



National Library  
of Canada

Acquisitions and  
Bibliographic Services Branch

395 Wellington Street  
Ottawa, Ontario  
K1A 0N4

Bibliothèque nationale  
du Canada

Direction des acquisitions et  
des services bibliographiques

395, rue Wellington  
Ottawa (Ontario)  
K1A 0N4

*Your file - Votre référence*

*Our file - Notre référence*

## NOTICE

The quality of this microform is heavily dependent upon the quality of the original thesis submitted for microfilming. Every effort has been made to ensure the highest quality of reproduction possible.

If pages are missing, contact the university which granted the degree.

Some pages may have indistinct print especially if the original pages were typed with a poor typewriter ribbon or if the university sent us an inferior photocopy.

Reproduction in full or in part of this microform is governed by the Canadian Copyright Act, R.S.C. 1970, c. C-30, and subsequent amendments.

## AVIS

La qualité de cette microforme dépend grandement de la qualité de la thèse soumise au microfilmage. Nous avons tout fait pour assurer une qualité supérieure de reproduction.

S'il manque des pages, veuillez communiquer avec l'université qui a conféré le grade.

La qualité d'impression de certaines pages peut laisser à désirer, surtout si les pages originales ont été dactylographiées à l'aide d'un ruban usé ou si l'université nous a fait parvenir une photocopie de qualité inférieure.

La reproduction, même partielle, de cette microforme est soumise à la Loi canadienne sur le droit d'auteur, SRC 1970, c. C-30, et ses amendements subséquents.

Canada

UNIVERSITY OF ALBERTA

FOUR CONTRIBUTIONS TO THE APPLICATION OF TURBULENT  
JET THEORY IN HYDRAULIC ENGINEERING

BY



SHOUHONG WU

A THESIS

SUBMITTED TO THE FACULTY OF GRADUATE STUDIES AND  
RESEARCH IN PARTIAL FULFILLMENT OF THE REQUIREMENT  
FOR THE DEGREE OF DOCTOR OF PHILOSOPHY

DEPARTMENT OF CIVIL ENGINEERING

EDMONTON, ALBERTA

SPRING, 1994



National Library  
of Canada

Acquisitions and  
Bibliographic Services Branch

395 Wellington Street  
Ottawa, Ontario  
K1A 0N4

Bibliothèque nationale  
du Canada

Direction des acquisitions et  
des services bibliographiques

395, rue Wellington  
Ottawa (Ontario)  
K1A 0N4

*Your file* *Votre référence*

*Our file* *Notre référence*

**The author has granted an irrevocable non-exclusive licence allowing the National Library of Canada to reproduce, loan, distribute or sell copies of his/her thesis by any means and in any form or format, making this thesis available to interested persons.**

**L'auteur a accordé une licence irrévocable et non exclusive permettant à la Bibliothèque nationale du Canada de reproduire, prêter, distribuer ou vendre des copies de sa thèse de quelque manière et sous quelque forme que ce soit pour mettre des exemplaires de cette thèse à la disposition des personnes intéressées.**

**The author retains ownership of the copyright in his/her thesis. Neither the thesis nor substantial extracts from it may be printed or otherwise reproduced without his/her permission.**

**L'auteur conserve la propriété du droit d'auteur qui protège sa thèse. Ni la thèse ni des extraits substantiels de celle-ci ne doivent être imprimés ou autrement reproduits sans son autorisation.**

ISBN 0-612-11420-1

**Canada**

UNIVERSITY OF ALBERTA

RELEASE FORM

NAME OF AUTHOR SHOUHONG WU

TITLE OF THESIS FOUR CONTRIBUTIONS TO THE  
APPLICATION OF TURBULENT JET THEORY  
IN HYDRAULIC ENGINEERING

DEGREE FOR WHICH THESIS WAS PRESENTED  
DOCTOR OF PHILOSOPHY

YEAR THIS DEGREE GRANTED 1994

Permission is hereby granted to THE UNIVERSITY OF ALBERTA LIBRARY to reproduce single copies of this thesis and to lend or sell such copies for private, scholarly or scientific research purposes only.

The author reserves other publication rights, and neither the thesis nor extensive extracts from it may be printed or otherwise reproduced without the author's written permission.

(Signed) *Shouhong Wu* .....

PERMANENT ADDRESS :

*#304 9130-82 Ave* .....

*Edmonton AB T6C 0Z5* .....

DATED *April 14* ..... 1994

THE UNIVERSITY OF ALBERTA  
FACULTY OF GRADUATE STUDIES AND RESEARCH

The undersigned certify that they have read, and recommended to the Faculty of Graduate Studies and Research for acceptance, a thesis entitled FOUR CONTRIBUTIONS TO THE APPLICATION OF TURBULENT JET THEORY IN HYDRAULIC ENGINEERING in partial fulfillment of the requirements for the degree of Doctor of Philosophy in Civil Engineering.

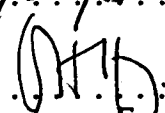
  
.....  
Supervisor

  
.....  
Co-Supervisor

  
.....

  
.....

  
.....

  
.....  
External Examiner

Date

..... 13th April 94 .....

**To the Memory of My Father**

## ABSTRACT

The thesis has been written in the paper format and includes four papers.

Paper 1 presents the results of an experimental study on the characteristics of a circular turbulent wall jet growing on a rough boundary, for the values of relative roughness  $k_s/D$  (equivalent sand height over nozzle diameter) varying from 0.16 to 2.16. The velocity profiles in the central vertical plane as well as the transverse velocity profiles were found to be similar. The length scale in the vertical plane was affected by the boundary roughness whereas the transverse expansion was almost unaffected. The boundary shear stress was affected considerably by the boundary roughness.

Paper 2 presents the results of an exploratory experimental study on intersecting circular turbulent jets of unequal momentum fluxes for an angle of intersection equal to 60 degrees. The flow can be divided into two regions, region 1 extending from the nozzle to the intersection point and region 2 covering the field downstream of the intersection point. In both regions, the velocity and pressure fields were measured, analyzed and correlated with the ratio of the jet velocities at the two nozzles.

Paper 3 presents an analysis of all the published data for wall jets, free jumps and submerged jumps and a study of three cases as a whole. The non-dimensional forward velocity profiles were found to be insensitive to submergence. The relative length scale  $L/y_0$  ( $L$  is the longitudinal distance from gate where the maximum velocity falls to one half of the gate velocity and  $y_0$  is the gate opening) for wall jet was found to be 60 and was independent of nozzle Reynolds number. For free jumps, it was found that the velocity scale decay is

similar, and  $L/y_0$  value is much smaller than that for wall jet and increases almost linearly with  $F_0$ . For submerged jumps, the velocity scale decay was found to have two types: free-jump-like and wall-jet-like. A criterion to distinguish a submerged jump with free-jump-like decay from that with a wall-jet-like decay is proposed.

Paper 4 presents the results of an exploratory experimental study on the effect of two dimensional baffle on submerged jumps. It was found that two critical values exist for the ratio of baffle height to downstream flow depth,  $(h/y_t)_{c1}$  and  $(h/y_t)_{c2}$ . When  $h/y_t$  is greater than  $(h/y_t)_{c2}$ , the main flow is deflected to form surface jet which is favorable for channel bed protection. When  $h/y_t$  is smaller than  $(h/y_t)_{c1}$ , the main flow reattaches the channel bed downstream the baffle. When  $h/y_t$  is between  $(h/y_t)_{c1}$  and  $(h/y_t)_{c2}$ , both deflected and reattached jets are possible depending on the initial condition. Detailed mean velocity and pressure fields were measured for deflected surface jets. The results were analyzed and correlated with the baffle size and position, gate Froude number and tail water depth.



## ACKNOWLEDGMENTS

I am greatly indebted to my supervisor, Dr. N. Rajaratnam for his guidance, encouragement, understanding and support throughout the research program. It is his great appreciation of the subject and sincere help that made this research work possible. I am also deeply grateful to my co-supervisor Professor P. M. Steffler for his patient explanation and instruction in the early stage of my research work when I worked with the LabView program for the LDA system and for his valuable advice in the writing of the thesis.

I deeply appreciate Mr. S. Lovell for setting up the experimental arrangements and his productive advice during the experiments.

Thanks to Dr. Dejiang Long for sending me all the diskettes of his experimental data. These data were very helpful for the study in Chapter 4.

Thanks to Dr. José Carlos de Araújo for his great help in my experiments of the study on baffle effects on submerged jumps during his stay at the T. Blench Hydraulics Laboratory.

Thanks to Ferdous and Femi for reading through the whole thesis to check my English.

Thanks to all my colleagues and all the professors of the Water Resources Group, Civil Engineering Department of the University of Alberta for their friendship during my stay at T. Blench hydraulics Laboratory.

Special thanks to my wife Cuihui, my daughter Danni and my son James for their patience, encouragement and support.

Finally I deeply appreciate the financial support from the Canadian Natural Science and Engineering Research council for my research programs, through an operating grant to my supervisor.

## TABLE OF CONTENTS

Chapter		page
<b>1</b>	<b>Introduction</b> .....	1
	References .....	4
<b>2</b>	<b>Circular Turbulent Wall Jets on Rough Boundaries</b>	7
	2.1 Introduction .....	7
	2.2 Experimental arrangement .....	9
	2.3 Experiments and experimental results .....	10
	2.4 Analysis of the experimental results .....	11
	2.4.1 Velocity distribution in the central vertical plane	11
	2.4.2 Velocity distribution in $y = \delta$ plane .....	13
	2.4.3 Velocity distribution in non-central vertical plane	13
	2.4.4 Boundary shear stress variation along center-line	13
	2.4.5 Roughness effect on length and velocity scales	14
	2.5 Conclusions .....	15
	2.6 References .....	16
<b>3</b>	<b>Intersecting Circular Jets of Unequal Momentum Flux</b>	38
	3.1 Introduction .....	38
	3.2 Experiments .....	40
	3.3 Experimental results and analysis for region 1 .....	42
	3.3.1 Velocity and pressure variation along jet axis .....	42
	3.3.2 Velocity and pressure distribution in region 1 .....	43
	3.4 Experimental results and analysis for region 2 .....	45
	3.4.1 Velocity and pressure variation along resultant jet axis	45
	3.4.2 Velocity and pressure distribution in region 2 .....	47
	3.5 Conclusions .....	48
	3.6 References .....	50
<b>4</b>	<b>Free Jumps, Submerged Jumps and Wall Jets</b> .....	95
	4.1 Introduction .....	95
	4.2 Wall jets .....	99
	4.3 Free jumps .....	100

4.4	Submerged jumps .....	103
4.4.1	Experimental setup .....	104
4.4.2	Experiments and results .....	106
4.4.3	Analysis of submerged jump results .....	107
4.4.3.1	Velocity profile similarity .....	107
4.4.3.2	Decay of Piezometric pressure defect ..	108
4.4.3.3	Decay of velocity scale .....	108
4.4.3.4	Variation of length scale $L$ .....	110
4.4.3.5	More about the velocity scale decay ...	111
4.4.3.6	Length scale $b$ .....	111
4.4.3.7	Length scale $\delta$ .....	111
4.4.3.8	Reverse flow .....	112
4.4	Conclusions .....	114
4.5	References .....	116
<b>5</b>	<b>Effect of Baffles on Submerged Jumps .....</b>	<b>163</b>
5.1	Introduction .....	163
5.2	Experimental arrangement .....	164
5.3	Possible flow states .....	166
5.3.1	Experimental results and analysis ( Series 1) .....	169
5.3.2	Mean flow structure .....	170
5.4	Conclusions .....	180
5.5	References .....	183
<b>5</b>	<b>General Discussion .....</b>	<b>219</b>
	References .....	222

## LIST OF TABLES

Table		page
2-1	Details of the experiments .....	10
2-2	Scale data for $\delta$ , $b_y$ , $b_z$ , $u_{m0}$ and $C_f$ .....	36
2-3	Scales in $x/D=16$ plane .....	37
2-4	Coefficients and length scale growth rates .....	37
3-1	Primary details of the experiments .....	42
3-2	Velocity and pressure scale data in region 1 .....	89
3-3	Maximum pressure data in region 1 .....	90
3-4	Length scale data in region 1 .....	90
3-5	Data for the axis of jet in region 2 .....	91
3-6	Velocity and pressure scale data in region 2 .....	92
3-7	Length scale data in region 2 .....	94
3-8	Data for $p_{min}$ , $a_1$ , $a_2$ , $db_y/dx$ ; $db_z/dx$ and $p_{max}$ .....	94
4-1	Data for the wall jet velocity scale .....	152
4-2	Data for the wall jet length scale $L$ .....	153
4-3	Data for the rate of growth of length scales for wall jet .....	153
4-4	Data for the velocity scale of free jumps .....	154
4-5	Data for the length scale $L$ of free jumps .....	155
4-6	Data for the length scale $b$ of free jumps .....	155
4-7	Details of experiments of Series 1 .....	106
4-8	Data of $F_0$ and $S$ for submerged jumps .....	156
4-9	Velocity scale data for submerged jumps .....	157
4-10	Data for the length scale $L$ for submerged jumps .....	159
4-11	Data for the length scale $b$ for submerged jumps .....	160
4-12	Data for the length scale $\delta$ for submerged jumps .....	161
4-13	Scale data for the reverse flow of present experiments .....	162
4-14	Surface profile data of present experiments .....	162
5-1	Experimental results for critical baffle height $h_{c1}$ .....	210
5-2	Experimental results for critical baffle height $h_{c2}$ .....	211
5-3	Details of experiments of series 2 .....	171
5-4	Regression equations for the scales on water surface .....	212
5-5	Data for vorticity, circulation and circulation discharge of the eddy upstream baffle .....	212

5-6	Magnitude and locus of the maximum velocity .....	213
5-7	Data for the surface profiles .....	214
5-8	Length scale and discharge data in the surface jet region .....	215
5-9(a)	Surface velocity data for varying gate Froude numbers	216
5-9(b)	Surface velocity data for varying baffle heights .....	216
5-9(c)	Surface velocity data for varying submergences .....	217
5-9(d)	Surface velocity data for varying baffle positions .....	217
5-10	Data of surface hump position, surface hump height, maximum surface velocity and its position for varying nozzle Froude numbers, submergences, baffle heights and baffle positions .....	218

## LIST OF FIGURES

Figure		page
1-1	Flow configuration of circular wall jet .....	5
1-2	Schematic representation of mixing of two jet .....	5
1-3(a-b)	Definition sketch for the free and submerged hydraulic jumps	6
1-4	Flow configuration of the submerged jump with a baffle .....	6
2-1	Definition sketch and experimental arrangement .....	17
2-2	Details of roughness .....	18
2-3(a-d)	Velocity profiles in the central vertical plane .....	19
2-4(a-d)	Velocity profiles in $y=\delta$ plane .....	20
2-5(a-b)	Velocity profiles in $x/D=16$ plane .....	21
2-6	Shear stress variation along the center line of the wall .....	21
2-7(a-d)	Non-dimensional velocity profiles in the central vertical plane	22
2-8	Consolidated non-dimensional velocity profiles in the central vertical plane .....	23
2-9(a-d)	Inner layer non-dimensional velocity profiles in the central vertical plane .....	24
2-10(a-b)	Plots of inner layer velocity data in non-dimensional form	25
2-11(a-d)	Non-dimensional velocity profiles in the free mixing region	26
2-12	Consolidated velocity profiles in the free mixing region of the central vertical plane .....	27
2-13(a-d)	Non-dimensional velocity profiles in $y=\delta$ plane .....	28
2-14	Consolidated non-dimensional velocity profiles in $y=\delta$ plane	29
2-15(a-c)	Non-dimensional velocity profiles at section $x/D=16$ .....	30
2-16	Skin friction coefficient variation along the wall center line	31
2-17	Effect of roughness on skin friction coefficient .....	31
2-18	Growth of boundary layer in the central vertical plane .....	32
2-19	Effect of roughness on boundary layer growth rate .....	32
2-20	Variation of boundary layer thickness in transverse direction at section $x/D=16$ .....	33
2-21	Roughness effect on the decreasing rate of the boundary layer thickness in the transverse direction .....	33
2-22	Growth of the length scale $b_y$ .....	34
2-23	Effect of roughness on the growth rate of length scale $b_y$	34

2-24	Growth of the length scale $b_z$ .....	35
2-25	Decay of the velocity scale $u_m$ .....	35
2-26	Effect of roughness on the coefficient C .....	35
3-1	Definition sketch for intersecting jets of equal momentum flux	51
3-2	Schematic diagram of the experimental set up .....	52
3-3	Definition sketch for intersecting jets of unequal momentum flux	53
3-4	Decay of the centerline velocity of jet in region 1 .....	54
3-5	Variation of the centerline pressure in jet region 1 .....	54
3-6	Variation of the maximum pressure in jet in region 1 with R	54
3-7(a-f)	Transverse velocity profiles in region 1 .....	55
3-8(a-f)	Dimensionless transverse velocity profiles in region 1 .....	57
3-9	Consolidated transverse velocity profiles in region 1 .....	59
3-10(a-b)	Growth of the transverse length scales in region 1 .....	60
3-11	Variation of the length scale $b_{z1}$ growth rate with R .....	61
3-12(a-f)	Vertical velocity profiles in region 1 .....	61
3-13(a-f)	Dimensionless vertical velocity profiles in region 1 .....	63
3-14	Consolidated dimensionless velocity profiles in region 1 .....	65
3-15	Growth of the vertical length scales in region 1 .....	65
3-16(a-f)	Transverse pressure profiles in jet in region 1 .....	66
3-17(a-f)	Vertical pressure profiles in jet in region 1 .....	68
3-18	Axis of jet in region 2 - comparison of predicted axis and measured axis .....	70
3-19(a-b)	Velocity scale decay in region 2 .....	70
3-20	Variation of the coefficients $a_1$ and $a_2$ with R .....	71
3-21	Pressure variation along the axis of the jet in region 2 .....	72
3-22	Correlation of the minimum pressure along the jet axis in region 2 with R .....	72
3-23(a-e)	Pressure field in the reverse flow region .....	73
3-24	Variation of the maximum pressure with R .....	74
3-25(a-f)	Transverse velocity profiles in region 2 .....	75
3-26(a-f)	Dimensionless transverse velocity profiles in region 2 .....	77
3-27	Consolidated dimensionless transverse velocity profiles in region 2 .....	79
3-28	Variation of the length scale $b_z$ with the distance from intersection point .....	79

3-29(a-f)	Vertical velocity profiles in region 2 .....	80
3-30(a-f)	Dimensionless vertical velocity profiles in region 2 .....	82
3-31	Consolidated plot for all the vertical velocity profile data in region 2 .....	84
3-32	Growth of the vertical length scale of the jet in region 2	84
3-33	Variation of the length scale growth rates in region 2 with R	84
3-34(a-f)	Transverse pressure profiles in region 2 .....	85
3-35(a-f)	Vertical pressure profiles in region 2 .....	87
4-1(a-b)	Definition sketch for the free and submerged hydraulic jumps	119
4-2	Typical longitudinal velocity distribution in (submerged) jumps	119
4-3	Non-dimensional velocity profiles of submerged jumps	120
4-4	Non-dimensional velocity profiles of free jumps .....	121
4-5	Decay of velocity scales of free jumps, submerged jumps and plane wall jets .....	122
4-6	Decay of the velocity scale of submerged jumps .....	123
4-7	Variation of the $L/y_0$ with $F_0$ and $S$ .....	123
4-8(a-b)	Decay of the velocity scale in plane turbulent wall jets	124
4-9	Variation of the length scale $L$ with the nozzle Reynolds number for plane turbulent wall jets .....	124
4-10(a-f)	Decay of the velocity scale in free jumps .....	125
4-11	Consolidated plot of the velocity scale decay in free jumps	127
4-12	Variation of the length scale $L$ with $F_0$ for the free jumps	128
4-13	Growth of the length scale $b$ for the free jumps .....	128
4-14(a-c)	Experimental arrangement .....	129
4-15	Flow chart for sub-VI " From voltages to magnitude and angle"	130
4-16	Comparison of longitudinal velocity profiles in $z=0$ and $z=0.1B$ planes .....	131
4-17	Mean velocity field of run 1 .....	131
4-18(a-c)	Longitudinal velocity profiles for runs 2, 3 and 4 .....	132
4-19(a-c)	Pressure profiles for runs 2, 3 and 4 .....	133
4-20(a-d)	Non-dimensional velocity profiles for runs 1~4 .....	134
4-21	Consolidated plot of the non-dimensional longitudinal velocity profiles of present experiments on submerged jumps .....	135
4-22	Longitudinal variation of the maximum pressure defect in submerged jumps .....	135



4-23(a-o)	Longitudinal variation of the velocity scale in submerged jumps	136
4-24	Variation of $S^*$ with $F_0$ .....	143
4-25	Variation of the length scale $L$ with $F_0$ and $S$ for submerged jumps .....	144
4-26	Correlation between $L/y_0$ and $F_0$ and $S$ for submerged jumps	144
4-27	Variation of $S^*$ and $S^\#$ with $F_0$ for submerged jumps .....	144
4-28	Variation of $x_d/L$ with $F_0$ and $S$ for submerged jumps .....	145
4-29	Velocity scale decay of WJL jump in the region off the wall jet curve .....	145
4-30	Longitudinal variation of the length scale $b$ for submerged jumps	146
4-31(a-b)	Growth of the inner layer of submerged jumps .....	147
4-32(a-d)	Similarity of velocity profiles of the reverse flow in submerged jumps .....	148
4-33	Consolidated non-dimensional plot of the reverse flow velocity profiles in submerged jumps .....	149
4-34	Longitudinal variation of the length scale $b_r$ of the reverse flow region of submerged jumps .....	149
4-35(a-b)	Longitudinal variation of the reverse flow surface velocity in submerged jumps .....	150
4-36	Velocity scale $u_{sm}$ as a function of $F_0$ and $S$ .....	151
4-37	Variation of the roller length with $S$ for submerged jumps	151
5-1	Flow configuration of hydraulic jump forced by a two-dimensional baffle .....	184
5-2	Experimental flume .....	185
5-3(a-b)	Experimental setup for velocity and pressure measurements	186
5-4(a-b)	Schematic flow patterns .....	187
5-5(a-b)	Variation of the critical baffle heights with baffle position	188
5-6(a-n)	Velocity and piezometric fields .....	189
5-7(a-d)	Distribution of the longitudinal velocity component before baffle	196
5-8(a-d)	Non-dimensional profiles of the longitudinal velocity component before baffle .....	197
5-9	Consolidated non-dimensional profiles of the longitudinal velocity component before baffle .....	198
5-10	Decay of the velocity scale before baffle .....	198
5-11	Variation of the length scale $b$ before baffle .....	198

5-12(a-b)	Effect of the nozzle gate number on the decay of maximum velocity and its locus .....	199
5-13(a-b)	Comparison of the decay and the locus of the maximum velocity for two different flow patterns .....	200
5-14(a-b)	Effect of the baffle position and height on the decay and locus of the maximum velocity of deflected surface jets .....	201
5-15(a-g)	Non-dimensional forward velocity profiles in the region of surface jet .....	202
5-16	Longitudinal variation of forward discharge of surface jets	204
5-17(a)	Longitudinal variation of surface jet boundary .....	204
5-17(b)	Growth of the length scale $b_s$ .....	204
5-18(a-c)	Effect of gate Froude number on the scales on water surface	205
5-19(a-c)	Effect of submergence on the scales on water surface	206
5-20(a-c)	Effect of baffle position on the scales on water surface	207
5-21(a-c)	Effect of baffle height on the scales on water surface	208
5-22	Consolidated plot for the surface velocity decay .....	209
5-23	Variation of circulation with baffle position .....	209

## NOTATIONS

(the numbers in squarebrackets [] denote relevant chapter numbers)

Symble	Description
$a_1, a_2$	coefficients [3]
$B$	flume width [4]
$b$	length scale equal to $y$ where $u = 0.5u_m$ and $\partial u/\partial y < 0$ [4, 5]
$b'_y$	length scale in vertical direction in the non-central planes [2]
$b_r$	water depth where $u = 0.75 u_s$ [4]
$b_s$	water depth where $u = 0.5u_s$ [5]
$b_y$	length scale in vertical direction [2, 3]
$b_z$	length scale in transverse direction [2]
$b_{z+}$	inner side length scale in the transverse direction in region 2 [3]
$b_{z-}$	outer side length scale in the transverse direction in region 2 [3]
$b_{z1+}$	inner side length scale in the transverse direction in region 1 [3]
$b_{z1-}$	outer side length scale in the transverse direction in region 1 [3]
$C$	coefficient [2]
$C_f$	coefficient of skin friction [2]
$D$	diameter of jet nozzle [2, 3]
$\Delta p_{cm}$	maximum value of the difference between the centerline pressure of $R \neq 0$ and that of $R=0$ in region 1 [3]
$F_0$	gate Froude number [1, 4, 5, 6]
$f_1$ to $f_4$	functions [2, 4]
$g$	gravitational acceleration [1, 4, 5]
$g_1, g_2$	functions [4]
$H$	distance from nozzle to intersection point [3]
$h$	baffle height [1, 5]
$h_{c1}$	lower critical baffle height [5]
$h_{c2}$	upper critical baffle height [5]
$h_h$	hump height above the tail water surface [5]
$k_1, k_2$	pitch probe calibration parameters [4]
$K_{21}$	$K_{21} = k_2 - k_1$ [4]
$k_s$	equivalent sand roughness [2]
$L$	length scale equal to the value of $x$ where $u_m = U_0/2$ [1, 4, 5, 6]
$L_{rj}$	length of the free jump roller [1, 4, 5]

$L_{rsj}$	length of the submerged jump roller [1, 4, 5]
$p$	piezometric pressure [4, 5]; pressure inside the jet (with reference to the surrounding atmospheric pressure [3])
$p_{21}$	pitch probe middle hole and upper hole pressure difference [4]
$p_{23}$	pitch probe middle hole and lower hole pressure difference [4]
$p_c$	value of $p$ on the centerline of jet [3]
$p_{max}$	maximum pressure in the reverse flow region [3]; maximum deviation of piezometric pressure from hydrostatic value [4]
$p_{min}$	minimum value of $p_c$ in region 2 [3]
$q$	forward discharge per unit flume width [5]
$q_{circIn}$	eddy circulation discharge per unit flume width [5]
$q_{nozl}$	nozzle discharge per unit flume width [5]
$R$	correlation coefficient [2, 4, 5]; ratio of jet velocity at nozzles B to that at nozzle A [3, 6]
$r$	distance from vortex center to the point of measurement [5]
$Re_0$	nozzle Reynolds number [4, 6]
$S$	submergence [1, 4, 5, 6]
$S^\#$	smallest value of $S$ required for a WJL jump to have the same length scale $L$ as wall jet [4]
$S^*$	critical value of $S$ to distinguish between WJL and FJL jumps [4]
$u$	time averaged longitudinal velocity at any point [2, 3, 4, 5]
$u', v', w'$	fluctuation velocity components in x, y and z directions [2]
$u'_m$	maximum value of $u$ in non-central vertical planes [2]
$u_\tau$	boundary shear velocity [2]
$U_0$	velocity of jet at nozzle [1, 2, 4, 5]
$u_m$	value of $u$ in the central vertical plane [2]; maximum value of $u$ at any section [3, 4, 5]
$u_{m0}$	maximum value of $u_m$ [2]
$u_{md}$	value of $u_m$ at the location where the decay of $u_m$ deviates from wall jet curve [4]
$u_s$	surface flow velocity [5]; reverse flow velocity on water surface [4]
$u_{sm}$	maximum value of $u_s$ [4]
$v, w$	time-averaged velocities in y and z directions [2]
$v_m$	magnitude of maximum velocity vector [5]
$v_\theta$	tangential velocity [5]

$x$	distance from the intersection point and along the theoretically predicted resultant jet axis [3]; longitudinal distance from nozzle [1, 2, 4, 5]
$x'$	distance from the intersection point and along the symmetry line [3]
$x_0$	distance from the baffle front to the gate [1, 5]
$x_1$	longitudinal distance from Nozzle A [3]
$x_d$	value of $x$ where submerged jump velocity scale decay starts to deviate from the wall jet curve [4]
$x_{sm}$	value of $x$ where the surface velocity has the maximum value [5]
$x_{top}$	the position of the top of surface hump [5]
$y$	coordinate in vertical direction [1, 2, 3, 4, 5]
$y_1$	nozzle opening [1, 4, 5, 6]
$y_2$	conjugate tail water depth of the free jump [1, 4, 5]
$y_3$	water depth behind the gate [1, 4, 5]
$y_{nozl}$	value of $y$ above which $q=q_{nozl}$ [5]
$y_s$	water depth [5]; distance below the free surface [4]
$y_t$	tail water depth [1, 4, 5]
$z$	transverse distance [2]; distance from the (theoretically predicted) resultant jet axis [3]
$z'$	distance from the symmetry line [2]
$z^*$	distance between the experimentally determined resultant jet axis and the theoretically predicted axis [3]
$z_1$	transverse distance from the axis of nozzle A [3]
$\alpha$	angle between the jets [3]
$\delta$	boundary layer thickness [4, 5]; boundary layer thickness in the central vertical plane [2]
$\delta'$	boundary layer thickness in the non-central vertical planes [2]
$\Gamma$	eddy circulation [5]
$\eta$	$= y/b$ [4]
$\nu$	kinematic viscosity of the fluid [2]
$\emptyset$	angle of attack [4]
$\rho$	density of the fluid [2, 3, 4, 5]
$\tau_{0m}$	boundary shear stress (in the central vertical plane) [2]
$\zeta$	vorticity [5]
$\bar{\alpha}$	the angle between (theoretically predicted) resultant jet axis and symmetry line [3]

## **Chapter 1      Introduction**

A turbulent jet is defined as a jet of high velocity fluid discharging into an ambient fluid which may be at rest or in motion. A systematic study of turbulent jets is believed to have begun with the theoretical studies of Tollmien (1926) and Goertler (1942) and the experimental work of Förthmann (1934) (Abramovich, 1963 ) and since then a large number of papers on jets have been published. The books written by Abramovich (1963) and by Rajaratnam (1976) provide a coherent treatment of the theory of turbulent jets.

Although the present knowledge on turbulent jets can be considered to be comprehensive, there are still several areas in which useful contributions can be made. In this thesis, the results of experimental studies on four practical problems in hydraulic engineering dealing with turbulent jets will be presented.

In Chapter 2, the results of an experimental investigation on circular wall jets on rough boundaries will be presented. A circular wall jet is defined as a jet of fluid discharging tangentially on a flat surface and Fig. 1-1 gives a definition of such a flow configuration. In the introduction section of Chapter 2 (section 2.1), the general characteristics of circular wall jets on smooth boundaries are given first. Following this, the experimental setup for the present study is described in section 2.2. In section 2.3, the details of the experiments of four different relative roughnesses and the direct experimental results are given. The analysis on the effect of roughness on the jet characteristics and the conclusions are given in sections 2.4 and 2.5 respectively.

The objective of Chapter 3 is to study the mean flow structure of two intersecting circular jets of unequal momentum flux (see Fig. 1-2 ). The original

inspiration for the study stems from the fact that in hydraulic engineering, it is possible to use jet intersection as a means to dissipate energy, in connection with hydraulic structures. Intersecting jets have been studied by a number of investigators and a brief review of the existing investigations is given in the introduction section (section 3.1) of Chapter 3. The experimental setup is described in detail in section 3.2. The experimental results for the flow region between the nozzles and the intersection point and the analysis on the results for this region are given in section 3.3. The experimental results and the analysis of the flow region downstream the intersection point are presented in section 3.4. The conclusions for the present study are formulated in section 3.5.

Chapter 4 is a major component of this thesis. In this chapter, free hydraulic jumps, submerged jumps and two-dimensional wall jets (referred to as classical wall jets, or CWJ) are studied as a whole. Fig. 1-3 illustrates the flow configuration of free jumps and submerged jumps. The classical wall jet can be viewed as the limiting case of submerged jumps when the tail water depth approaches infinity. In the introduction section of Chapter 4 (section 4.1), the existing published papers which reveal the flow structure of free and submerged jumps are reviewed briefly and some of the results on the mean velocity profiles are reproduced. Section 4.2 focuses on classical wall jets. In this section, the existing published data on the decay of velocity scale of CWJ and the corresponding length scale data are collected and analyzed.

For free jumps, a collection of all the available data on velocity and length scales are presented in section 4.3. By analyzing the velocity scale data, an attempt was made to obtain a general decay law for free jumps. A second attempt in section 4.3 is to show how the length scale  $L$  of free jumps changes with nozzle Froude number  $F_0$  ( here  $L$  equals to the longitudinal distance from nozzle

where the maximum velocity falls to one half of the nozzle velocity, and  $F_0$  equals to  $U_0/\sqrt{gy_0}$  in which  $U_0$  and  $y_0$  are the nozzle velocity and the opening respectively, and  $g$  is the gravitational acceleration).

Much attraction has been given to submerged jumps since they serve as the transition from free jumps to wall jets. In section 4.4, all the available existing scale data on submerged jumps are collected. In addition, some more experiments were done to supplement the data. The experimental set up for the experiments will be described first in section 4.4. Following that, an analysis on the characteristics of submerged jumps based on the collected data and the new experimental data will be performed. This analysis is done mainly in the following two aspects: (1) for jumps of different  $F_0$ , how the decay of the velocity scale changes from the style of free jump to the style of wall jet with an increase of submergence  $S$  (equal to  $(y_t - y_2)/y_2$ , where  $y_t$  is the tail water depth and  $y_2$  is the tail subcritical sequent depth of free jump for a given  $F_0$ ); (2) how the length scales of submerged jumps vary with  $F_0$  and  $S$ . The conclusions of the present study on free jumps, submerged jumps and wall jets are formulated in section 4.5.

In Chapter 5, some experimental results on the effect of two-dimensional baffles on wall jets with finite submergences are presented. The flow configuration of this problem is shown in Fig. 1-4. Chapter 5 consists of 4 sections. In the brief introductory section (section 5-1), the necessity of the present study is described. Section 5-2 describes the experimental setup for the present study. The experimental results and the analysis on the results are presented in section 5-3. First of all, this section describes the flow characteristics of the two different flow states found in the experiments, the deflected surface jet and reattaching wall jet. Following this, the formation conditions for the two flow



states are discussed and empirical curves are presented to describe these conditions. Based on the detailed experimental data, section 5-3 discusses the baffle effects on the mean flow structure of both flow states, especially the deflected surface jet state. This includes: the decay of velocity scale, the development of length scales and the characteristics of baffle induced eddies. In the last section of Chapter 5, section 5-4, the conclusions on the effects of baffle on submerged jumps are formulated.

In the last chapter of this thesis, Chapter 6, a general discussion is presented on the four contributions presented in Chapters 2 to 5. For each of these contributions, Chapter 6 gives a brief summary and suggests possible directions for further study.

#### **References:**

1. Abramovich, G. N. (1963), *The Theory of Turbulent Jets*, English Translation published by M. I. T. Press, Massachusetts, 671 p.
2. Rajaratnam, N. (1976). *Turbulent Jets*, Elsevier Scientific Publishing Co., 304p.

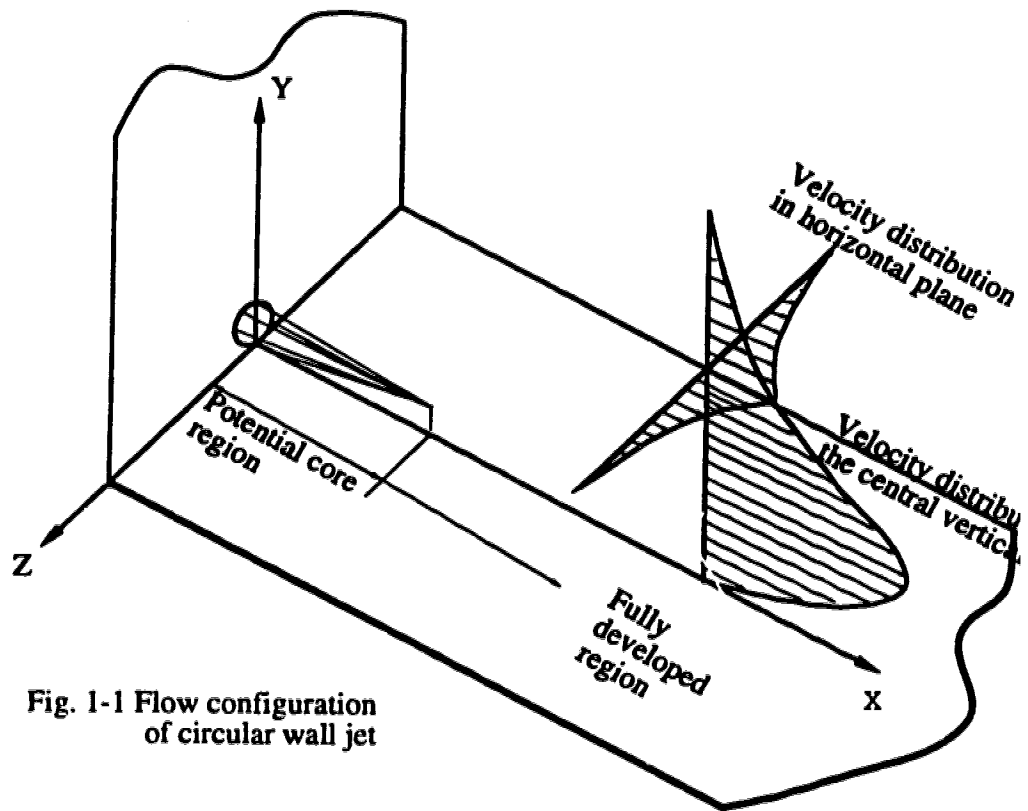


Fig. 1-1 Flow configuration of circular wall jet

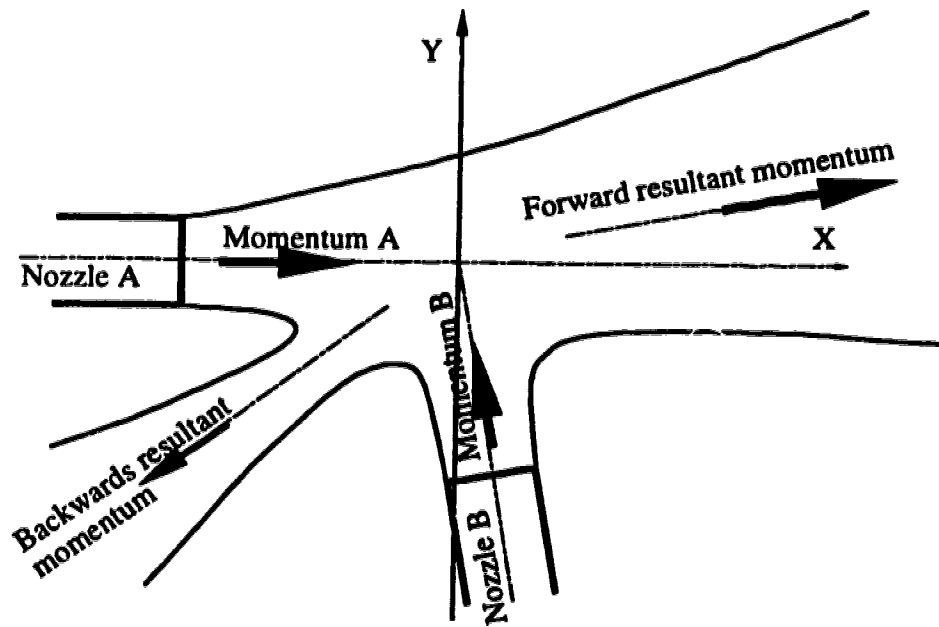


Fig. 1-2 Schematic representation of mixing of two jets

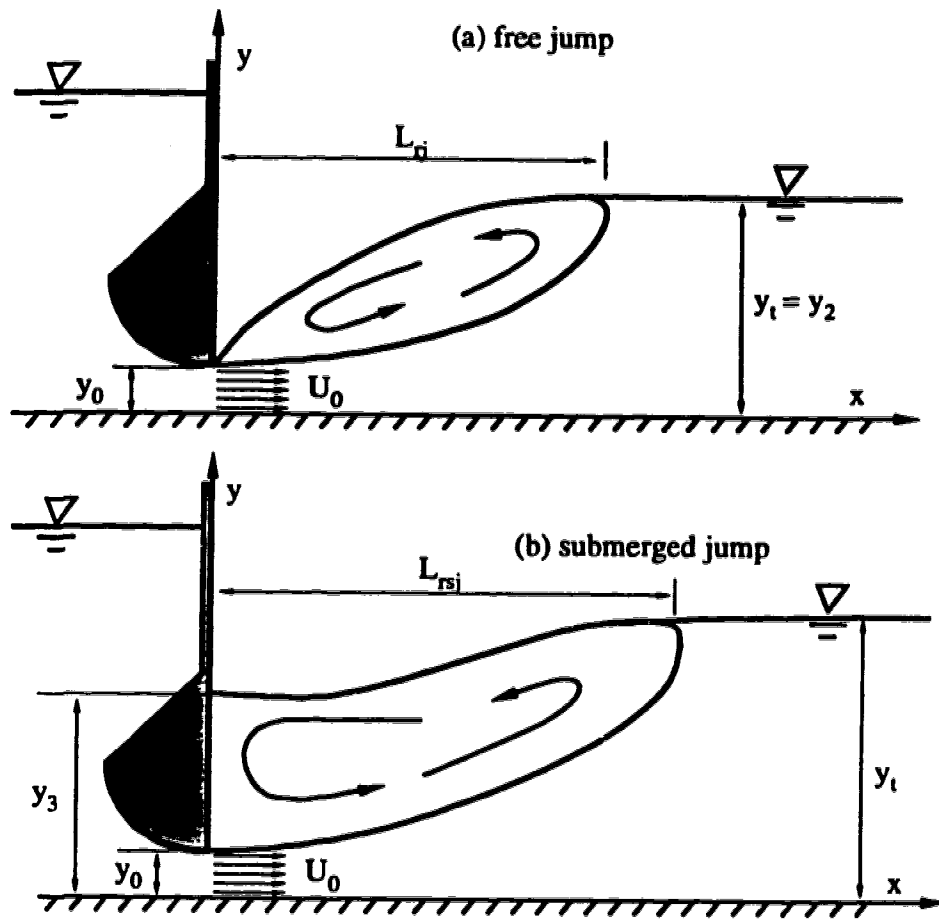


Fig. 1-3(a-b) Definition sketch for free and submerged hydraulic jumps

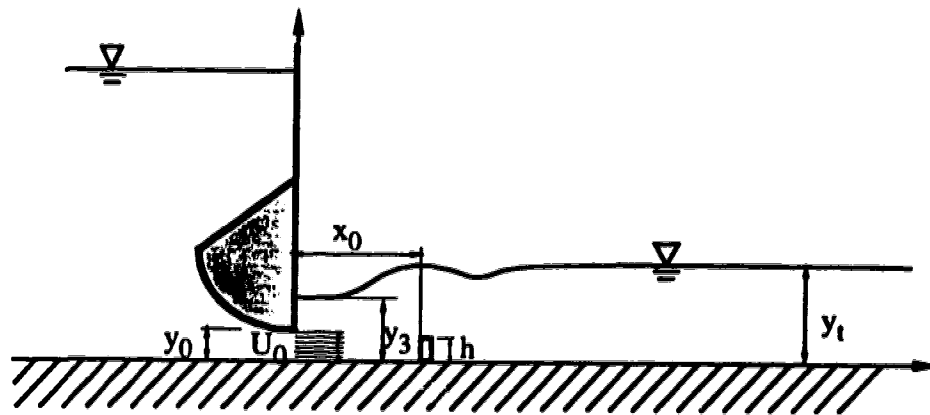


Fig. 1-4 Flow configuration of submerged jump with baffle

## Chapter 2 Circular Turbulent Wall Jets on Rough Boundaries \*

### 2.1 Introduction

Consider a circular wall jet of diameter  $D$  issuing from a nozzle with an (almost) uniform velocity  $U_0$  tangential to a boundary into a large mass of the same fluid (essentially) at rest. Such a flow configuration is referred to as a circular wall jet ( all boundaries are generally referred to as walls in the Fluid Mechanics literature and hence the name wall jet ). Fig. 2-1(a) shows the definition sketch of such a configuration. The circular wall jet belongs to the family of bluff wall jets ( Rajaratnam, 1976 ). If the Reynolds number of the jet (equal to  $U_0 D/\nu$  where  $\nu$  is the kinematic viscosity of the fluid) is greater than a few hundred, the jet is likely to be turbulent. Based on the investigations of Newman, Patel, Savage and Tjio (1972), Rajaratnam and Pani (1974) and others ( see review by Launder and Rodi (1983) for a list of other investigations ), we understand that in the region of fully developed flow, which occurs downstream of the potential core, in the central plane where  $z = 0$ , the distribution of time averaged axial velocity  $u_m$  in the  $Y$  direction is similar. That is  $u_m/u_{m0} = f_1(y/b_y)$  where  $f_1$  denotes a functional relation and  $u_{m0}$  and  $b_y$  are respectively the velocity and length scales. The velocity scale  $u_{m0}$  is defined as the maximum value of  $u_m$  which occurs at a normal distance  $\delta$  from the wall and  $b_y$  is the value of  $y$  where  $u_m = u_{m0}/2$  and  $\partial u_m/\partial y$  is negative. The inner region where  $y < \delta$  is known as the boundary layer ( with  $\delta$  referred to as the thickness of the

---

\* The main content of this chapter has been published in the Journal of Hydraulic Research, 1990, Vol. 28, No. 5.

boundary layer ) whereas the outer region with  $y \geq \delta$  is known as the free mixing region. The  $u$  velocity profiles in the transverse direction ( see Fig. 2-1 (a)) are also similar. That is  $u/u_m = f_2(z/b_z)$  where  $u_m$  is equal to the maximum value of  $u$ ,  $b_z$  is the value of  $z$  where  $u = u_m/2$  and  $f_2$  denotes another function. This function  $f_2$  is well approximated by the exponential equation

$$f_2 = \exp(-0.693(z/b_z)^2) \quad (2-1)$$

In the fully-developed flow region,  $u_{m0} \propto 1/x$  and both the length scales grow linearly with the longitudinal distance  $x$ . From a review of the available results, Launder and Rodi (1983) suggest the following values for growth rates of scales  $b_y$  and  $b_z$ :

$$\frac{db_y}{dx} = 0.048 \quad \text{and} \quad \frac{db_z}{dx} = 0.26 \quad (2-2)$$

which indicate a transverse to vertical spreading rate of about 5.5. If  $\tau_{0m}$  is the boundary shear stress in the central plane, dimensional arguments suggest that  $\tau_{0m} \propto 1/x^2$ . The variation of  $u_{0m}$  and  $\tau_{0m}$  with  $x$  has been evaluated in a unified manner for bluff wall jets of several shapes by Rajaratnam and Pani (1974).

Considering bluff wall jets on rough boundaries, comparatively very little work has been done. Pani (1972) performed one experiment with a sand-paper of roughness with a relative equivalent roughness  $k_s/D$  of 0.20 and found that the main difference was that  $\delta$  increases somewhat at a larger rate. Since the boundaries are more likely to be rough in practical cases, an experimental study was done with four values for the relative roughness  $k_s/D$  equal to 0.16, 0.32, 1.08 and 2.16 and the results are presented in this chapter.

## 2.2 Experimental arrangement

The experiments were performed in a jet tank 1.1 m wide, 1.22 m deep and 3.5 m long. The circular wall jet from a nozzle entered the tank, tangentially on a flat plate kept horizontal at about the mid-depth in the tank (see Fig. 2-1(b)). Jets of desired velocities were produced by means of a standpipe of different heights and the jets were deeply submerged by maintaining the water level very near the top of the jet tank.

Time-averaged mean velocity field in the jet was measured with a Prandtl tube of external diameter of 2.4 mm. No turbulence correction was made to the velocity since the turbulence field was not known. This tube was also used to measure the boundary shear stress in the center plane.

Two types of roughnesses were used in the experiments. The first roughness was provided by a (hardened) rubber mat with rectangular ridges running perpendicular to the direction of the jet. The second roughness was provided by a flower-type mat and the details of these roughnesses are shown in Fig. 2-2. The mats were fixed to the horizontal support plate in such a way that the jets issued tangentially at the top level of the roughness elements. When roughnesses were calculated, it was assumed that there exists the semi-logarithmic type of the law of the wall in the inner region of the boundary layer part. This semi-log law is described as

$$u_m = 5.75u_* \log\left(30 \frac{y}{k_s}\right) \quad (2-3)$$

in which  $u_*$  is wall shear velocity. By eqn. (2-3), if the datum for the roughness was chosen correctly, the plot of  $u_m$  against  $y$  data for the inner layer of the jet would form a straight line on a semi-log paper. This was exactly the way the datum for the two materials were found. Once the datum was found, the  $k_s$  value

could be obtained by extending the straight line in the semi-log paper to cross  $u_m=0$  line and multiplying the y value at this point by 30. The roughness values for the strip and flower-typed roughness materials were found to be respectively 4.0 mm and 27.4 mm.

### 2.3 Experiments and experimental results

Four experiments were performed, the primary details of which are given in table 2-1. Two nozzles of diameters of 12.7 and 25.4 mm were used with the two roughnesses, giving  $k_s/D$  values of 0.16, 0.32, 1.08 and 2.16. The jet velocity at the nozzle was given two values of 3.35 and 4.27 m/s and the Reynolds number of the jet was varied from about 5200 to 8100.

Table 2-1. Details of the experiments

run	D(mm)	$U_0$ (m/s)	$k_s$ (mm)	$k_s/D$	$U_0D/\nu$
1	12.7	4.27	4.0(strip)	0.32	5160
2	25.4	3.35	4.0(strip)	0.16	8110
3	25.4	3.35	27.4(flower)	1.08	8110
4	12.7	4.27	27.4(flower)	2.16	5160

For each experiment, the variation of time-averaged longitudinal velocity  $u_m$  was measured in the central vertical plane ( $z=0$ ) at several longitudinal distances from the nozzle. The  $u_m(y)$  profiles for all the four runs are shown in Fig. 2-3(a-d). In the figure, we can see the potential core at  $x/D=1$ , the boundary layer and the free mixing regions, the fall of  $u_m$  with  $x/D$  as well as the growth of  $b_y$  and  $\delta$  with  $x/D$ .

The variation of  $u(z)$  in the plane of  $u_{m0}$  was also measured in all the four runs and the results are shown in Fig. 2-4(a-d). In these profiles we can see the decay of  $u_{m0}$  with  $x/D$  as well as the growth of  $b_z$  with  $x/D$ .

Fig. 2-5(a-b) shows the velocity profiles for several non-zero values of  $z/D$  for one longitudinal section ( $x/D=16$ ) and these profiles show us the decay of longitudinal velocity in transverse direction. In Fig. 2-5, we can see that the boundary layer becomes somewhat thinner as we move transversely away from the central plane.

It was attempted to measure the boundary shear stress  $\tau_{0m}$  in the central plane by means of the 2.4 mm Prandtl tube as the Preston tube using the calibration diagram of Hollingshead and Rajaratnam (1980), but for the values of  $k_s$  and diameter of Prandtl tube involved, the results were found to be very approximate. Hence  $\tau_{0m}$  was calculated by the log-law with the characteristic constants having the values of 5.75 and 8.5 for the Prandtl tube resting on top of the roughness elements and the results are shown in Fig. 2-6. In Fig. 2-6 it is seen that  $\tau_{0m}$  decreases rather rapidly with the distance from the nozzle.

## **2.4 Analysis of the experimental results**

### **2.4.1 Velocity distribution in the central vertical plane**

The velocity profiles in the central vertical plane are plotted in non-dimensional forms for each run in Fig. 2-7(a-d). It is seen from the figures that the profiles are similar in each run for  $x > 8D$  but only those for small  $k_s/D$  values (runs 1 and 2) agree well with the corresponding curve for the plane turbulent wall jet under zero pressure gradient on a smooth wall, referred to as the classical wall jet (CWJ). For the high  $k_s/D$  value cases, it is clearly seen from the figure that the boundary layer is much thicker than that of CWJ. All the profile



data are shown together in a consolidated form in Fig. 2-8 wherein the experimental results form a similarity ribbon, at least in the free mixing region.

Let us now consider separately the boundary layer and free-mixing regions. The data for the boundary region are non-dimensionalized by using the maximum velocity and the boundary thickness as scales and are plotted in Fig. 2-9(a-d). In Fig. 2-9, it is found that except the first section at  $x = 8D$ , at all other sections, the profiles are similar in each run, and that the similarity profile for each run can be described by a power law of the form

$$\frac{u_m}{u_{m0}} = \left(\frac{y}{\delta}\right)^{(1/n)} \quad (2-4)$$

with  $n$  varying from about 19 to 3.

All the boundary layer data are plotted together in Fig. 2-10(a). In Fig. 2-10(a), the data show a wide band indicating the effect of boundary roughness. The velocity data are also plotted in semi-log form in Fig. 2-10(b) in which  $u_* = \sqrt{\tau_{0m}/\rho}$ , and the results are approximately described by the Karman-Prandtl type semi-logarithmic equation with the respective characteristic constants of 5.75 and 8.5.

Fig. 2-11(a-d) show the data in the free mixing region for each run, and all the data in this region are plotted together in Fig. 2-12. It is seen from Figs. 2-11 and 2-12 that in the free mixing region the velocity profiles are similar and they can be represented well by the straight line passing the two points (1, 0.05) and (0.5, 1). The exponential curves represented by the equation

$$\frac{u_m}{u_{m0}} = \exp[-0.693\left(\frac{y-\delta}{b_y-\delta}\right)^2] \quad (2-5)$$

are also plotted in Figs 2-11 and 2-12 and they are seen to be close to the data.

#### 2.4.2 Velocity distribution in $y = \delta$ plane

The  $u(z)$  profiles in  $y = \delta$  plane are found to be similar and the non-dimensional velocity profiles are plotted in Fig. 2-13(a-d) for each run and together in Fig. 2-14 for all runs. The data seem to scatter somewhat when the values of  $z/b_z$  are greater than about 1.5. Although the data are around the exponential curves represented by

$$\frac{u}{u_{m0}} = \exp[-0.693 \left(\frac{z}{b_z}\right)^2] \quad (2-6)$$

they are better described by the straight line passing the two points (1, 0.05) and (0.5, 1).

#### 2.4.3 Velocity distribution in non-central vertical plane

All the velocity data in the non-central planes measured at  $x = 16D$  from the nozzle are plotted in non-dimensional form in Fig. 2-15(a-c). In the figure the prime denotes the scales in non-central plane and the curves in Fig. 2-15(c) are the same as the curves in Fig. 2-9. Just as in the central vertical plane, the data show very good similarity in the free mixing region and are well described by the same straight line. The curve in Fig. 2-15(b), which is close to the data, is represented by

$$\frac{u}{u'_m} = \exp[-0.693 \left(\frac{y-\delta'}{b'_y-\delta'}\right)^2] \quad (2-7)$$

The data in the boundary layer region are seen to fall around the power law curves for the central vertical plane.

#### 2.4.4 Boundary shear stress variation along center-line

To see the variation of the boundary shear stress along center-line, let us define the skin friction coefficient  $C_f$  as

$$C_f = \frac{\tau_{0m}}{\frac{1}{2}\rho u_{m0}^2} \quad (2-8)$$

The variation of  $C_f$  with  $x/D$  is shown in Fig. 2-16, and it was found that for  $x/D$  greater than about 10-15,  $C_f$  becomes approximately constant for each of the four experiments. The variation of this constant value of  $C_f$  with the relative roughness  $k_s/D$  is shown in Fig. 2-17, and it was found that this variation can be described approximately by the equation

$$C_f \pm 0.0049 = 0.0116 \pm 0.0030 + 0.0212 \pm 0.0027 \frac{k_s}{D} \quad (2-9)$$

with the correlation coefficient  $R$  equal to 0.976. The subscripts in equation 2-9 are the standard errors. In Fig. 2-17, we find that for a rough boundary with  $k_s/D = 2.0$ ,  $C_f$  is about nine times that of the corresponding smooth boundary value.

#### 2.4.5 Roughness effect on length and velocity scales

Considering the relative boundary layer thickness  $\delta/D$ , its variation with  $x/D$  is shown in Fig. 2-18 and was found to be essentially linear. The variation of the growth rate of  $\delta$  with  $k_s/D$  is shown in Fig. 2-19 wherein this variation is described by the linear equation

$$\frac{d\delta}{dx} \pm 0.0008 = 0.093 \pm 0.0004 + 0.008 \pm 0.0004 \frac{k_s}{D} \quad (R=0.994) \quad (2-10)$$

Contrary to the trend in the longitudinal direction, the boundary layer thickness was found to decrease linearly in the transverse direction, and this can be seen from the  $\delta'/\delta$  data measured at section  $x/D=16$  plotted against  $z/D$  in Fig. 2-20. This decreasing rate as a function of  $k_s/D$  is shown in Fig. 2-21 and was found to be well described by the quadratic equation

$$\frac{d(\delta'/\delta)}{d(z/D)} \pm 0.006 = -0.332 \pm 0.006 + 0.188 \pm 0.016 \frac{k_s}{D} - 0.047 \pm 0.007 \left(\frac{k_s}{D}\right)^2 \quad (R=0.999) \quad (2-11)$$

Regarding the relative length scale  $b_y/D$  its variation with  $x/D$  was also found to be linear as shown in Fig. 2-22. It was found that the rate of increase of  $b_y/D$  with  $x/D$  increased approximately linearly with the relative roughness  $k_s/D$  as shown in Fig. 2-23 and that this rate of increase is described by the equation

$$\frac{db_y}{dx} \pm 0.0053 = 0.0504 \pm 0.0028 + 0.02 \pm 0.0026 \frac{k_s}{D} \quad (R=0.946) \quad (2-12)$$

For the lateral expansion of the wall jet, Fig. 2-24 indicates that the roughness of the boundary does not affect the growth of  $b_z/D$ . Observations on the variation of  $U_0/u_{m0}$  with  $x/D$  show that  $u_{m0} \propto (1/x)$  (see Fig. 2-25). Further the coefficient  $C$  in the velocity scale equation

$$\frac{u_{m0}}{U_0} = \frac{C}{\left(\frac{x}{D} - 3.6\right)} \quad (2-13)$$

decreases linearly with  $k_s/D$  as shown in Fig. 2-26. In Fig. 2-26, we see that  $C$  decreases from the smooth boundary value of 6.25 to about 4.2 for  $k_s/D = 2.16$ . the variation of  $C$  with  $k_s/D$  is described roughly by the equation

$$C \pm 0.502 = 5.60 \pm 0.307 - 0.741 \pm 0.281 \frac{k_s}{D} \quad (R=0.836) \quad (2-14)$$

## 2.5 Conclusions

Based on the experimental observations of circular wall jets growing on rough boundaries with the relative roughness  $k_s/D$  equal to 0.16, 0.32, 1.08 and 2.16, the following conclusions can be formulated.

(1) The longitudinal velocity profiles are approximately similar. This similarity characteristic is improved if the profiles are considered separately in the boundary layer and in the free mixing regions.

(2) The length scales of the whole wall jet as well as the boundary layer thickness grow linearly with the distance  $x$  from the nozzle but the growth rates increase linearly with the relative roughness. The boundary layer thickness decreases linearly in the transverse direction, and the decreasing rate is a quadratic function of the relative roughness.

(3) The velocity scale was found to vary inversely with  $x$ , with the characteristic coefficient decreasing with the relative roughness.

(4) The boundary shear stress in the central plane was found to vary inversely with  $x^2$  and the characteristic skin friction coefficient indicated a rapid linear increase with the relative roughness.

## **2.6 References**

1. Hollingshead, A. B. and Rajaratnam, N., A Calibration chart for the Preston tube, *J. Hyd. Res, IAHR*, 1980, Vol. 18, pp. 313-326.
2. Launder, B. E. and Rodi, W., The turbulent wall jet - measurements and modeling, *Ann. Rev. of fluid Mech.*, Vol. 15, 1983, pp. 429-459.
3. Newman, B. G., Patel, R. P., Savage, S. B. and Tjio, H. K., Three dimensional wall jet originating from a circular orifice, *Aero. Quarterly*, Vol. 23, 1972, pp. 188-200.
4. Pani, B. S., Three dimensional turbulent wall jets, Ph.D. thesis, Univ. of Alberta, 1972.
6. Rajaratnam, N. and Pani, B. S., Three dimensional turbulent wall jets, *Proc. ASCE, J. Hyd. Engrg.*, Vol. 100, 1974, pp. 69-83.
7. Rajaratnam, N., *Turbulent Jets*, Elsevier Publishing Co., Amsterdam, 1976, 304 p.

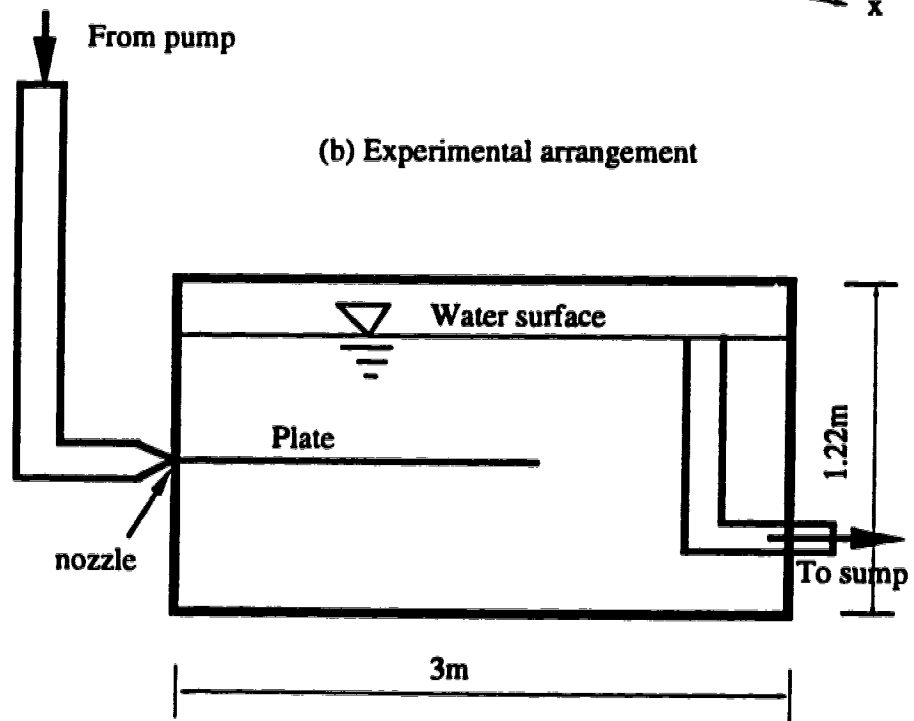
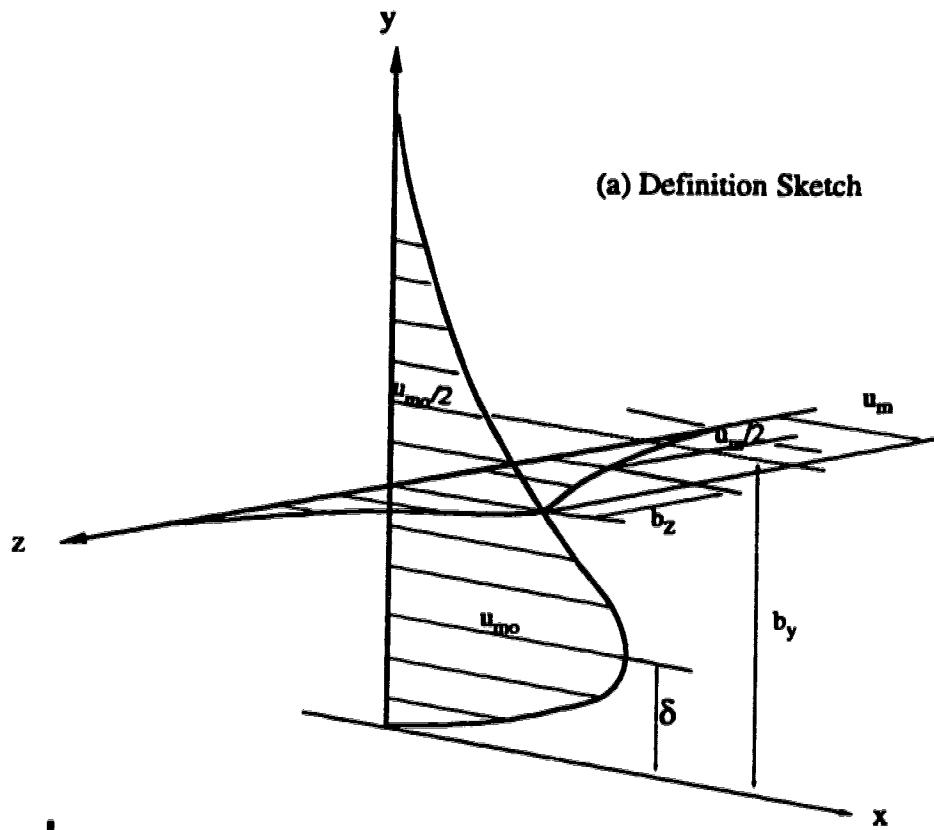
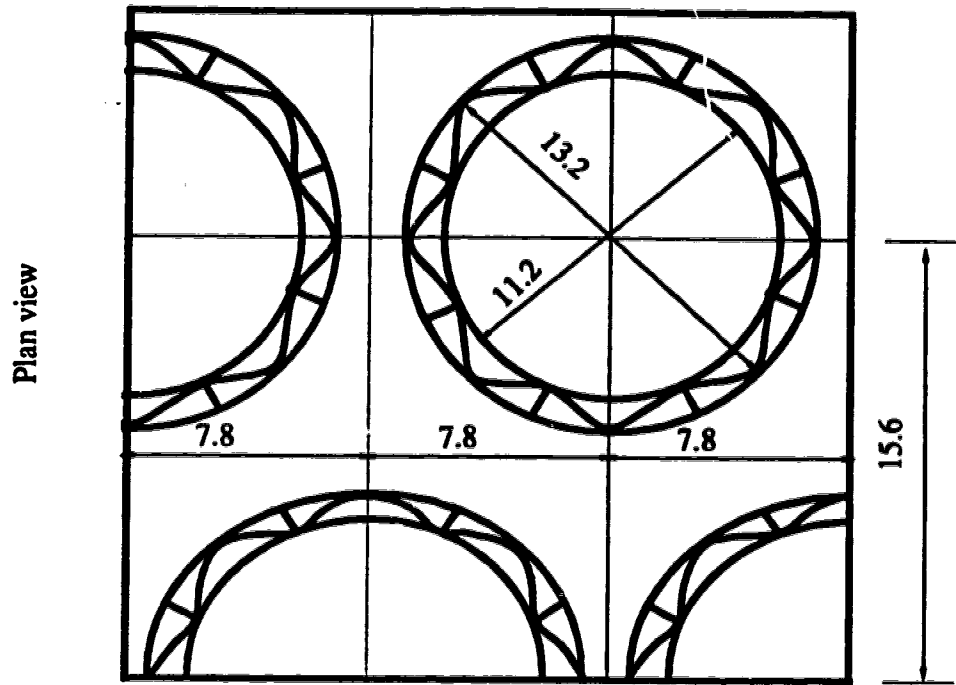
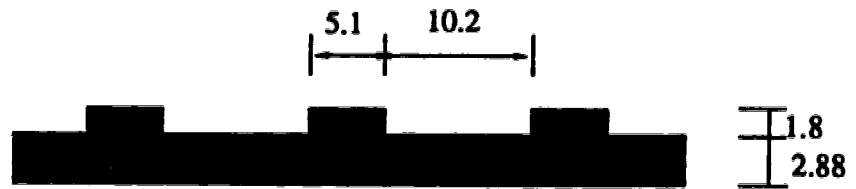


Fig. 2-1 Definition sketch and experimental arrangement



(a) Flower shaped roughness



(b) Strip roughness

Fig. 2-2 Details of the Roughnesses (Dimensions shown are in mm)

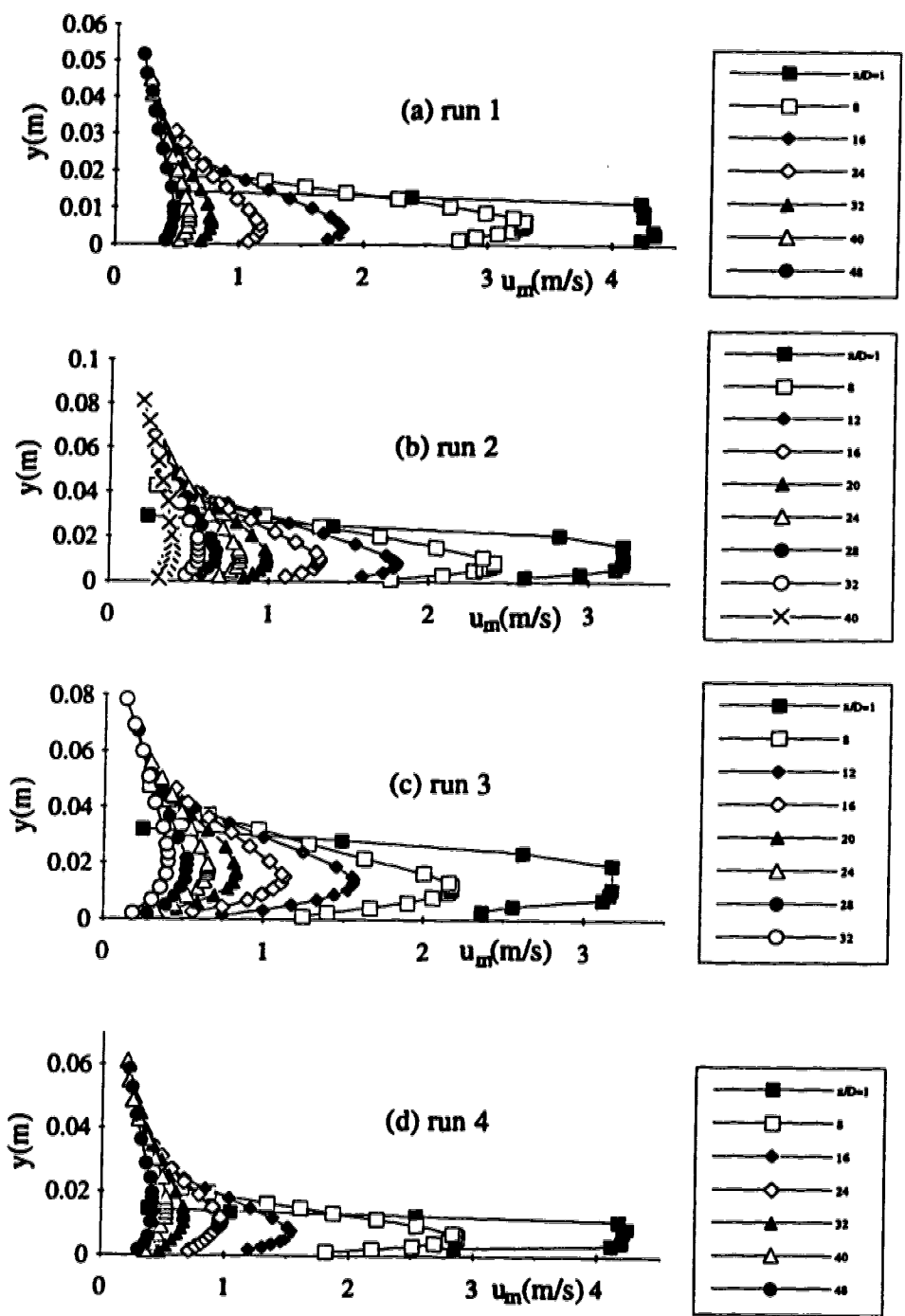


Fig. 2-3(a-d) Velocity profiles in the central vertical plane



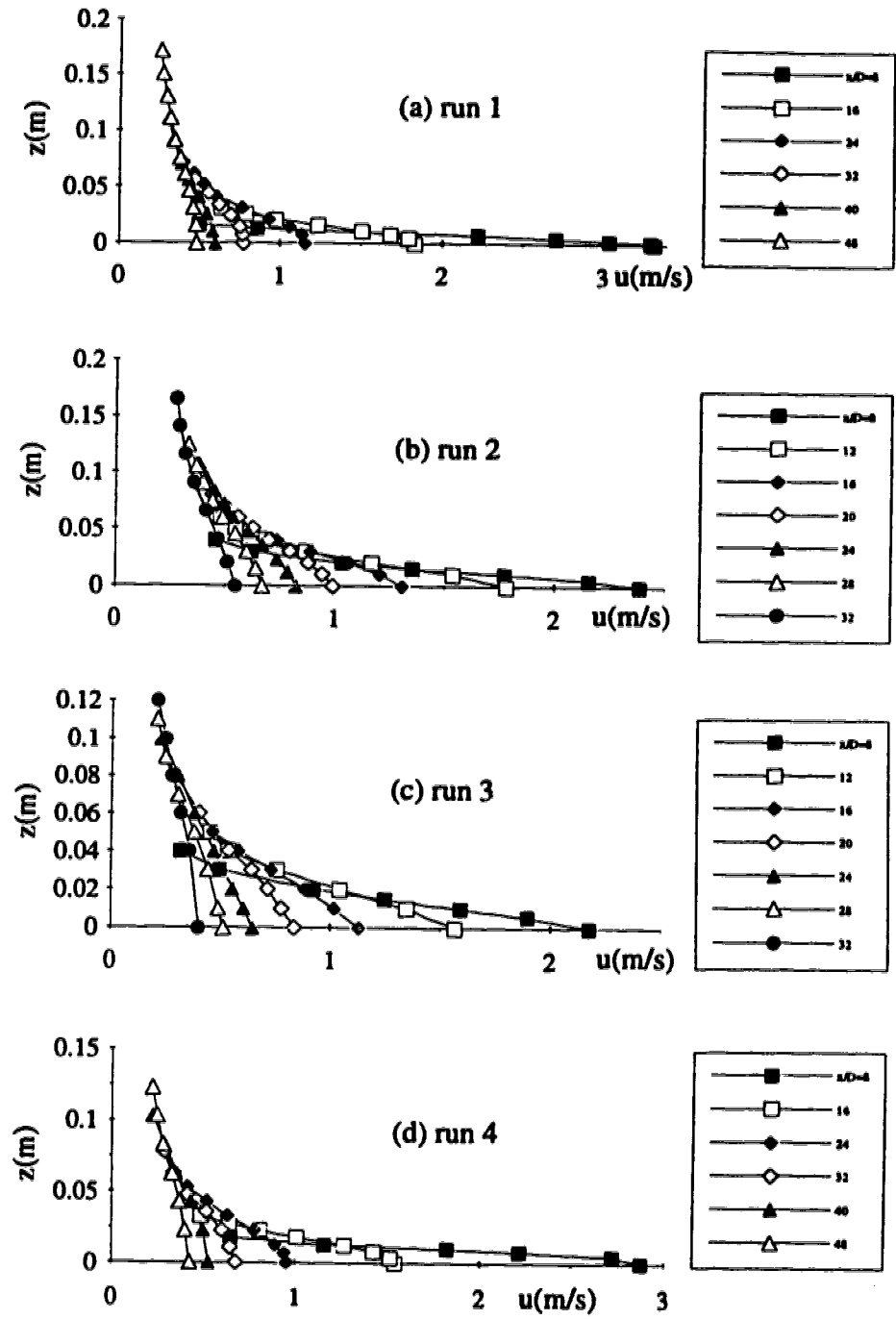


Fig. 2-4(a-d) Velocity profiles in  $y = \delta$  plane

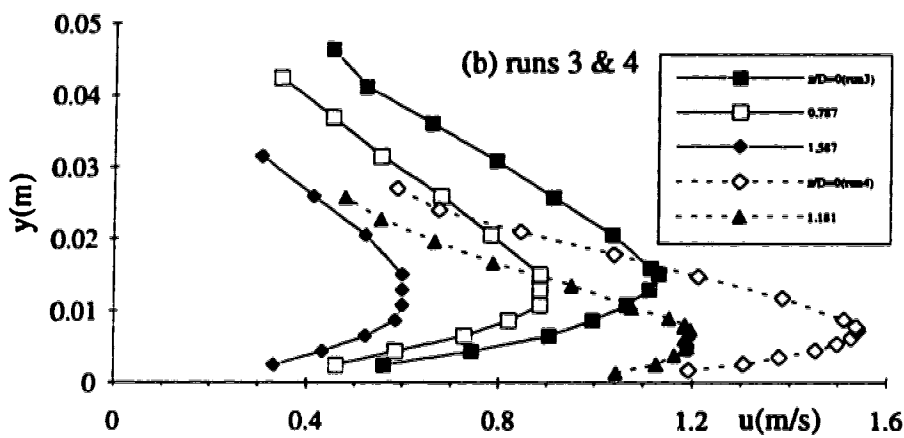
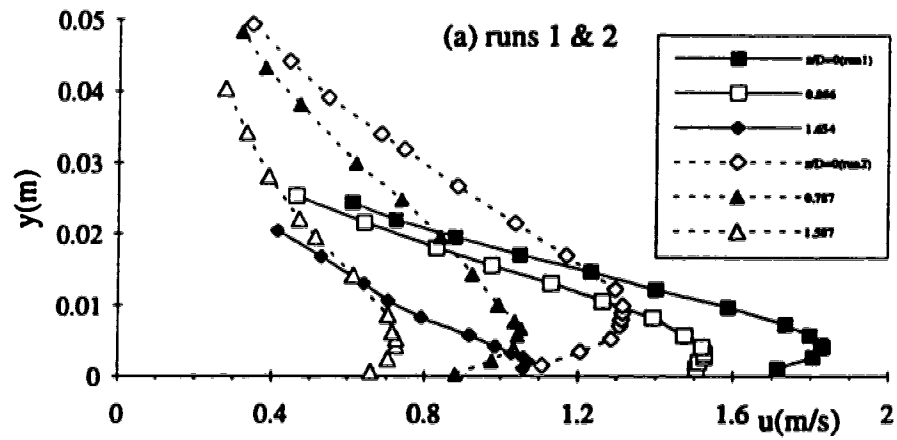


Fig. 2-5(a-b) Velocity profiles in  $x/D=16$  plane

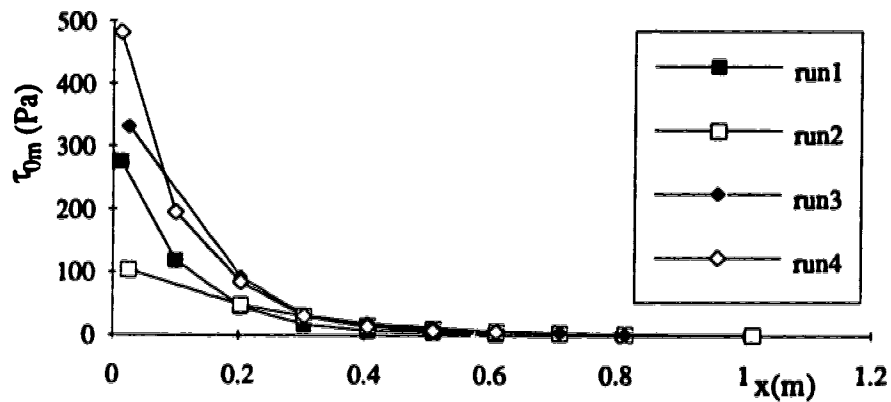


Fig. 2-6 Shear stress variation along the center line of the wall

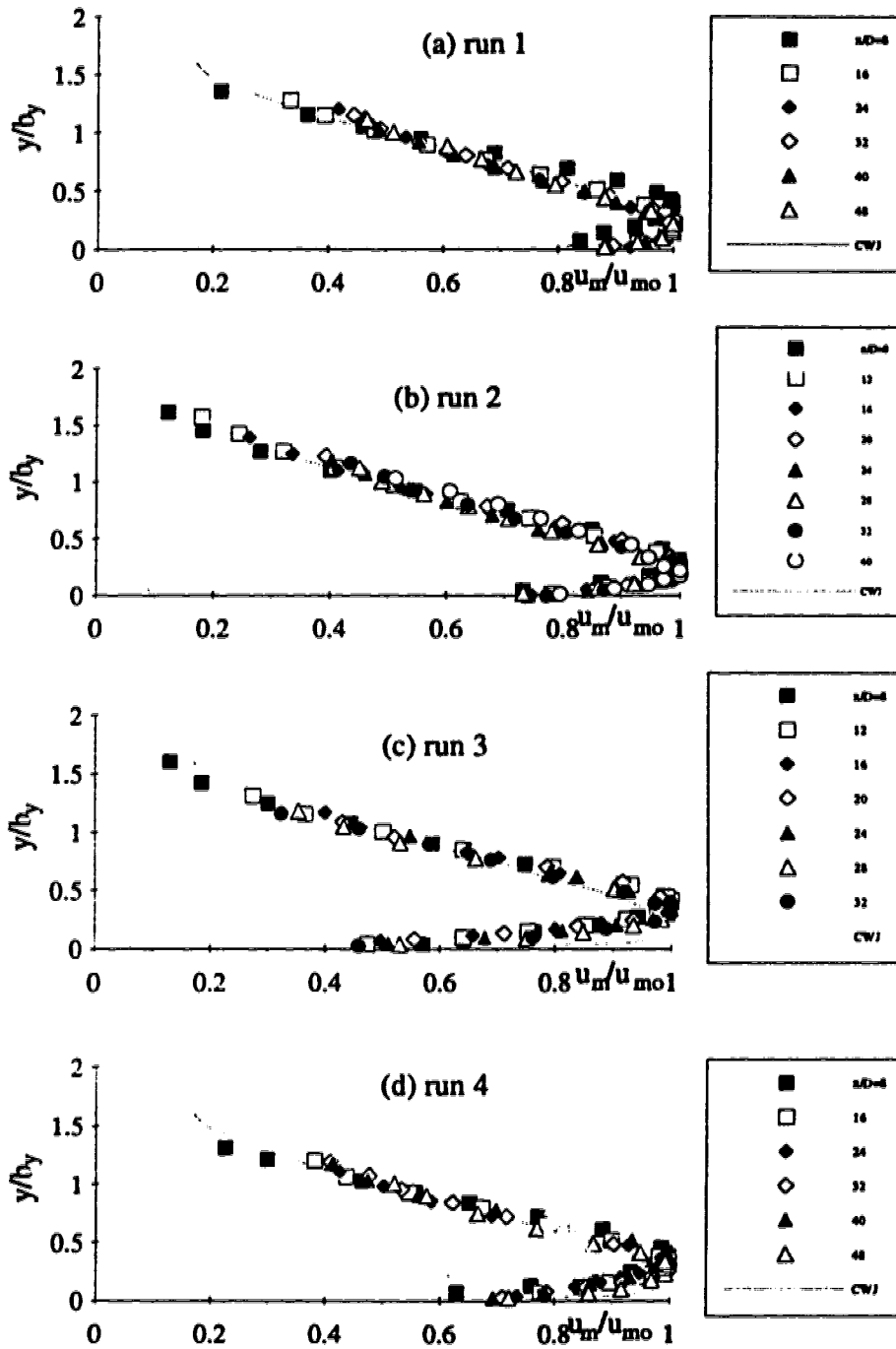


Fig. 2-7(a-d) Non-dimensional velocity profiles in the central vertical plane

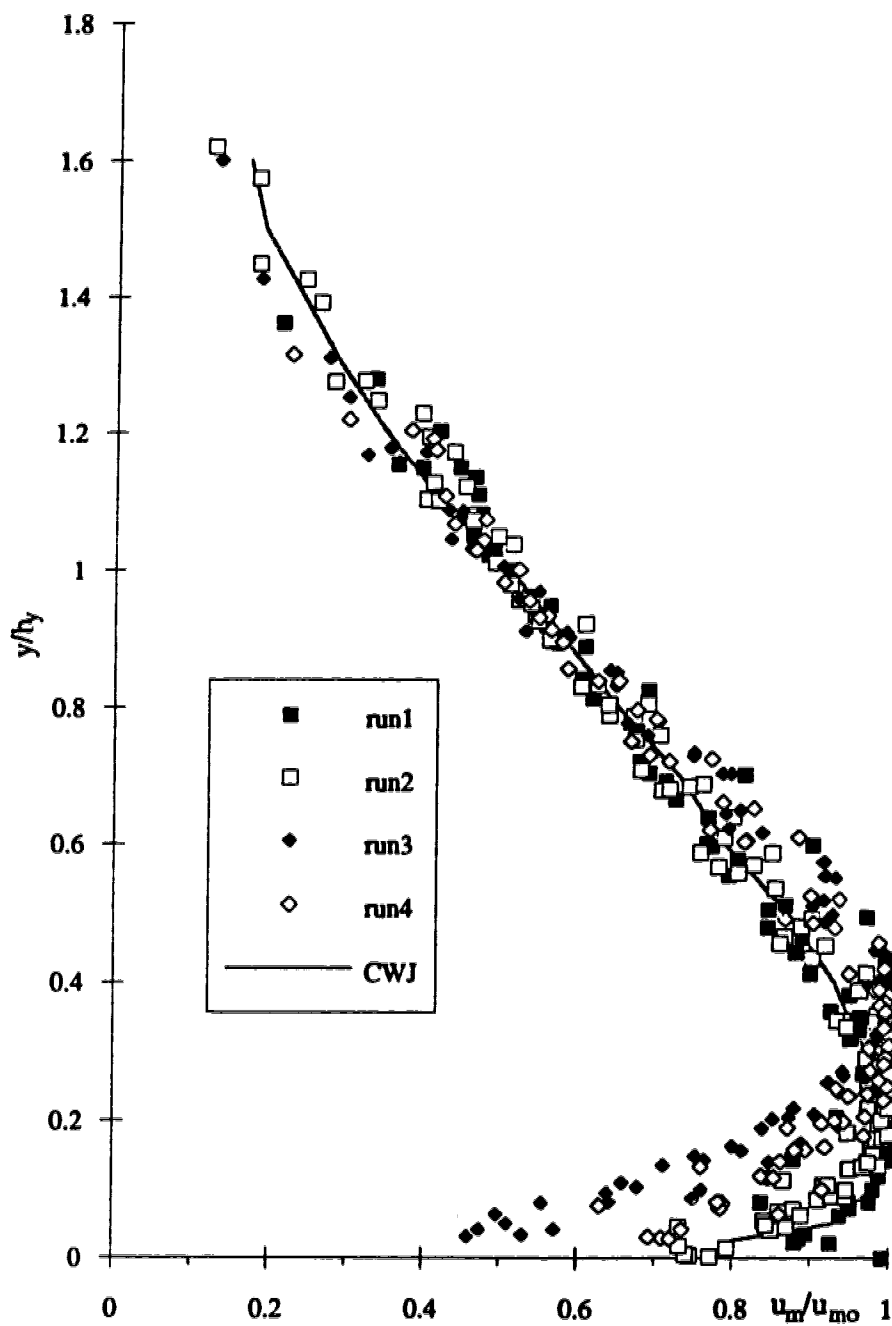


Fig. 2-8 Consolidated non-dimensional velocity profiles in the central vertical plane

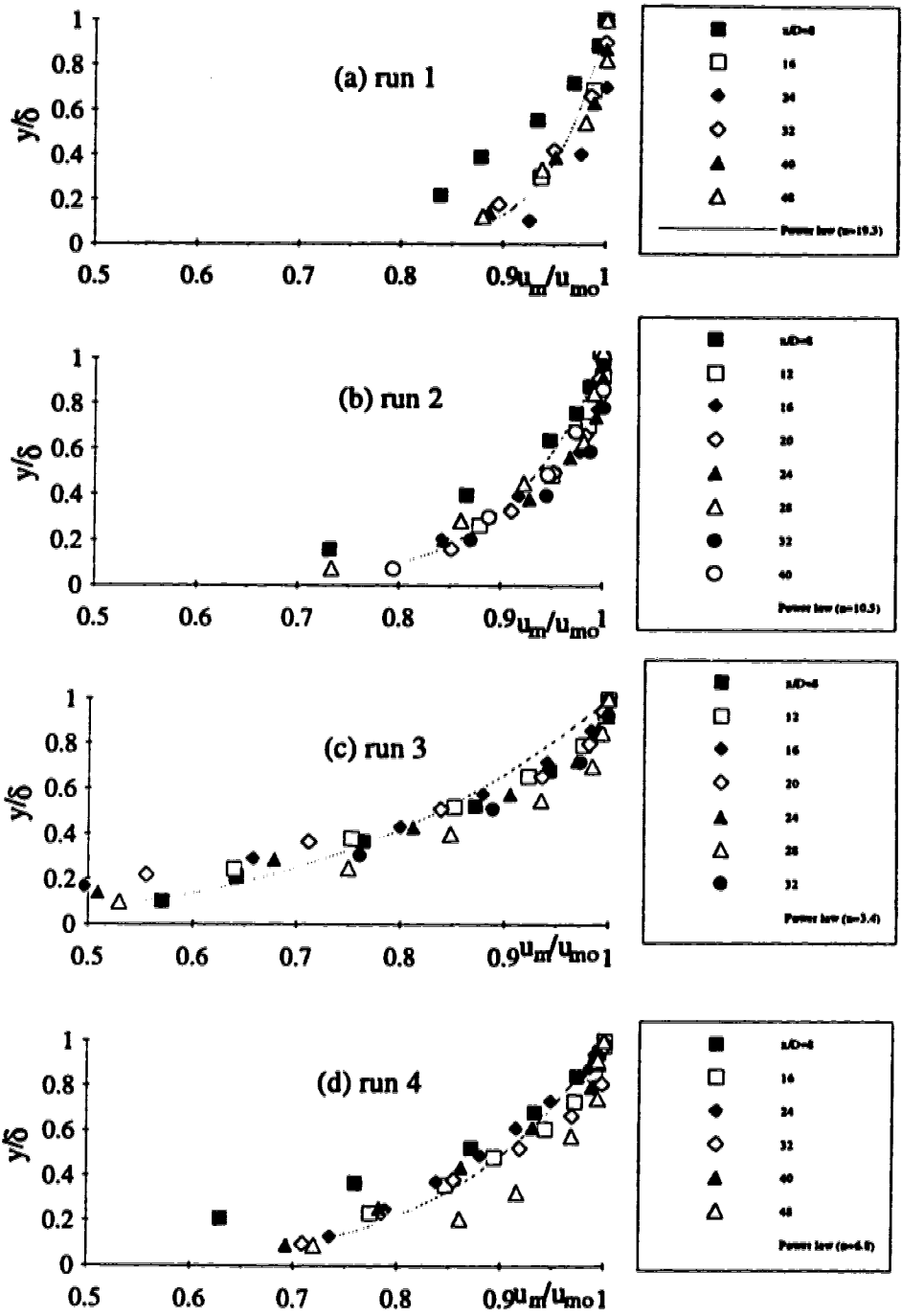


Fig. 2-9(a-d) Inner layer non-dimensional velocity profiles in the central vertical plane

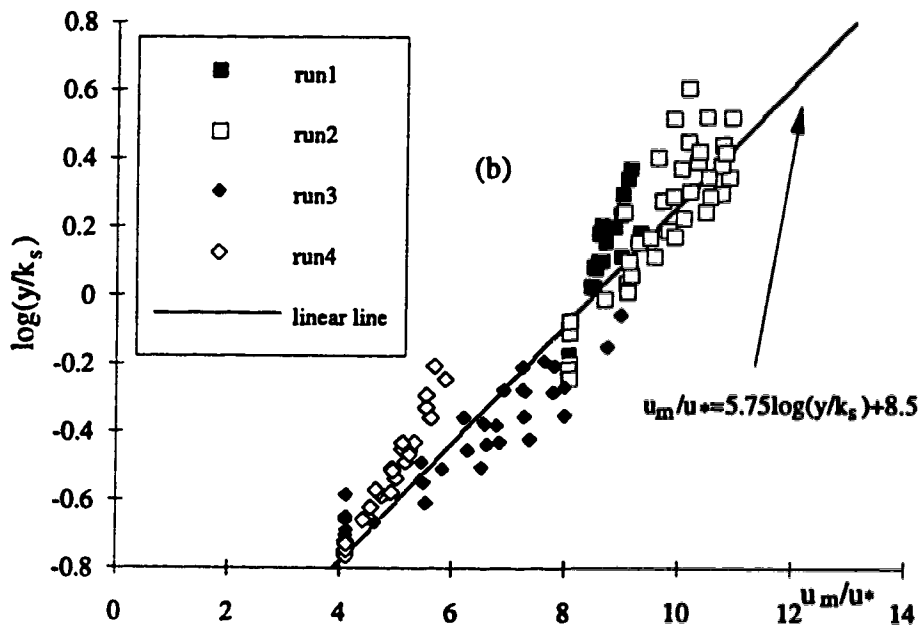
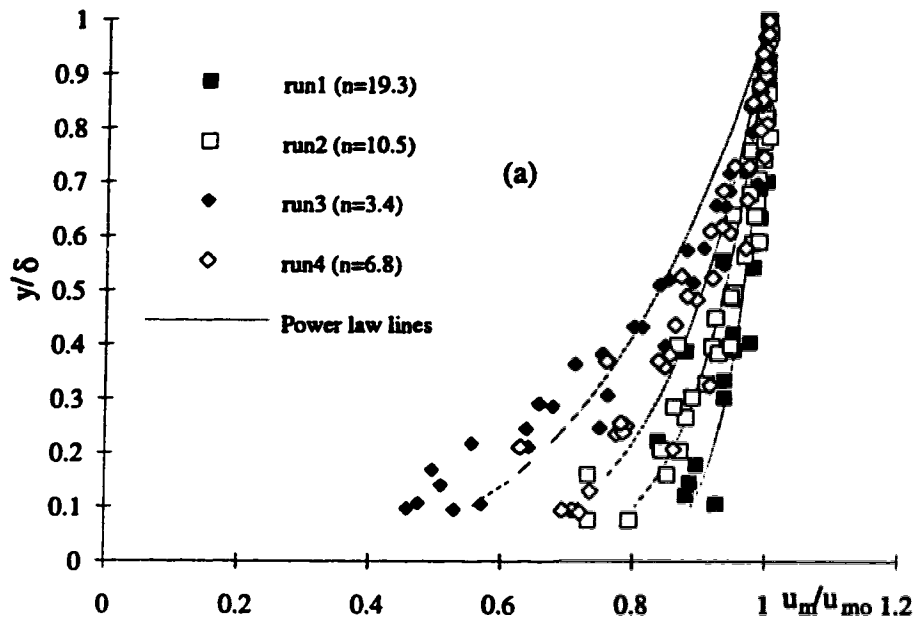


Fig. 2-10(a-b) Plots of inner layer velocity data in non-dimensional form

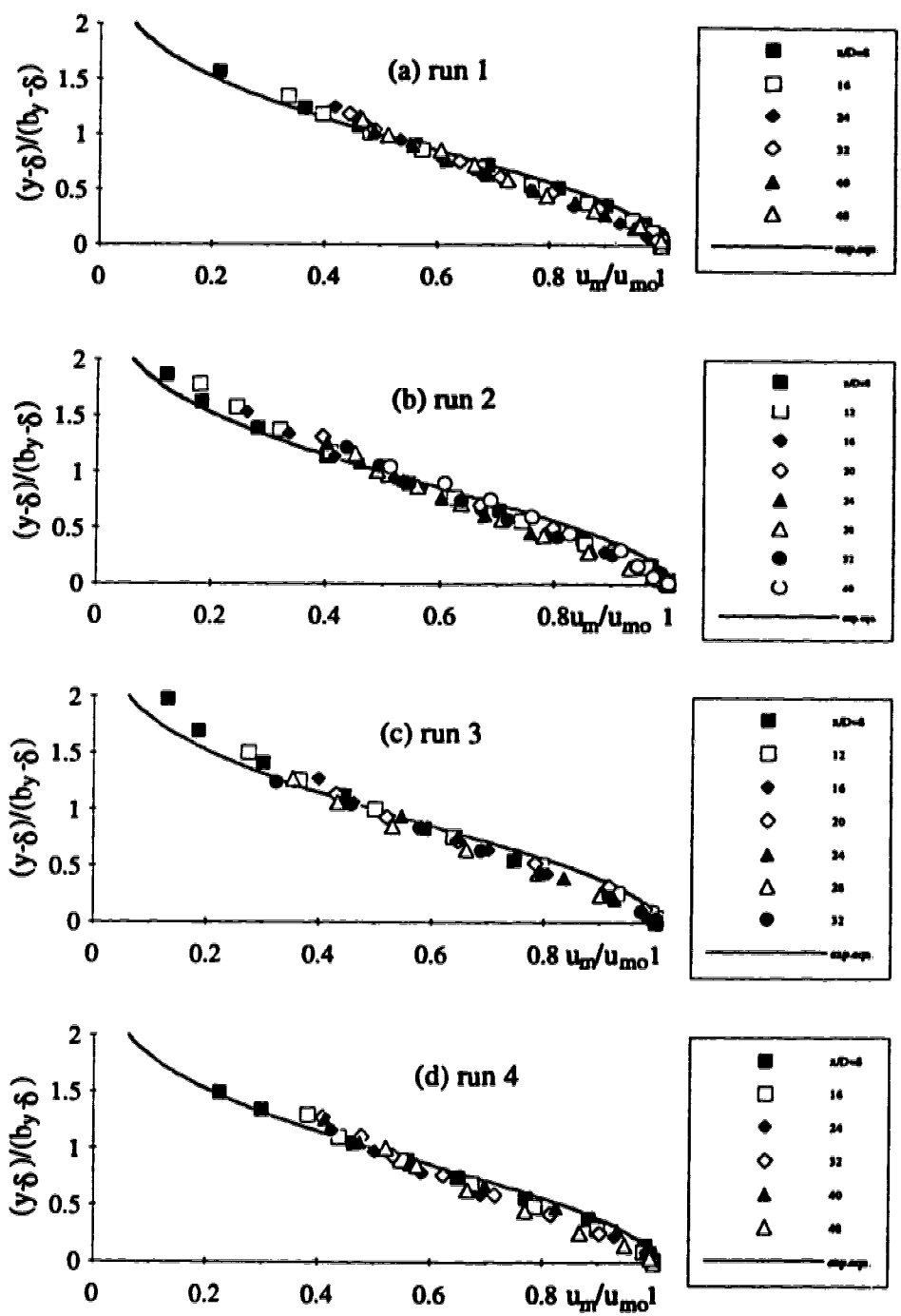


Fig. 2-11(a-d) Non-dimensional velocity profiles in the free mixing region

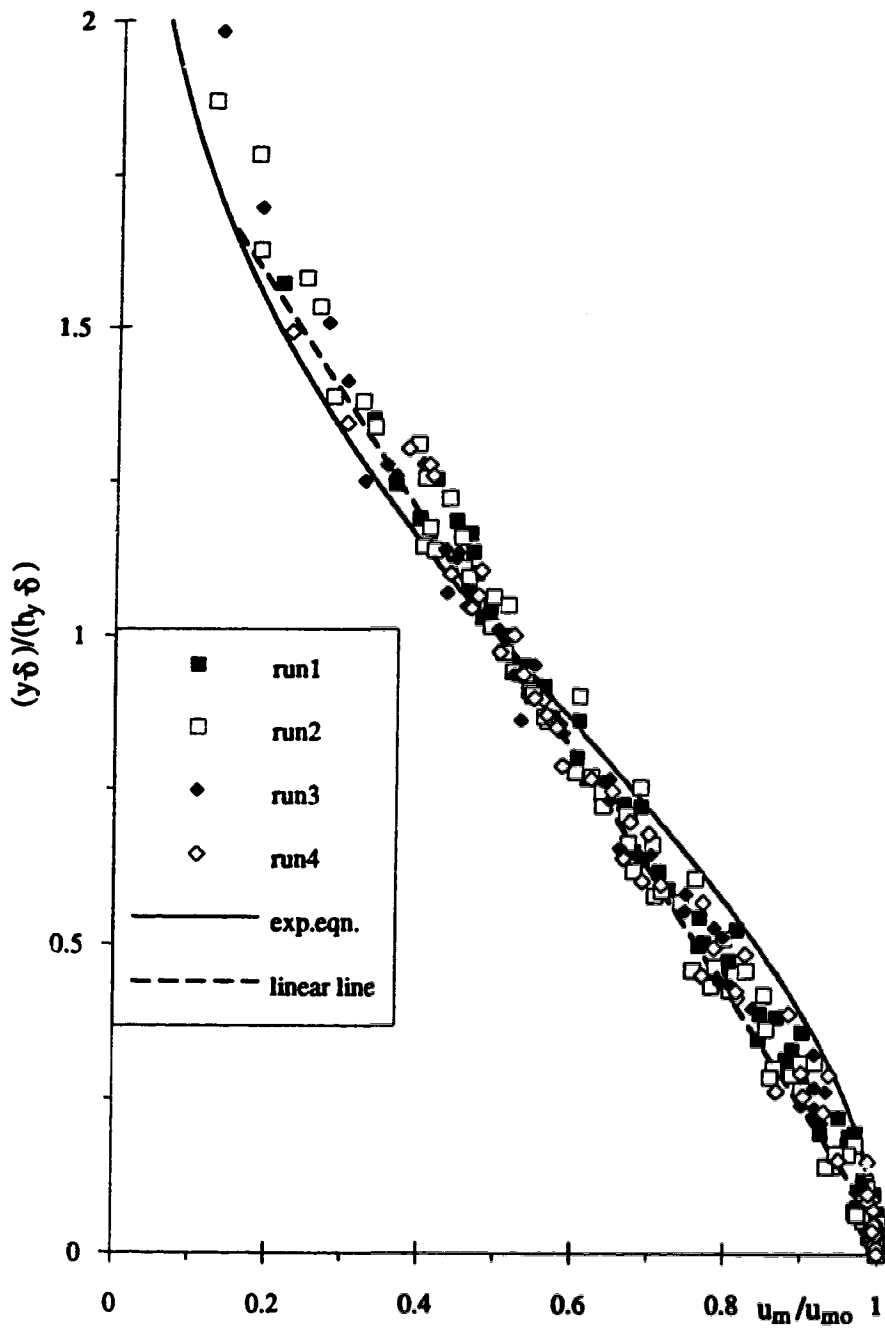


Fig. 2-12 Consolidated velocity profiles in the free mixing region of the central vertical plane



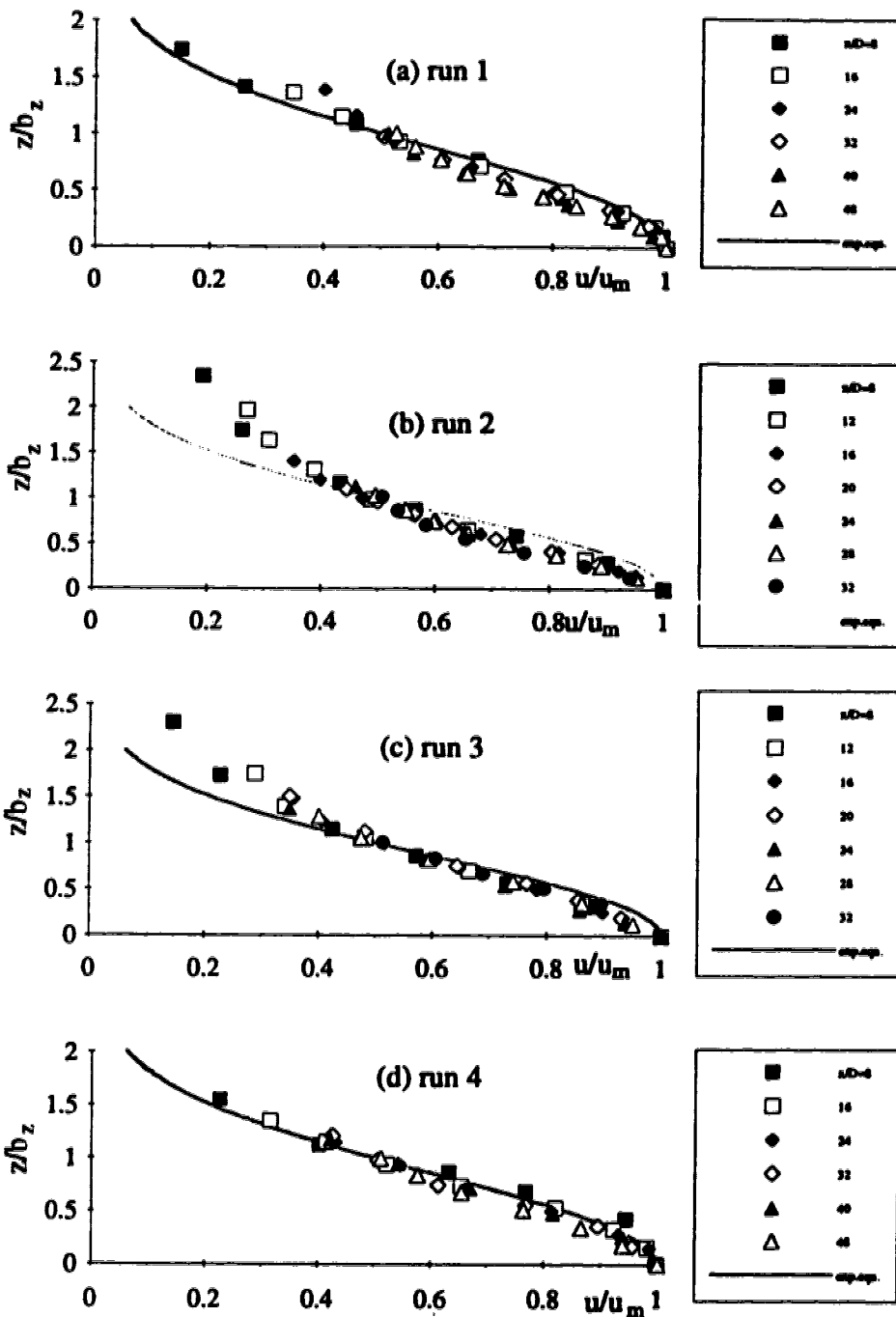


Fig. 2-13(a-d) Non-dimensional velocity profiles in  $y=\delta$  plane

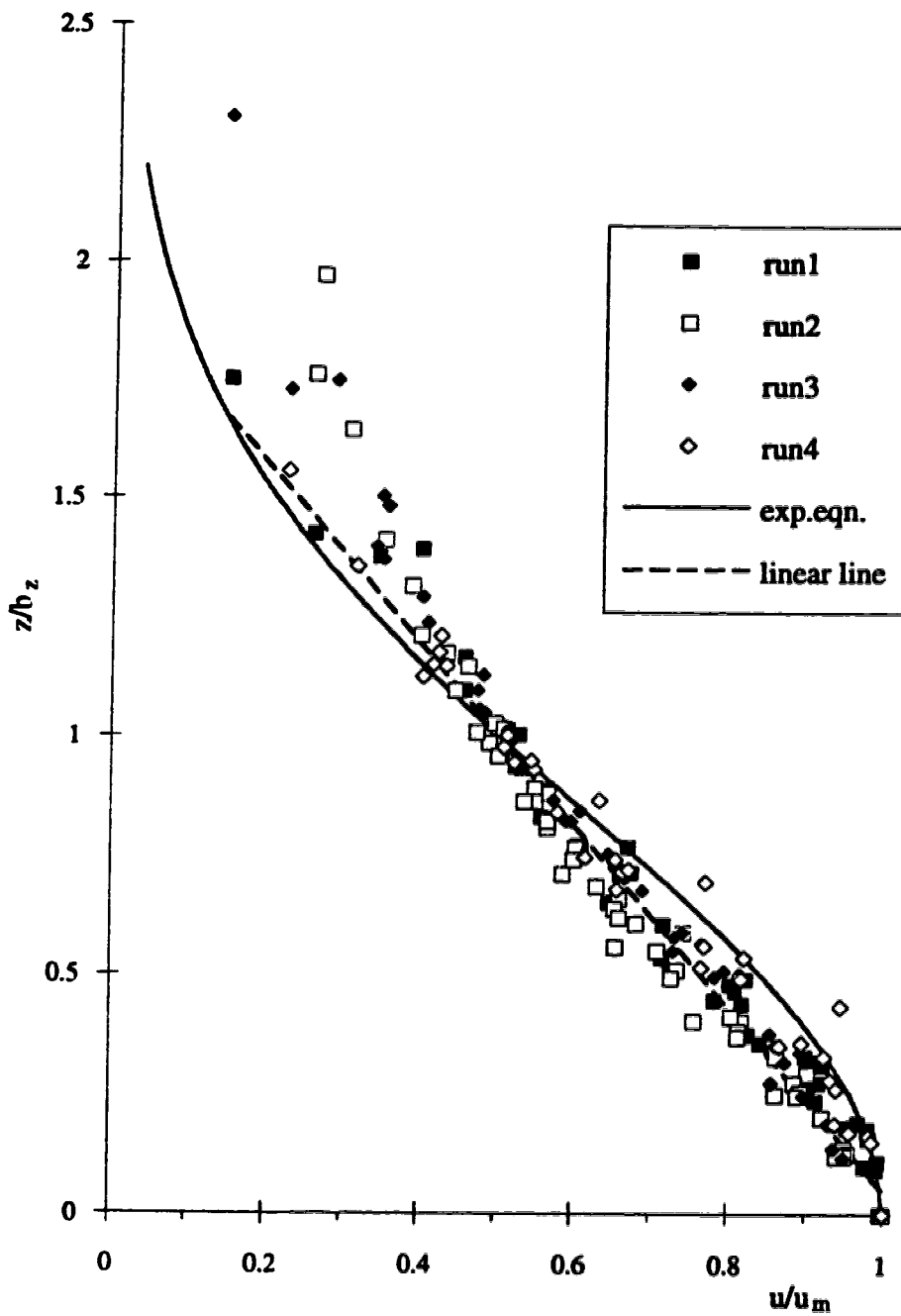


Fig. 2-14 Consolidated non-dimensional velocity profiles in  $y = \delta$  plane

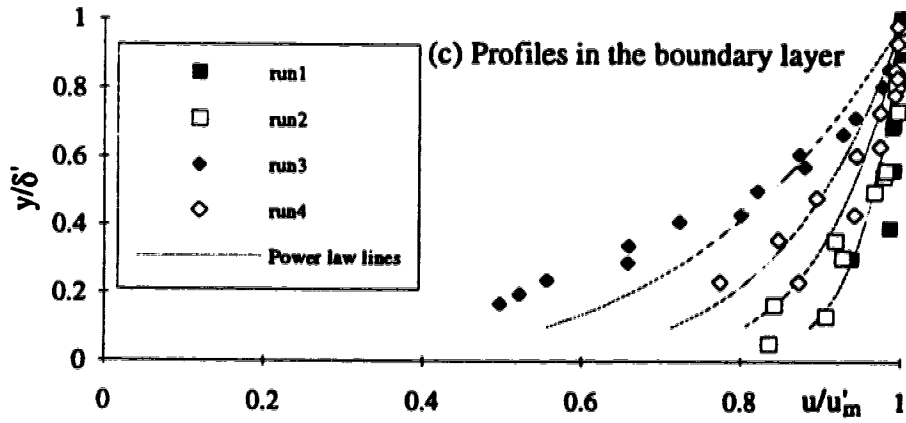
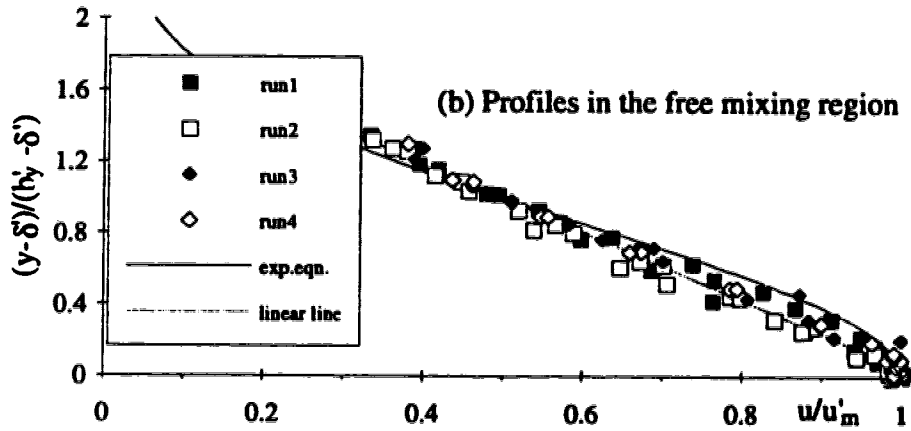
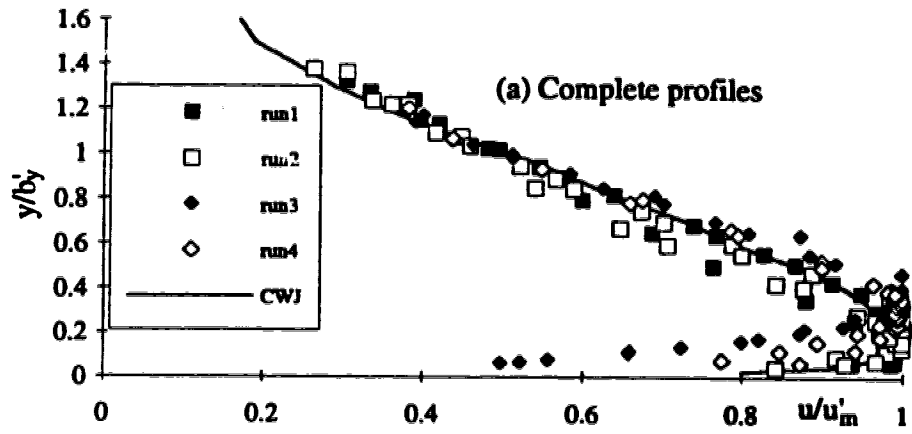


Fig. 15(a-c) Non-dimensional velocity profiles at section  $x/D=16$

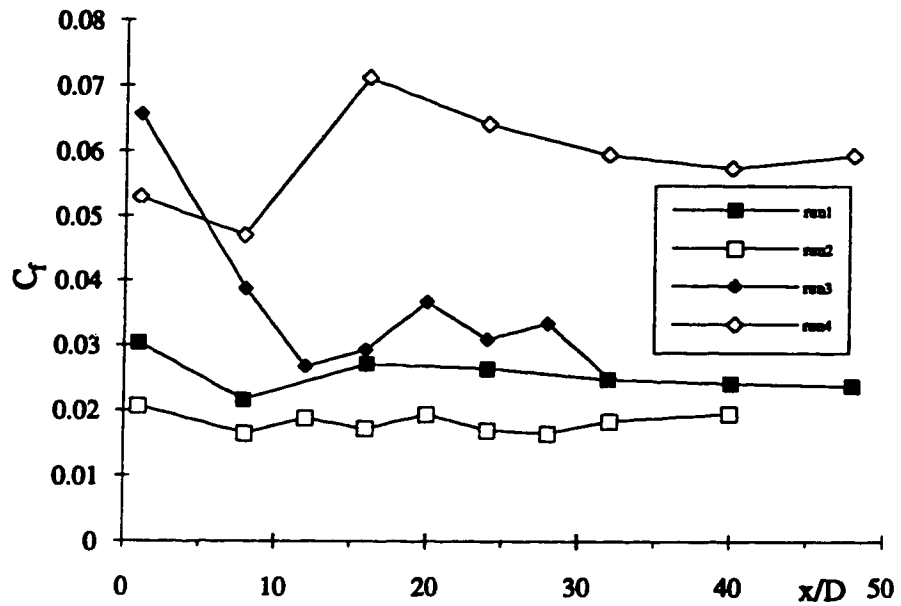


Fig. 2-16 Skin friction coefficient variation along the wall center line

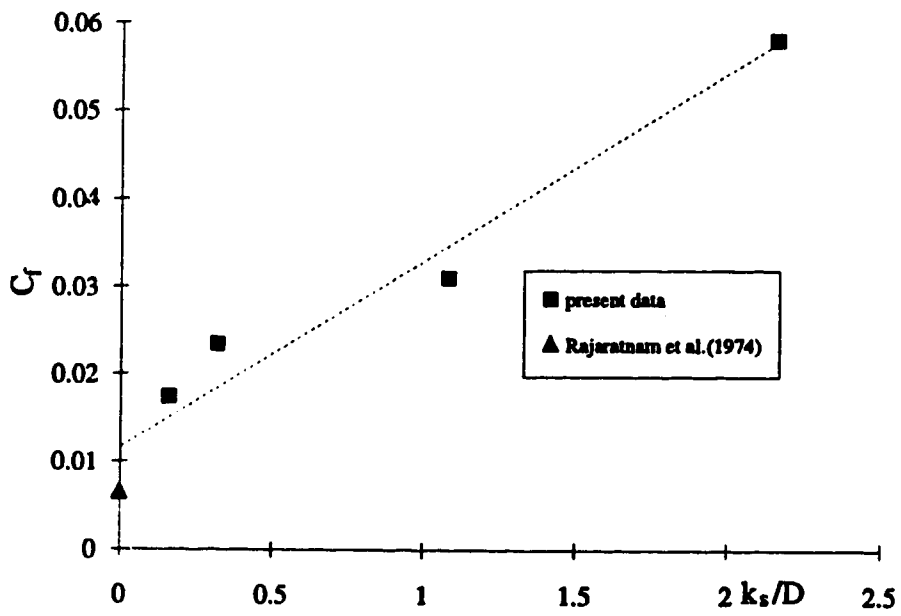


Fig. 2-17 Effect of roughness on skin friction coefficient

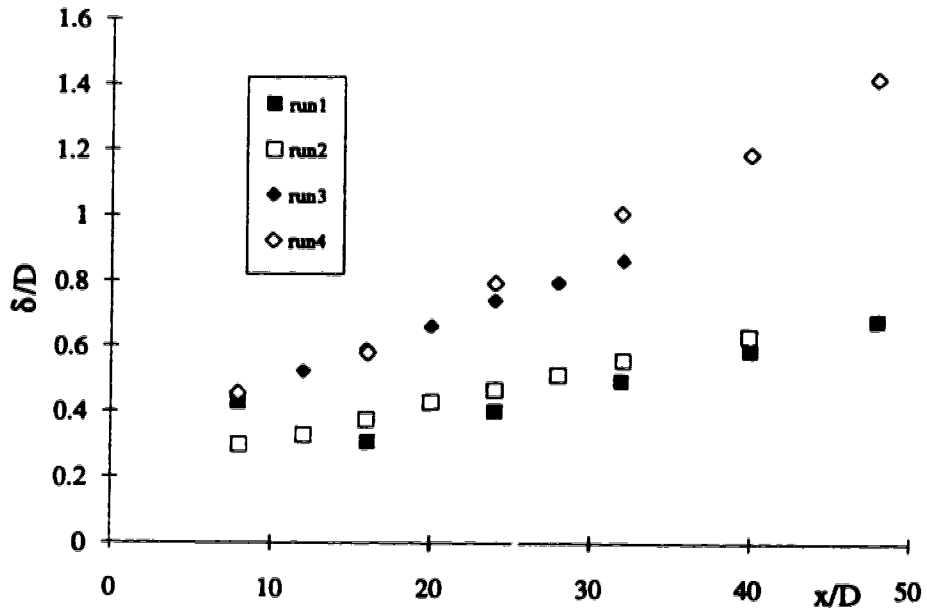


Fig. 2-18 Growth of boundary layer in the central vertical plane

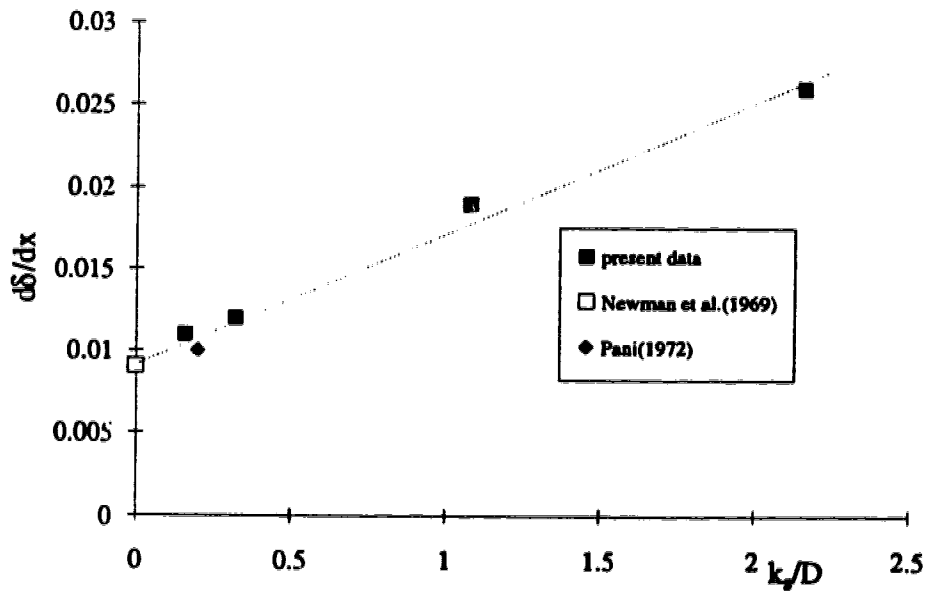


Fig. 2-19 Effect of roughness on boundary layer growth rate

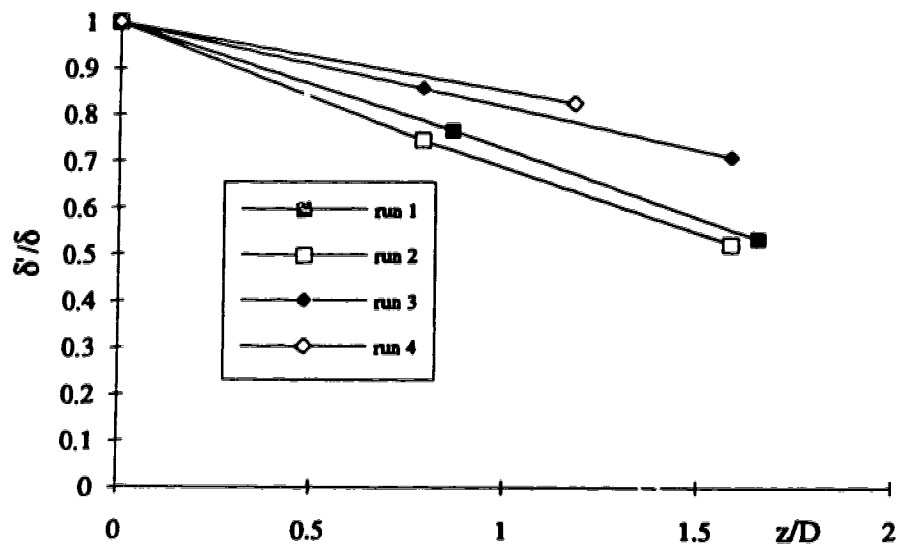


Fig. 2-20 Variation of boundary layer thickness in the transverse direction at section  $x/D=16$

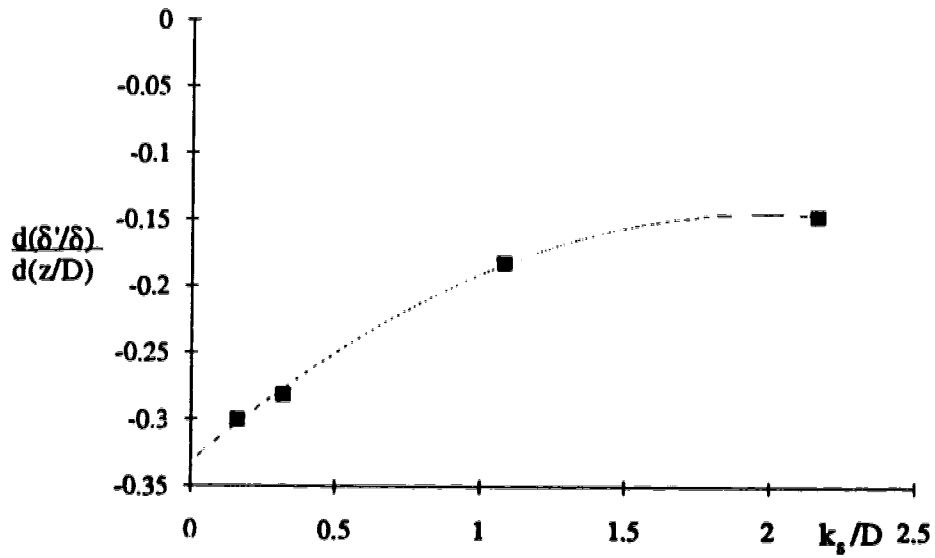


Fig. 2-21 Roughness effect on the decreasing rate of boundary layer thickness in transverse direction

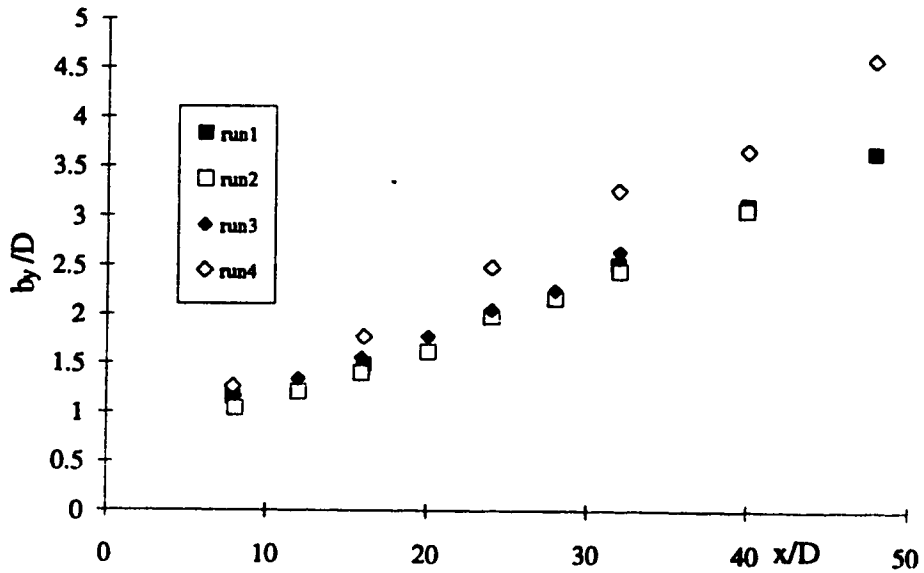


Fig. 2-22 Growth of the length scale by

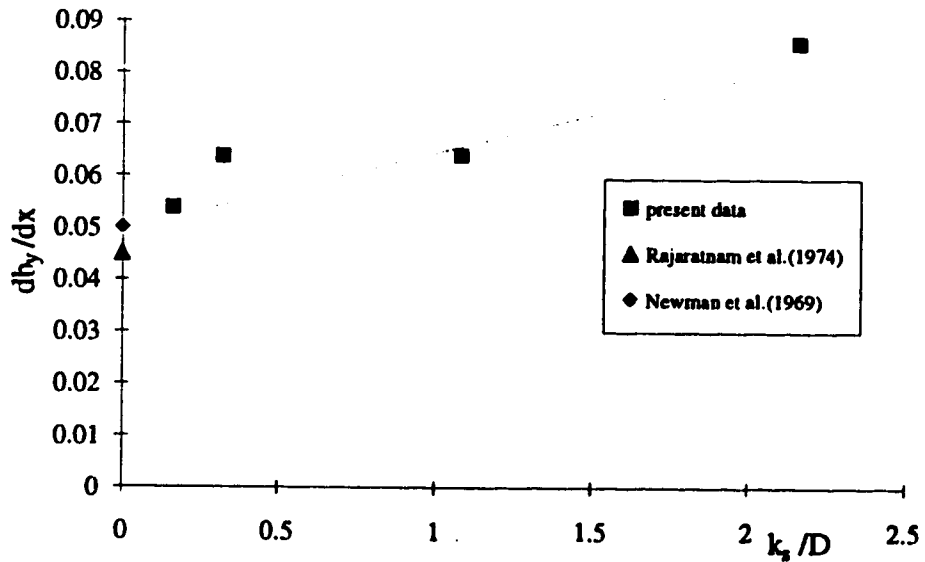


Fig. 2-23 Effect of roughness on the growth rate of length scale by

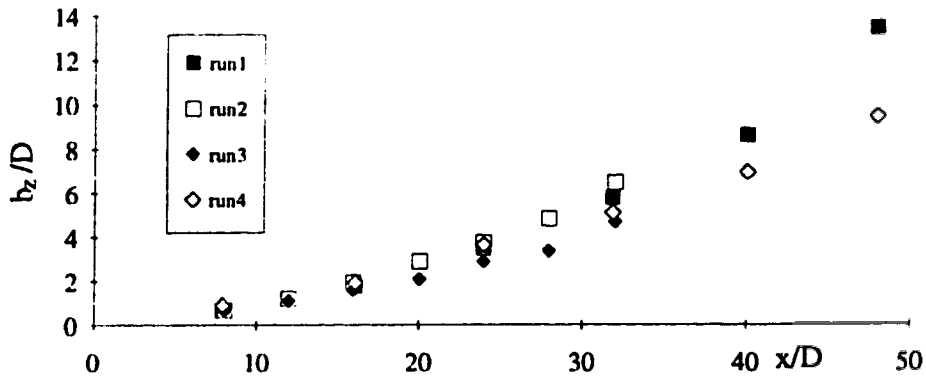


Fig. 2-24 Growth of the length scale  $b_z$

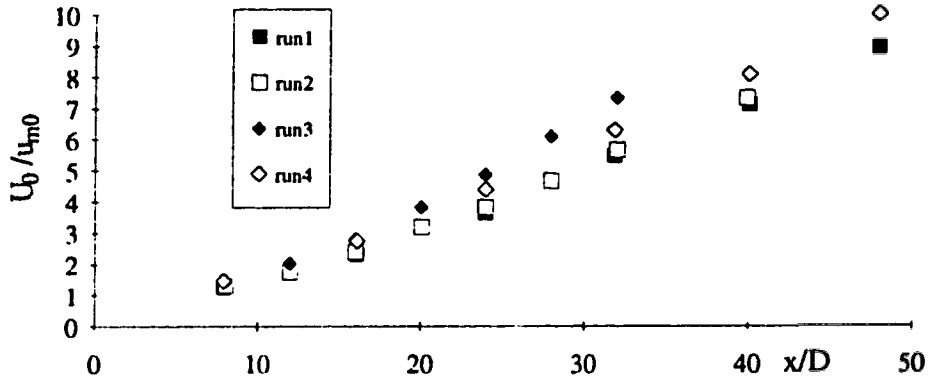


Fig. 2-25 Decay of the velocity scale  $u_m$

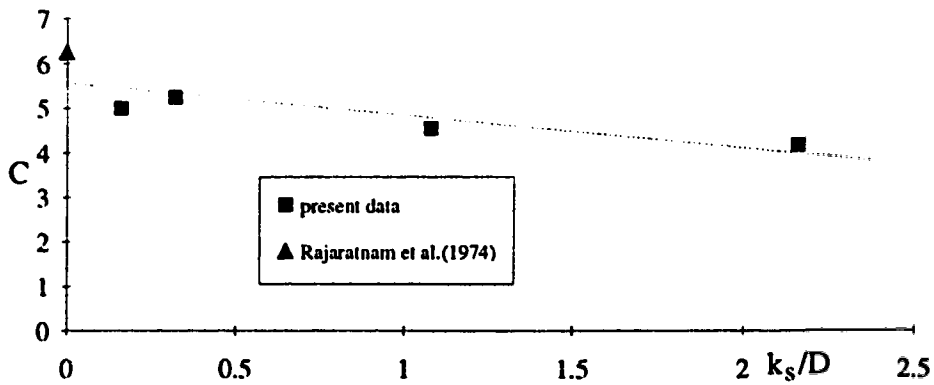


Fig. 2-26 Effect of roughness on the coefficient C



Table 2-2. Scale data for  $\delta$ ,  $b_y$ ,  $b_z$ ,  $u_{m0}$  and  $C_f$

run #	$x/D$	$\delta/D$	$b_y/D$	$U_0/u_{m0}$	$b_z/D$	$C_f$
1	1.00			1.00		0.0303
	7.92	0.43	1.16	1.29	0.72	0.0216
	16.08	0.31	1.50	2.33	1.78	0.0271
	24.00	0.40	1.99	3.66	3.46	0.0264
	31.92	0.50	2.52	5.49	5.76	0.0247
	40.08	0.59	3.12	7.13	8.64	0.0242
	48.00	0.68	3.66	8.96	13.44	0.0238
2	1.00			1.00		0.0207
	8.04	0.30	1.04	1.32	0.67	0.0165
	12.00	0.33	1.22	1.76	1.20	0.0188
	15.96	0.38	1.41	2.41	1.96	0.0171
	20.04	0.43	1.63	3.19	2.88	0.0194
	24.00	0.47	1.98	3.84	3.72	0.0169
	27.96	0.51	2.16	4.67	4.80	0.0165
	32.04	0.56	2.44	5.65	6.44	0.0184
39.96	0.64	3.07	7.32		0.0195	
3	1.00			1.00		0.0658
	8.04	0.46	1.17	1.46	0.68	0.0387
	12.00	0.52	1.34	2.03	1.13	0.0267
	15.96	0.59	1.56	2.81	1.60	0.0292
	20.04	0.66	1.78	3.82	2.10	0.0366
	24.00	0.74	2.04	4.86	2.88	0.0308
	27.96	0.80	2.24	6.08	3.36	0.0334
	32.04	0.86	2.64	7.34	4.68	0.0250
4	1.00			1.00		0.0529
	7.92	0.46	1.26	1.48	0.91	0.0470
	16.08	0.58	1.77	2.77	1.92	0.0711
	24.00	0.79	2.48	4.39	3.65	0.0641
	31.92	1.01	3.26	6.31	5.09	0.0594
	40.08	1.19	3.67	8.09	6.91	0.0574
	48.00	1.42	4.61	10.00	9.45	0.0594

Table 2-3. Scales in  $x/D=16$  plane

run #	$z/D$	$\delta'/\delta$	$b'_y/b_y$	$u'_m/u_m$
1	0.000	1.000	1.000	1.000
	0.866	0.767	1.000	0.835
	1.654	0.535	0.864	0.585
2	0.000	1.000	1.000	1.000
	0.787	0.746	0.991	0.800
	1.587	0.524	0.923	0.553
3	0.000	1.000	1.000	1.000
	0.787	0.858	0.938	0.783
	1.587	0.710	0.808	0.529
4	0.000	1.000	1.000	1.000
	1.181	0.826	0.950	0.777

Table 2-4. Coefficients and length scale growth rates

run #	$\frac{db_y}{dx}$	$\frac{d\delta}{dx}$	C	$C_f$	$\frac{d(\delta'/\delta)}{d(z/D)}$ (at $\frac{x}{D}=16$ )
1	0.064	0.012	5.26	0.0235	-0.281
2	0.054	0.011	5.00	0.0175	-0.300
3	0.064	0.019	4.55	0.0310	-0.183
4	0.086	0.026	4.17	0.0580	-0.147

## **Chapter 3 Intersecting Circular Jets of Unequal Momentum Flux \***

### **3.1 Introduction**

Intersecting turbulent jets can be used for many purposes. In industry, their application can be found in gas mixing chambers, combustion chambers and spray drying equipment. In hydraulic engineering, intersecting turbulent jets could be used as the design element in energy dissipators. Merging of two streams can be interpreted as a limiting case of intersecting jets.

There have been relatively few investigations on intersecting circular turbulent jets. From their early experiments on dual intersecting jets with intersecting angles  $\alpha$  (see Fig. 3-1 for a definition sketch) from 0 to 30 degrees Baron and Bollinger [1952] found that there exist significant static pressure gradients. Maxwell (1979) found that when two jets intersect, the direction of the resulting jet can be found by using elementary momentum consideration and neglecting entrainment. Maxwell and Snorrason (1981) made a preliminary experimental study of two intersecting air jets with approximately equal momentum fluxes, with an intersecting angle  $\alpha$  equal to 90 degrees. They explored the velocity field in the vicinity of the (geometrical) intersection point. When analyzing parallel jets, Knystautas (1964) found that the Reichardt hypothesis is very useful. In this hypothesis, it is assumed that the fluid viscosity is negligible and that the pressure field is constant. This enables the linearization of the equation of motion and allows the resultant flow to be obtained by adding

---

\* The main content of this chapter has been published in the Journal of Hydraulic Research, 1992, Vol. 30, No. 6.

the squares of the velocities of the individual jets For intersecting jets with  $\alpha$  greater than about 14 degrees, the observations of Baron and Bollinger (1952) and Maxwell and Snorrason (1981) both indicated that due to the violation of these assumptions, this procedure is not valid any more.

Witze (1974) performed a series of experiments with opposing circular (air) jets ( $\alpha = 180^\circ$ ) with the separation distance between the nozzles equal to 20, 30 and 40 times the diameter of the jet. He found that impingement produced a radial jet, which grew at about three times the rate of a radial jet produced from a nozzle. A similar rapid growth of a plane jet produced by impingement of two plane wall jets ( $\alpha = 180^\circ$ ) was observed by Kind and Suthanthiran (1973).

Rajaratnam and Khan (1992) studied intersecting circular turbulent jets of equal momentum flux for  $\alpha$  equal to 30, 60, 90 and 120 degrees. They divided the flow into two regions (see Fig. 3-1). Region 1 extended from nozzle to the intersection point (IP) and the region downstream of IP formed region 2. In region 1, using axial pressure measurements, they found that the flow was affected by the stagnation pressure for  $x_1/H$  greater than 0.5 for  $\alpha = 30^\circ$  where  $H$  is the distance between the nozzle to the IP and  $x_1$  is the axial distance from the nozzle. This value increased to 0.85 for normal impingement on a plate (Beltaos and Rajaratnam, 1974). If  $p_s$  is the pressure at the stagnation point,  $p_s[\frac{H}{D}]^2 / \rho U_0^2$  was a function of  $\alpha$  where  $\rho$  is the fluid density and  $U_0$  is the jet velocity at the nozzle of diameter  $D$ . The velocity profiles in the jet in the transverse ( $z_1$ ) and vertical ( $y$ ) directions were similar for  $x_1/H$  up to about 0.88.

In region 2, the pressure and velocity profiles along the axis of the jet were found to be approximately similar and expressions were found for the velocity, pressure and length scales. In the early part of region 2, the vertical growth of the jet was about three times its transverse growth. In the later part of region 2, these

two growth rates tend to become equal but were still greater than the growth rate of simple circular jets by about 50%. The velocity profiles in the vertical and transverse directions were found to be similar and this similarity curve was well described by the (familiar) exponential equation.

The results of an attempt to extend this investigation to intersecting jets of unequal momentum fluxes are presented in this chapter.

### 3.2 Experiments

A schematic diagram of the experimental set up is shown in Fig. 3-2. The jets were produced by two well designed nozzles with internal diameter ( $D$ ) of 12.7 mm. These nozzles were connected to the air supply (from the university air compressor through a pressure reducer) with tygon tubing with a separate control valve in each line. The nozzles were mounted on a work bench and the intersection angle  $\alpha$  between the jets could be adjusted to any desired value. For this study, the valves were adjusted to produce jets of desired velocity at each nozzle. The jet velocity at the nozzle was calculated by measuring the excess pressure in the approaching pipe, just before the nozzle, above that of the atmospheric pressure. It was observed that the nozzle pressure was very stable and there was no obvious fluctuation of the water levels in the two manometer tubes measuring the nozzle pressure. The dominant random error in the nozzle velocity calculation comes from the manometer reading which can be expected not to exceed 0.5 mm. This equates to a maximum error of about 2.8m/s in nozzle velocity calculation for the specific weight of 0.0012 of air under room temperature.

A three dimensional traverse system was set up so that the measuring instrument (Prandtl probe) could be placed at any required position. The minimum recordable distances in the longitudinal, vertical and transversal directions were 0.1 mm, 0.3 mm and 1.27 mm respectively.

A Prandtl-type pitot-static probe of external diameter of 1.5 mm was used to obtain the time average velocity as well as the pressure field in the intersecting jets. This Prandtl tube was connected to two micro-manometers. Alcohol of specific gravity of 0.81 was used as the micro-manometer fluid. The micro-manometer scale was divided into millimeters.

At every section, the probe was aligned with the flow on the jet axis with a tuft probe so as to reduce the errors that might be introduced otherwise due to angle of attack. The slope for the micro-manometer connected to the static pressure holes was set to 1/25 all the time while the slope for the other micro-manometer, which was used to measure the total head, was set to from  $11.31^\circ$  (slope 1/5) to  $60^\circ$ . The alcohol levels in the two micro-manometers were very stable during measurement. Considering that the random errors in reading the manometers could not exceed 0.5 mm, the maximum error in the pressure calculation was about 0.02 mm of alcohol column height and that in the total head calculation was 0.1 to 0.433 mm. The resulting maximum error in the velocity calculation was 1.2 (for 1/5 slope) to 2.4 m/s (for 60 degree slope). No corrections were made to velocity and pressure measurements for the effect of turbulence and this aspect should be kept in mind especially when considering the results in the region near the intersection point.

The arrangement of the nozzles A and B for the present study is shown in Fig. 3-3. The angle of the intersection was fixed at 60 degrees with H/D equal to 7.9. Region 1 extends from nozzle A to the intersection point and region 2 lies

downstream of the intersection point. The ratio of the velocity at nozzle B to that at nozzle A is termed the velocity ratio R. Six experiments were performed for R = 0, 0.39, 0.47, 0.59, 0.68 and 0.79. The respective velocities at the nozzles are shown in Table 1 and were varied from zero to about 42 m/s. In this range of velocities, compressibility effects can be neglected.

**Table 3-1 Primary details of the experiments**

Expt.	$U_{0A}$ (m/s)	$U_{0B}$ (m/s)	$R = \frac{U_{0B}}{U_{0A}}$
1	42.14	0	0.00
2	42.15	16.46	0.39
3	35.19	16.5	0.47
4	42.2	25.03	0.59
5	42.16	28.67	0.68
6	42.14	33.36	0.79

In each of these six experiments, the time-averaged axial velocity and pressure were measured along AC (see Fig. 3-3) and the axis of the resulting jet after the intersection. In Fig. 3-3, CX represents the theoretically calculated axis of the resulting jet. Fig. 3-3 shows the co-ordinate system used. The profiles of  $u$  in the vertical ( $y$ ) and transverse directions were measured at several sections in both region 1 and region 2. Measurements also included the pressure field in the jets. These results are presented and discussed in the following sections.

### **3.3 Experimental results and analysis for region 1**

#### **3.3.1 Velocity and pressure variation along jet axis**

Considering the axis of the jet from nozzle A, Fig. 3-4 shows the variation of the axial velocity along the axis of the jet A. In Fig. 3-4, one can see the extent

of the potential core. After the end of the potential core, it is seen that the decay of the centerline velocity is increased as  $R$  increases. Fig. 3-5 shows the variation of the centerline pressure in terms of  $\frac{1}{2} \rho U_0^2$  with  $x_1/D$ . At  $x_1/D = 4.5$ , the pressure begins to increase due to the presence of the pressure hill in the intersection region. If  $x_{1*}$  is the value of  $x_1$  at which the pressure begins to increase,  $x_{1*}/H = 5.7$  which is approximately equal to the value found for jets of equal momentum flux for  $\alpha = 60$  degrees. If  $\Delta p_{cm}$  is the maximum value of the difference between the centerline pressure of  $R \neq 0$  and that of  $R=0$  in region 1, the variation of  $\Delta p_{cm}$  with  $R$  is shown in Fig. 3-6. From Fig. 3-6, it is seen that  $\Delta p_{cm}/\frac{1}{2} \rho U_0^2$  increases continuously with  $R$  from 0 for  $R = 0$  to about 0.021 for  $R = 0.79$ . For  $R = 1$ ,  $\Delta p_{cm}/\frac{1}{2} \rho U_0^2$  for  $H/D = 9.8$  was equal to 0.88. The variation of  $\Delta p_{cm}/\frac{1}{2} \rho U_0^2$  with  $R$  can be described well by the following polynomial equation.

$$\frac{\Delta p_{cm}}{\frac{1}{2} \rho U_0^2} \pm 0.00062 = 0.053 \pm 0.006 R - 0.148 \pm 0.015 R^2 + 0.210 \pm 0.010 R^3 \quad (3-1)$$

with the correlation coefficient equal to 1.000.

### 3.3.2 Velocity and pressure distribution in region 1

In region 1, the velocity profiles  $u(z_1)$  were measured at several sections with  $x_1/D$  ranging from 4.9 to 7.4. These profiles are shown in Fig. 3-7(a-f) for  $R = 0, 0.39, 0.47, 0.59, 0.68$  and  $0.79$ . One can see from Fig. 3-7 that as the intersection point is approached, on the inner side (i.e. the side of the other jet) the jet does not grow as fast as on the outer side. When the velocity on the inner side was measured near the intersection point, the results can only be considered as approximate because of the strong flow attack from the other jet to the Prandtl tube (for this reason the data were not taken for  $R = 0.79$  in this region). In Fig. 3-8(a-f), the transverse velocity profiles are plotted in non-dimensional form, and



we can see that these profiles are similar and can be described well by the exponential equation

$$\frac{u}{u_m} = \exp(-0.693(\frac{z_1}{b_{z1}})^2) \quad (3-2)$$

except for the section with  $x_1/D = 7.4$ . The data for all values of R are collected in Fig. 3-9 where the exponential equation appears to describe the data well, except for the station  $x_1/D = 7.4$ . In Figs. 3-8 and 3-9,  $u_m$  is maximum velocity, and  $b_{z1}$  is the transverse length scale defined as the value of  $z_1$  where  $u = \frac{1}{2} u_m$ .

The variations of length scales  $b_{z1+}$  (on the inner side) and  $b_{z1}$ . ( on the outer side ) with R are shown respectively in Fig. 3-10 (a) and (b). It is seen that both scales grow approximately linearly, but while the growth rate on the outer side was not affected by the jet B it decreased on the inner side when R increased. The variation of the growth rate of length scale  $b_{z1}$  with R is shown in Fig. 3-11, and it is seen that the growth rate on the inner side decreases approximately linearly with R and the relation can be expressed as

$$\frac{d(b_{z1+})}{d(x_1)} \pm 0.004 = 0.028 \pm 0.003 + 0.078 \pm 0.006 R \quad (3-3)$$

with the correlation coefficient equal to 0.989.

The velocity profiles in vertical direction are shown in Fig. 3-12(a-f) and they are found similar when plotted in non-dimensional form in Fig. 3-13(a-f). The data for all values of R are plotted together in consolidated form in Fig. 3-14. In Figs. 3-13 and 3-14,  $b_y$  is the value of y where  $u = \frac{1}{2} u_m$ . It is seen from Figs. 3-13 and 3-14 that the familiar exponential equation described the data very well. The growth of the vertical length scale  $b_y$  with distance from the nozzle is shown in Fig. 3-15 where one can see that as the intersection point is approached, the jet grows faster in the vertical direction, especially so when R value is large.

Fig. 3-16(a-f) displays the pressure profiles in transverse direction for several  $x_1/D$  values and all the six R values. These profiles highlight the asymmetry of the jets especially for big R values. The pressure profiles in vertical direction are shown in Fig. 3-17(a-f).

### 3.4 Experimental results and analysis for region 2

#### 3.4.1 Velocity and pressure variation along resultant jet axis

For the region 2 extending from the intersection point, firstly the direction of the resulting jet can be predicted from momentum consideration. Referring to Fig. 3-3, let us denote the momentum from nozzles A and B as  $M_A$  and  $M_B$ , and the angle between the resultant jet and the line of symmetry (shown by the line CX' in Fig. 3-3) as  $\bar{\alpha}$ . Let us further assume that the pressure inside the resultant jet is the same as that of the ambient fluid we can write the momentum balance equation in Z direction as

$$M_A \sin\left(\frac{\alpha}{2} - \bar{\alpha}\right) + M_B \cos\left(\frac{\pi}{2} + \bar{\alpha} + \frac{\alpha}{2}\right) = 0 \quad (3-4)$$

Solving  $\bar{\alpha}$  from equation (3-4), we obtain

$$\begin{aligned} \bar{\alpha} &= \tan^{-1}\left\{ \frac{M_A - M_B}{M_A + M_B} \tan\left(\frac{1}{2}\alpha\right) \right\} \\ &= \tan^{-1}\left\{ \frac{1 - R^2}{1 + R^2} \tan\left(\frac{1}{2}\alpha\right) \right\} \end{aligned} \quad (3-5)$$

Eq. (3-5) has been reported earlier by Maxwell and Snorrason [1979] in a different form. Fig. 3-18 shows a comparison of experimental results with Eq. (3-5). In experiments, the axis of the resulting jet was defined as the locus of maximum velocity points. It is seen from Fig. 3-18 that the theoretical prediction is satisfactory away from the point of intersection whereas near the intersection

point the agreement is not good especially for large values of R due to the violation of the constant pressure field assumption.

The variation of maximum velocity in the deflected jet (in the direction of the resulting jet) in terms of  $U_0$  (velocity at nozzle A), with  $x/D$  is shown in Fig. 3-19(a). The decay of the maximum velocity appears to be enhanced with the increase of R. In Fig. 3-19(b), the data are presented in a different form. As is seen from Fig. 3-19(b) that after  $x/D=3$ ,  $U_0/u_m$  increases linearly with  $x/D$ . If we assume

$$\frac{U_0}{u_m} = a_1 + a_2 \frac{x}{D} \quad (3-6)$$

the variation of coefficients  $a_1$  and  $a_2$  with R is shown in Fig. 3-20, and the relations can be expressed as

$$a_1|_{\pm 0.006} = 1.085|_{\pm 0.006} - 0.723|_{\pm 0.0029}R + 0.363|_{\pm 0.0036} R^2 \quad (3-7)$$

$$a_2|_{\pm 0.007} = 0.140|_{\pm 0.006} + 0.227|_{\pm 0.0011}R \quad (3-8)$$

with correlation coefficients equal to 0.999 and 0.995 respectively.

The variation of the pressure along the axis of the jet with distance from the intersection point is shown in Fig. 3-21 wherein for all the non-zero values of R, one can notice the drop from the increased pressure area before the intersection point to a low pressure and a recovery for further increase with  $x/D$ . For  $R = 0.79$ , the lowest value of  $p/\frac{1}{2} \rho U_0^2 \approx -0.04$ . Fig. 3-22 shows the variation of the minimum pressure  $p_{\min}$  (measured along the jet axis) in terms of  $\frac{1}{2} \rho U_0^2$  with R, wherein  $p_{\min}$  decreases continuously as R increases. Fig. 3-21 also shows for all non-zero values of R, the minimum pressure occurs at  $x/D \approx 4$ .

The maximum pressure ( $p_{\max}$ ) occurred in the region of backward flow, as indicated by Fig. 3-23 (a-e). It did occur at the stagnation point possibly

because of the high turbulence energy around this point. The variation of the maximum pressure in the backward flow region, in terms of  $\frac{1}{2} \rho U_0^2$ , with R is shown in Fig. 3-24, wherein  $p_{\max}/\frac{1}{2} \rho U_0^2$  increases continuously with R and becomes equal to about 0.11 at R = 1 (The result for R=1 is from the work of Rajaratnam and Khan).

### 3.4.2 Velocity and pressure distribution in region 2

The transverse velocity profiles in region 2 are shown in Fig. 3-25(a-f), and they were found to be essentially symmetric about the experimentally determined resulting jet axis (EDRJA). These profiles were also found to be similar as shown in Fig. 3-26(a-f). When all the profiles are shown together in Fig. 3-27, it was found that the exponential equation appears to describe the data extremely well. In Figs. 3-26 and 3-27,  $z_*$  is the distance between the x axis and EDRJA, and  $b_z$  is a length scale and is equal to  $z-z_*$  where velocity is half of the maximum velocity. The growth of the length scale  $b_z$  in terms of D is shown in Fig. 3-28. It was found that the jet growth was almost symmetric about EDRJA, and the growth was approximately linear (after a short region of no growth). The variation of the growth rate of the length scale  $b_z$  with R is shown in Fig. 3-33 (with that in y direction ) from which we can see that the growth rate increases almost linearly with R and can be expressed as

$$\frac{db_z}{dx} \Big|_{z_0.012} = 0.073_{z_0.007} + 0.085_{z_0.012} R \quad (3-9)$$

with the correlation coefficient equal to 0.909.

The vertical velocity profiles in region 2 are shown in Fig. 3-29(a-f), and they were found to be similar when plotted in non-dimensional form as shown in Fig. 3-30(a-f). A consolidated plot is given for all the vertical velocity profile data in Fig. 3-31, and the exponential equation was found to describe all the data very

well. The variation of relative length scale  $b_y/D$  with  $x/D$  is shown in Fig. 3-32 for  $R = 0$  to 0.79 in which the growth rates are approximately linear. The length scale growth rate  $db_y/dx$  was found to increase continuously with  $R$  as shown in Fig. 3-33 and can be described by the following equation:

$$\frac{db_y}{dx} \pm_{\pm 0.015} = 0.082_{\pm 0.015} + 0.023_{\pm 0.058} R + 0.417_{\pm 0.056} R^2 \quad (3-10)$$

with the correlation coefficient equal to 0.996. For  $R$  in the approximate range of 0.4 to 0.8, the ratio of the growth rate in the vertical to transverse direction varies from 1 to 2.5. For  $R = 1$ , this ratio was found to be 3.3 by Rajaratnam and Khan.

The transverse pressure profiles are shown in Fig. 3-34(a-f), and they are found to be essentially symmetric about EDRJA. The vertical pressure profiles are shown in Fig. 3-35(a-f).

### 3.5 Conclusions

This chapter presents the results of an exploratory experimental study on the intersection of unequal momentum flux. For jets of equal diameter, the ratio  $R$  of the velocities at the nozzle was given values of 0.39, 0.47, 0.59, 0.68 and 0.79 for an angle of intersection of 60 degrees. A control experiment with  $R = 0$  was also performed. Based on the results, the following conclusions can be formulated.

(1) The flow can be divided into two regions, region 1 from nozzle to the intersection point and region 2 from downstream of intersection point.

(2) Along the jet axis in region 1, the pressure hill associated with the jet intersection begins to affect the jet for  $x_1/H$  greater than about 0.57. As  $R$

increases the maximum velocity in the jet decays faster and the pressure increase is also larger.

(3) The transverse and vertical distributions of velocity are similar for  $x_1/H$  up to about 0.9 but as the intersection point is approached, the transverse growth of the jet on the inner side (i.e. the side of the other jet) is retarded. In vertical direction the jet growth rate increases as  $R$  is increased.

(4) Near the intersection point, the start point of the jet axis in region 2 lie on the outer side of the intersection point and the distance increases as  $R$  is increased. Away from the intersection point, the jet axis approach the lines predicted by simple momentum consideration.

(5) As  $R$  increases the velocity scale  $u_m$  in region 2 decays faster, and for all  $R$  values the ratio  $U_0/u_m$  increases linearly with relative distance  $x/D$ .

(6) Along the axis of the resulting jet, the pressure decreases to minimum value at  $x/D = 4$ , and after that it recovers. The minimum pressure, in terms of  $\frac{1}{2}\rho U_0^2$ , decrease continuously as  $R$  is increased and is as low as -0.04 for  $R = 0.79$ . The maximum pressure exists in the backward flow region and in terms of  $\frac{1}{2}\rho U_0^2$  reaches a value of about 0.1 for  $R = 0.79$ .

(7) In region 2, the transverse velocity profiles are symmetric about the experimentally determined axis. The velocity profiles in both transverse and vertical directions have been found similar. The transverse jet growth rate is not affected significantly by  $R$  whereas the vertical growth rate increases with  $R$  and is generally larger than the transverse growth rate.

### **3.6 References**

1. Baron, T. and Bollinger, E. H. (1952), **Mixing of high velocity air jets**, Tech. Rept. CML-3, Univ. of Illinois Engrg., Expt. Stn, 101p.
2. Beltaos, S. (1975), **Oblique Impingement of Circular Turbulent Jets**, J. Hyd. Res., IAHR, Vol. 14, pp. 17-36.
3. Beltaos, S. and Rajaratnam, N. (1974), **Impinging Circular Turbulent Jets**, J. Hyd. Div., ASCE, Vol. 100, No. Hy10, October, pp. 1313-1328.
4. Kind, R. J. and Suthanthiran, K. (1973), **The Intersection of Two Opposing Plane Turbulent Wall jets**, J. Fluid Mech., Vol. 58, Part 2, pp. 389-402.
5. Knystautas, R. (1964), **The Turbulent Jet from a Series of Holes in Line**, Aero. Quat., Vol. 15, pp. 1-28.
6. Maxwell, W. H. C. (1979), **Crossing Submerged Jets**, Proc. ASCE., J. Hyd. Engrg., Vol. 105, No. HY12, pp. 1557-1560.
7. Maxwell, W. H. C. and Snorrason, A. (1981), **Measurement of Merging Flow**, UILU-WRC-81-0155, Department of Civil Engineering, The University of Illinois at Urbana-Champaign, Illinois, U.S.A.
8. Rajaratnam, N. (1976), **Turbulent Jet**, Elsevier Scientific Publishing Co., 304p.
9. Rajaratnam, N. and Khan, A. A. (1990), **Intersecting Circular Turbulent Jets**, Journal of Hyd. Res., IAHR, 1992, Vol. 30, No. 3, pp. 373-387.
10. Witze, P. O. (1974), **A Study of Impinging Axisymmetric turbulent Flows: The Wall jet, The Radial and Opposing free jets**, Ph.D. Dissertation, University of California, Davis, 164p.

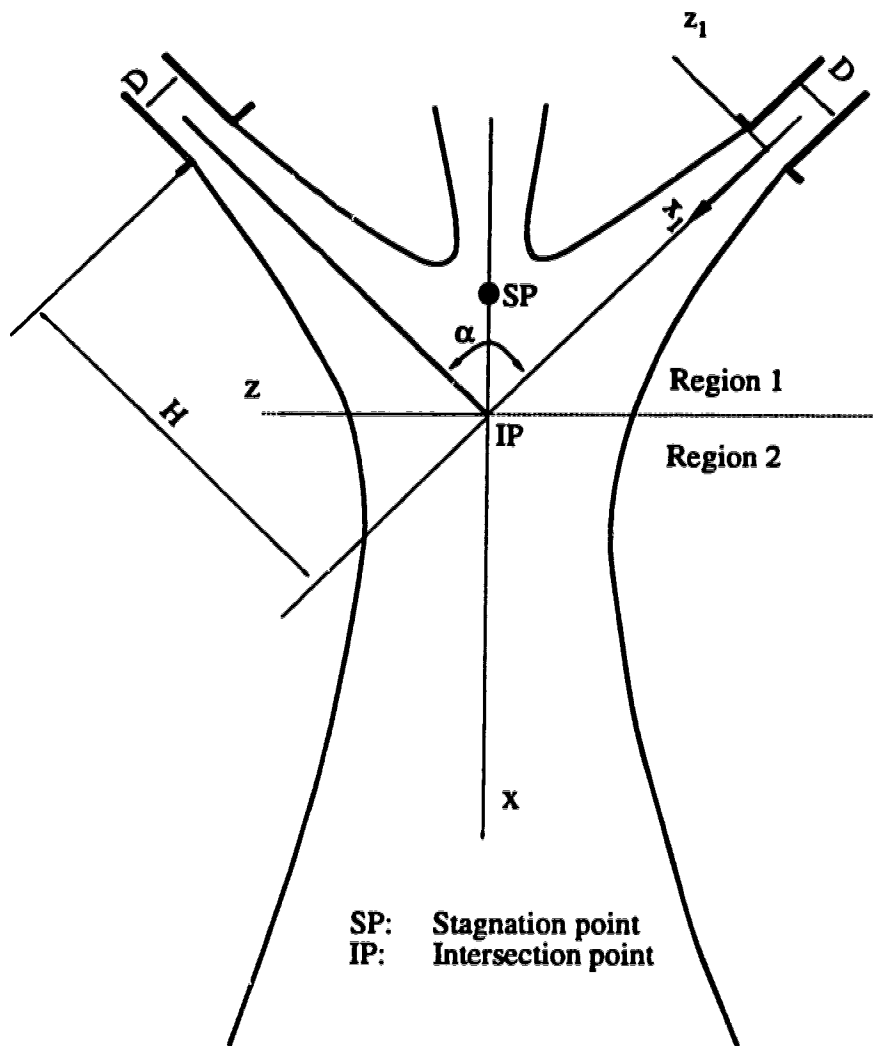
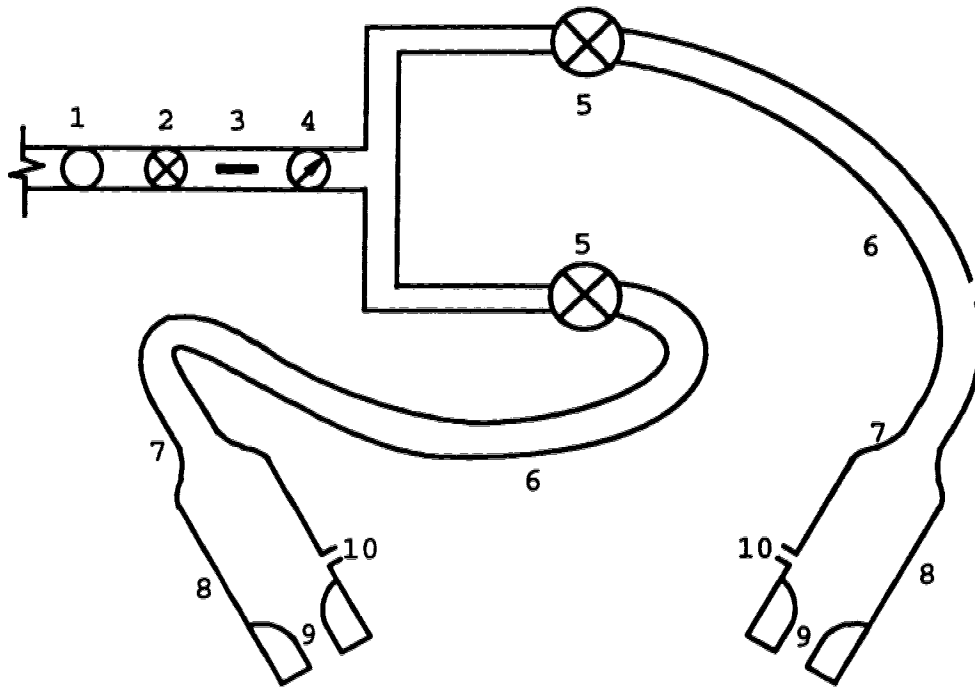


Fig. 3-1 Definition sketch for intersecting jets of equal momentum flux





1. Moisture trap
2. Main pressure regulating valve
3. Heating element
4. Pressure gauge
5. Pressure regulating valve
6. 19 mm internal diameter tygon tubing
7. Expansion joint connecting 19 mm internal diameter copper pipe to 38 mm internal diameter copper pipe
8. 380 mm long, 38 mm internal diameter copper tube
9. 25.4 mm long, 12.7 mm internal diameter nozzle
10. 3 mm taps connected to vertical differential water manometer by means of tygon tubing

Fig. 3-2. Schematic diagram of the experimental set up

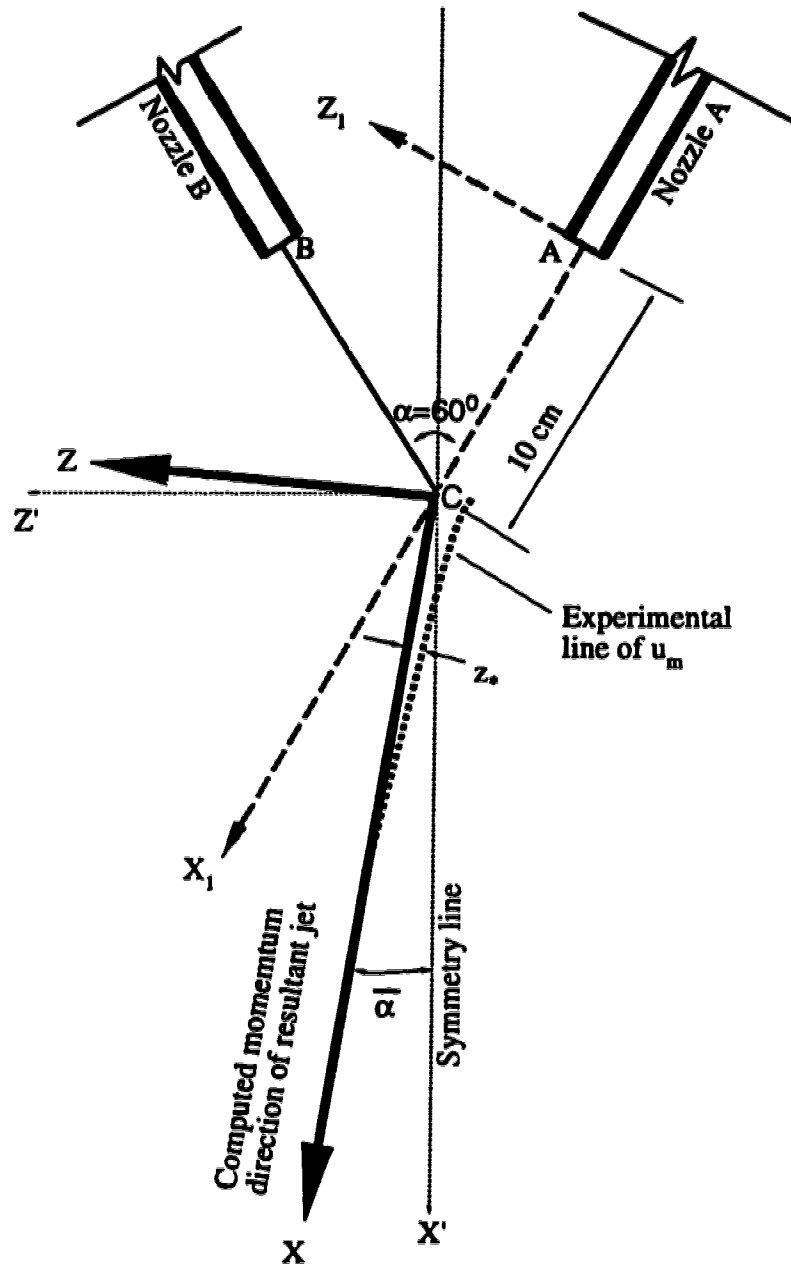


Fig. 3-3 Definition sketch for the intersecting jets of unequal momentum flux

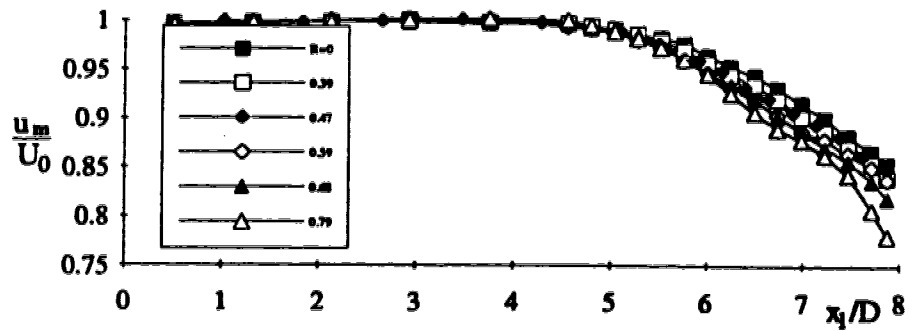


Fig. 3-4 Decay of the centerline velocity of jet in region 1

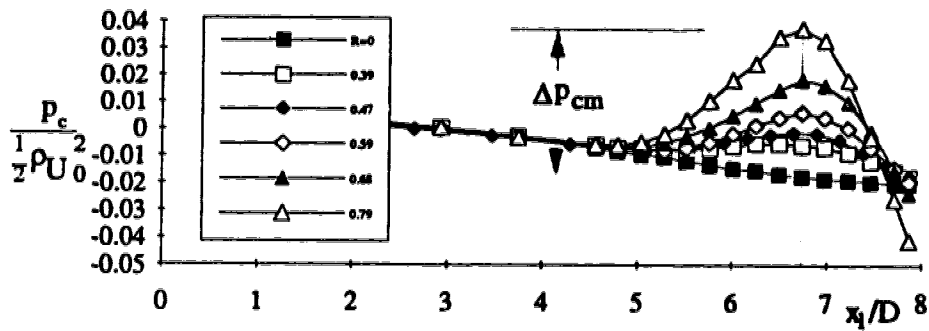


Fig. 3-5 Variation of the centerline pressure in jet in region 1

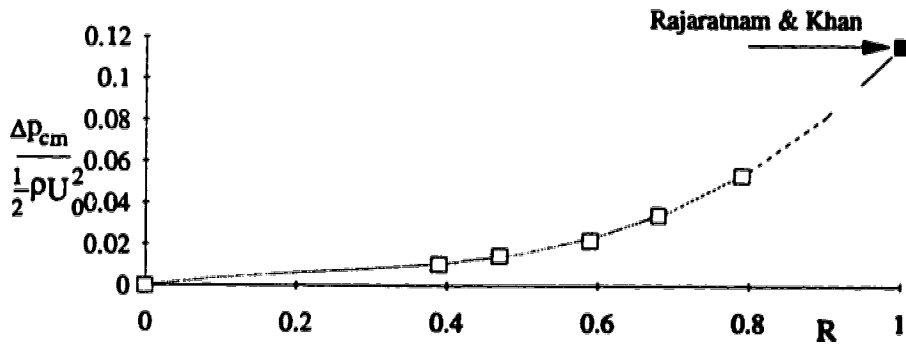


Fig. 3-6 Variation of the maximum pressure difference in jet in region 1 with R

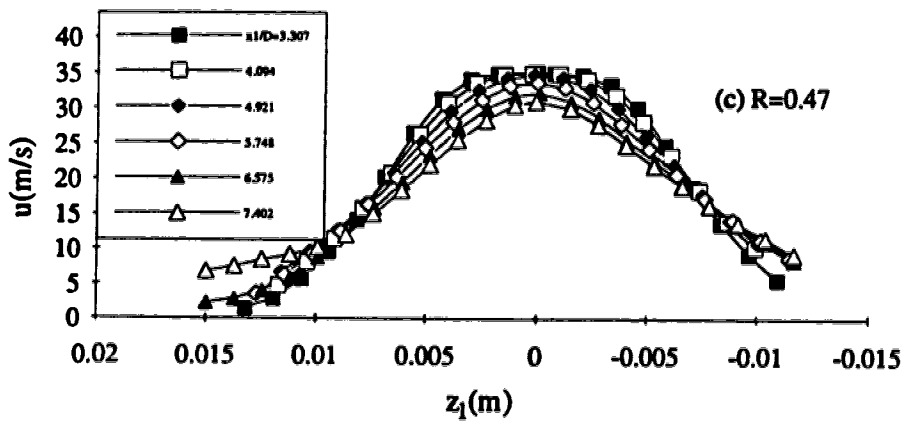
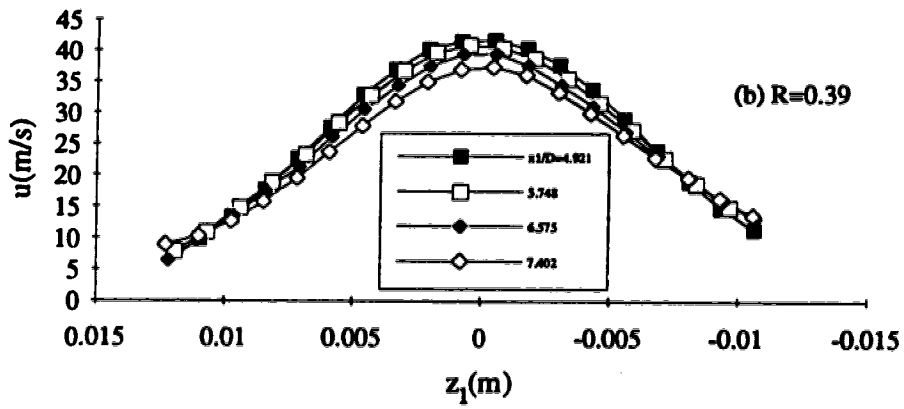
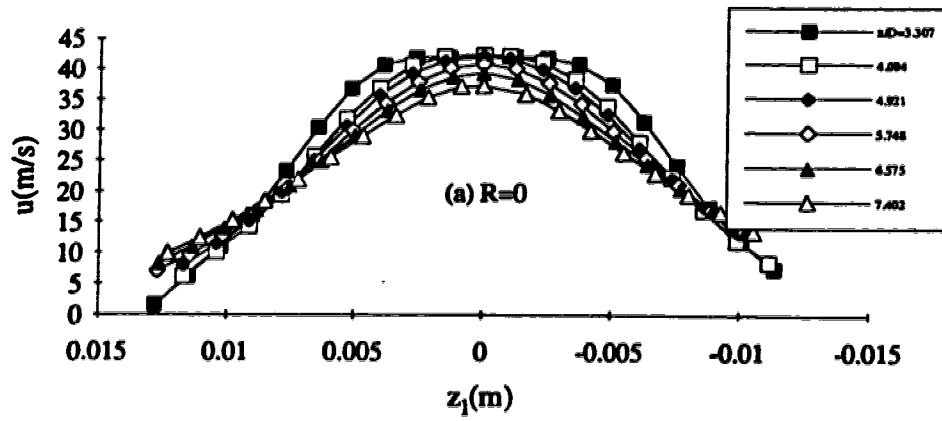


Fig. 3-7(a-c) Transverse velocity profiles in region 1

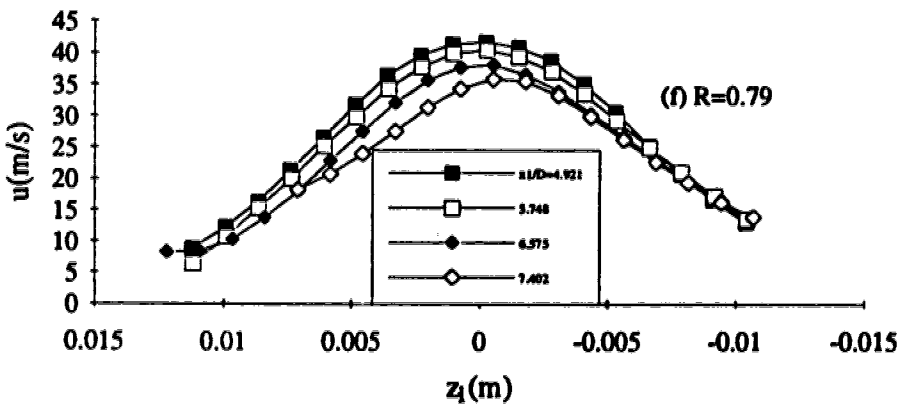
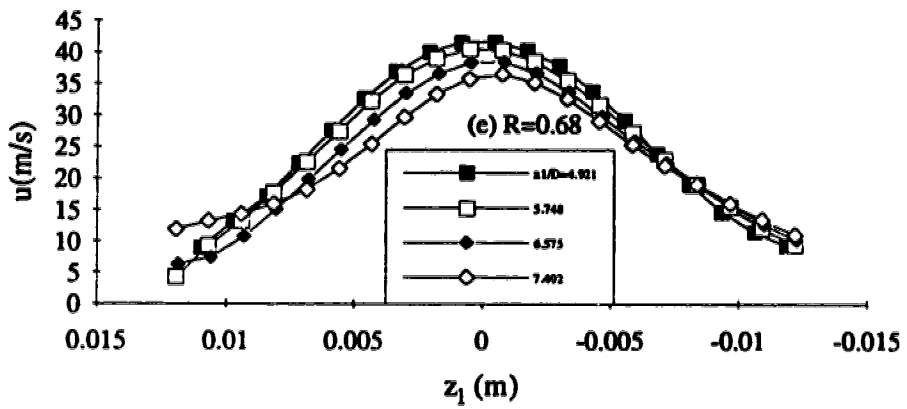
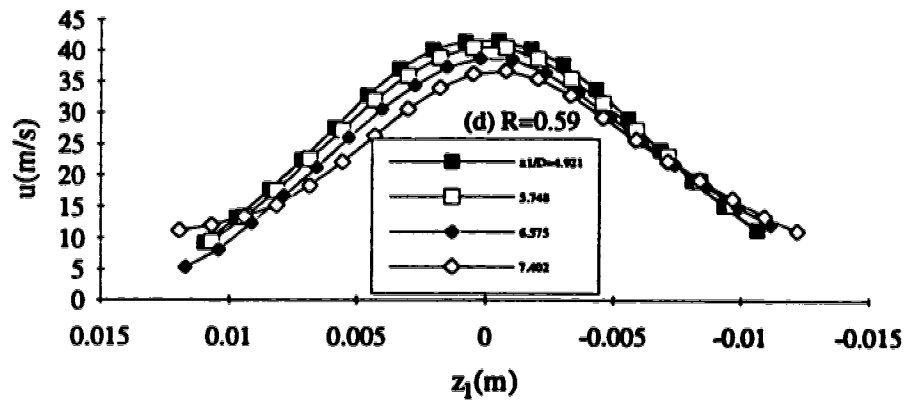


Fig. 3-7(d-f) Transverse velocity profiles in region 1

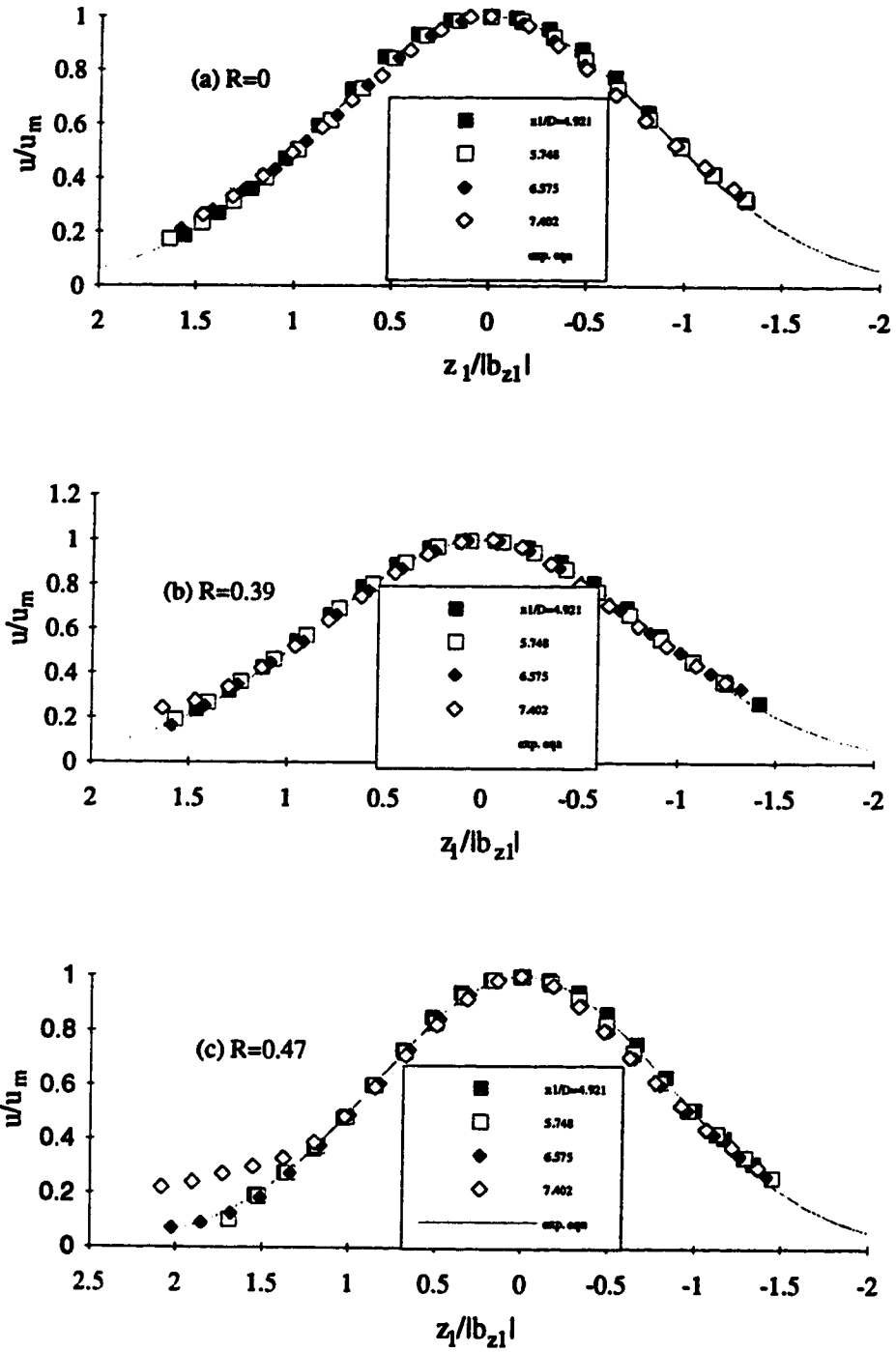


Fig. 3-8(a-c) Dimensionless transverse velocity profiles in region 1

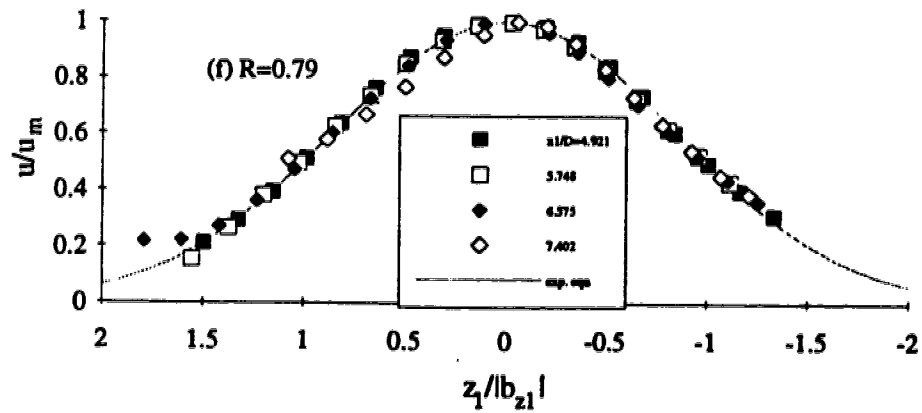
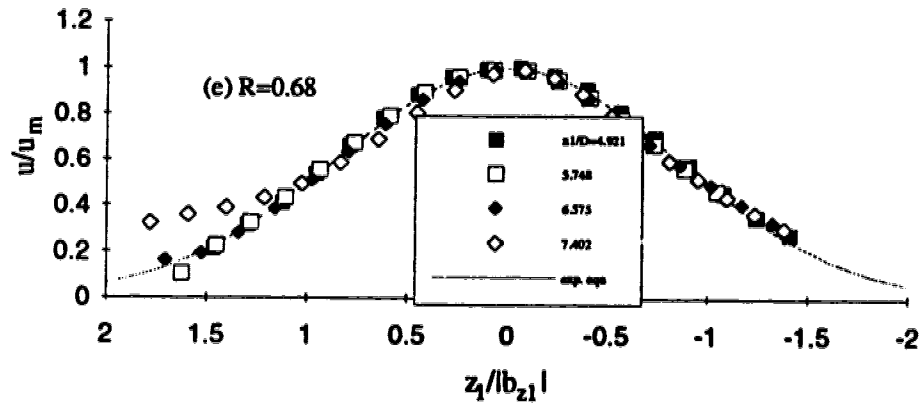
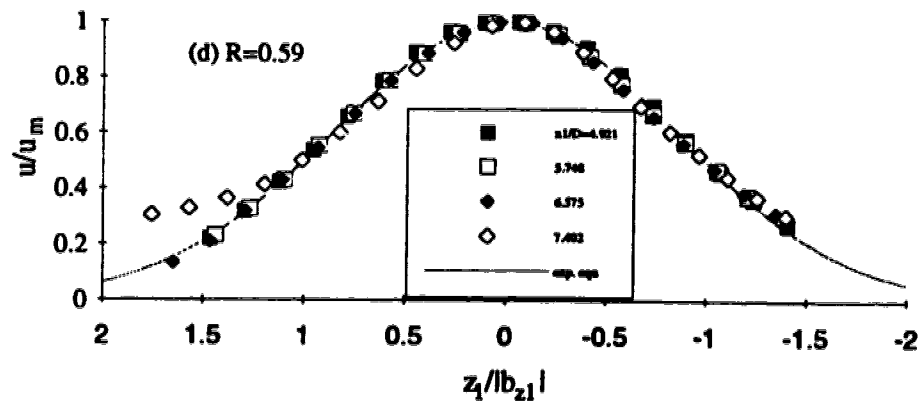


Fig. 3-8(d-f) Dimensionless transverse velocity profiles in region 1

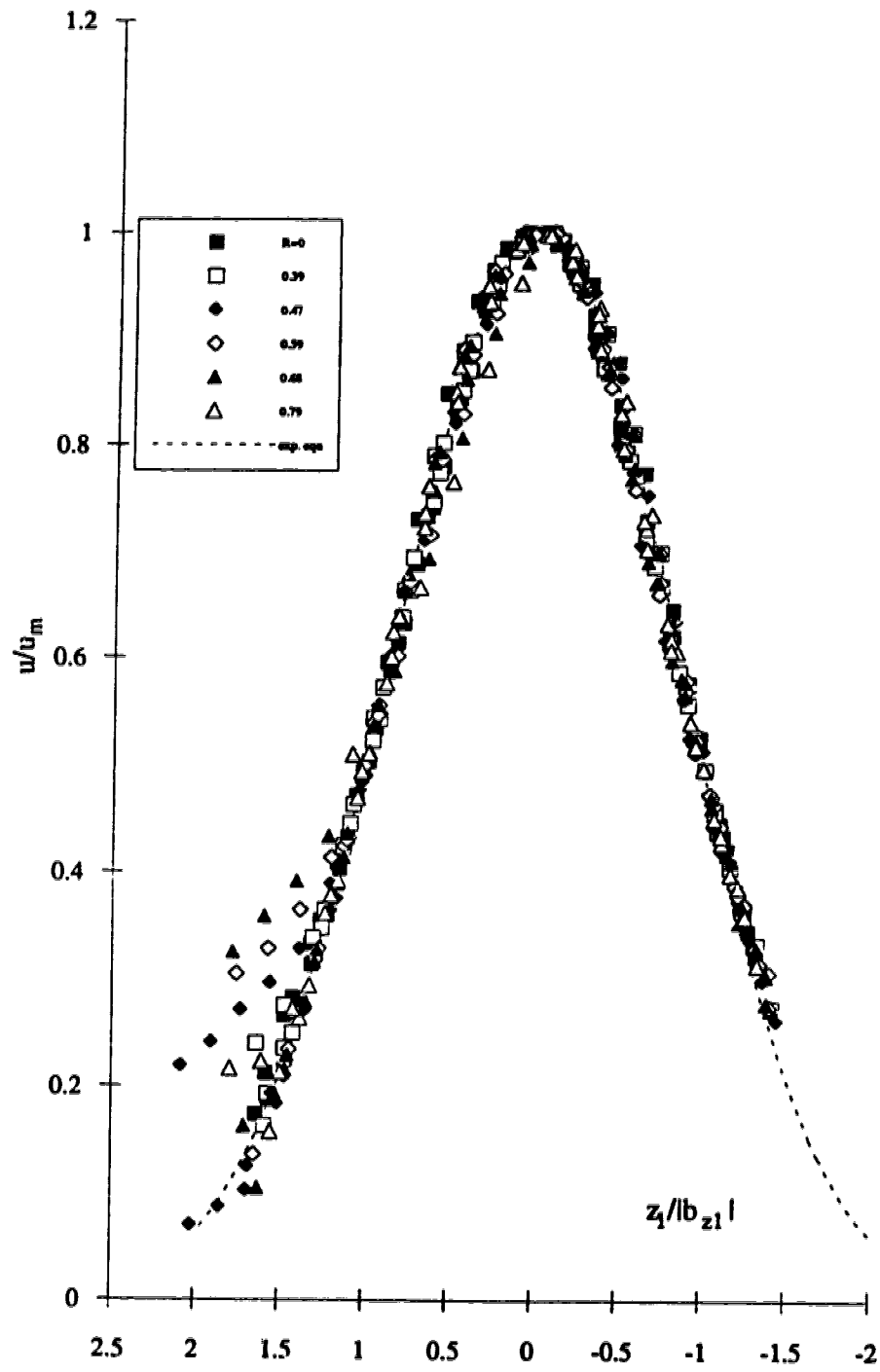


Fig. 3-9 Consolidated transverse velocity profiles in region 1



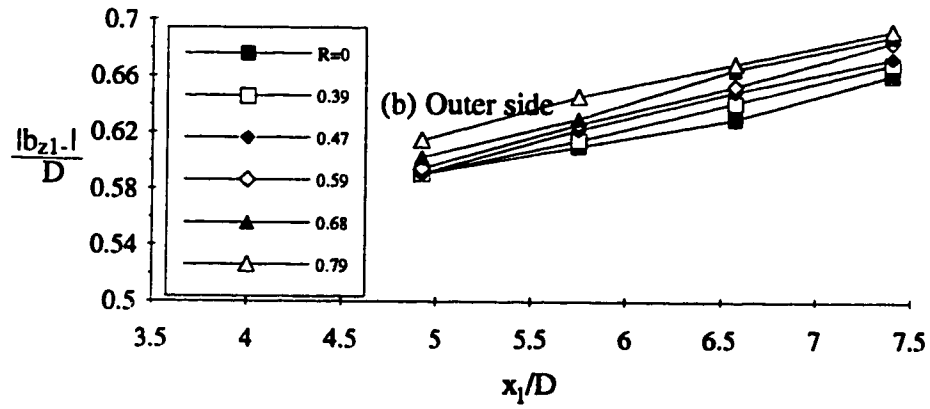
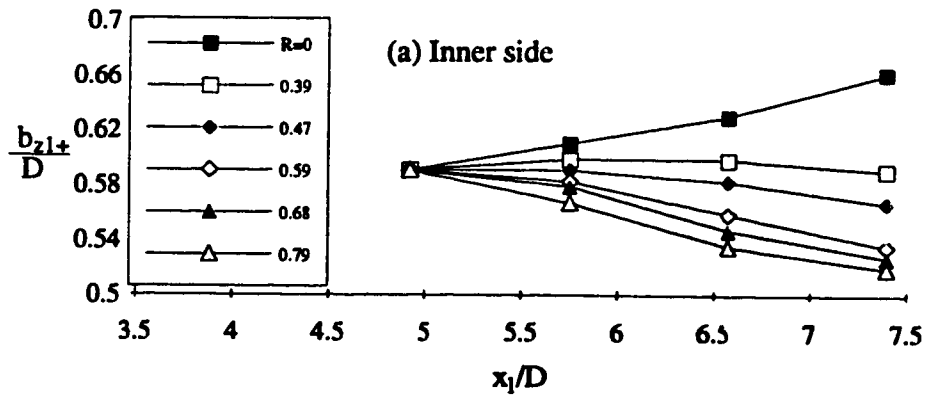


Fig. 3-10(a-b) Growth of the transverse length scales in region 1

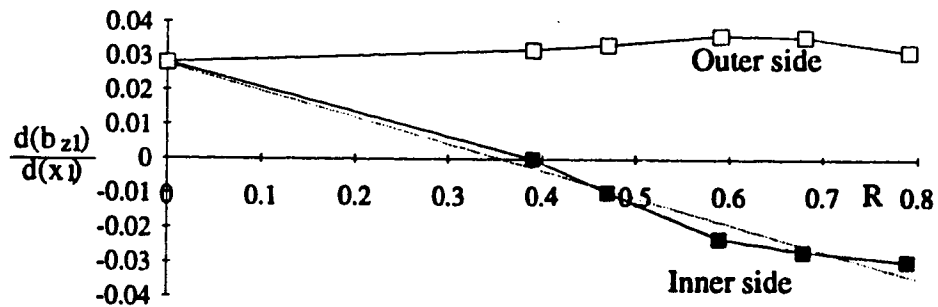


Fig. 3-11 Variation of the growth rate of length scale  $b_{z1}$  with R

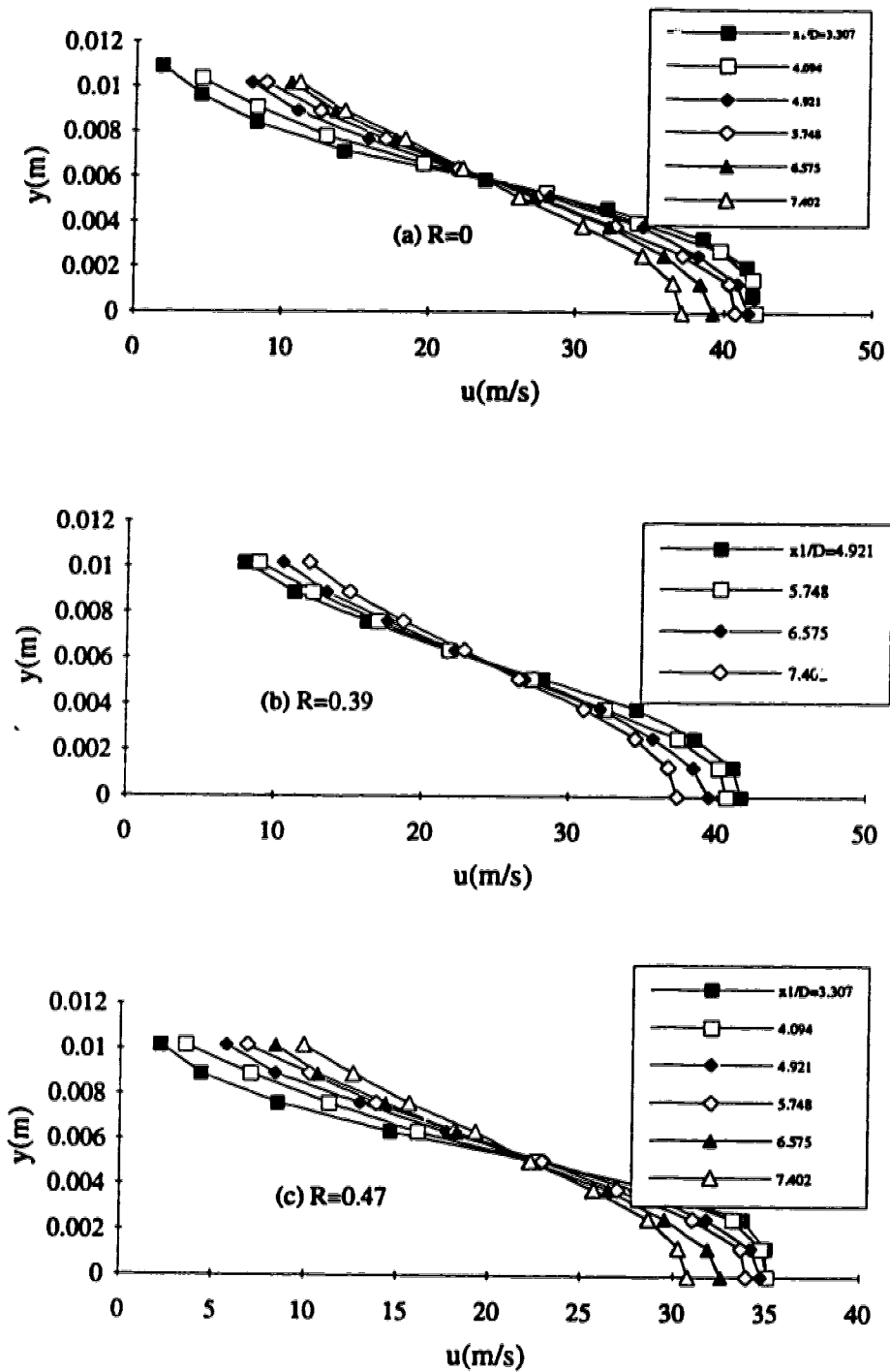


Fig. 3-12(a-c) Vertical velocity profiles in region 1

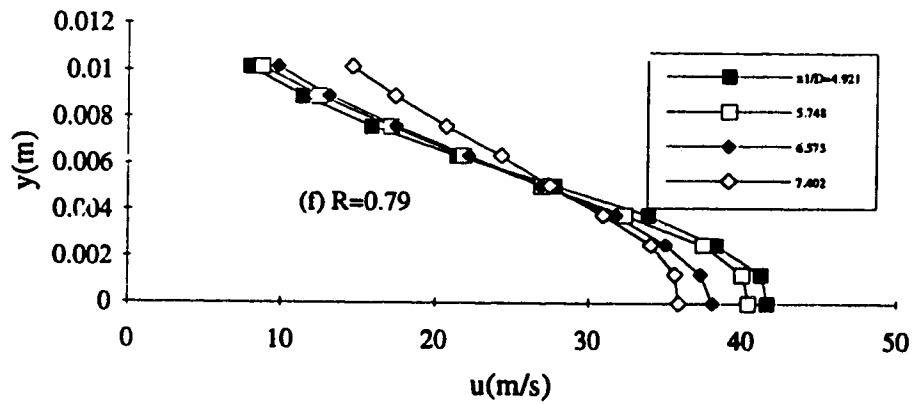
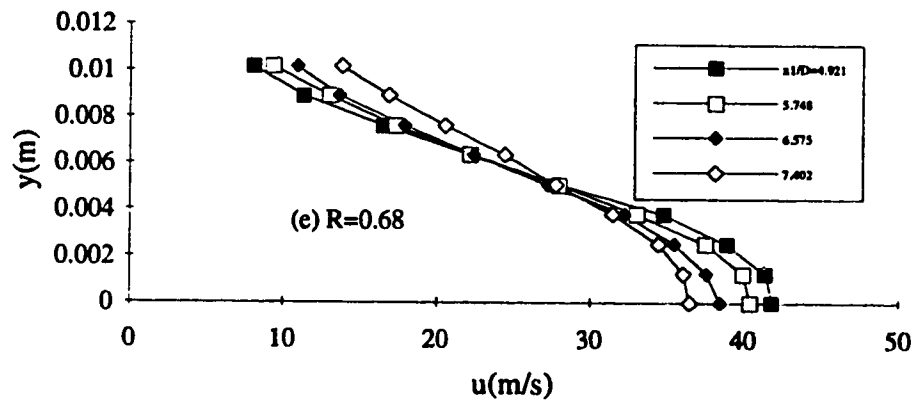
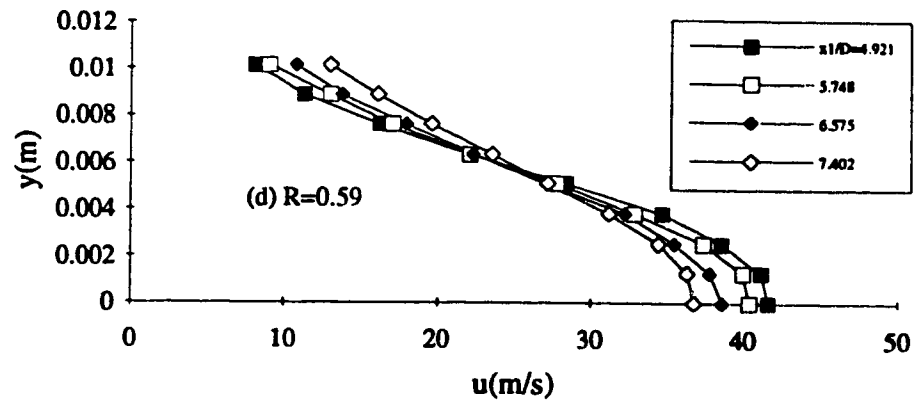


Fig. 3-12(d-f) Vertical velocity profiles in region 1

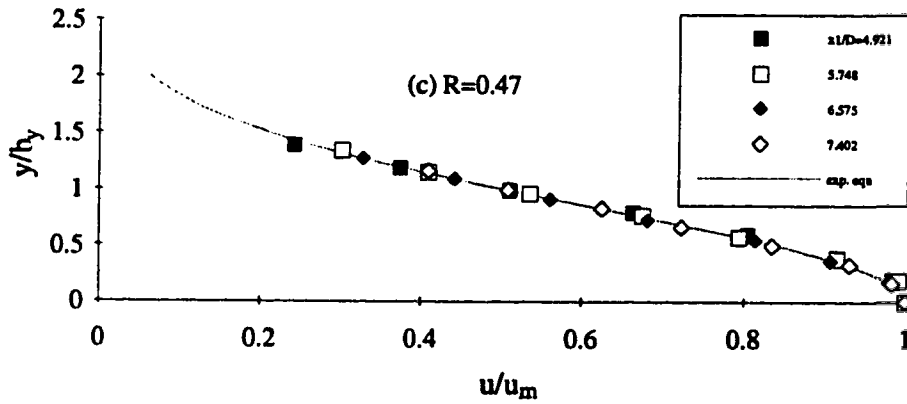
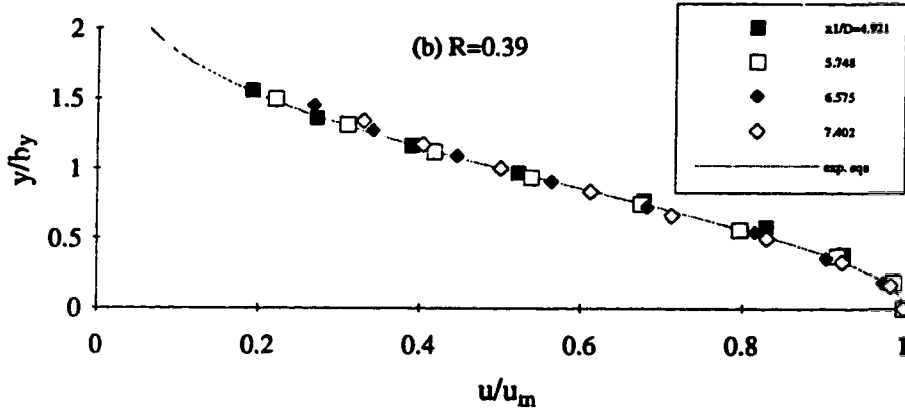
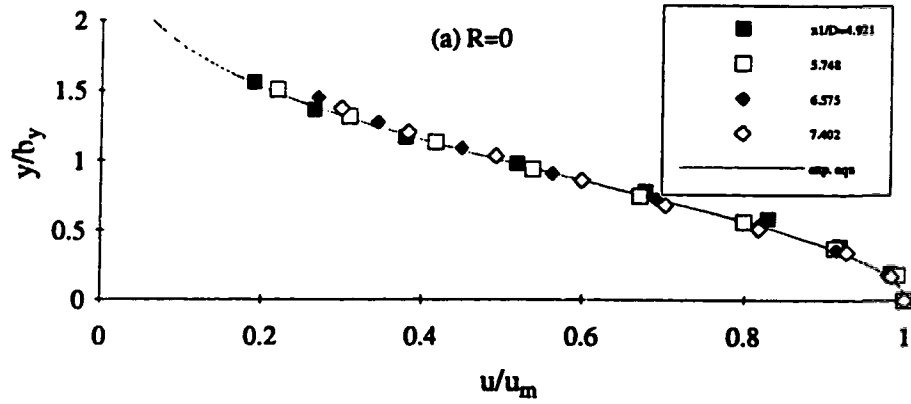


Fig. 3-13(a-c) Dimensionless vertical velocity profiles in region 1

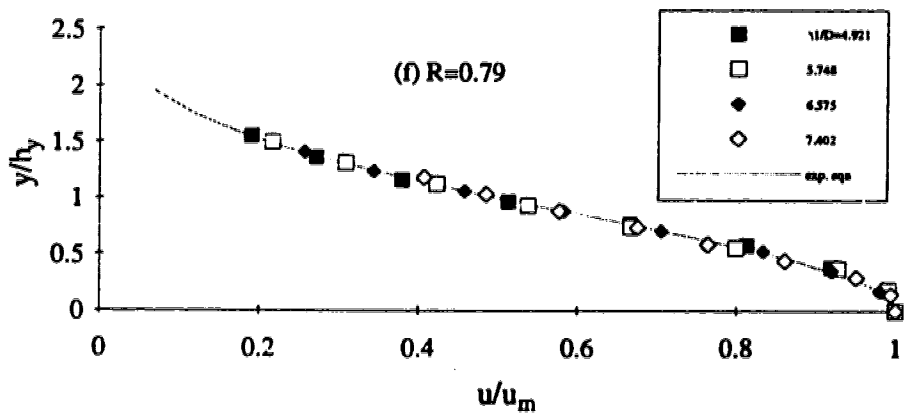
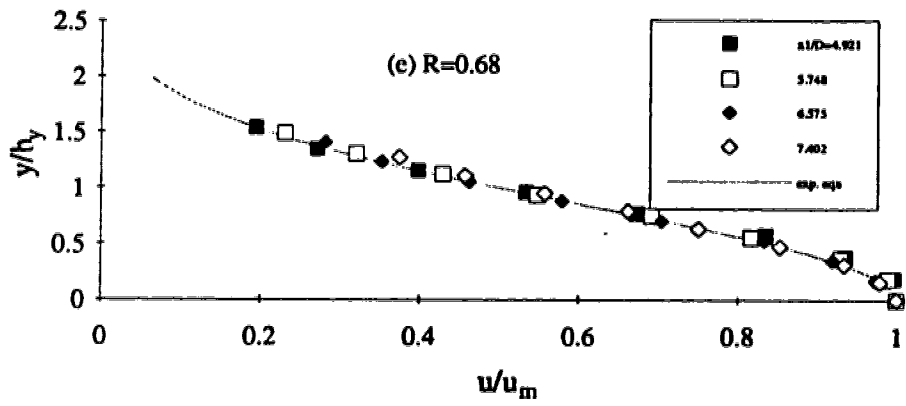
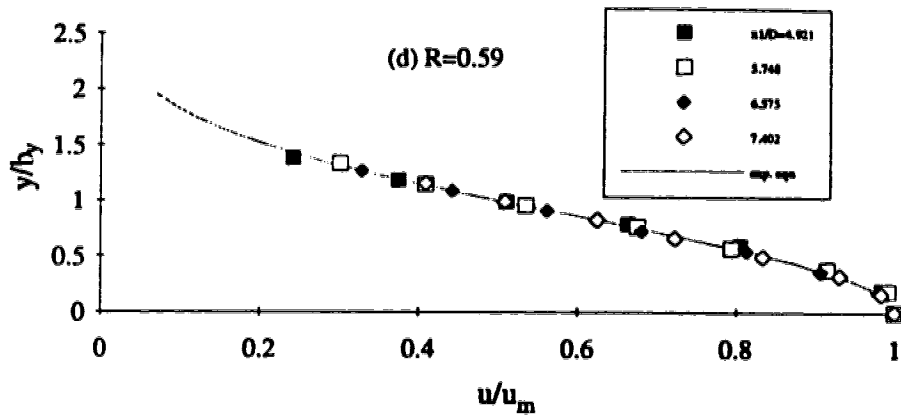


Fig. 3-13(d-f) Dimensionless vertical velocity profiles in region 1

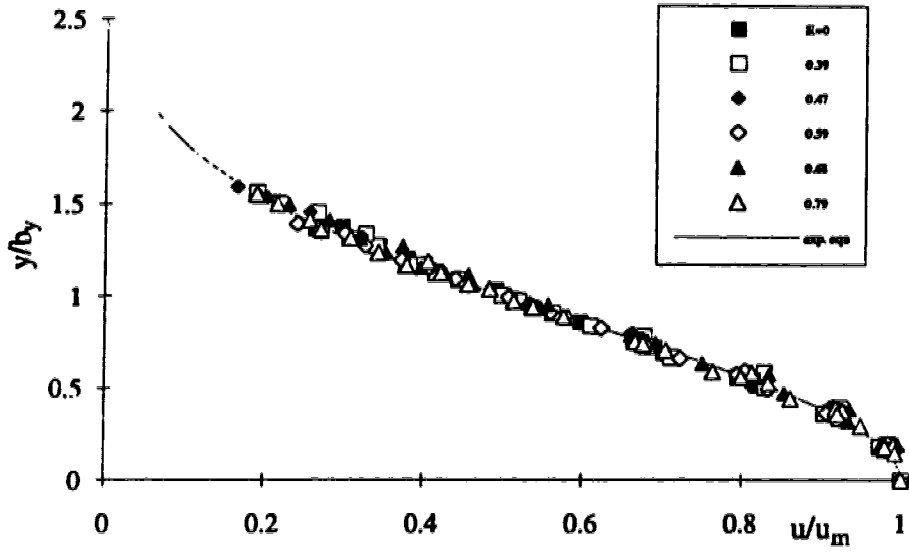


Fig. 3-14 Consolidated dimensionless vertical velocity profiles in region 1

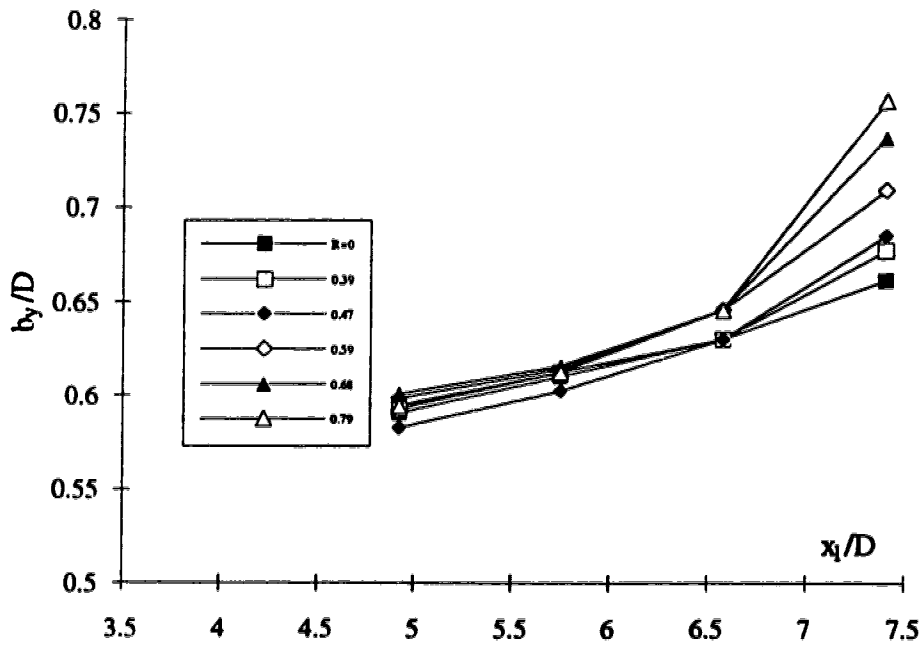


Fig. 3-15 Growth of the vertical length scales in region 1

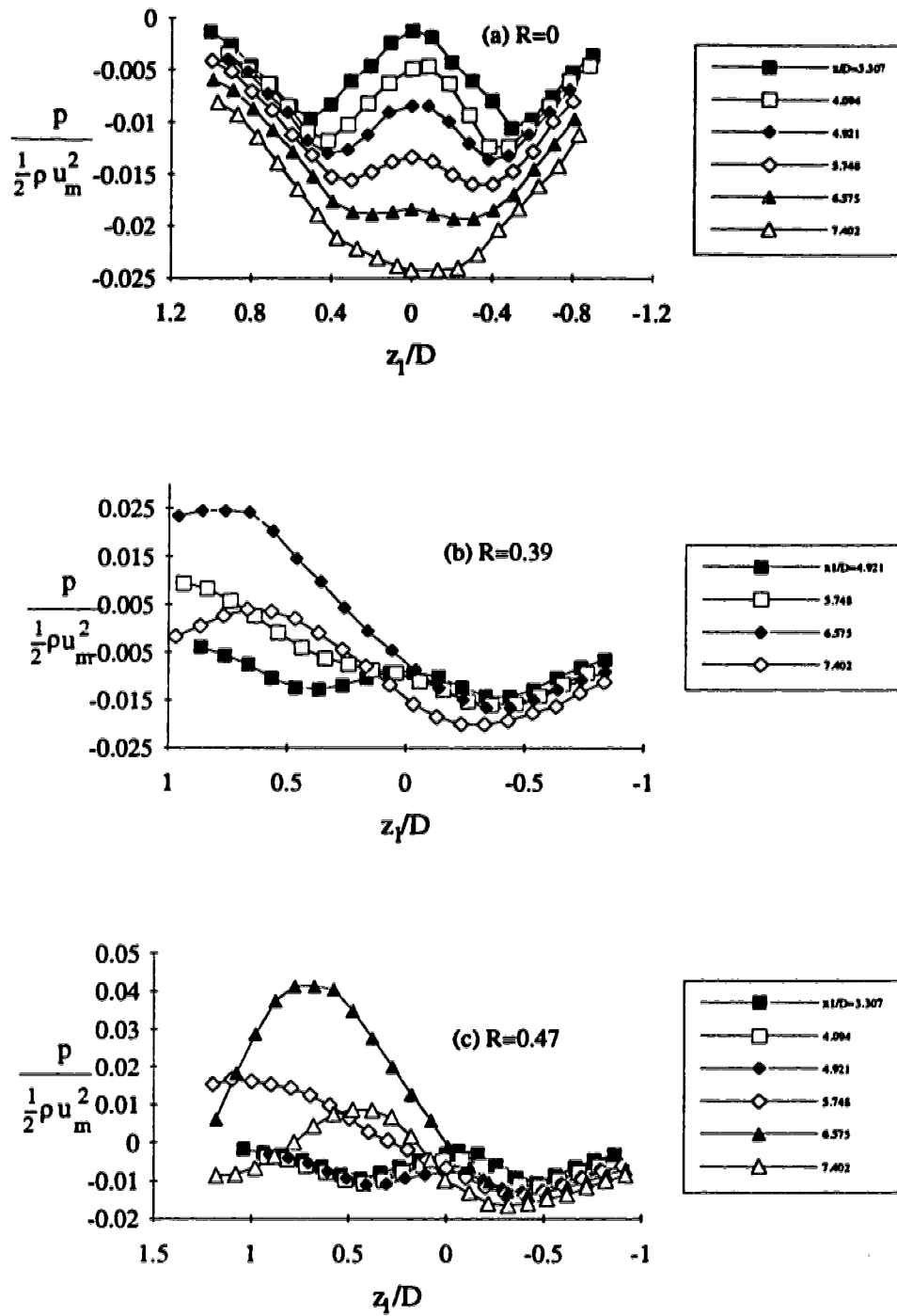


Fig. 3-16(a-c) Transverse pressure profiles in the jet in region 1

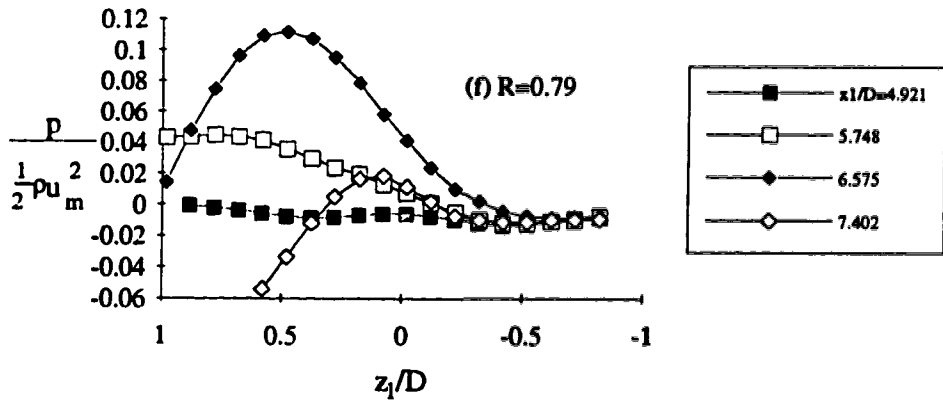
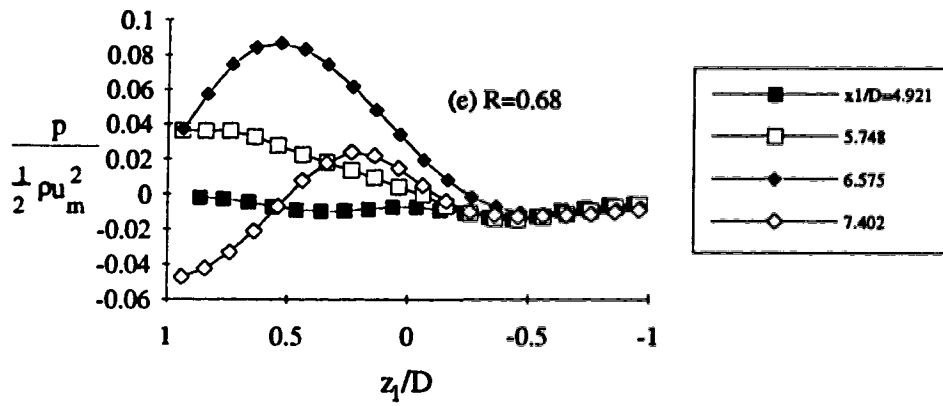
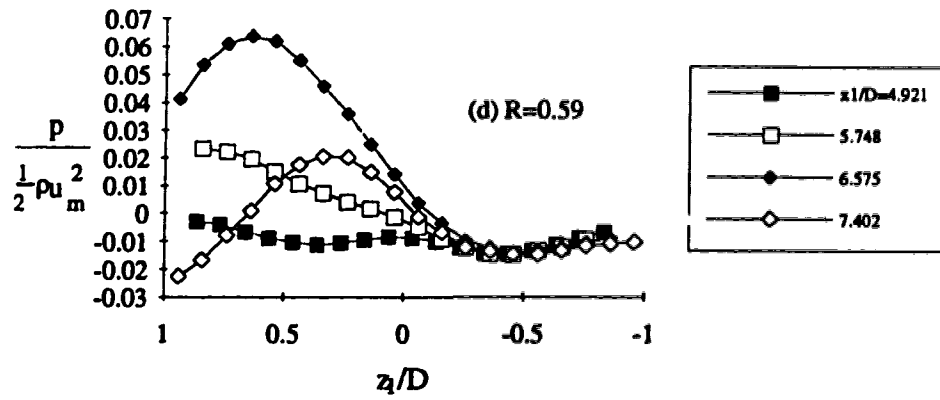


Fig. 3-16(d-f) Transverse pressure profiles in the jet in region 1



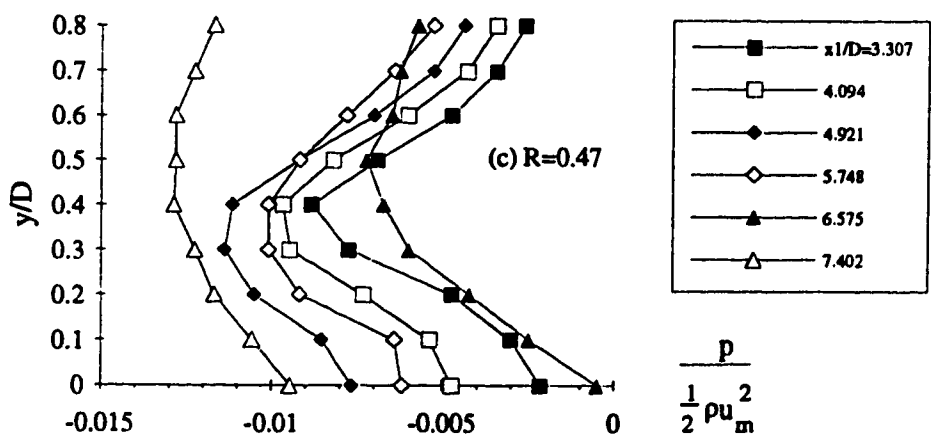
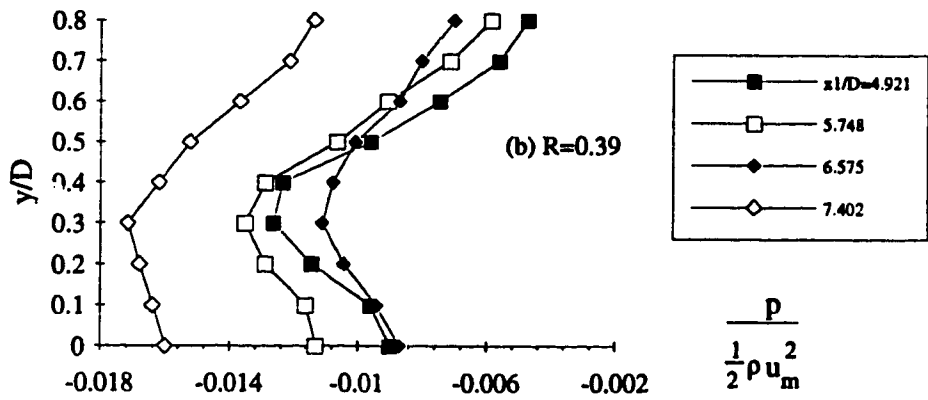
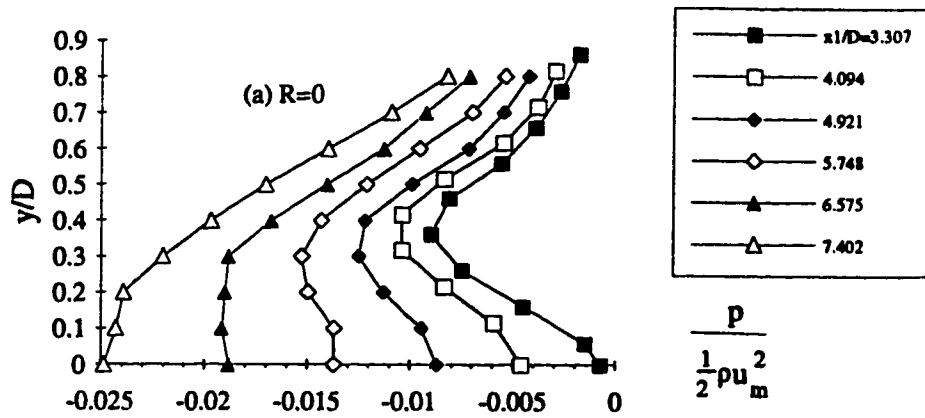


Fig. 3-17(a-c) Vertical pressure profiles in the jet in region 1

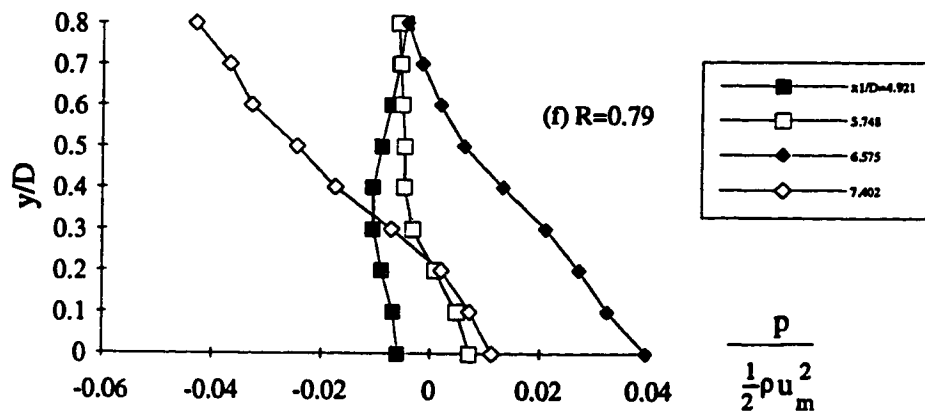
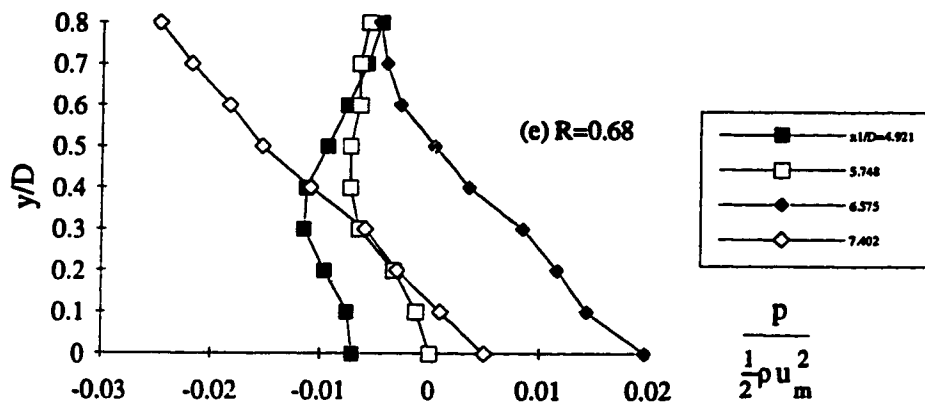
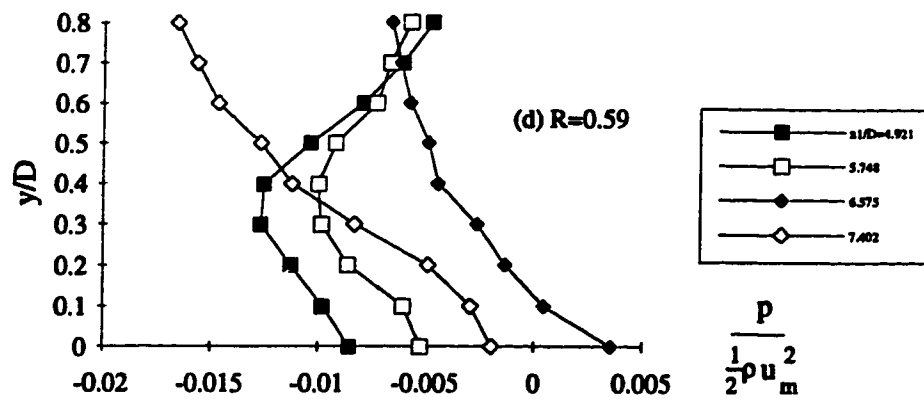


Fig. 3-17(d-f) Vertical pressure profiles in the jet in region 1

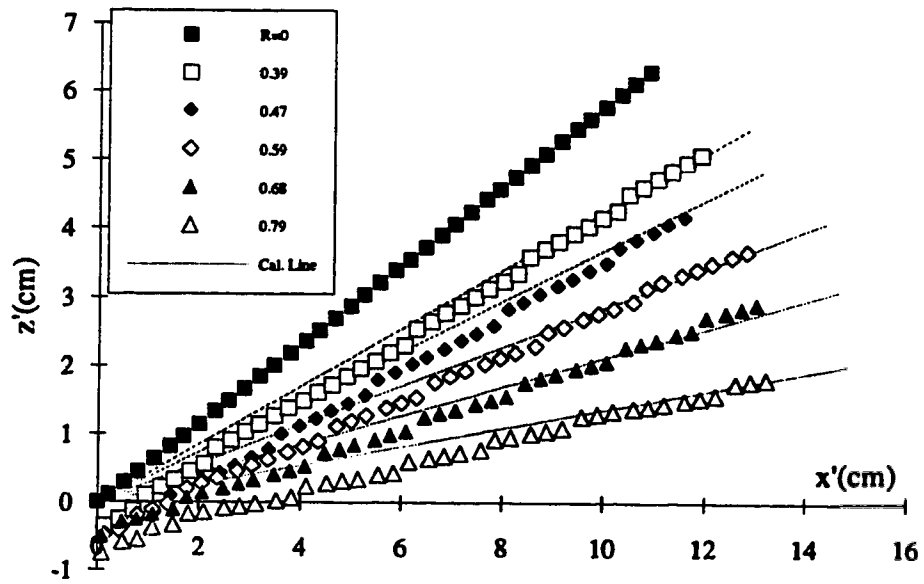


Fig. 3-18 Axis of jet in region 2 - comparison of predicted axis and measured axis

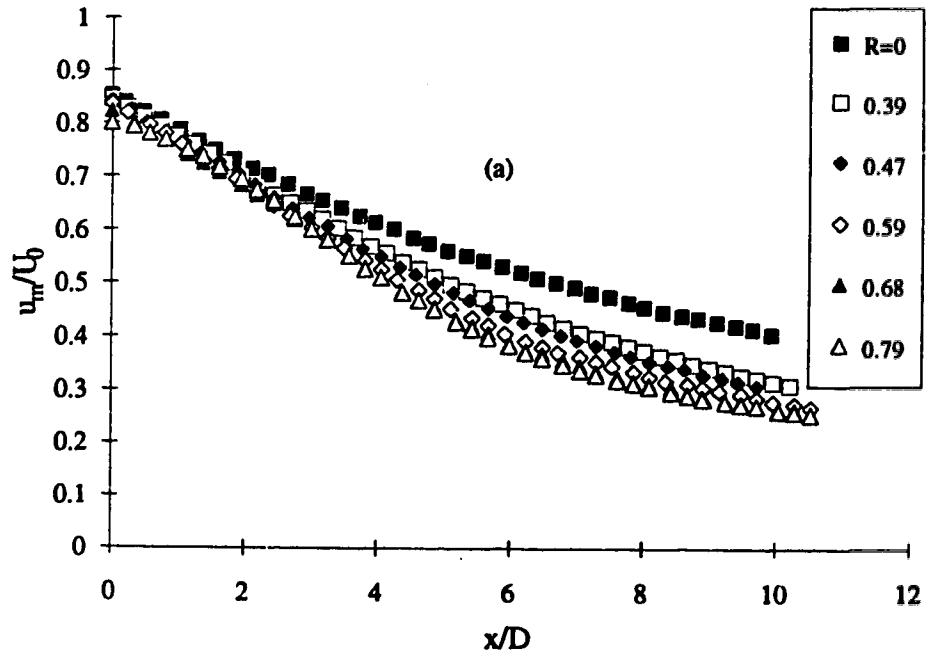


Fig. 3-19(a) Velocity scale decay in region 2

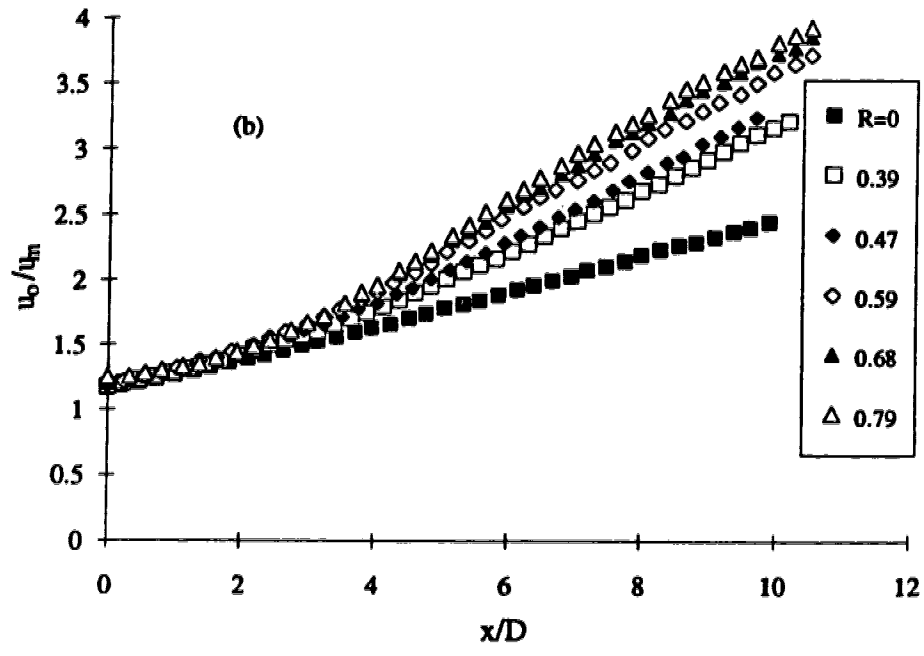


Fig. 3-19(b) Velocity scale decay in region 2

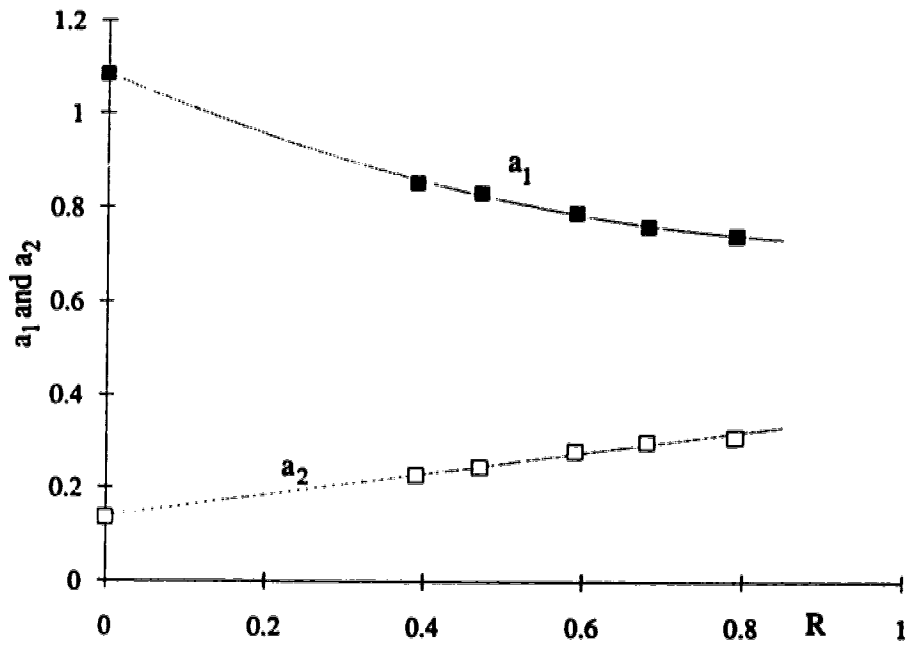


Fig. 3-20 Variation of the coefficients  $a_1$  and  $a_2$  with  $R$

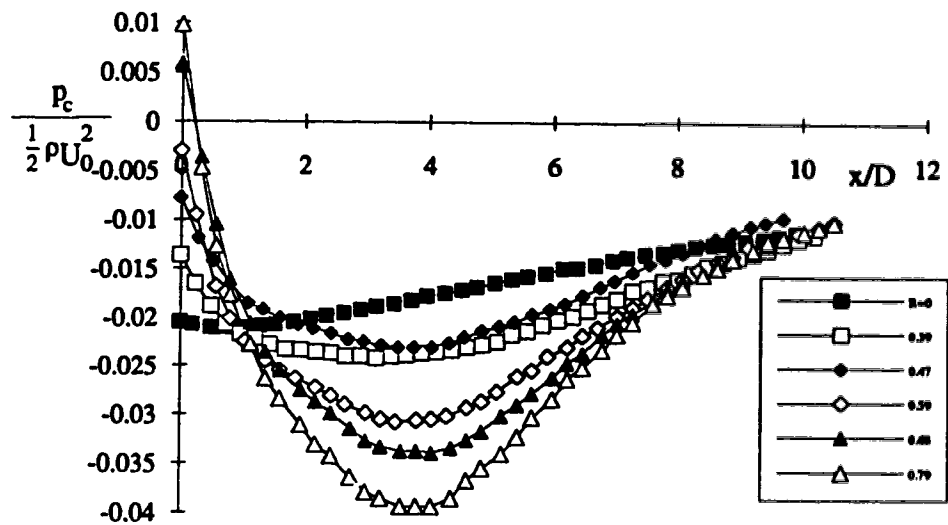


Fig. 3-21 Pressure variation along the axis of the jet in region 2

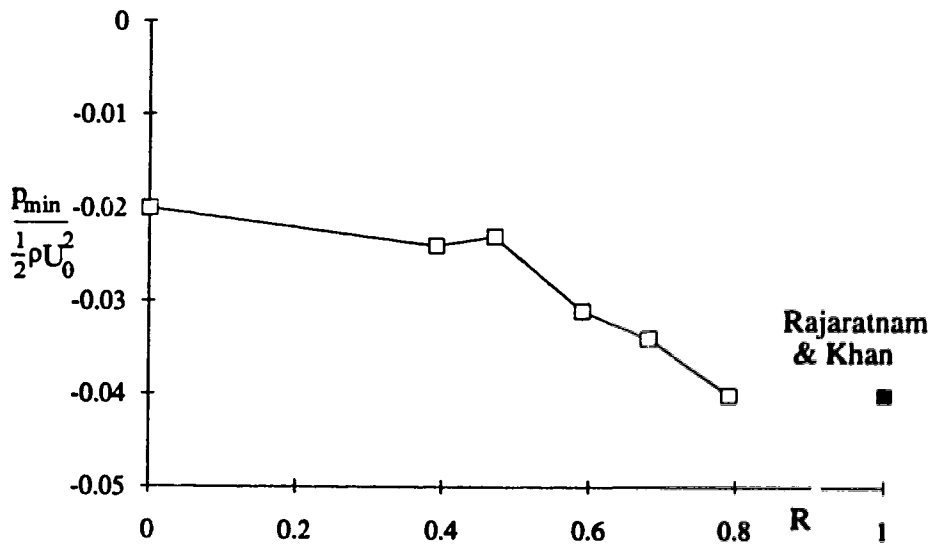


Fig. 3-22 Correlation of the minimum pressure along the jet axis in region 2 with R

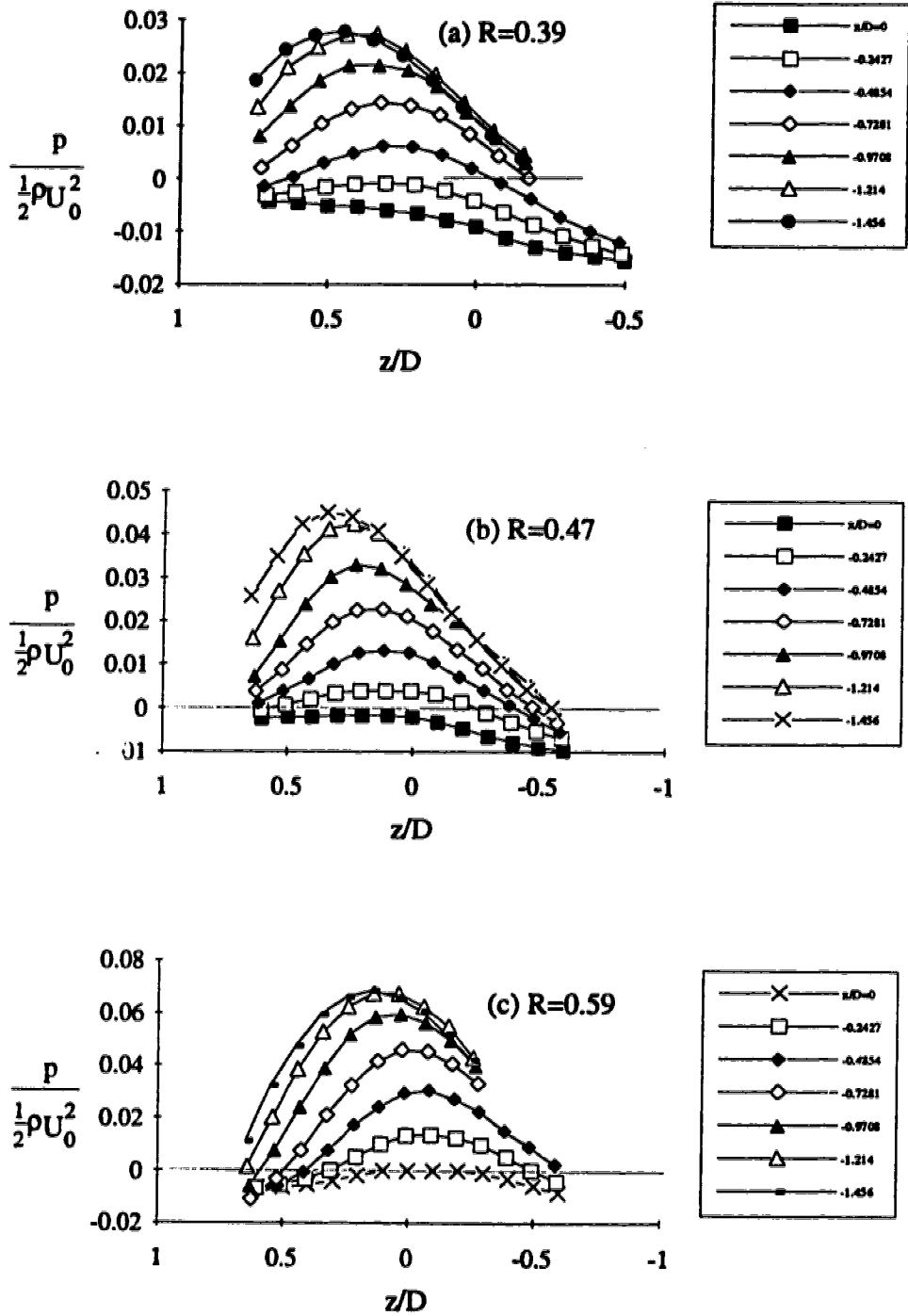


Fig. 3-23(a-c) Pressure field in the reverse flow region

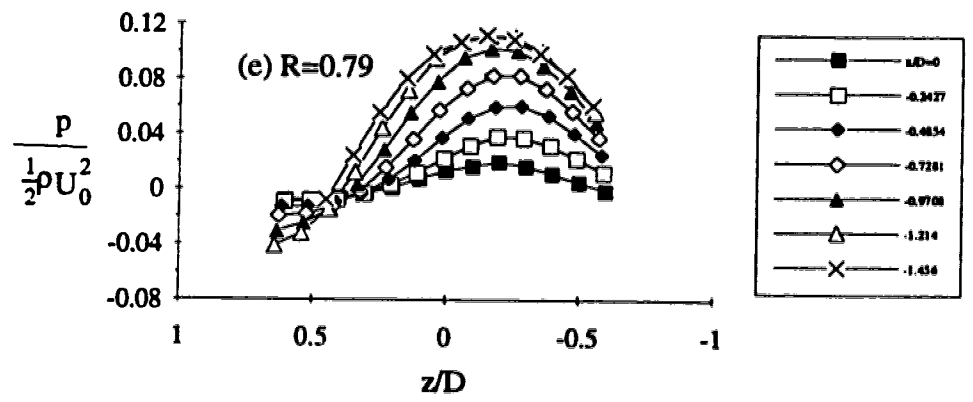
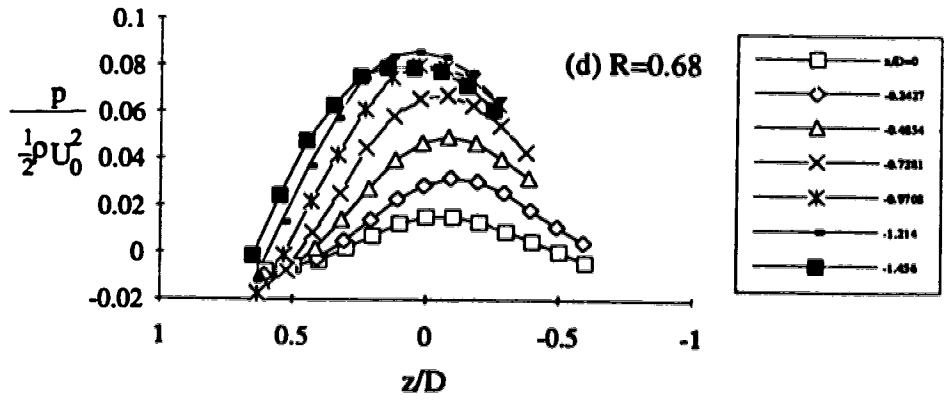


Fig. 3-23(d-e) Pressure field in the reverse flow region

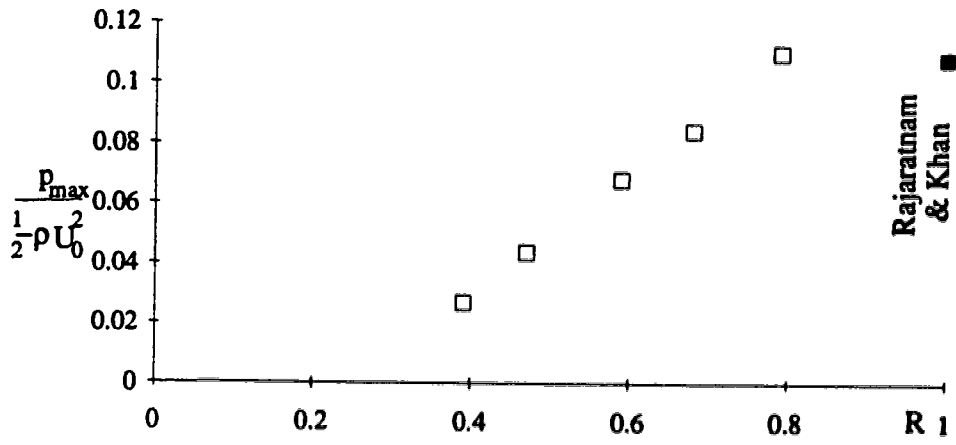


Fig. 3-24 Variation of the maximum pressure with R

Rajaratnam  
& Khan

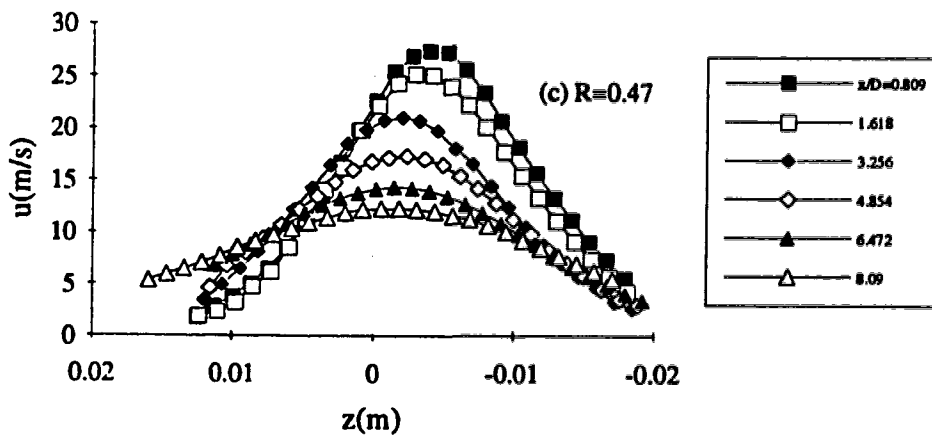
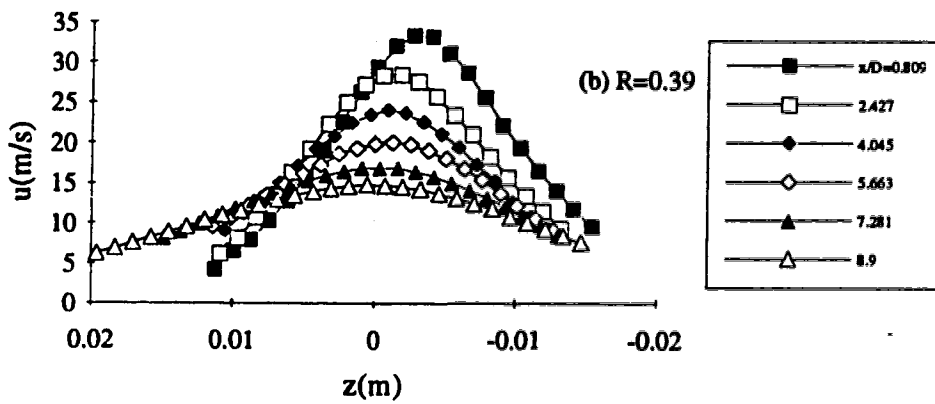
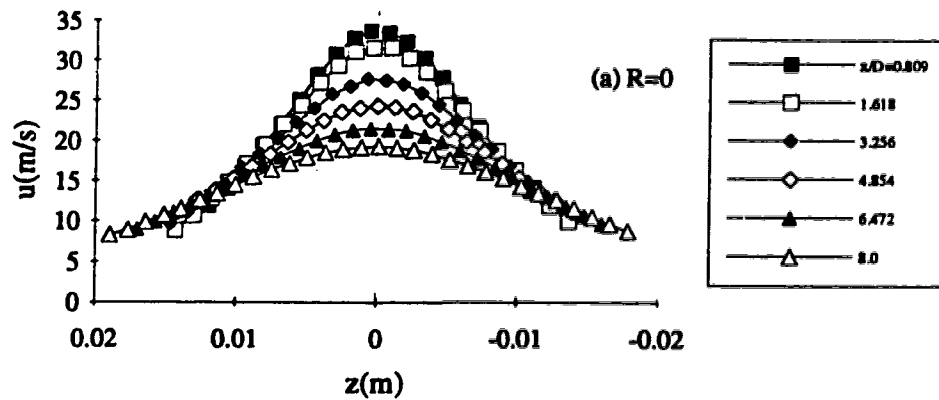


Fig. 3-25(a-c) Transverse velocity profiles in region 2



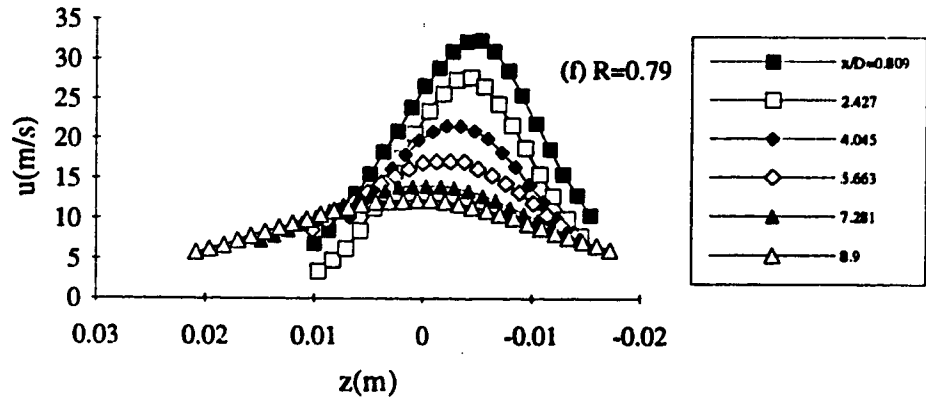
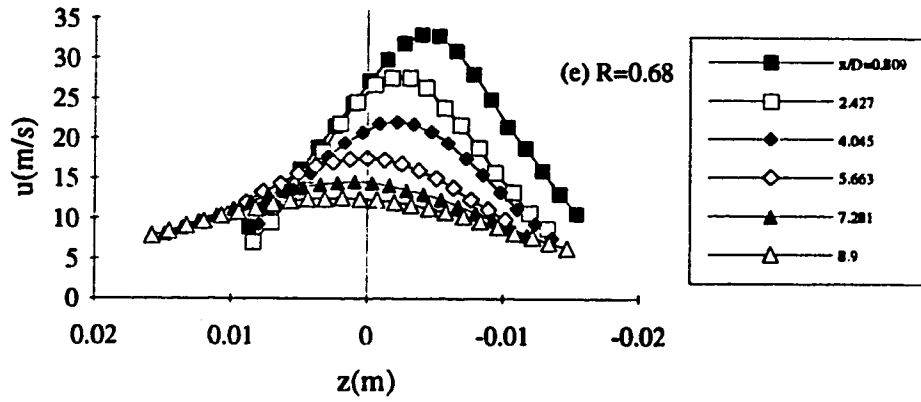
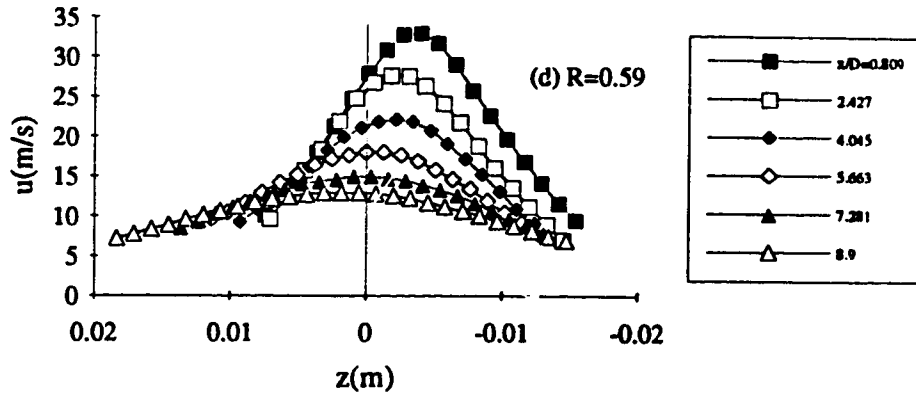


Fig. 3-25(d-f) Transverse velocity profiles in region 2

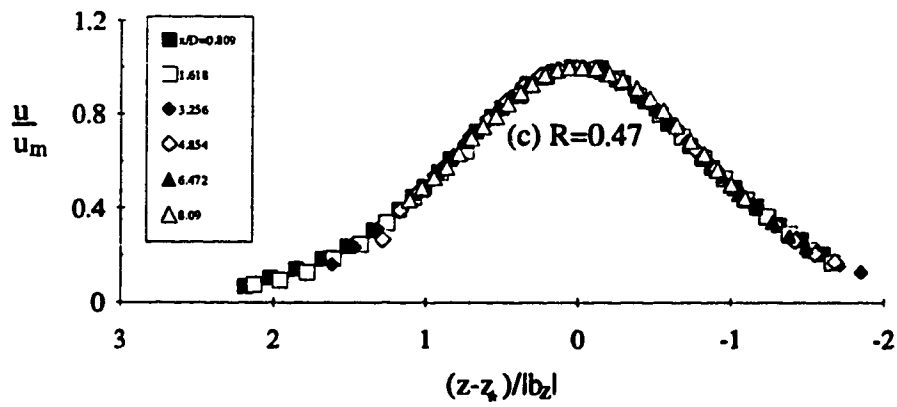
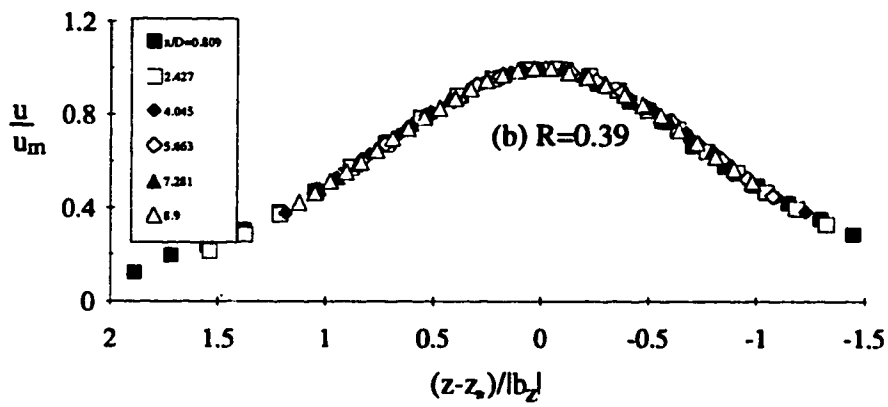
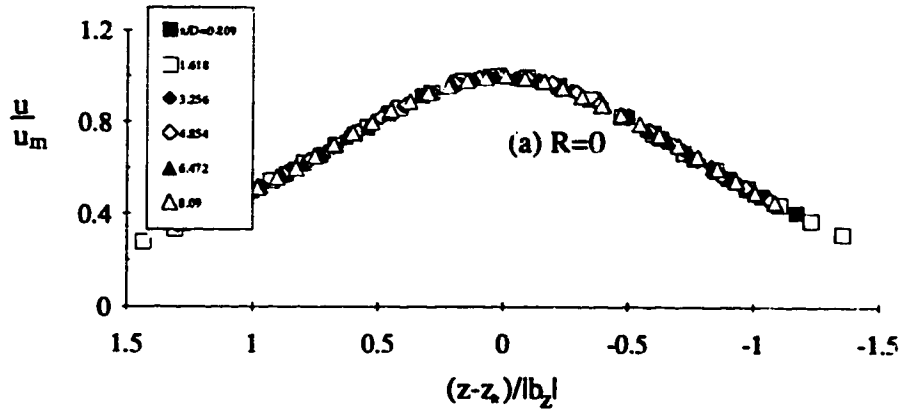


Fig. 3-26(a-c) Dimensionless transverse velocity profiles in region 2

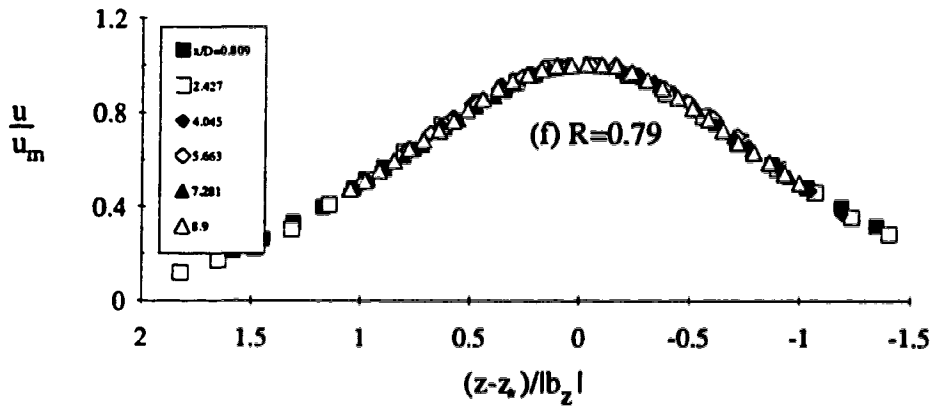
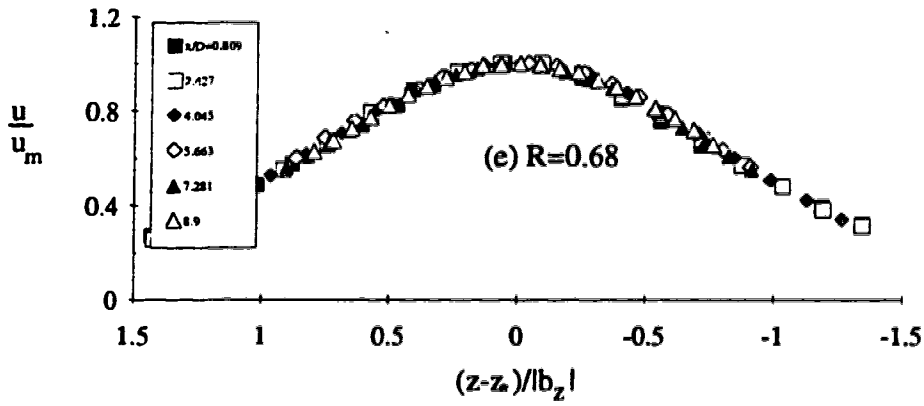
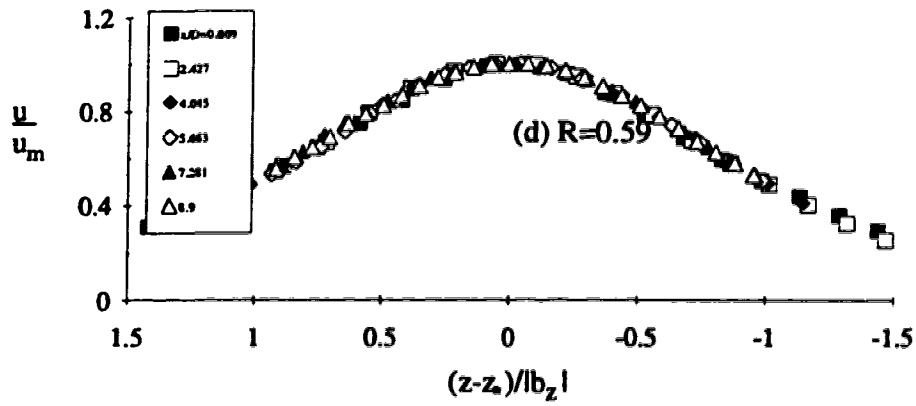


Fig. 3-26(d-f) Dimensionless transverse velocity profiles in region 2

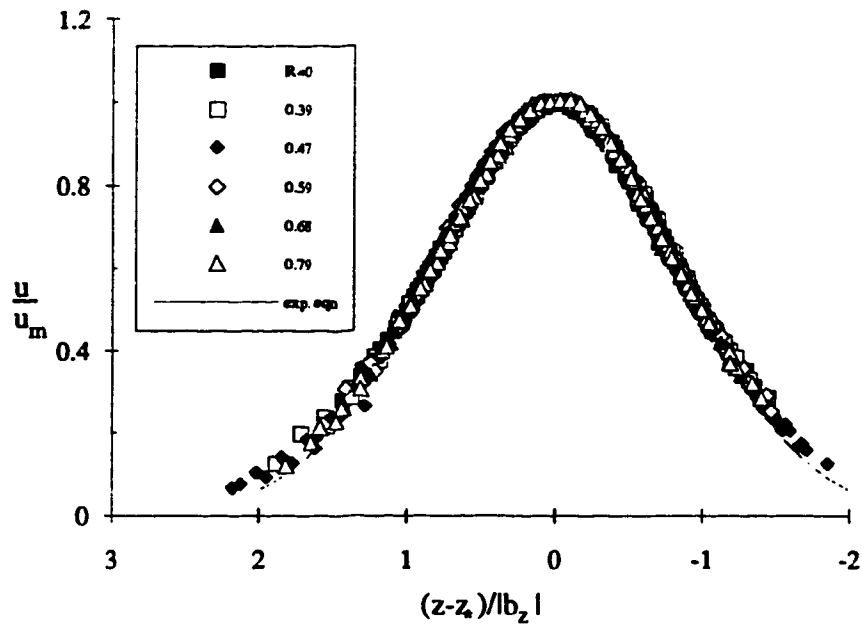


Fig. 3-27 Consolidated dimensionless transverse velocity profiles in region 2

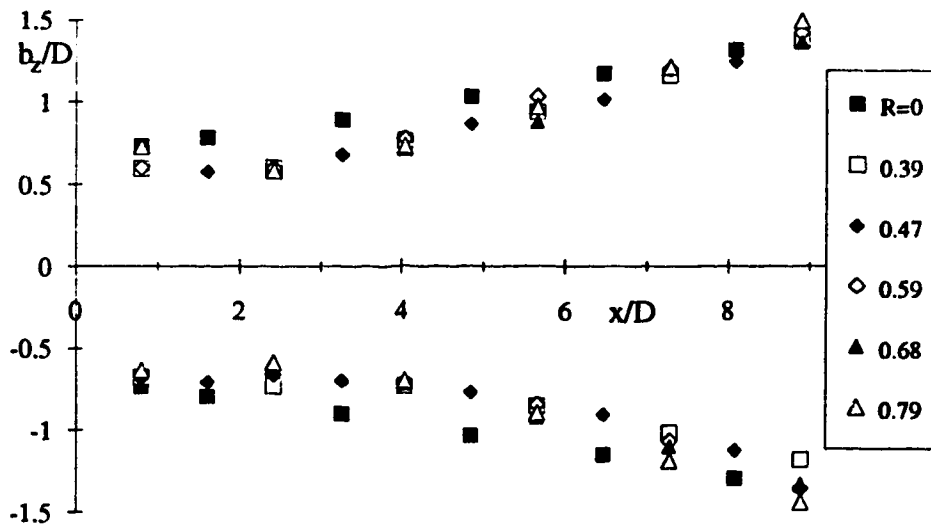


Fig. 3-28 Variation of the length scale  $b_z$  with the distance from intersection point

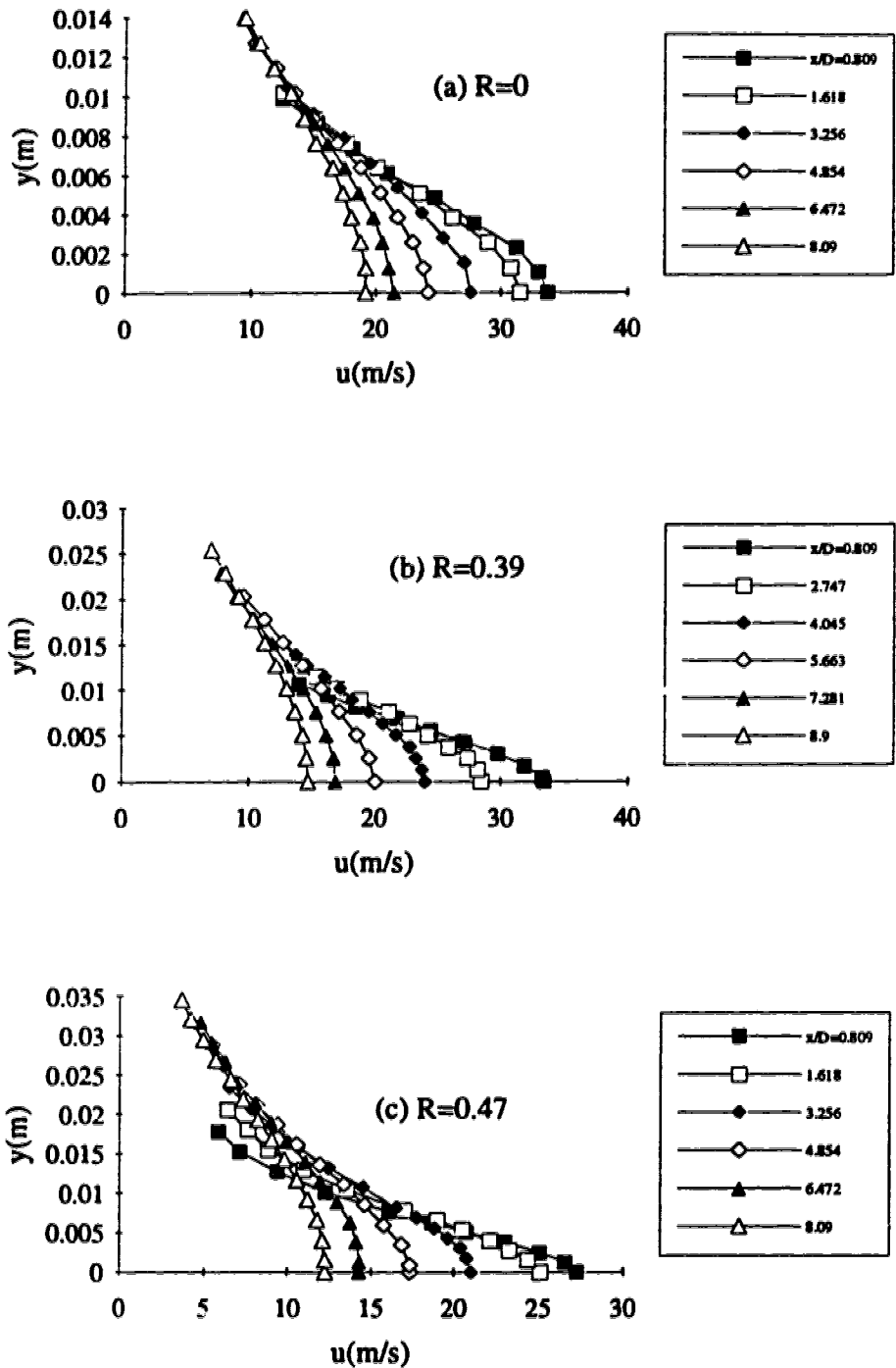


Fig. 3-29(a-c) Vertical velocity profiles in region 2

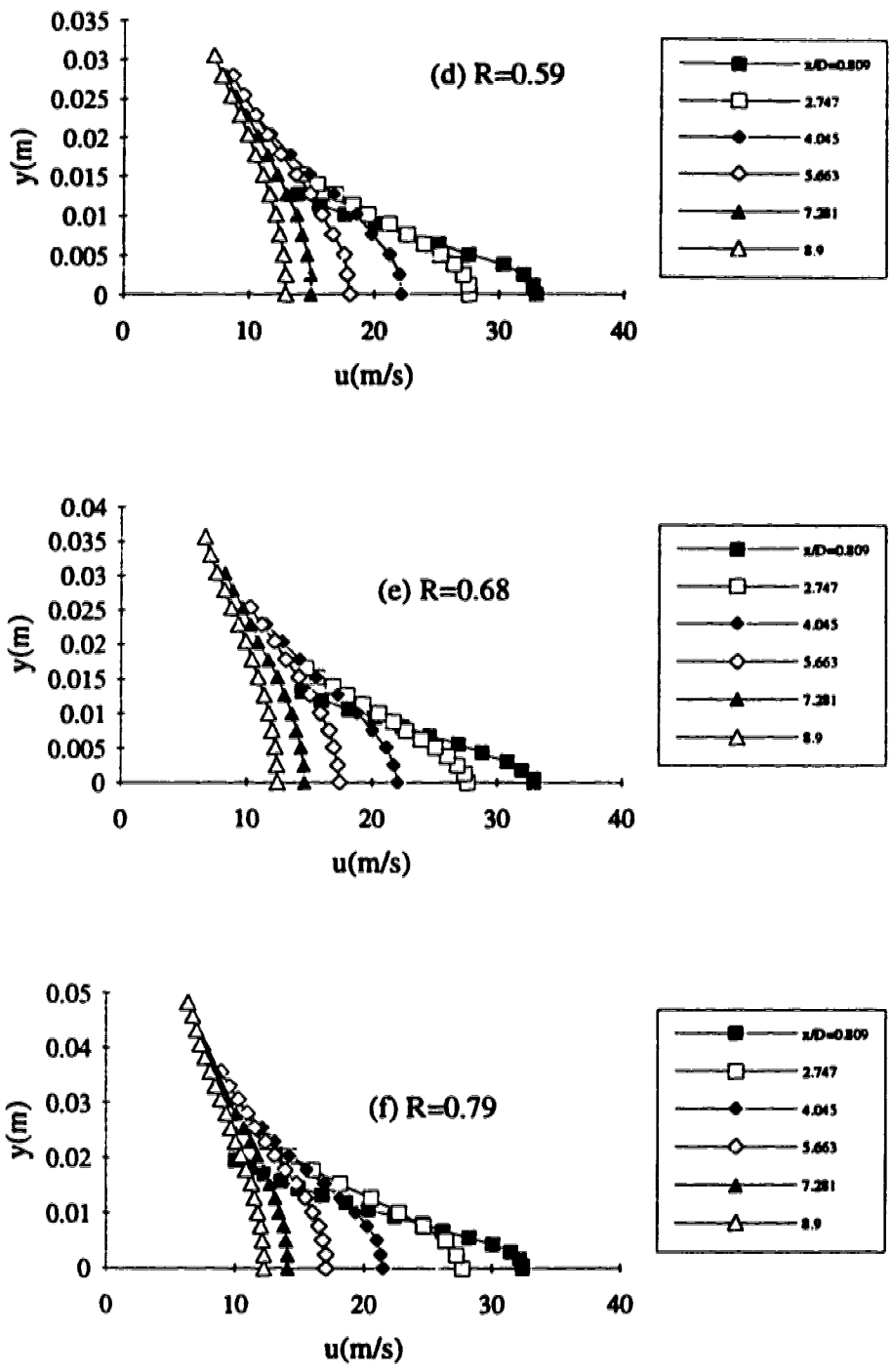


Fig. 3-29(d-f) Vertical velocity profiles in region 2

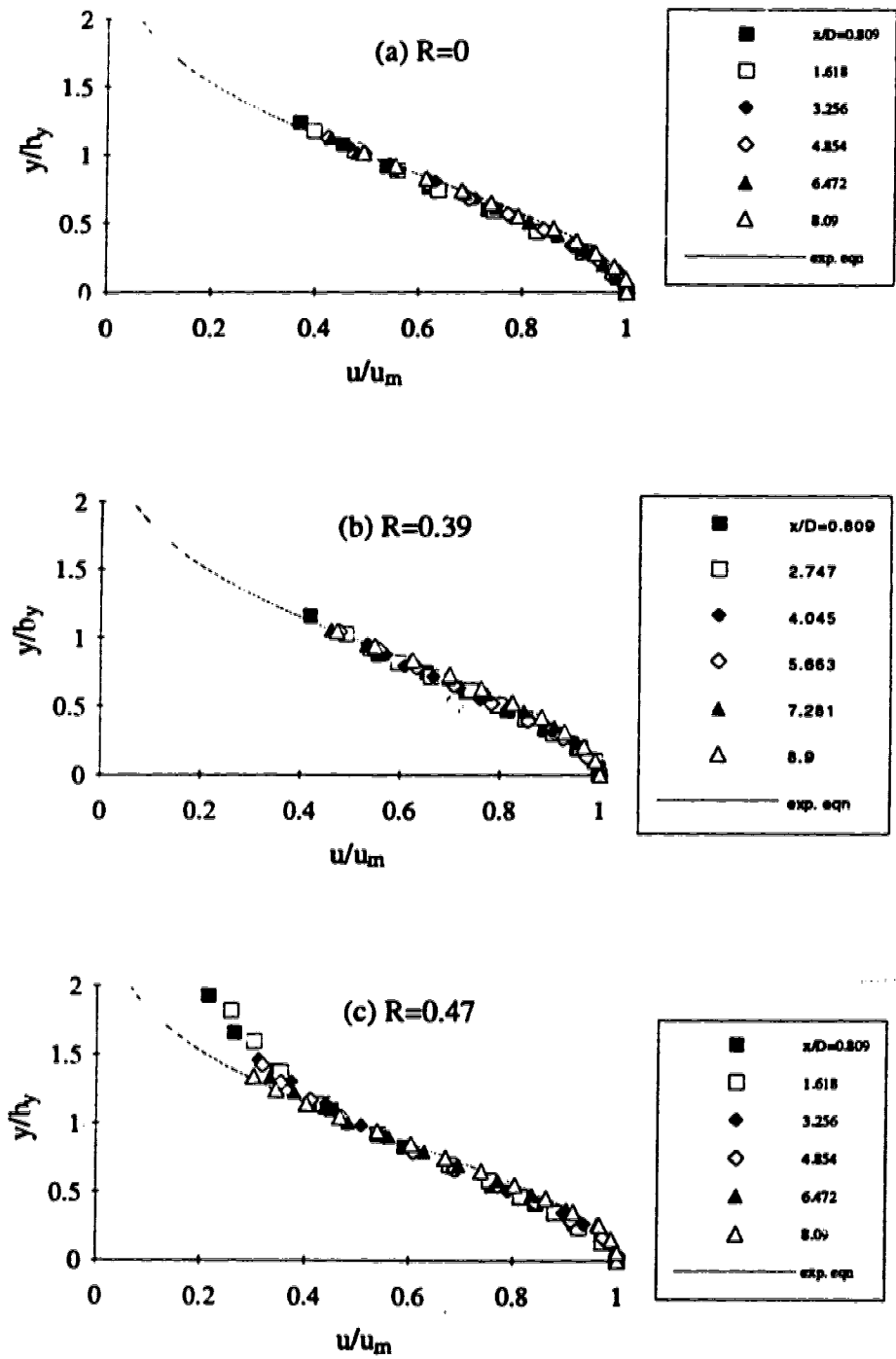


Fig. 3-30(a-c) Dimensionless vertical velocity profiles in region 2

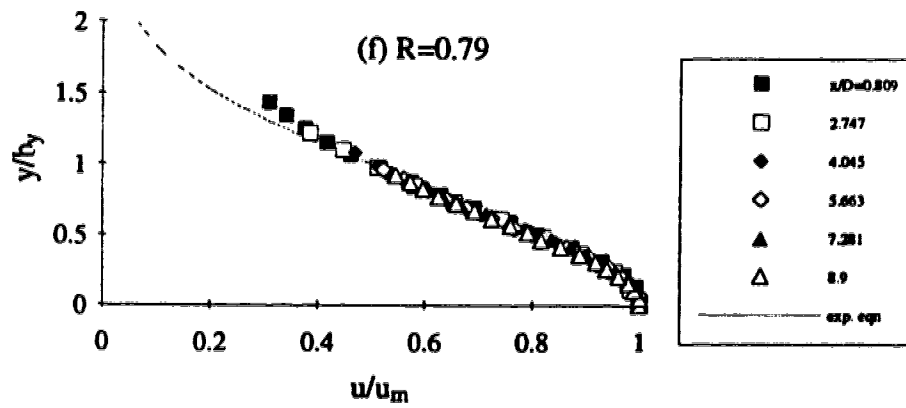
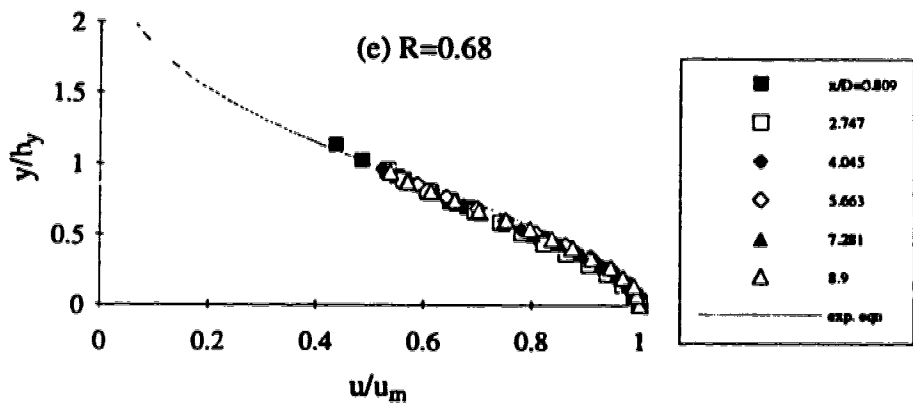
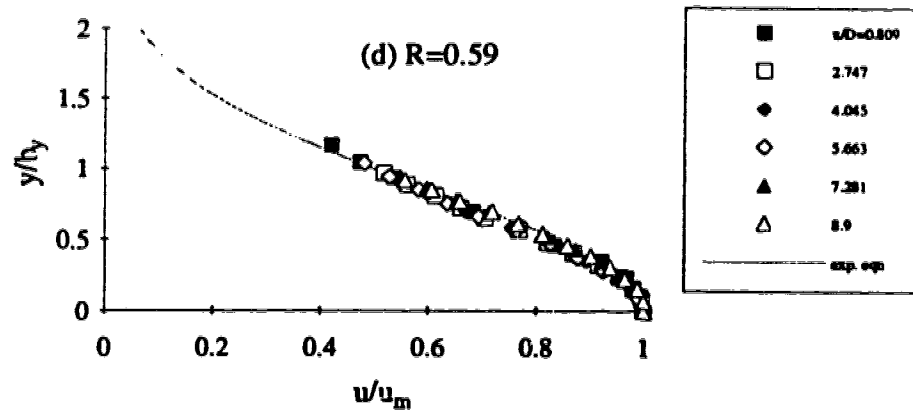


Fig. 3-30(d-f) Dimensionless vertical velocity profiles in region 2



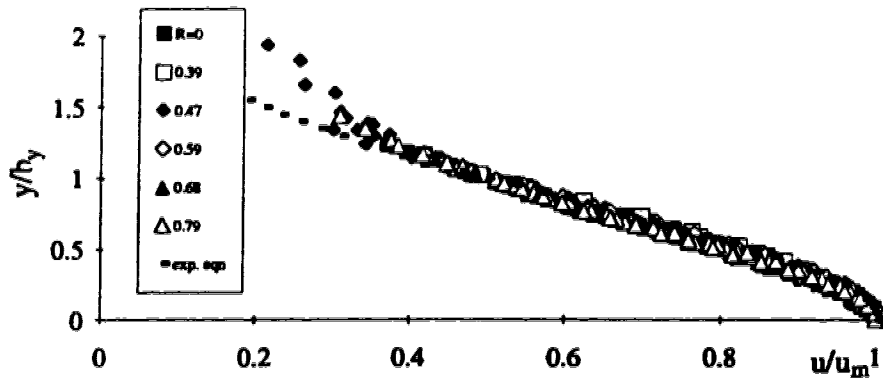


Fig. 3-31 Consolidated plot for all the vertical velocity profile data in region 2

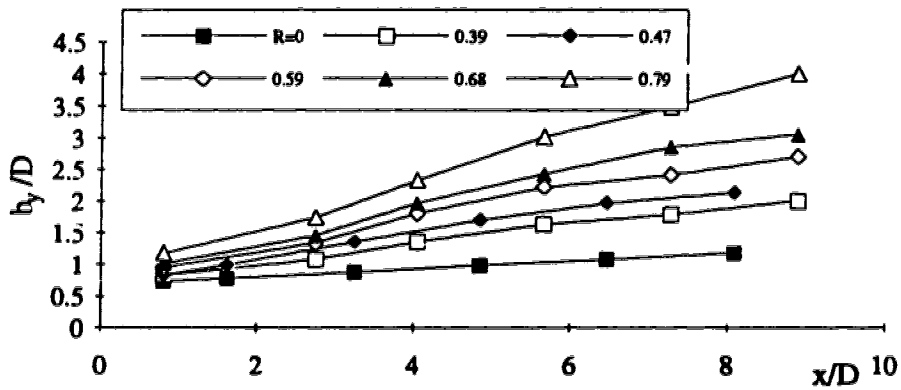


Fig. 3-32 Growth of the vertical length scales of the jet in region 2

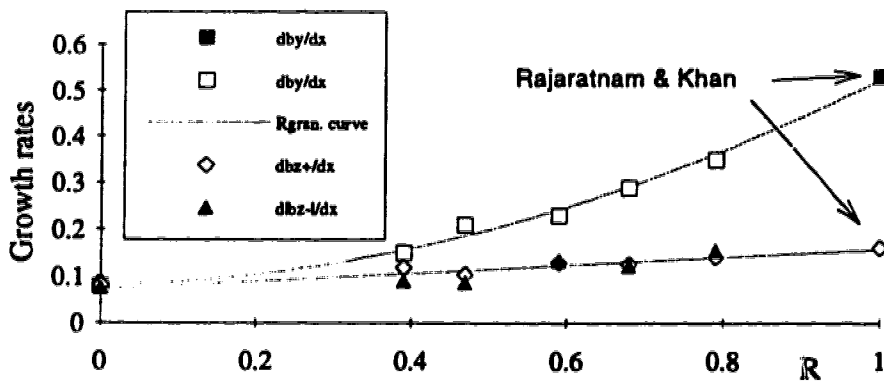


Fig. 3-33 Variation of the length scale growth rates in region 2 with R

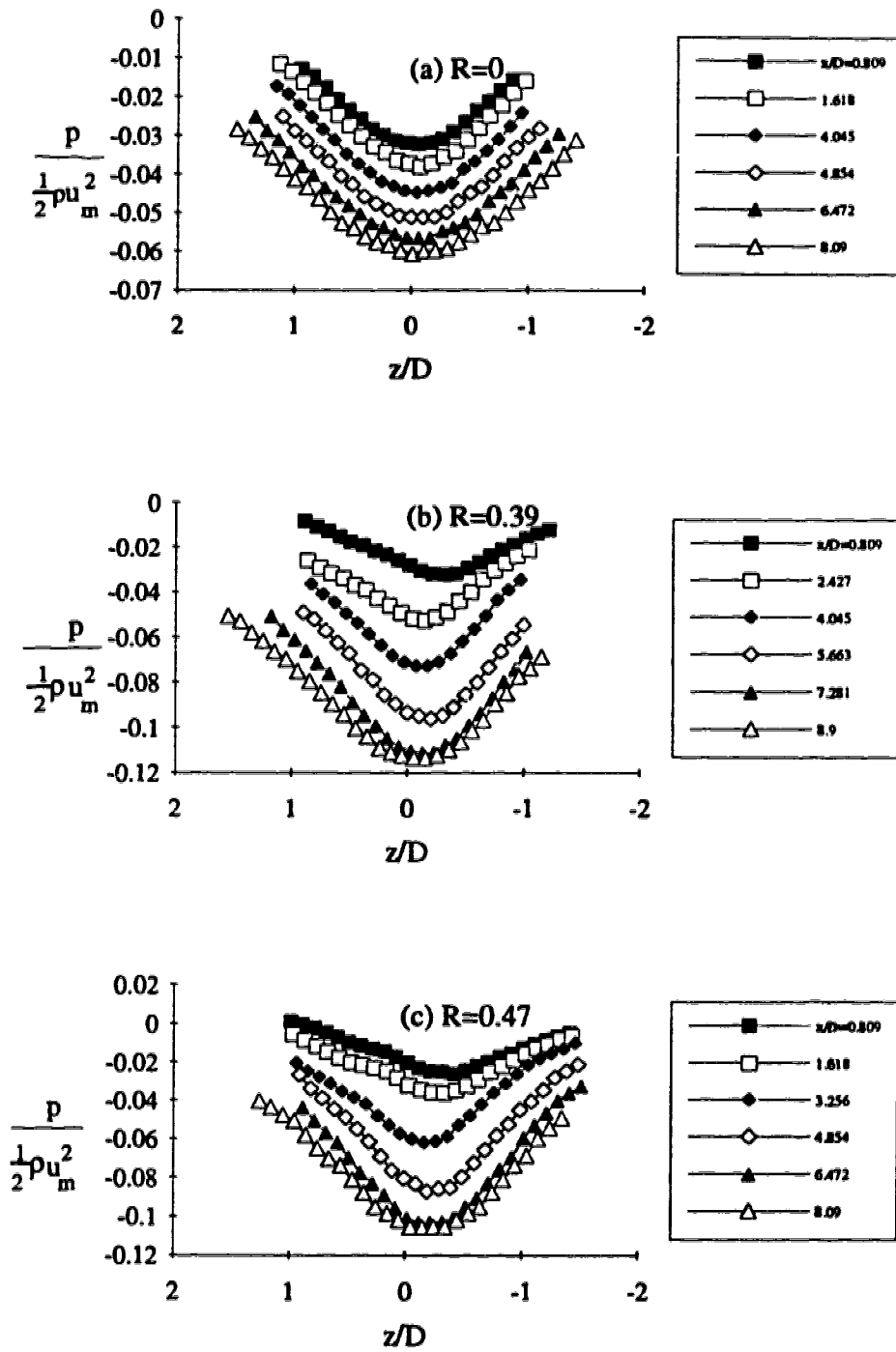


Fig. 3-34(a-c) Transverse pressure profiles in region 2

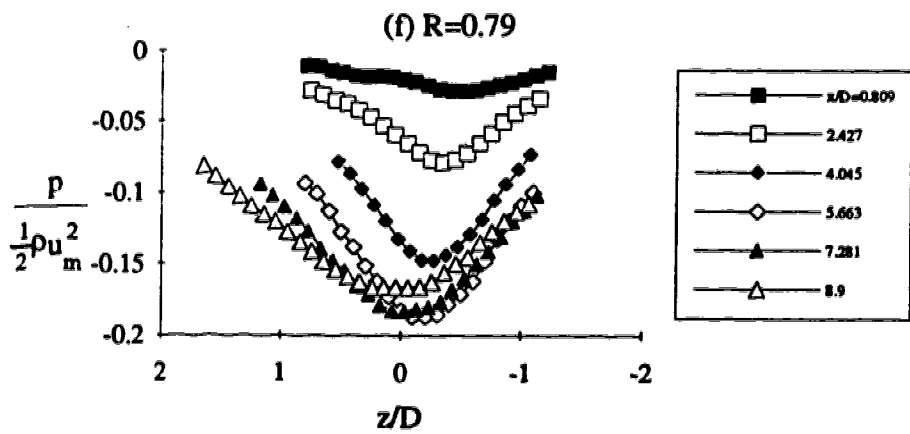
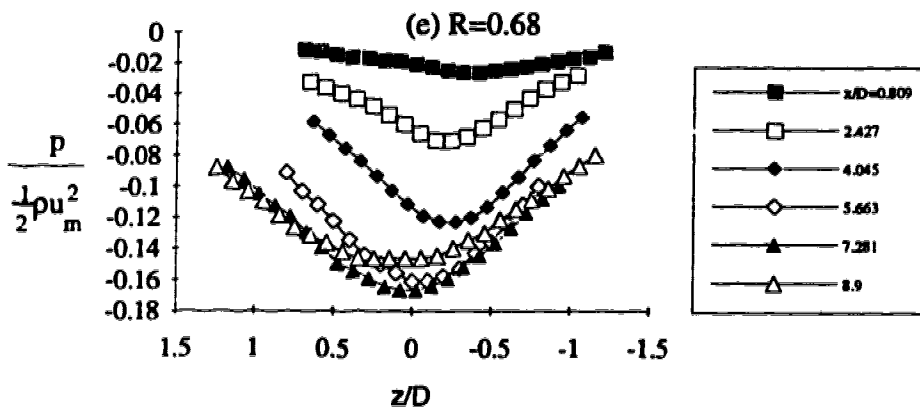
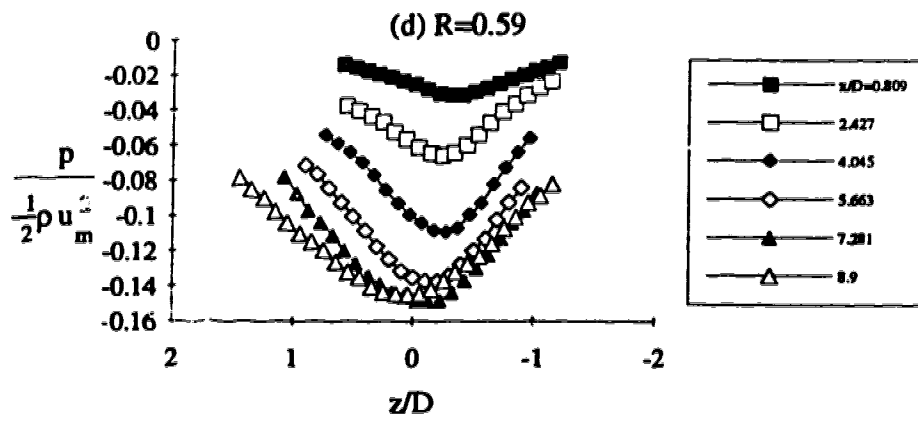


Fig. 3-34(d-f) Transverse pressure profiles in region 2

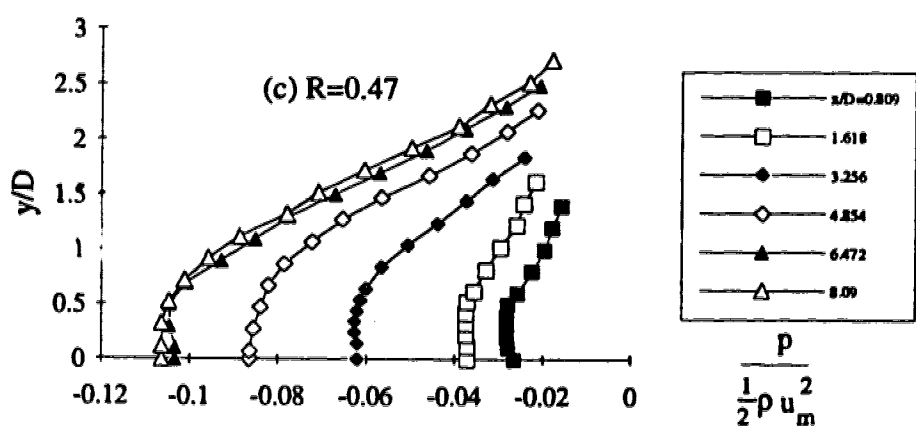
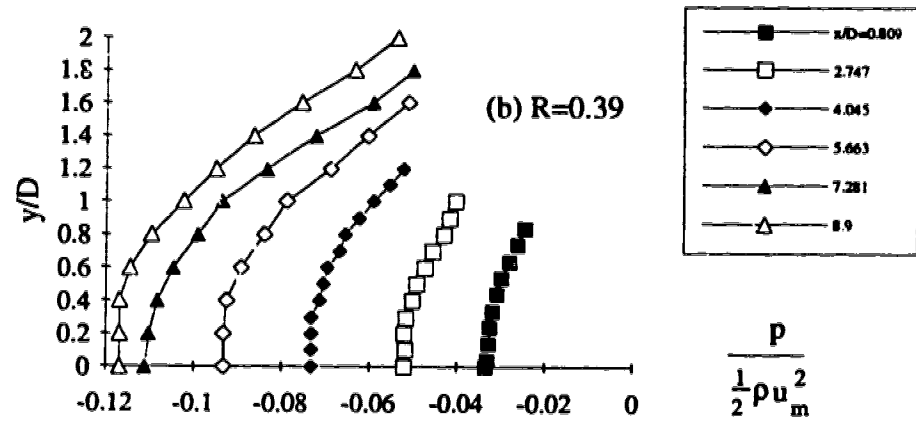
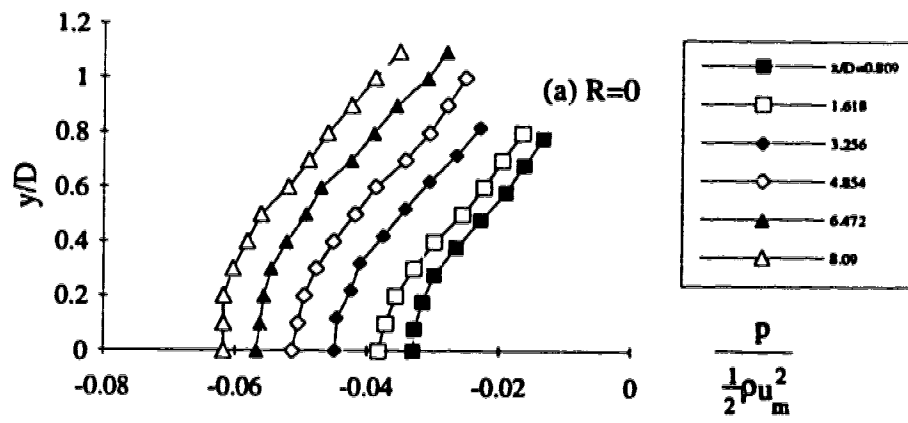


Fig. 3-35(a-c) Vertical pressure profiles in region 2

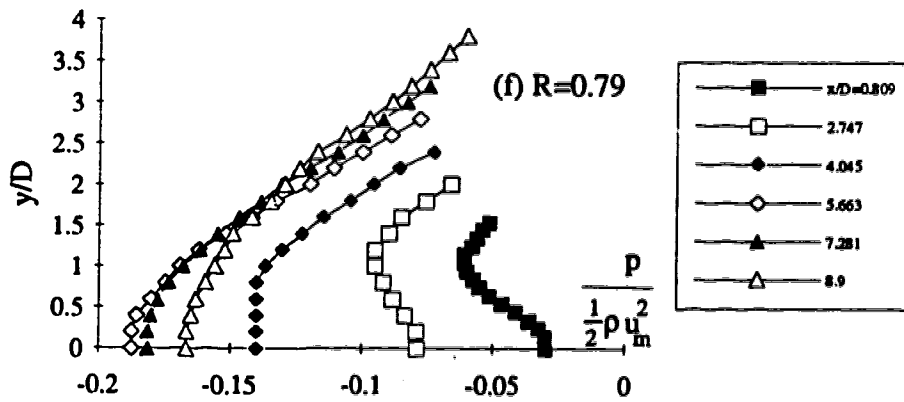
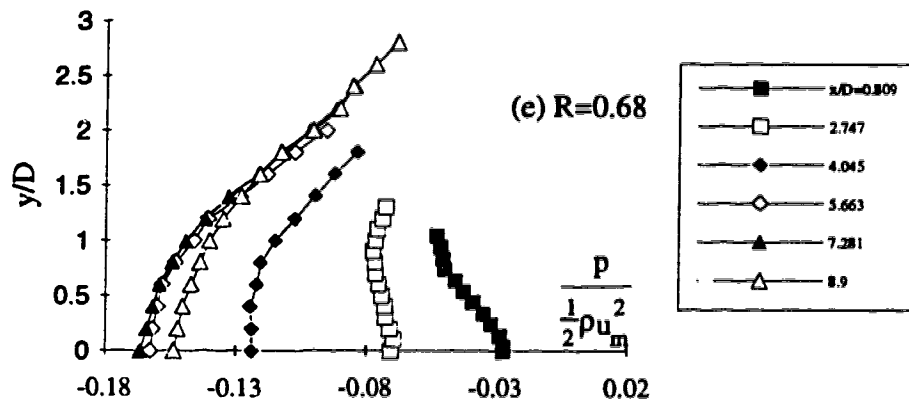
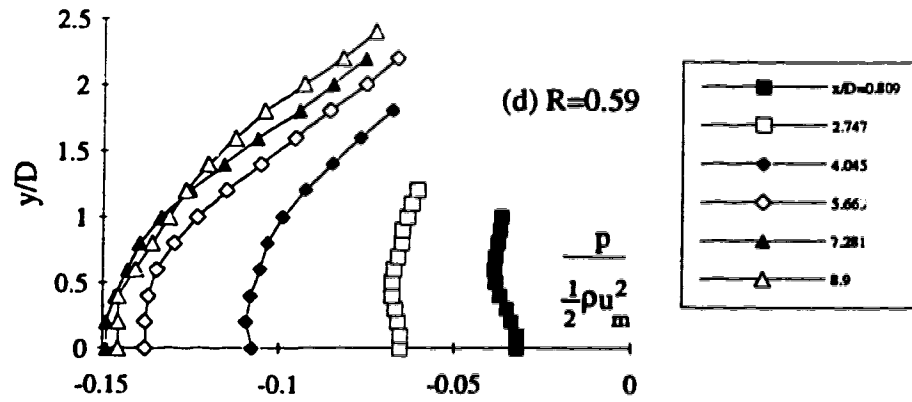


Fig. 3-35(d-f) Vertical pressure profiles in region 2

Table 3-2. Velocity and pressure scale data in region 1

R=0		R=0.39		R=0.47		R=0.59		R=0.68		R=0.79		
$\frac{x_1}{D}$	$\frac{P_c}{\frac{1}{2}\rho U_0^2}$	$\frac{x_1}{D}$	$\frac{P_c}{\frac{1}{2}\rho U_0^2}$	$\frac{x_1}{D}$	$\frac{P_c}{\frac{1}{2}\rho U_0^2}$	$\frac{x_1}{D}$	$\frac{P_c}{\frac{1}{2}\rho U_0^2}$	$\frac{x_1}{D}$	$\frac{P_c}{\frac{1}{2}\rho U_0^2}$	$\frac{x_1}{D}$	$\frac{P_c}{\frac{1}{2}\rho U_0^2}$	
0.512	0.0086	0.512	0.0080	1.024	0.0056	1.000	0.512	0.0089	0.998	0.512	0.0083	0.996
1.321	0.0053	1.321	0.0053	1.839	0.0026	0.999	1.321	0.0053	0.999	1.321	0.0053	0.998
2.130	0.0030	2.130	0.0030	2.655	0.0000	1.000	2.130	0.0028	1.001	2.130	0.0030	0.999
2.939	0.0003	2.939	0.0003	3.470	-0.0026	1.001	2.939	0.0000	1.002	2.939	0.0004	0.999
3.748	-0.0031	3.748	-0.0027	4.286	-0.0058	0.999	3.748	-0.0027	1.000	3.748	-0.0027	0.997
4.557	-0.0068	4.557	-0.0056	5.101	-0.0079	0.990	4.557	-0.0062	0.994	4.557	-0.0062	0.997
4.800	-0.0083	4.800	-0.0068	5.509	-0.0075	0.977	4.800	-0.0074	0.991	4.800	-0.0065	0.992
5.042	-0.0093	5.042	-0.0074	5.917	-0.0051	0.960	5.042	-0.0077	0.988	5.042	-0.0065	0.989
5.285	-0.0104	5.285	-0.0077	6.161	-0.0032	0.949	5.285	-0.0080	0.980	5.285	-0.0053	0.985
5.528	-0.0118	5.528	-0.0075	6.406	-0.0021	0.932	5.528	-0.0068	0.973	5.528	-0.0027	0.976
5.771	-0.0133	5.771	-0.0071	6.651	-0.0013	0.921	5.771	-0.0047	0.960	5.771	0.0003	0.961
6.013	-0.0145	6.013	-0.0061	6.895	-0.0017	0.907	6.013	-0.0018	0.947	6.013	0.0052	0.947
6.256	-0.0152	6.256	-0.0053	7.140	-0.0038	0.895	6.256	0.0012	0.932	6.256	0.0098	0.936
6.499	-0.0166	6.499	-0.0053	7.385	-0.0085	0.882	6.499	0.0044	0.920	6.499	0.0148	0.921
6.741	-0.0174	6.741	-0.0058	7.629	-0.0132	0.864	6.741	0.0062	0.904	6.741	0.0186	0.903
6.984	-0.0180	6.984	-0.0065	7.874	-0.0175	0.849	6.984	0.0044	0.888	6.984	0.0169	0.888
7.227	-0.0188	7.227	-0.0086				7.227	0.0003	0.879	7.227	0.0104	0.872
7.469	-0.0192	7.469	-0.0118				7.469	-0.0068	0.865	7.469	-0.0003	0.858
7.712	-0.0198	7.712	-0.0154				7.712	-0.0142	0.851	7.712	-0.0148	0.838
7.874	-0.0201	7.874	-0.0172				7.874	-0.0192	0.839	7.874	-0.0237	0.820
												0.807
												0.781

**Table 3-3 Maximum pressure data in region 1**

R	$P_{cm}/\frac{1}{2}\rho U_0^2$
0	-0.016
0.39	-0.0053
0.47	-0.0013
0.59	0.0062
0.68	0.0186
0.79	0.0377
1	0.1

**Table 3-4 Length scale data in region 1**

R	$x_1/D$	$b_{z+}/D$	$b_z/D$	$b_y/D$
0	4.921	0.5906	-0.5906	0.5906
	5.748	0.6102	-0.6102	0.6102
	6.575	0.6299	-0.6299	0.6299
	7.402	0.6614	-0.6614	0.6614
0.39	4.921	0.5906	-0.5906	0.5929
	5.748	0.5984	-0.6142	0.6126
	6.575	0.5984	-0.6417	0.6299
	7.402	0.5906	-0.6693	0.6772
0.47	4.921	0.5906	-0.5906	0.5827
	5.748	0.5906	-0.622	0.6024
	6.575	0.5827	-0.6496	0.6299
	7.402	0.5669	-0.6732	0.6850
0.59	4.921	0.5906	-0.5945	0.5984
	5.748	0.5827	-0.626	0.6142
	6.575	0.5591	-0.6535	0.6457
	7.402	0.5354	-0.685	0.7087
0.68	4.921	0.5906	-0.6024	0.6008
	5.748	0.5787	-0.6299	0.6157
	6.575	0.5472	-0.6654	0.6457
	7.402	0.5276	-0.689	0.7362
0.79	4.921	0.5906	-0.6142	0.5945
	5.748	0.5669	-0.6457	0.6126
	6.575	0.5354	-0.6693	0.6457
	7.402	0.5197	-0.6929	0.7339

Table 3-5. Data for the axis of the jet in region 2

R=0		R=0.39		R=0.47		R=0.59		R=0.68		R=0.79	
x'(cm)	z'(cm)	x'(cm)	z'(cm)	x'(cm)	z'(cm)	x'(cm)	z'(cm)	x'(cm)	z'(cm)	x'(cm)	z'(cm)
0	0	0.149	-0.351	0.176	-0.477	0.139	-0.489	0.105	-0.497	0.103	-0.755
0.222	0.128	0.435	-0.235	0.515	-0.358	0.437	-0.409	0.483	-0.294	0.494	-0.581
0.534	0.308	0.721	-0.12	0.806	-0.257	0.8	-0.182	0.785	-0.236	0.8	-0.544
0.801	0.462	0.957	0.113	1.146	-0.138	1.097	-0.102	1.088	-0.177	1.089	-0.382
1.112	0.642	1.243	0.228	1.442	0.1	1.395	-0.023	1.491	-0.099	1.497	-0.334
1.424	0.822	1.528	0.344	1.733	0.201	1.758	0.205	1.768	0.084	1.786	-0.172
1.691	0.976	1.814	0.459	2.072	0.32	2.056	0.284	2.07	0.143	2.092	-0.136
2.002	1.156	2.1	0.575	2.412	0.438	2.354	0.363	2.474	0.221	2.5	-0.087
2.313	1.336	2.336	0.807	2.703	0.54	2.751	0.469	2.776	0.28	2.807	-0.051
2.58	1.49	2.622	0.922	3.043	0.659	3.049	0.548	3.079	0.338	3.113	-0.015
2.892	1.67	2.908	1.038	3.382	0.777	3.347	0.627	3.483	0.416	3.521	0.034
3.203	1.849	3.194	1.153	3.629	0.998	3.744	0.733	3.785	0.475	3.827	0.07
3.47	2.004	3.48	1.269	3.969	1.116	4.042	0.812	4.088	0.534	4.116	0.232
3.782	2.183	3.766	1.384	4.309	1.235	4.34	0.891	4.465	0.736	4.524	0.28
4.093	2.363	4.051	1.5	4.6	1.337	4.702	1.119	4.768	0.795	4.83	0.317
4.36	2.517	4.337	1.615	4.939	1.455	5	1.198	5.07	0.854	5.136	0.353
4.671	2.697	4.623	1.731	5.279	1.574	5.298	1.277	5.474	0.932	5.545	0.401
4.983	2.877	4.909	1.846	5.526	1.794	5.696	1.383	5.776	0.99	5.851	0.438
5.25	3.031	5.195	1.962	5.866	1.913	5.994	1.462	6.079	1.049	6.14	0.6
5.561	3.211	5.481	2.077	6.205	2.031	6.292	1.542	6.456	1.252	6.548	0.648
5.873	3.391	5.766	2.193	6.496	2.133	6.654	1.769	6.759	1.31	6.854	0.684
6.14	3.545	6.052	2.308	6.836	2.252	6.952	1.849	7.062	1.369	7.16	0.721
6.451	3.725	6.288	2.541	7.176	2.37	7.25	1.928	7.465	1.447	7.568	0.769
6.762	3.904	6.574	2.656	7.467	2.472	7.647	2.033	7.768	1.506	7.857	0.931
7.029	4.059	6.86	2.771	7.806	2.59	7.945	2.113	8.07	1.564	8.164	0.968
7.341	4.238	7.146	2.887	8.102	2.828	8.243	2.192	8.448	1.767	8.572	1.016
7.652	4.418	7.432	3.002	8.393	2.93	8.64	2.297	8.75	1.826	8.878	1.052
7.919	4.572	7.718	3.118	8.733	3.048	8.903	2.499	9.053	1.884	9.184	1.088
8.231	4.752	8.003	3.233	9.072	3.167	9.201	2.578	9.456	1.962	9.575	1.263
8.542	4.932	8.289	3.349	9.363	3.268	9.599	2.684	9.759	2.021	9.881	1.299
8.809	5.086	8.526	3.581	9.703	3.387	9.897	2.763	10.062	2.08	10.187	1.335
9.12	5.266	8.811	3.697	10.042	3.505	10.194	2.842	10.439	2.282	10.595	1.384
9.432	5.446	9.097	3.812	10.29	3.726	10.592	2.948	10.741	2.341	10.902	1.42
9.699	5.6	9.383	3.928	10.629	3.845	10.855	3.149	11.044	2.4	11.208	1.456
10.01	5.78	9.669	4.043	10.969	3.963	11.153	3.228	11.448	2.478	11.616	1.505
10.322	5.959	9.955	4.159	11.26	4.065	11.55	3.334	11.75	2.536	11.922	1.541
10.589	6.113	10.241	4.274	11.599	4.183	11.848	3.413	12.026	2.719	12.228	1.577
10.9	6.293	10.477	4.506			12.146	3.492	12.43	2.798	12.619	1.751
		10.763	4.622			12.543	3.598	12.733	2.856	12.925	1.788
		11.048	4.737			12.841	3.677	13.035	2.915	13.231	1.824
		11.334	4.853								
		11.62	4.968								
		11.906	5.084								



Table 3-6 Velocity and pressure scale data in region 2

R=0			R=0.39			R=0.47		
$\frac{x}{D}$	$\frac{P_c}{\frac{1}{2}\rho U_0^2}$	$\frac{u_m}{U_0}$	$\frac{x}{D}$	$\frac{P_c}{\frac{1}{2}\rho U_0^2}$	$\frac{u_m}{U_0}$	$\frac{x}{D}$	$\frac{P_c}{\frac{1}{2}\rho U_0^2}$	$\frac{u_m}{U_0}$
0.000	-0.0204	0.854	0.000	-0.0136	0.847	0.000	-0.0078	0.843
0.202	-0.0207	0.840	0.243	-0.0166	0.831	0.283	-0.0119	0.826
0.485	-0.0210	0.821	0.485	-0.0188	0.813	0.526	-0.0143	0.801
0.728	-0.0210	0.806	0.728	-0.0207	0.796	0.809	-0.0166	0.779
1.011	-0.0210	0.788	0.971	-0.0216	0.776	1.092	-0.0186	0.763
1.294	-0.0209	0.766	1.214	-0.0222	0.760	1.335	-0.0192	0.743
1.537	-0.0207	0.750	1.456	-0.0228	0.742	1.618	-0.0201	0.725
1.820	-0.0204	0.733	1.699	-0.0232	0.725	1.901	-0.0207	0.705
2.103	-0.0201	0.716	1.942	-0.0234	0.703	2.144	-0.0212	0.684
2.346	-0.0198	0.704	2.184	-0.0235	0.681	2.427	-0.0216	0.660
2.629	-0.0195	0.687	2.427	-0.0237	0.665	2.710	-0.0222	0.640
2.913	-0.0192	0.667	2.670	-0.0240	0.651	2.953	-0.0225	0.623
3.155	-0.0188	0.656	2.913	-0.0240	0.635	3.236	-0.0229	0.606
3.438	-0.0186	0.641	3.155	-0.0241	0.621	3.519	-0.0231	0.583
3.722	-0.0182	0.627	3.398	-0.0240	0.603	3.762	-0.0231	0.565
3.964	-0.0178	0.614	3.641	-0.0238	0.585	4.045	-0.0231	0.550
4.247	-0.0175	0.602	3.883	-0.0237	0.571	4.328	-0.0227	0.530
4.531	-0.0172	0.586	4.126	-0.0235	0.558	4.571	-0.0220	0.516
4.773	-0.0169	0.576	4.369	-0.0234	0.541	4.854	-0.0214	0.500
5.056	-0.0164	0.561	4.611	-0.0231	0.527	5.137	-0.0210	0.483
5.340	-0.0160	0.553	4.854	-0.0228	0.512	5.380	-0.0205	0.468
5.582	-0.0157	0.542	5.097	-0.0225	0.497	5.663	-0.0197	0.454
5.865	-0.0154	0.531	5.340	-0.0217	0.485	5.946	-0.0191	0.439
6.149	-0.0149	0.521	5.582	-0.0213	0.473	6.189	-0.0186	0.427
6.391	-0.0148	0.511	5.825	-0.0207	0.462	6.472	-0.0177	0.416
6.675	-0.0145	0.502	6.068	-0.0203	0.450	6.755	-0.0168	0.403
6.958	-0.0140	0.492	6.310	-0.0198	0.440	6.998	-0.0162	0.394
7.200	-0.0138	0.483	6.553	-0.0192	0.427	7.281	-0.0153	0.385
7.484	-0.0135	0.475	6.796	-0.0186	0.418	7.564	-0.0145	0.372
7.767	-0.0133	0.466	7.039	-0.0180	0.407	7.807	-0.0140	0.363
8.009	-0.0130	0.457	7.281	-0.0172	0.399	8.090	-0.0134	0.355
8.293	-0.0127	0.449	7.524	-0.0169	0.391	8.373	-0.0125	0.346
8.576	-0.0124	0.441	7.767	-0.0163	0.383	8.616	-0.0119	0.340
8.818	-0.0123	0.436	8.009	-0.0160	0.373	8.899	-0.0112	0.329
9.102	-0.0120	0.429	8.252	-0.0154	0.366	9.183	-0.0106	0.323
9.385	-0.0118	0.422	8.495	-0.0146	0.357	9.425	-0.0102	0.316
9.627	-0.0115	0.416	8.738	-0.0142	0.349	9.708	-0.0097	0.308
9.911	-0.0112	0.408	8.980	-0.0138	0.342			
			9.223	-0.0133	0.335			
			9.466	-0.0129	0.328			
			9.708	-0.0123	0.321			
			9.951	-0.0118	0.316			
			10.194	-0.0114	0.311			

Table 3-6 (continued) Velocity and pressure scale data in region 2

R=0.59			R=0.68			R=0.79		
$\frac{x}{D}$	$\frac{P_c}{\frac{1}{2}\rho U_0^2}$	$\frac{u_m}{U_0}$	$\frac{x}{D}$	$\frac{P_c}{\frac{1}{2}\rho U_0^2}$	$\frac{u_m}{U_0}$	$\frac{x}{D}$	$\frac{P_c}{\frac{1}{2}\rho U_0^2}$	$\frac{u_m}{U_0}$
0.000	-0.0030	0.838	0.000	0.0059	0.824	0.000	0.0098	0.801
0.243	-0.0095	0.820	0.324	-0.0035	0.800	0.324	-0.0047	0.794
0.566	-0.0169	0.797	0.566	-0.0104	0.786	0.566	-0.0127	0.780
0.809	-0.0201	0.780	0.809	-0.0160	0.769	0.809	-0.0177	0.769
1.052	-0.0225	0.760	1.133	-0.0206	0.742	1.133	-0.0228	0.751
1.375	-0.0245	0.729	1.375	-0.0235	0.726	1.375	-0.0263	0.738
1.618	-0.0254	0.715	1.618	-0.0254	0.709	1.618	-0.0284	0.717
1.861	-0.0263	0.694	1.942	-0.0275	0.686	1.942	-0.0311	0.695
2.184	-0.0272	0.668	2.184	-0.0287	0.666	2.184	-0.0331	0.675
2.427	-0.0281	0.646	2.427	-0.0299	0.649	2.427	-0.0343	0.654
2.670	-0.0290	0.626	2.751	-0.0314	0.619	2.751	-0.0364	0.623
2.993	-0.0299	0.604	2.993	-0.0327	0.601	2.993	-0.0379	0.600
3.236	-0.0305	0.585	3.236	-0.0333	0.579	3.236	-0.0384	0.582
3.479	-0.0308	0.566	3.560	-0.0337	0.552	3.560	-0.0393	0.550
3.802	-0.0306	0.542	3.802	-0.0337	0.531	3.802	-0.0393	0.526
4.045	-0.0305	0.525	4.045	-0.0339	0.514	4.045	-0.0393	0.510
4.288	-0.0302	0.507	4.369	-0.0334	0.488	4.369	-0.0384	0.483
4.611	-0.0293	0.487	4.611	-0.0325	0.469	4.611	-0.0367	0.468
4.854	-0.0287	0.471	4.854	-0.0316	0.456	4.854	-0.0355	0.450
5.097	-0.0277	0.452	5.178	-0.0300	0.434	5.178	-0.0340	0.428
5.421	-0.0260	0.435	5.421	-0.0290	0.422	5.421	-0.0322	0.414
5.663	-0.0254	0.422	5.663	-0.0278	0.409	5.663	-0.0303	0.398
5.906	-0.0240	0.407	5.987	-0.0262	0.389	5.987	-0.0284	0.384
6.230	-0.0231	0.392	6.230	-0.0247	0.377	6.230	-0.0263	0.372
6.472	-0.0219	0.381	6.472	-0.0237	0.370	6.472	-0.0251	0.361
6.715	-0.0210	0.372	6.796	-0.0217	0.356	6.796	-0.0234	0.349
7.039	-0.0198	0.363	7.039	-0.0206	0.348	7.039	-0.0217	0.338
7.281	-0.0189	0.353	7.281	-0.0195	0.337	7.281	-0.0204	0.329
7.524	-0.0180	0.345	7.605	-0.0183	0.326	7.605	-0.0186	0.320
7.848	-0.0169	0.335	7.848	-0.0170	0.319	7.848	-0.0177	0.314
8.090	-0.0160	0.325	8.090	-0.0163	0.312	8.090	-0.0169	0.307
8.333	-0.0151	0.318	8.414	-0.0154	0.305	8.414	-0.0155	0.297
8.657	-0.0142	0.311	8.657	-0.0143	0.296	8.657	-0.0148	0.289
8.899	-0.0136	0.305	8.899	-0.0136	0.290	8.899	-0.0139	0.285
9.142	-0.0127	0.298	9.223	-0.0130	0.285	9.223	-0.0130	0.278
9.466	-0.0124	0.293	9.466	-0.0124	0.278	9.466	-0.0121	0.274
9.708	-0.0118	0.285	9.708	-0.0115	0.272	9.708	-0.0117	0.270
9.951	-0.0112	0.279	10.032	-0.0109	0.268	10.032	-0.0111	0.262
10.275	-0.0106	0.274	10.275	-0.0105	0.264	10.275	-0.0106	0.259
10.517	-0.0101	0.269	10.517	-0.0101	0.259	10.517	-0.0101	0.255

Table 3-7 Length scale data in region 2

R=0		0.39		0.47		0.59		0.68		0.79	
x/D	bz+	x/D	bz+	x/D	bz+	x/D	bz+	x/D	bz+	x/D	bz+
0.8090	0.7350	0.8090	0.5946	0.8090	0.5955	0.8090	0.6028	0.8090	0.7259	0.8090	0.7261
1.6180	0.7834	2.4270	0.6070	1.6180	0.5749	2.4270	0.5989	2.4270	0.5891	2.4270	0.5886
3.2560	0.8898	4.0450	0.7635	3.2560	0.6809	4.0450	0.7733	4.0450	0.7196	4.0450	0.7333
4.8540	1.0201	5.6630	0.9369	4.8540	0.8661	5.6630	1.0310	5.6630	0.8800	5.6630	0.9656
6.4720	1.1734	7.2810	1.1601	6.4720	1.0164	7.2810	1.1975	7.2810	1.2115	7.2810	1.2120
8.0900	1.3171	8.9000	1.3718	8.0900	1.2446	8.9000	1.4222	8.9000	1.3662	8.9000	1.4928
x/D	bz-	x/D	bz-	x/D	bz-	x/D	bz-	x/D	bz-	x/D	bz-
0.8090	-0.7348	0.8090	-0.6759	0.8090	-0.6853	0.8090	-0.6571	0.8090	-0.6403	0.8090	-0.6315
1.6180	-0.7923	2.4270	-0.7281	1.6180	-0.7068	2.4270	-0.6587	2.4270	-0.6399	2.4270	-0.5884
3.2560	-0.8949	4.0450	-0.7264	3.2560	-0.6999	4.0450	-0.7071	4.0450	-0.7141	4.0450	-0.7009
4.8540	-1.0289	5.6630	-0.8542	4.8540	-0.7661	5.6630	-0.8451	5.6630	-0.9220	5.6630	-0.8960
6.4720	-1.1508	7.2810	-1.0129	6.4720	-0.9073	7.2810	-1.0660	7.2810	-1.0991	7.2810	-1.1880
8.0900	-1.2974	8.9000	-1.1772	8.0900	-1.1232	8.9000	-1.3573	8.9000	-1.3277	8.9000	-1.4398
x/D	by	x/D	by	x/D	by	x/D	by	x/D	by	x/D	by
0.8090	0.7346	0.8090	0.8291	0.8090	0.8291	0.8090	0.9591	0.8090	1.0181	0.8090	1.1756
1.6180	0.7819	2.7470	1.0811	1.6180	0.9945	2.7470	1.3409	2.7470	1.4591	2.7470	1.7425
3.2560	0.8764	4.0450	1.3646	3.2560	1.3646	4.0450	1.8134	4.0450	1.9709	4.0450	2.3331
4.8540	0.9945	5.6630	1.6402	4.8540	1.7031	5.6630	2.2228	5.6630	2.4354	5.6630	3.0181
6.4720	1.0811	7.2810	1.7976	6.4720	1.9787	7.2810	2.4197	7.2810	2.8606	7.2810	3.4906
8.0900	1.1913	8.9000	2.0181	8.0900	2.1362	8.9000	2.7031	8.9000	3.0654	8.9000	4.0024

Table 3-8 Data for  $P_{min}$ ,  $a_1$ ,  $a_2$ ,  $db_y/dx$ ,  $db_z/dx$  and  $P_{max}$

R	$P_{min}/\frac{1}{2}\rho U_0^2$	$P_{max}/\frac{1}{2}\rho U_0^2$	$a_1$	$a_2$	$db_z/dx$	$d^2b_z/dx^2$	$db_y/dx$
0.00	-0.0210		1.0857	0.1369	0.0810	0.0770	0.0800
0.39	-0.0241	0.0270	0.8514	0.2296	0.1190	0.0930	0.1500
0.47	-0.0231	0.0440	0.8299	0.2457	0.1036	0.0880	0.2100
0.59	-0.0308	0.0680	0.7900	0.2800	0.1280	0.1340	0.2300
0.68	-0.0339	0.0840	0.7596	0.2993	0.1260	0.1250	0.2900
0.79	-0.0393	0.1100	0.7397	0.3093	0.1410	0.1550	0.3500
1.00	-0.0400	0.1080			0.1600	0.1600	0.5300

## Chapter 4 Free Jumps, Submerged Jumps and Wall Jets \*

### 4.1 Introduction

The hydraulic jump is one of the most interesting phenomena in the field of hydraulic engineering. It forms a rapid transition from supercritical to subcritical flow and is shown in Fig. 4-1 (a). In Fig. 4-1 (a), a free hydraulic jump is formed just downstream of a (streamlined) gate which produces a supercritical stream with an almost uniform velocity of  $U_0$  and a depth of  $y_0$ , and the tail water depth  $y_t$  is equal to the subcritical sequent depth  $y_2$ , given by the Belanger equation

$$\frac{y_2}{y_0} = \frac{1}{2} (\sqrt{1+8F_0^2} - 1) \quad (4-1)$$

where  $F_0$  is the supercritical Froude number, equal to  $U_0/\sqrt{gy_0}$  and  $g$  is the acceleration due to gravity. If the tail water depth is less than  $y_2$ , the jump would form somewhere downstream and is referred to as a repelled jump. If  $y_t$  is greater than  $y_2$ , a submerged jump is formed at the gate as shown in Fig. 4-1 (b). A submerged jump is characterized by the supercritical Froude number  $F_0$  and the Submergence factor  $S$ , defined as  $(y_t - y_2)/y_t$  (Rajaratnam, 1965(a)). Obviously,  $S$  is equal to zero for the jump at the gate, which we will refer to as the free jump and as  $S$  increases above zero, we get submerged jumps of different degrees of submergence. When  $S$  becomes large, the submerged jump looks like a plane turbulent jet. If  $S$  is very large, it would behave like the classical plane turbulent wall jet (which is a plane turbulent wall jet with an unbounded stagnant ambient and zero longitudinal pressure gradient) (Rajaratnam, 1976 (a)).

---

\* The main content of this chapter has been sent to the Journal of Hydraulics Research for Publication.

Leonardo da Vinci, in the 16th century, was the first to describe the hydraulic jump and since then, it has been investigated extensively. A general review of these publications on the hydraulic jump, can be found in a recent book by Hager (1992). It should be mentioned that most of these papers deal with the global characteristics of the jump and only a few investigators have considered the internal structure of flow in the jump.

In 1965, Rajaratnam (1965 a) studied submerged jumps treating them as plane turbulent wall jets with finite submergence. For Froude number  $F_0$  ( at the gate) varying from 4.38 to 7.66 and  $S$  in the range of 0.18 to 1.17, Rajaratnam found that the velocity profiles in the forward flow were similar if they are normalized with a velocity scale equal to the maximum velocity  $u_m$  at that section and a length scale  $b$  equal to the distance from the boundary (bed) where the local velocity is equal to  $0.5 u_m$  and  $du/dy < 0$  (see Fig. 4-2 for a definition sketch). Further, this normalized velocity profile was described well by the corresponding curve of the wall jet for  $\eta$  up to about 1 where  $\eta = y/b$  and  $y$  is vertical distance from the wall or boundary which is the channel bed in our case. (see Fig. 4-3). For  $\eta$  greater than 1, the experimental observations deviated downwards from the wall jet curve. For his own data, Rajaratnam used straight lines to describe the longitudinal decay of the velocity scale  $u_m$  and found that the slope of the straight lines was only a function of submergence. Rajaratnam also found that the length scale  $b$  grew linearly and the slope only depended upon the nozzle Froude number. In a later study, with a much wider range of the flow parameters  $F_0$  and  $S$  (Rajaratnam, 1965 c ;  $F_0$  varying from 3.01 to 6.44 and  $S$  from 1.60 to 2.24), Rajaratnam found that the decay of the velocity scale followed the -0.515 power law which is very close to the wall jet decay rate of

-0.5 power law. The growth rate of the length scale  $b$  for these cases was found to be essentially the same as that for wall jets.

Rajaratnam also investigated the free jump as a wall jet (Rajaratnam, 1965 b). The velocity profiles, non-dimensionlized with  $u_m$  and  $b$ , were also found to be similar (Fig. 4-4). In the boundary layer part which lies between the wall and the plane of  $u_m$ , the velocity data followed the defect law when plotted with  $u/u_m$  vs.  $y/\delta$  where  $\delta$  is the thickness of the layer between the bed and the plane of the maximum velocity. In the free mixing region which lies above the  $u_m$  plane, the velocity measurements were well described by the corresponding curve of the wall jet for  $\eta$  up to about 1, beyond which the observations fell off to join the curve for submerged jumps (curve in Fig. 4-3). The length scale data were located slightly above the straight line found by Sigalla (1958) for wall jets and that for submerged jumps found earlier by the author himself. For the decay of velocity scale of free jumps, Rajaratnam found that the velocity scale of free jumps decayed considerably faster in comparison with that of the wall jet (Fig. 4-5). In Fig. 4-5, it is seen that the data points for free jumps, submerged jumps and wall jets are not described by one curve or equation and are spread over a zone.

Long, Rajaratnam and Steffler (1990) introduced a different length scale for the velocity scale decay in their studies on submerged jump and its comparison with the wall jet. Instead of using the gate opening, they used the length scale  $L$  which is the longitudinal distance from the gate where  $u_m$  is equal to  $U_0/2$  (Fig. 4-6). There are two advantages of using  $L$  instead of  $y_0$ . Firstly, its use in place of  $y_0$  brings the velocity scale data for jumps, submerged jumps and wall jets into a relatively narrow band and this is shown clearly in Fig. 4-6 (this

is obvious when Fig. 4-6 is compared with Fig. 4-5). Further, Long, Rajaratnam and Steffler also found that the length scale  $L$  is also useful in analyzing the longitudinal variation of turbulence properties.

Although the study of Long, Rajaratnam and Steffler can be viewed as a notable contribution, there are still some questions that have to be resolved. These are :

(1) Since Long, Rajaratnam and Steffler were focusing on submerged jumps they did not look deeply into wall jet and free jumps. For wall jet, they simply used the value 49 for  $L/y_0$  which was obtained simply by transferring the coefficient in the  $u_m/U_0 \sim x/y_0$  relation found by Rajaratnam (1976 a). In fact, the  $L/y_0$  value for wall jet might be affected by the nozzle Reynolds number  $R_0$  (defined as  $U_0 y_0/\nu$  where  $\nu$  is the kinematic viscosity of the fluid). Whether this is true or not needs to be verified. For decay of velocity scale of free jumps, Long, Rajaratnam and Steffler did not do any further analysis. They just used the experimental results from Rajaratnam (1965 b). In fact, a lot more data are available since Rajaratnam's work and therefore we can have a closer look at free jumps by analyzing the existing data.

(2) It is seen from Fig. 4-6 that for some submerged jumps, the decay of the velocity scale data is wall-jet-like (WJL), that is, they fall on the wall jet curve for some distance and then fall off from it, whereas for some other submerged jumps, the decay is free-jump-like (FJL), following the free jump curve. Long, Rajaratnam and Steffler did not distinguish between these different trends and it is not known under what conditions either of these occurred.

(3) To predict the length scale  $L$  for submerged jumps, Long, Rajaratnam and Steffler presented a similarity model, but as can be seen in Fig. 4-7, there is considerable scatter in the data presented. Hence, it appears that there is a need to consider this problem further.

The main objective of this chapter is to consider firstly the three cases of free jumps, submerged jumps of varying degrees of submergences and the classical plane turbulent wall jet . Secondly, we want to quantify clearly the differences between the free jump and the wall jet. Thirdly, we want to establish under what conditions the decay of the velocity scale in a submerged jump is free-jump-like, and under what conditions it is wall-jet-like. Finally we also want to recognize any overall similarity between these three classes of flows, if they exist.

## 4.2 Wall jet

For a plane turbulent wall jet under zero pressure gradient in an infinite expanse of the same fluid ( referred to herein as the classical wall jet ), it is easy to show (Rajaratnam, 1976 a) that  $u_m \propto x^{-0.5}$  in which  $x$  is the longitudinal distance from the nozzle. Following the general practice, available observations on the variation of the velocity scale are plotted together in Fig. 4-8 (a) with  $U_0$  and  $y_0$  as the scales. These observations are described by the equation

$$u_m/U_0 = 3.50(x/y_0)^{-0.5} \quad (4-2)$$

which was obtained by Rajaratnam (1976 a). In Fig. 4-8 (b), the same data are replotted with  $U_0$  and  $L$  as the scales. Correlation of the data appears to be better and the experimental results are described well by the equation



$$u_m/U_0 = 0.50(x/L)^{-0.5} \quad (4-3)$$

The variation of the non-dimensional length scale  $L/y_0$  with the nozzle Reynolds number  $R_0$  is shown in Fig. 4-9. In Fig. 4-9,  $L/y_0$  does not appear to vary systematically with the Reynolds number. The scatter of the data in Fig. 4-9 might be due to the differences in nozzle shape and the initial turbulence in the jet. The mean value of  $L/y_0$  is 59.85 and the standard deviation is 9.20. If converted to the  $u_m/U_0 \sim x/y_0$  system, the coefficient in eqn. (4-2) corresponding to this mean value of  $L/y_0$  would be 3.87. The mean value obtained here is about 20% bigger than the value used by Long, Rajaratnam and Steffler and if this mean value were used by them, the curve in Fig. 4-7 would be even further away from most of the data points.

For the growth rate  $db/dx$  of the length scale  $b$ , Launder and Rodi (1981) presented 22 sets of data in their table ( table 1 in Launder and Rodi (1981)). According to this table, the mean value of  $db/dx$  is 0.0728 and the standard deviation is 0.0071. According to Launder and Rodi, the mean value of the boundary layer growth rate,  $d\delta/dx$ , is 0.011 with a standard deviation of 0.0014. The data on the velocity and length scales  $L$ ,  $b$  and  $\delta$  are given in Table 4-1 to 4-3 at the end of the chapter.

### 4.3 Free jump

Let us consider the experimental observations available in the literature on the variation of the velocity scale in the free hydraulic jump. The presently available experimental observations on the variation of the velocity scale  $u_m$  for free jump, in terms of the velocity just before the jump  $U_0$ , are shown in Fig. 4-10 (a-f).

Rouse, Siao and Nagaratnam (1959) studied three jumps with a Froude number of 2, 4 and 6 in an air model and their results are shown in Fig 4-10 (a), with  $u_m/U_0$  against  $x/L$ . The channel inlet was rounded for all the three runs. As can be seen in Fig. 4-10 (a), while the data for  $F_0 = 4$  and 6 fall together, the data for  $F_0 = 2$  appear to behave differently possibly because at very low Froude numbers, the flow in the jump may not be as turbulent as that in jumps with relatively large Froude numbers (Jones, 1964).

The observations of Schröder (1963) on free jumps with the Froude number varying from 3.85 to 6.92 are shown in Fig. 4-10 (b). The results of Rajaratnam (1965 b) on jumps formed just downstream of sluice gates with the Froude number varying from 3.90 to 9.05 are shown in Fig. 4-10 (c). Fig. 4-10 (d) shows the results of Hager (1992, 1993) for the Froude number varying from 4.30 to 8.90. Fig. 4-10 (e) and (f) show the results of Ohtsu, Yasuda and Awazu (1990) for jumps formed near the gate as well as for jumps formed some distance downstream (repelled jumps). All these observations, except those of Ohtsu, Yasuda and Awazu on repelled jumps and the results of Rouse, Siao and Nagaratnam for the Froude number of 2.0, appear to indicate a well-ordered decay of the velocity scale, as can be observed in Fig. 4-10. It also appears that the non-uniformity of the velocity distribution in the supercritical stream before the jump has only a minor effect on the decay of the velocity scale as evidenced by a study of the data of Ohtsu, Yasuda and Awazu on the repelled jump as well as the data from one experiment of Hager with  $F_0 = 4.95$  in which the jump was formed at the foot of a spillway.

All the velocity scale data are plotted together in a consolidated form in Fig. 4-11 and a mean curve has been found to describe most of the observations for the free jump. This mean curve is described by the equation

$$\frac{u_m}{U_0} \pm_{0.040} = 1.173 \pm_{0.010} - 0.843 \pm_{0.017} \frac{x}{L} + 0.174 \pm_{0.006} \left(\frac{x}{L}\right)^2 \quad (4-4)$$

( with a value of correlation coefficient R of 0.987). In Fig. 4-11, it can be seen that this equation describes the experimental observations for  $x/L$  from about 0.25 to about 3, where  $u_m/U_0$  falls to about 0.20. Fig. 4-11 also shows the corresponding curve for the classical wall jet and it can be seen that the wall jet curve is located slightly below the jump curve for  $x/L$  less than about 1.0, whereas for  $x/L$  greater than 1.0,  $u_m/U_0$  for the free jump falls below the wall jet curve. For  $x/L = 2.5$ ,  $u_m/U_0$  for the jump is about 0.15 whereas for the wall jet, the corresponding value is 0.31.

Let us next consider the behavior of the length scale  $L$  for the free jump. The experimental results for the free jump are shown in Fig. 4-12 in which the data of Rouse, Siao and Nagaratnam for the air model of the free jump appear to be somewhat different from the rest of the data. Even though there is considerable scatter in the data, it may be said that  $L/y_0$  appears to increase (almost linearly) with the Froude number. For  $F_0=3$ ,  $L/y_0$  is about 13 whereas for  $F_0=9$ ,  $L/y_0$  is about 30. For the classical wall jet,  $L/y_0$  is about 60 and compared to this value, the length scales for free jumps are considerably smaller, which indicates a faster decay of the maximum velocity. The results for the free jump are described approximately by the equation

$$L/y_0 \pm_{2.921} = 5.06 \pm_{1.955} + 2.91 \pm_{0.323} F_0 \quad (4-5)$$

with a value of correlation coefficient  $R$  of 0.877. According to eqn. (4-5), to get the same length scale  $L$  as the wall jet, the Froude number of the jump has to be equal to 19.

As far as the length scale  $b$  is concerned, not many data sets are available. Fig. 4-13 shows all the available data along with the wall jet line with a slope of 0.0728 which is the mean value for wall jet data as mentioned in the previous section. The virtual origin for wall jet  $b$  is chosen as  $x_0/y_0 = -10$  which was used by Rajaratnam (1976 a). It appears from Fig. 4-13 that the length scale  $b$  for the free jump grows at about the same rate as that of the wall jet in the early stage and grows faster later on. One can also see that the Froude number only affects the starting position of the faster growth part. A summary of the data for the velocity scale, length scales  $L$  and  $b$  is given in Tables 4-4 to 4-6 at the end of the chapter.

#### **4.4 Submerged jumps**

The submerged jump appears to serve as a transition from the free jump to the classical wall jet. Even though considerable amount of data is available on submerged jumps, from the investigations of Rajaratnam (1965 a, 1965 c, 1967 a, 1967 b, 1976 b), Narasimhan and Bhargava (1976), Long, Rajaratnam and Steffler (1990) and others, it appeared desirable to perform some detailed experiments, especially for relatively large values of the submergence factor  $S$  and relatively large values of the Froude number. Hence four detailed experiments were performed with the Froude number in the range of 5 to 8 and the submergence factor in the range of 1.5 to 6. Five further skeleton experiments were also performed with the Froude number in the range of 1 to

1.5 and the submergence factor in the range of 2 to 7.5. In the following subsections, we discuss the experimental arrangement, measurement techniques and the results obtained which will be followed by a general discussion of the structure of flow in submerged jumps.

#### **4.4.1 Experimental setup**

The experiments were done in the T. Blench Hydraulics Laboratory of the University of Alberta. Fig. 4-14 (a) shows the experimental arrangement used in the experiments. The flume was 7.60 m long, 0.466 m wide and 0.60 m deep. The horizontal bottom was made of aluminum and the side walls were made of glass. The tail water depth was controlled by a vertical tail gate located at the downstream end of the flume. Water entered the flume through a sluice gate with a streamlined lip, which produced a supercritical stream with a thickness equal to the gate opening. Water was pumped to the tank from the sump and the flow discharge was measured by a magnetic flow meter located in the supply line.

For the measurement of the time-averaged velocity field, two arrangements were used and these are shown in Fig. 4-14(b) and (c). The arrangement shown in Fig. 4-14(b) was used with a pitch probe. The pitch probe was made of three tubes of diameters of 1.0 mm. and was made and calibrated in the Hydraulics laboratory (Rajaratnam and Muralidhar, 1967). Two transducers of the Validyne model DP45-16 were used to measure the pressure differences. Transducer #1 measured the pressure difference between the middle and the upper tubes and #2 between the middle and the lower tubes. The output ends of the transducers were connected to a flat cable which in turn was connected to a Macintosh IIfx computer. The computer program used in the measurement was

written in LabView language. The program was designed for use with both transducers and manometers. When the pressure differences were within the range of the transducers (-2.54 cm to 2.54 cm), the transducers were used. When the observations were made, the computer coupled every two signals, one from each transducer, to obtain the magnitude of the velocity and attack angle and displayed the magnitude and angle on a strip chart on the screen in real time. When the desired number of samples were taken at the desired sampling interval, the computer processed all the samples and saved the results in an open file. If the pressure differences were out of the range of the transducers, the three horizontal tube stoppers in Fig. 4-14(b) were opened and results were obtained from the manometers and typed into the computer. The flow chart for the program is shown in Fig. 4-15 which was designed according to the pitch probe charts obtained by Rajaratnam and Muralidhar (1967). In Fig.4-15,  $p_{21}$  and  $p_{23}$  are the two pressure differences,  $f_1$  to  $f_4$  stand for four different calibration functions,  $\emptyset$  is the angle of the velocity vector and  $K_{21}$  is a non-dimensional parameter

$$K_{21} = k_2 - k_1 \quad (4-6)$$

In eqn. (4-6),  $k_1$  and  $k_2$  are two calibration parameters and both are the functions of  $\emptyset$ .

Fig. 4-14(c) shows the arrangement for use with the Pitot tube with an external diameter of 2.4 mm. Again, two transducers were used. Transducer #1 was used to measure the pressure difference between the dynamic pressure hole and a reference water level. Transducer #2 was used to measure the difference between the static pressure hole and another reference level. The two reference levels could be adjusted and read from the manometer table in Fig. 4-14(c). The

computer program was also written in LabView language and it was originally designed for multi-channel resource real time data taking. The above mentioned two programs are rather large and are available in the computer in T Blench Hydraulics Laboratory.

#### 4.4.2 Experiments and results

In the first series, four experiments were done and the details are given in Table 4-7. In these experiments, the gate opening and hence the depth of the supercritical stream leaving the gate was equal to 10 and 15 mm. For experiment 1,  $F_0$  was equal to 5.08 whereas for the other three experiments,  $F_0$  was equal to 7.46 but the submergence factor  $S$  was varied from 1.59 to 2.51. For experiment 1,  $S$  was equal to 5.08. To check if the flow was two dimensional when the tail water was deep, the velocity field was measured in the central vertical plane (CVP) and another vertical plane located at a transverse distance  $z$  equal to 0.1 times the width of the flume from the CVP. A comparison of the longitudinal velocity profiles in these two planes, shown in Fig. 4-16, indicates that at least in the central part of the flume the flow was two dimensional.

Table 4-7 Details of experiments of Series 1

Run	$y_0$ (m)	$y_1$ (m)	$U_0$ (m/s)	$F_0$	$S$	Tube used
1	0.010	0.44	1.72	5.48	5.08	pitch probe
2	0.015	0.53	2.86	7.46	2.51	Pitot tube
3	0.015	0.46	2.86	7.46	2.07	Pitot tube
4	0.015	0.39	2.86	7.46	1.59	Pitot tube

In the second series, five skeleton experiments were performed, in which the gate opening height was 35 mm and the ( $F_0$ ,  $S$ ) values were (1.45,

1.80), (1.21, 2.98), (1.23, 3.74), (1.15, 5.12) and (1.07, 7.42). A Pitot tube of 2.4 mm external diameter, connected to a transducer was used for measuring the pressure difference between the dynamic pressure hole and static pressure hole. Each sample of the pressure difference was changed to velocity and shown on the computer screen in real time. The LabView program used was the same as the one for the set-up shown in Fig. 4-14 (c). For each run, only the maximum longitudinal velocity was measured at several sections in the central vertical plane, after checking for the location of the maximum velocity.

Fig. 4-17 shows the velocity field of run 1 in series 1. As can be seen from Fig. 4-17, the flow is essentially horizontal for a distance up to about 1.2 m ( $120 y_0$ ) and the vertical velocity component becomes significant only after this section. The longitudinal velocity fields for runs 2, 3 and 4 in series 1 are shown in Fig. 4-18 (a-c). The corresponding Piezometric head fields are shown in Fig. 4-19 (a-c). From Fig. 4-19 we can see that for all the three runs, the maximum defect in the Piezometric head occurs at the upper edge of the gate, and it decays as we move away from the gate. The velocity profiles in Figs. 4-17 and 4-18 show clearly the wall jet structure near the bed and the recirculating flow near the water surface. The observations of series 2 will be presented in non-dimensional form in the next subsection.

### **4.4.3 Analysis of submerged jump results**

#### ***4.4.3.1 Velocity profile similarity***

Let us consider in detail the general features of the velocity profiles for the four experiments of the first series with relatively large submergences. In Fig. 4-20 (a-d), the longitudinal velocity profiles are plotted in non-dimensional form for each experiment, using  $u_m$  and  $b$  as the scales. It is seen that except for



the sections very close to the gate (within the potential core region) and far away from the gate (near the end of the jump), the velocity profiles at all the sections, in the forward flow region, are all similar. All the similar profiles are plotted together in Fig. 4-21 and we can see that they are described by the corresponding plane wall jet curve very well, except near the upper end, due to the presence of the reverse flow.

#### 4.4.3.2 Decay of Piezometric pressure defect

The longitudinal variation of  $p_{\max}$ , the maximum deviation of the Piezometric pressure from the hydrostatic value in terms of  $(0.5\rho U_0^2)$  for runs 2 to 4 is shown in Fig. 4-22 where  $\rho$  is the fluid density. It appears that this deviatory pressure is independent of submergence and decays linearly in the longitudinal direction. The regression line in Fig. 4-22 has the equation

$$\frac{p_{\max}}{0.5\rho U_0^2} \Big|_{\pm 0.0017} = -0.039735_{\pm 0.00107} + 0.000374_{\pm 0.000025} \frac{x}{y_0} \quad (4-7)$$

and the correlation coefficient  $R = 0.974$ .

#### 4.4.3.3 Decay of velocity scale

Considering the velocity scale  $u_m$ , the available data in the literature and the results obtained in the present study are shown plotted in Fig. 4-23(a-o) with  $u_m/U_0$  against  $x/L$ . Fig. 4-23 (a) shows the results of Narasimhan and Bhargawa for  $F_0$  equal to 3.12 and 4.0 with  $S$  varying from 0.33 to 2.24. (Narasimhan and Bhargawa (1976)). Fig. 4-23 (b) shows their results for  $F_0 = 4, 5$  and 6 for different submergences. In both these figures, the velocity scales decay in a way similar to that for free jumps. Rajaratnam's observations ( 1965 a, 1965 c, 1967 a, 1967 b, 1976 b) for a wide range of Froude numbers and submergences are shown in Fig. 4-23 (c) to (g). In Fig. 4-23 (c) and (g), the velocity scale decay is very much like that in the free jumps or FJL, whereas in Fig. 4-23 (e) and (f) the

decay is like that in the wall jet or WJL. Fig. 4-23 (h) shows the results of Ohtsu, Yasuda and Awazu (1990), and as can be seen that the velocity scale decay of the run with  $(F_0, S) = (7.34, 0.34)$  is FJL whereas those of the other two runs are WJL. The observations of Long, Rajaratnam and Steffler (1990) shown in Fig. 4-23 (i) indicate a FJL decay whereas the results in Fig. 4-23 (j) indicate a WJL decay. Fig. 4-23 (k) and (l) present the results of Liu (1949). The results of Bakhmeteff and Feodoroff (1941) shown in Fig. 4-23 (m) indicate a FJL decay. Fig. 4-23 (n) shows the results of the experiments from series 1 of the present work and these results show a WJL decay. The results of experiment series 2 are shown in Fig. 4-23 (o) and it is interesting to see that the decay of the velocity scale is approximately FJL even though the submergence is large.

Considering all these results on the decay of the velocity scale  $u_m/U_0$ , except perhaps the results for the smaller values of the Froude number shown in Fig. 4-23 (o), all the other results can be described as either WJL or FJL decay. In most of the FJL cases, the velocity scale has a slight increase before it decays probably because of the existence of the negative water surface slope and favorable pressure gradient near the gate. In the case of WJL decay, after a certain distance, the data appears to decay faster, to join the free jump decay curve, or drop even further. From the above discussion, we may argue that for any submerged jump of a given  $F_0$ , there exists a certain value of  $S$  which we might write as  $S^*$  and when  $S > S^*$ , the decay of the velocity scale is wall-jet-like or WJL, and when  $S < S^*$  it is free-jump-like or FJL.

In Fig. 4-24, the available results based on Fig. 4-23 (a-o) are plotted with open symbols representing WJL decay and the filled-in symbols for FJL decay. An approximate boundary is shown in Fig. 4-24 between these two

classes of flows. It appears that when  $F_0$  is close to 1,  $S^*$  is large and as  $F_0$  increases,  $S^*$  continues to fall. For  $F_0 = 6.5$ ,  $S^* \approx 1.0$ . It should be pointed out that more experiments should be carried out to define the  $S^*$  curve more precisely in the range of  $F_0$  from 1.5 to about 3.0. The  $S^*$  curve in Fig. 4-24 can be described by the following equation:

$$S^* = 12 F_0^{-1.3} \quad (4-8)$$

#### 4.4.3.4 Variation of length scale $L$

Let us consider the length scale  $L$  for the submerged jumps. In Fig. 4-25, all the available data for  $L$  are plotted with  $L/y_0$  against  $S$  for different ranges of  $F_0$ . In Fig. 4-25, we see that for each range of the Froude number,  $L/y_0$  increases with  $S$  to eventually reach the wall jet value of 59.85 for a certain value of  $S$ . The experimental results are replotted in Fig. 4-26 and the following equation

$$\frac{L}{y_0} \pm 1.114 = 7.26 \pm 1.065 F_0^{0.64 \pm 0.030} (1+S)^{0.77 \pm 0.034} \quad (R=0.947) \quad (4-9)$$

describes all the data except the five points separated by the broken lines in Fig. 4-25. In eqn. (4-9), if we set  $L/y_0 = 59.85$  we can solve for  $S$  as a function of  $F_0$ . Let us denote this particular value of  $S$  as  $S^\#$ . It is the submergence required for a jump to have the same length scale  $L$  as that of the classical wall jet.  $S^\#$  can be described by the equation

$$S^\# = 15.28 F_0^{-0.81} - 1 \quad (4-10)$$

Eqn. (4-10) is plotted in Fig. 4-27 together with eqn. (4-8) and it is interesting to see that both curves have the same trend. The two curves in Fig. 4-27 divide the  $(F_0, S)$  plane into three zones. Above the broken line defining  $S^\#$ , the submerged jump behaves as a wall jet with a WJL decay of  $u_m$  and a length scale  $L$  same as that of a wall jet whereas in the zone in between the two curves,

even though the decay of  $u_m$  is WJL, the length scale  $L$  is smaller than that of the wall jet. Below the  $S^*$  curve, the decay of the velocity scale is FJL and the length scale is described by eqn. 4-5.

#### 4.4.3.5 More about the velocity scale decay

It has been mentioned before that when the decay of the velocity scale in a submerged jump is WJL, after a certain distance of  $x_d$ , the velocity scale data fall off the wall jet decay curve. Fig. 4-28 shows that this distance  $x_d$  in terms of  $L$  is a function of  $F_0$  and  $S$  and is described by the linear equation

$$\frac{x_d}{L} \pm 0.054 = 0.208 \pm 0.066 + 0.132 \pm 0.009 F_0 + 0.124 \pm 0.013 S \quad (R=0.98) \quad (4-11)$$

If  $u_{md}$  is the value of  $u_m$  at the location where the departure from the wall jet curve occurs, the variation of  $u_m/u_{md}$  in the accelerated decay region, was found to be function of mainly  $(x-x_d)/y_t$  which is shown in Fig. 4-29. The mean curve in Fig. 4-29 is described by the equation

$$\frac{u_m}{u_{md}} \pm 0.049 = 1.015 \pm 0.011 - 0.539 \pm 0.028 \frac{x-x_d}{y_t} + 0.106 \pm 0.014 \left(\frac{x-x_d}{y_t}\right)^2 \quad (4-12)$$

with a correlation coefficient of 0.975.

#### 4.4.3.6 Length scale $b$

All the available data for submerged jump length scale  $b$  are shown in Fig. 4-30 together with the corresponding line for the wall jet. It is seen in Fig. 4-30 that most of the observations for submerged jumps are contained within a standard deviation and only the data points near the jump end show an accelerated growth rate.

#### 4.4.3.7 Length scale $\delta$

The available data for the boundary layer thickness  $\delta$  of submerged jumps are plotted in Fig. 4-31(a-b) together with the corresponding line for the

wall jet. Fig. 4-31(a) shows the data for FJL submerged jumps, and it appears that in the early part, the FJL jumps have thinner boundary layer than the wall jet (probably because of fact that the minimum water surface depth occurs at some distance from the gate) and near the jump end the boundary layer grows rapidly. For the WJL submerged jumps, the data are plotted in Fig. 4-31(b) which also shows vertical lines of  $x = x_d$ . Fig. 4-31(b) also indicates that for  $x \leq x_d$ , the WJL jumps have the same boundary layer thickness as the wall jet and that when  $x > x_d$ , the boundary begins to grow rapidly.

#### *4.4.3.8 Reverse flow*

In this subsection, we consider the reverse flow which occurs in the upper portion of the submerged jumps. Since there is a paucity of experimental observations on the velocity distribution in the reverse flow region in the literature, this velocity field was measured in the present work and the results are presented here. Fig. 4-32 (a-d) shows the present results in a non-dimensional form, with  $u/u_s$  against  $y/b_r$ , where  $u_s$  is the surface velocity,  $y_s$  is the vertical distance from the water surface and  $b_r$  is the value of  $y_s$  where  $u=0.75 u_s$ . From Fig. 4-32, it appears that velocity distribution is approximately similar in the reverse flow region. This similarity is demonstrated in a more general form in Fig. 4-33, where the results for all the four experiments are shown together.

The data for the length scale  $b_r$  are shown in Fig. 4-34. Here the jump roller length  $L_{Tsj}$  and tail water depth  $y_t$  are used as scales. In fact, instead of  $y_t$ , a more appropriate vertical length scale would be the thickness of the roller, were it easy to measure. The few data points shown in Fig. 4-34 show considerable scatter and at this time an average value of 0.2 might perhaps be used. The

present observations for the velocity scale are shown in Fig. 4-35(a-b) along with the few data points of Liu (1949) in two different non-dimensional forms. In Fig. 4-35(a) the inlet velocity  $U_0$  is used as the velocity scale and in Fig. 4-35 (b), the maximum value of the surface velocity  $u_{sm}$  is used as the scale whereas in both these figures, the length of the surface roller is used as the length scale. The correlation appears to be somewhat better in Fig. 4-35 (b) and the mean curve shown therein is described by the equation

$$\frac{u_s}{u_{sm}} \Big|_{\pm 0.066} = -0.215_{\pm 0.070} + 4.049_{\pm 0.280} \frac{x}{L_{rsj}} - 3.425_{\pm 0.260} \left(\frac{x}{L_{rsj}}\right)^2 \quad (4-13)$$

for  $x/L_{rsj}$  in the range of 0.2 to 0.9 with correlation coefficient of 0.912. It can also be seen ( Fig. 4-35 (b)) that the surface velocity has a maximum value at about  $x/L_{rsj} = 0.6$ . By a process of dimensional reasoning and trial and error, the following equation was found to describe the variation of the velocity scale for the reverse flow in terms of the jet velocity  $U_0$  for  $F_0$  from 2.12 to 8.48 and  $S$  from 0.44 to 5.08.

$$\begin{aligned} \frac{u_{sm}}{U_0} \Big|_{\pm 5\%} &= ag_1(F_0)g_2(S) \\ &= 0.342_{\pm 0.023} F_0^{0.263 \pm 0.034} e^{0.165(\pm 0.029)\sin(S)} \end{aligned} \quad (4-14)$$

The performance of this equation can be seen in Fig. 4-36 (correlation coefficient of 0.969).

Present observations on the length of the roller of the submerged jump are shown in Fig. 4-37, along with the available results in the literature, wherein, the length  $L_{rsj}$  is normalized by the subcritical sequent depth of the corresponding free jump ( following the general practice). In Fig. 4-37, the experimental observations are well described by the equation

$$\frac{L_{rsj}}{y_2} \Big|_{\pm 1.282} = 6_{\pm 0.225} + 4.14_{\pm 0.145} S \quad (R=0.961) \quad (4-15)$$

#### **4.4 Conclusions**

In this chapter, we have considered free jumps, submerged jumps and wall jets and have attempted to study the characteristics which are common to all of them as well the features that are different. This will help us to analyze submerged hydraulic jumps of any given Froude number and submergence.

For all the three flows, the distribution of the longitudinal velocity  $u$  at different sections are essentially the same, if expressed in a non-dimensional form with the maximum velocity at that station  $u_m$  as the velocity scale and the distance from the bed  $b$  where the local velocity is equal to half the maximum value and the velocity gradient in the vertical direction is negative, as the length scale. There are of course some differences in the upper part of the flow. In particular, for the free jump and submerged jumps, there is a region of reverse flow in the upper part of the flow, whereas for the classical wall jet, the entrainment will be essentially perpendicular the main jet.

For the classical wall jet, the decay of the velocity scale in terms of the velocity at the nozzle, with the longitudinal distance  $x$  in terms of the nozzle opening  $y_0$  follows the inverse square root equation. We found it necessary to normalize  $x$  with the length scale  $L$  which is the value of  $x$  where  $u_m=U_0/2$ . For the classical wall jet,  $L/y_0=59.85$ , with a standard deviation of 9.18. The decay equation for the wall jet becomes

$$u_m/U_0 = 0.50 (x/L)^{-0.5} \quad (4-3)$$

For the free jumps, we have assembled all the available experimental results ( from the investigations of Rouse, Siao and Nagaratnam, Schröder,

Rajaratnam, Ohtsu, Yasuda and Awazu and Hager) on the decay of the velocity scale in terms of  $U_0$  with the longitudinal distance  $x$  in terms of  $L$  and found a generalized decay curve which is different from that of the wall jet. This curve is given by the equation

$$\frac{u_m}{U_0} = 1.173 - 0.843\frac{x}{L} + 0.174\left(\frac{x}{L}\right)^2 \quad (4-4)$$

The length scale  $L$  in terms of  $y_0$  is a function of  $F_0$  and is given by the equation

$$L/y_0 = 5.06 + 2.91F_0 \quad (4-5)$$

It can be seen that  $L/y_0$  increases with  $F_0$  and for  $F_0 = 9$ ,  $L/y_0$  is 31.3 which is about half that of the wall jet. In general, it appears that the velocity scale decays rapidly in a free jump compared to that of a wall jet.

After a thorough study of the existing data in the literature and our detailed observations on a few more submerged jumps, we found that in certain submerged jumps, the decay of the velocity scale may be wall-jet-like (or WJL) and in others, it may be free-jump-like (or FJL). We found that for any given value of  $F_0$ , for  $S$  greater than  $S^*$ , the decay will be WJL whereas for  $S$  smaller than  $S^*$ , the decay will be FJL. We also found that this parameter  $S^*$  is given by the equation

$$S^* = 12 F_0^{-1.3} \quad (4-8)$$

For the submerged jumps, the length scale  $L$  in terms of  $y_0$  is given by the equation

$$\frac{L}{y_0} = 7.26F_0^{0.64}(1+S)^{0.77} \quad (4-9)$$

For a submerged jump to have a length scale the same as that of a wall jet,  $S$  has to be greater than  $S^*$  which is given by the equation



$$S^* = 15.28F_0^{-0.81} - 1 \quad (4-10)$$

The length scales  $b$  and  $\delta$  which describe the vertical distribution of the longitudinal velocity  $u$ , in the submerged jumps are essentially the same as in a wall jet up to some distance approximately near the end of the roller, beyond which they grow much more rapidly.

This study also presents some observations on the structure of the reverse flow for a few submerged jumps and some general conclusions have been drawn regarding the structure of the reverse flow.

#### 4.5 References

1. Bakhmeteff, B. A. and Feodoroff, N. V. (1941), Discussion of " Energy Loss at the Base of a Free Overfall", ASCE Trans., Vol. 108, pp. 1364-1373.
2. Gartshore, I. S. and Newman, B. G. (1969), The Turbulent Wall Jet in an Arbitrary Pressure Gradient, Aeronautical Quarterly, Vol. 20, Feb., pp. 25-56.
3. Hager, W. H. (1992), Energy Dissipators and Hydraulic Jump, Kluwer Academic Publishers, 288p.
4. Hager, W. H. (1993), Classical Hydraulic Jump: Free Surface Profile, Canadian Jour. of Civil Engrg, Vol. 20, No. 3, June, pp. 536-539.
5. Jones, L. E. (1964), Some Observations on the Undular Jump, ASCE Jour. of Hyd. Div., Vol. 90., HY3, pp. 69-82
6. Launder, B. E. and Rodi, W. (1981), The Turbulent Wall Jet, Progress in Aerospace Science, Vol. 19, pp. 81-128.

7. Liu, H. K. (1949), Diffusion of Flow from Submerged Sluice Gate, Thesis presented to the State Univ. of Iowa, Iowa, in partial fulfillment of the requirements for the degree of M. Sc., 32p.
8. Long, D, Rajaratnam, N. and Steffler, P. M. (1990), LDA Study of Flow Structure in Submerged Hydraulic Jump, Jour. of Hyd. Res., Vol. 28, No. 4, pp. 437-460.
9. Myers, G. E., Schauer, J. J. and Eustis, R. H. (1963), Plane Turbulent Wall Jet Flow Development and Friction Factor, Jour. of Basic Engineering, Trans. ASME, March, pp. 47-53.
10. Narasimhan, S. and Bhargava, V. P. (1976), Pressure Fluctuations in Submerged Jump, ASCE Jour. of Hyd. Div., Vol. 102, HY3, pp. 339-350.
11. Ohtsu, I., Yasuda, Y. and Awazu, S. (1990), Free and Submerged Hydraulic Jumps in Rectangular Channels, Report of the Research Institute of Science and Technology, Nihon University, No. 35, Feb. 1990, 50 p.
12. Rajaratnam, N. (1965a), Submerged Hydraulic Jump, ASCE Jour. of Hyd. Div., Vol. 91, HY4, pp. 71-96.
13. Rajaratnam, N. (1965b), The Hydraulic Jump as a Wall Jet, ASCE Jour. of Hyd. Div., Vol. 91, HY5, pp. 107-132.
14. Rajaratnam, N. (1965c), Flow below a Submerged Sluice Gate as a Wall Jet Problem, 2nd Australation Conf. on Hydraulics and Fluid Mechanics, Auckland, New Zealand, pp. B131-146.
15. Rajaratnam, N. (1976a), Turbulent Jets, Elsevier Scientific Publishing Co., 304p.

16. Rajaratnam, N. (1976b), Discussion of Pressure Fluctuations in Submerged Jump, ASCE Jour. of Hyd. Div., Vol. 102, HY12, pp. 1785-1787.
17. Rajaratnam, N. and Subramanya, K. (1967a), Plane Turbulent Reattached Wall Jets, Contributions to Turbulent Wall Jets in Hydraulic Engineering and Other Related Problems, Dept. of Civil Engineering, Univ. of Alberta, Edmonton, Canada.
18. Rajaratnam, N. and Subramanya, K. (1967b), Diffusion of Rectangular Wall Jets in Wider Channels, Contributions to Turbulent Wall Jets in Hydraulic Engineering and Other Related Problems, Dept. of Civil Engineering, Univ. of Alberta, Edmonton, Canada.
19. Rao, N. S. G. and Rajaratnam, N. (1963), The Submerged Hydraulic Jump, ASCE Jour. of Hyd. Div., Vol. 89, HY1, pp. 139-162.
20. Rouse, H. Siao, T. T. and Nagaratnam, S. (1959), Turbulence Characteristics of the Hydraulic Jump, Trans. ASCE, Vol. 124, pp. 926-966.
21. Schröder, R. (1963), Die turbulente Stromung im freien Wechselsprung, Habilitationsschrift, Mitteilung 59, Institut für Wasserbau und Wasserwirtschaft, TU Berlin, Berlin.
22. Schwarz, W. H. and Coasart W. P. (1961), The Two Dimensional Turbulent Wall Jet, Jour. of Fluid Mech. Vol. 10 pp. 481-495.
23. Sigalla, A. (1958), Measurement of Skin Friction in a Plane Turbulent Wall Jet, Jour. of Royal Aero. Soc., Vol. 62, pp. 873-877.

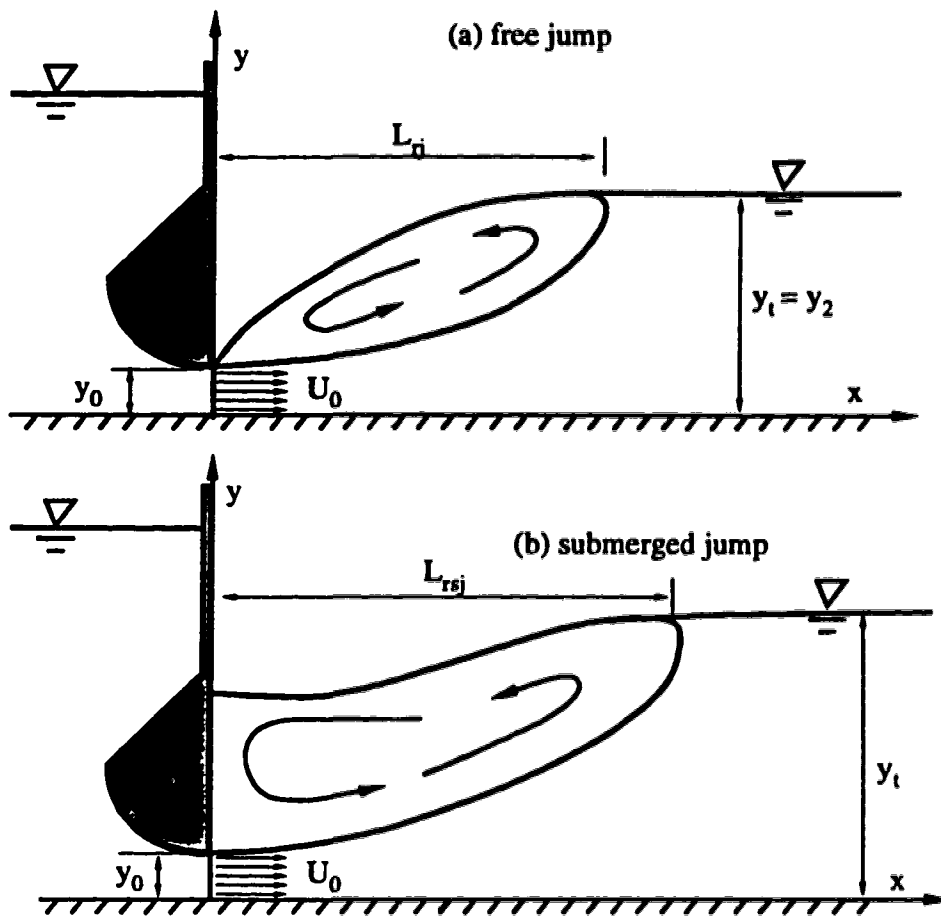


Fig. 4-1(a-b) Definition sketch for the free and submerged hydraulic jumps

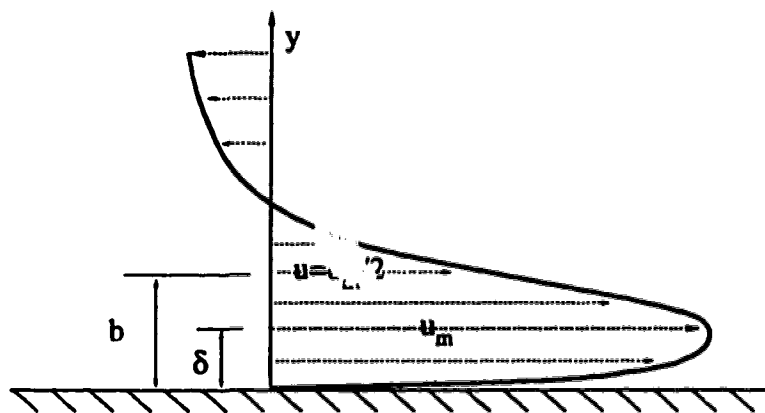


Fig. 4-2 Typical longitudinal velocity distribution in (submerged) jumps

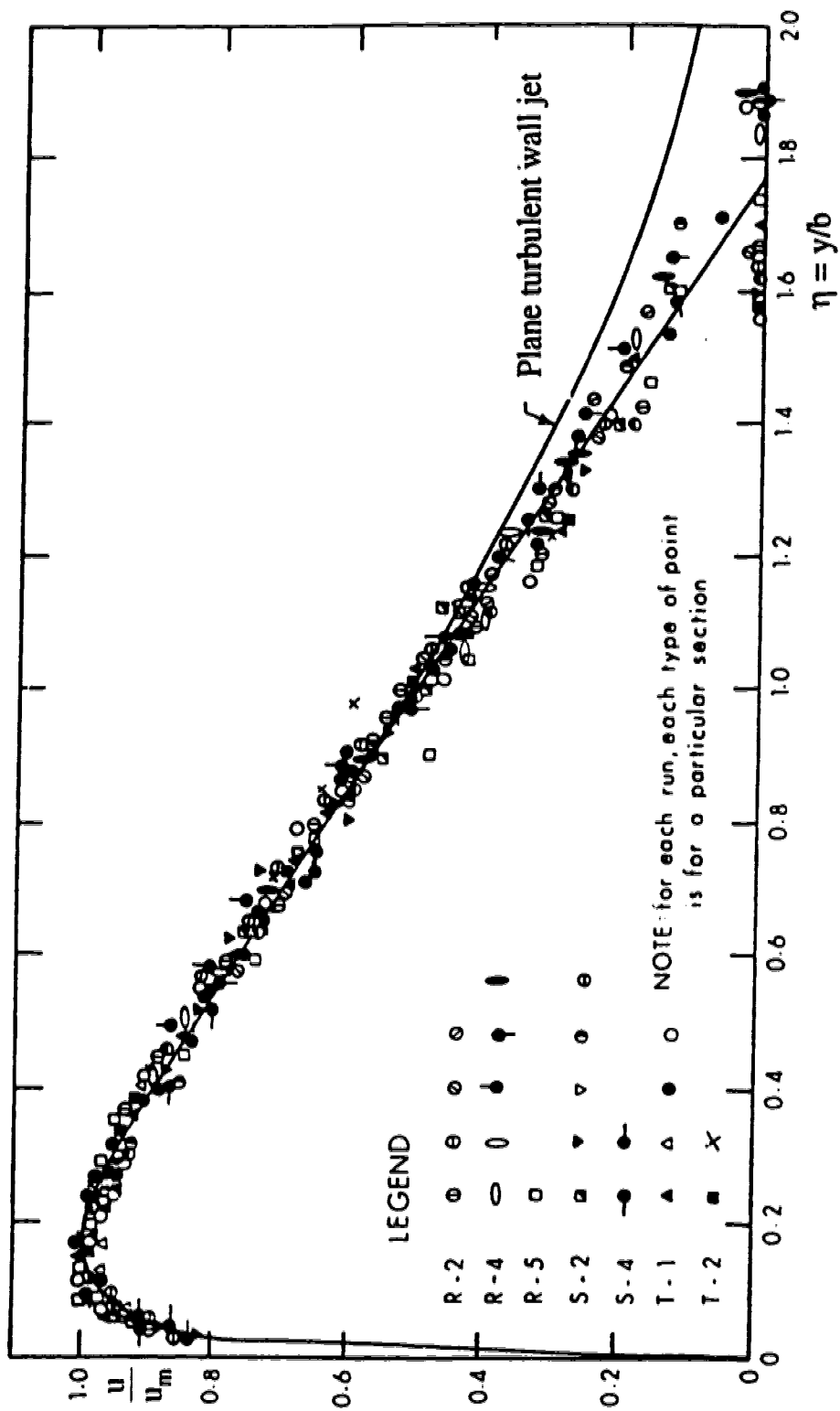


Fig. 4-3 Non-dimensional velocity profiles of submerged jumps (reproduced from Rajaratnam (1965 b))

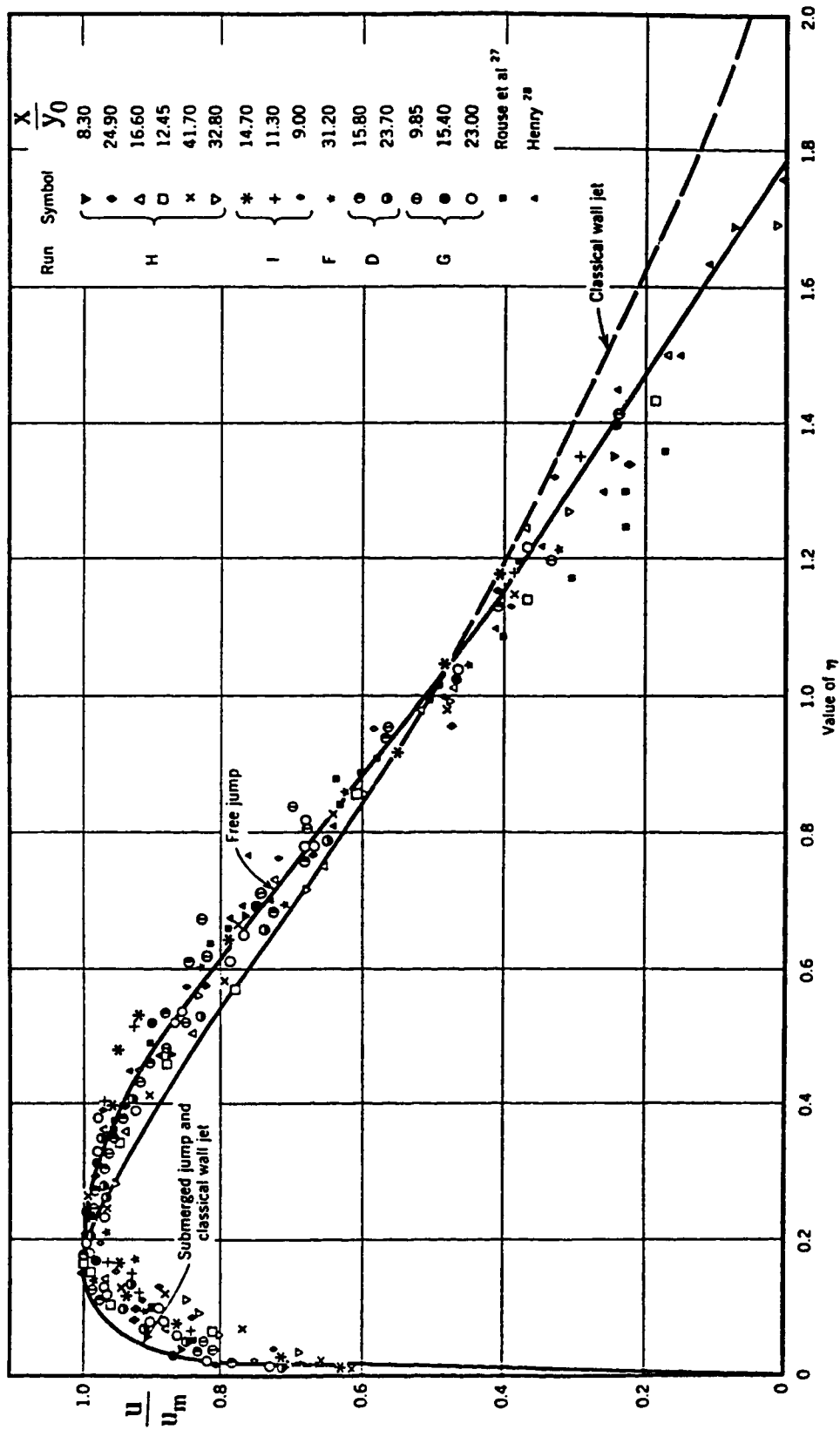


Fig. 4-4 Non-dimensional velocity profiles of free jumps (reproduced from Rajaratnam (1965 a))

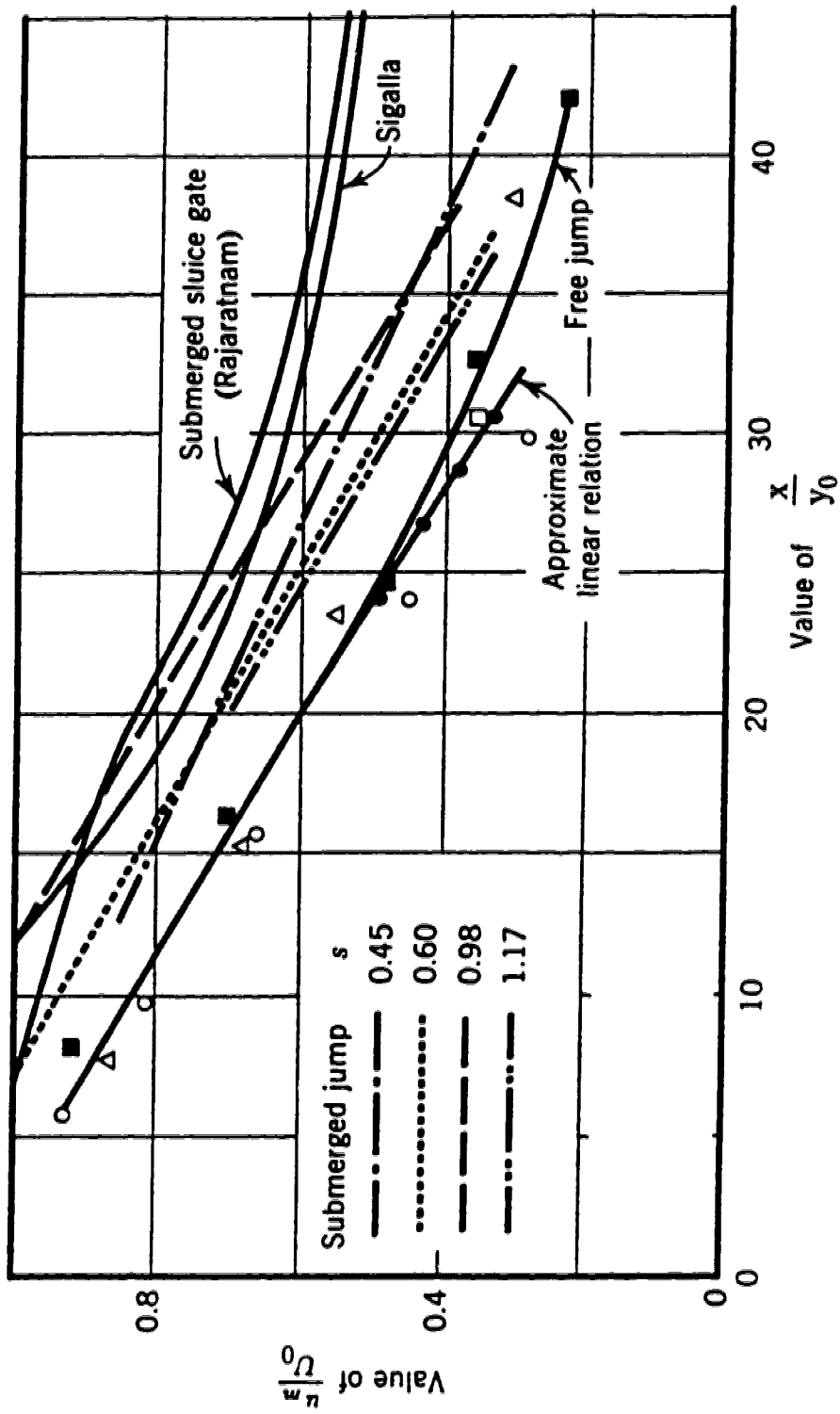


Fig. 4-5 Decay of velocity scales of free jumps, submerged jumps and plane wall jets  
(reproduced from Rajaratnam (1965 b))

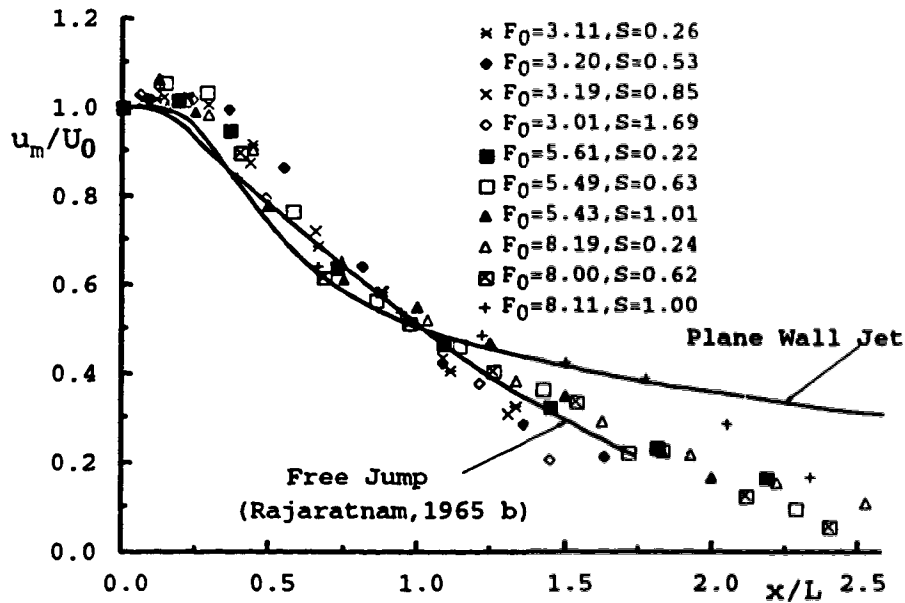


Fig. 4-6 Decay of the velocity scale of submerged jumps (reproduced from Long, Rajaratnam and Steffler (1990))

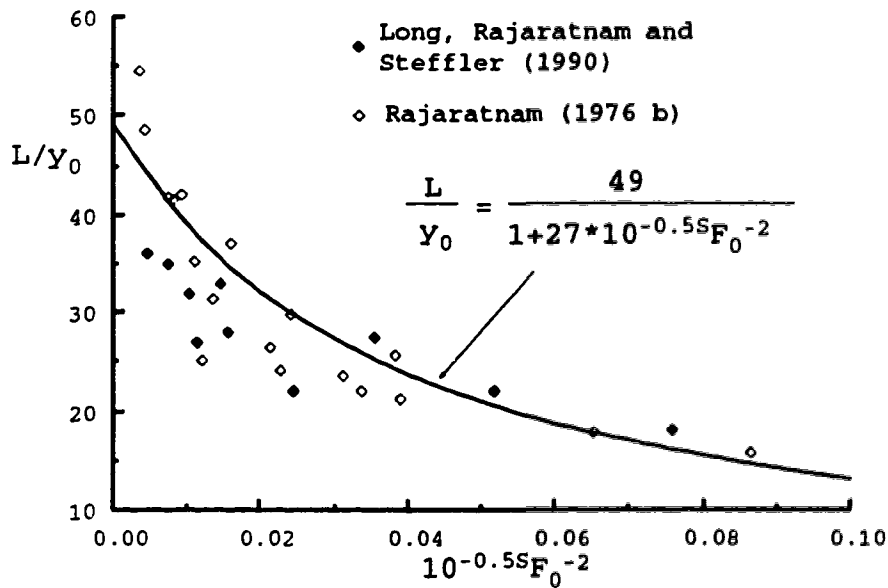


Fig. 4-7 Variation of  $L/y_0$  with  $F_0$  and  $S$  (reproduced from Long, Rajaratnam and Steffler (1990))



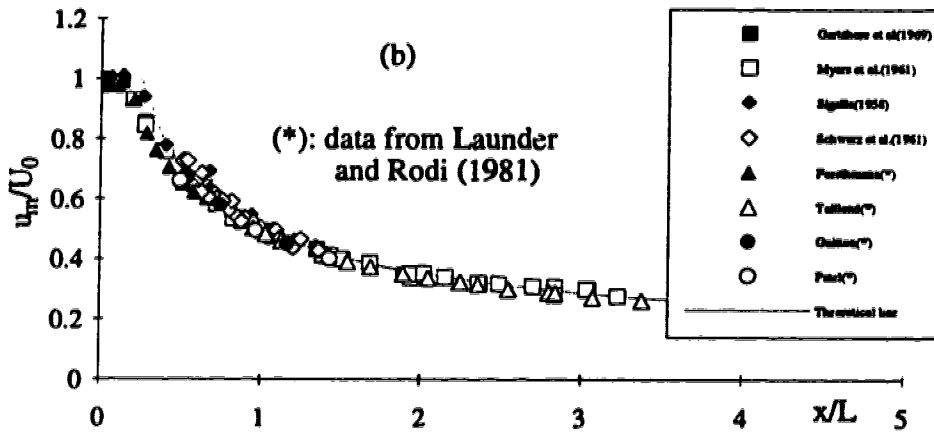
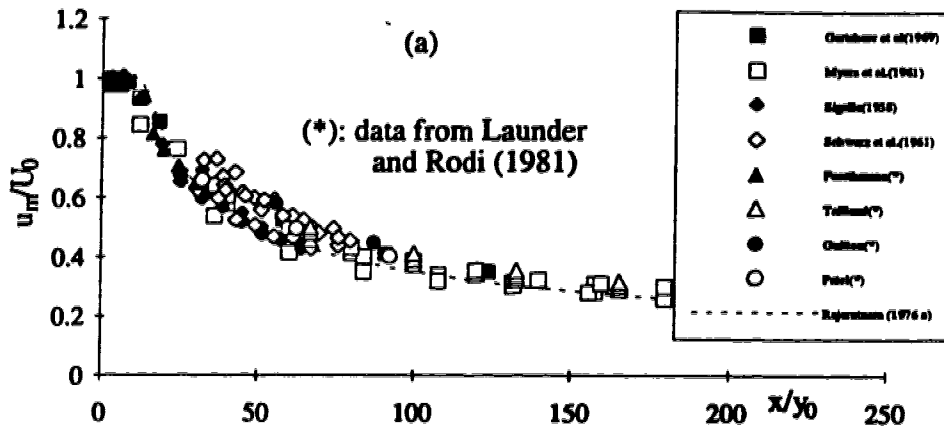


Fig. 4-8(a-b) Decay of the velocity scale in plane turbulent wall jets

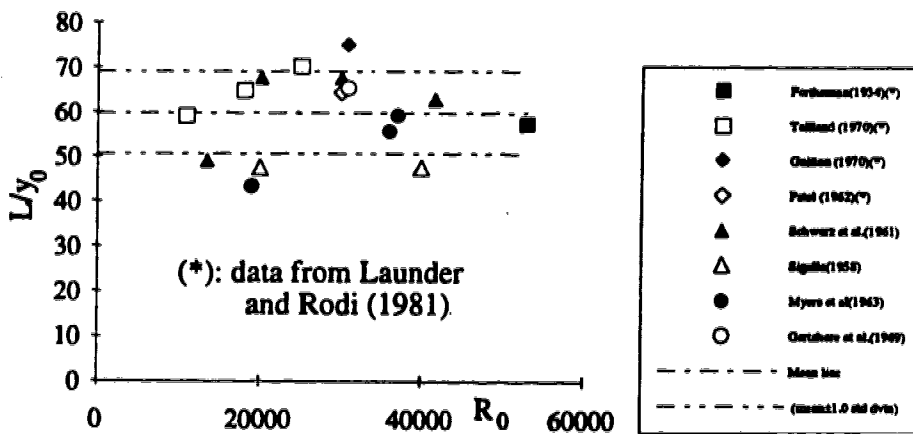


Fig. 4-9 Variation of the length scale  $L$  with nozzle Reynolds number for plane turbulent wall jets

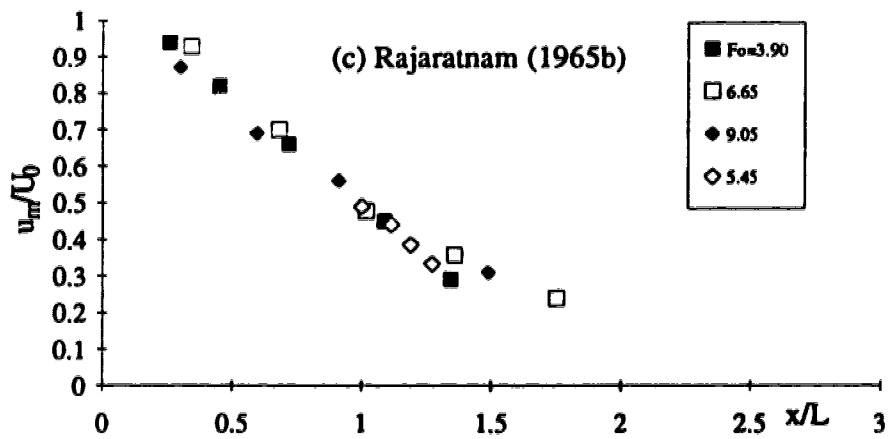
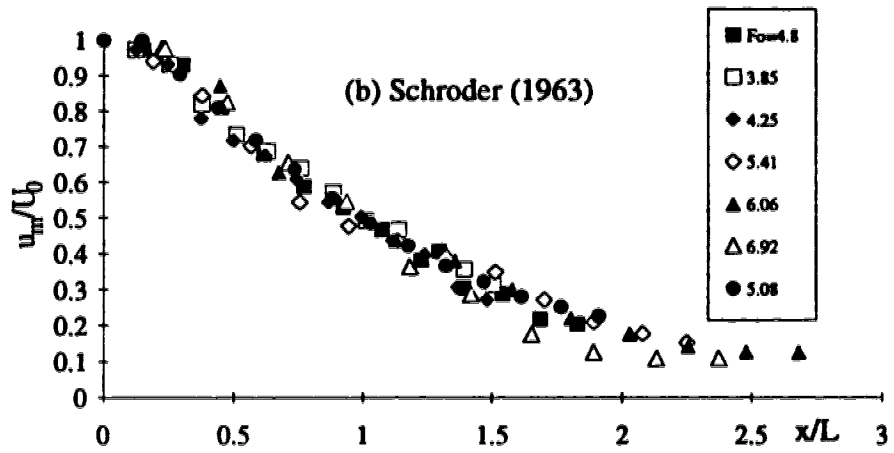
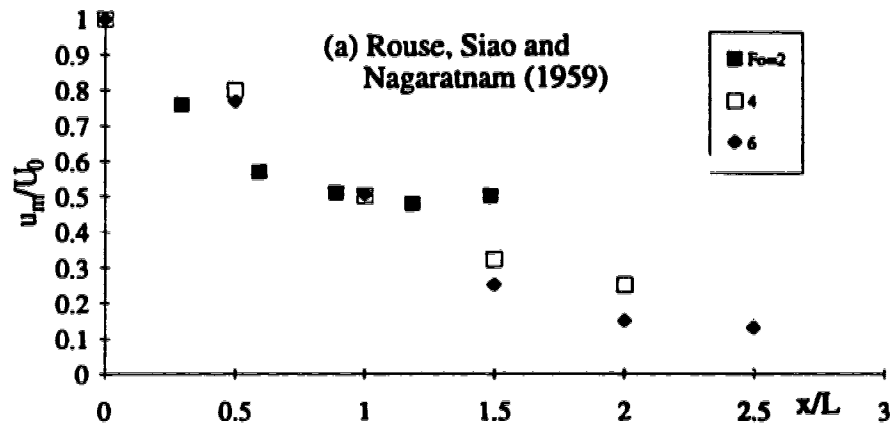


Fig. 4-10(a-c) Decay of the velocity scale in free jumps

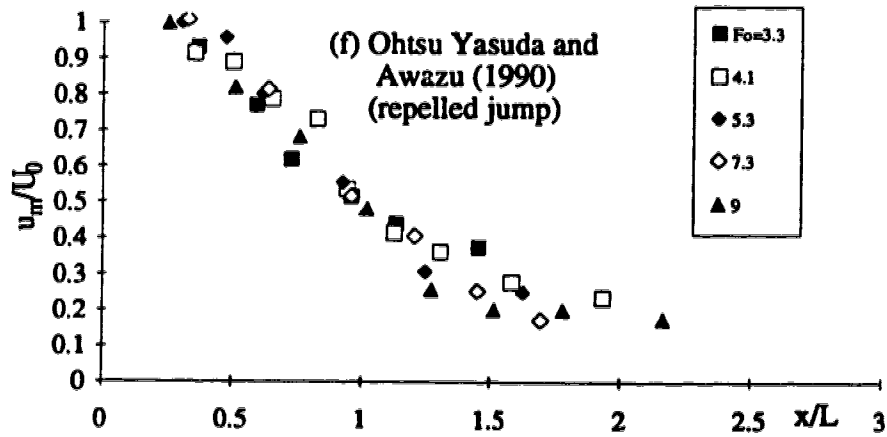
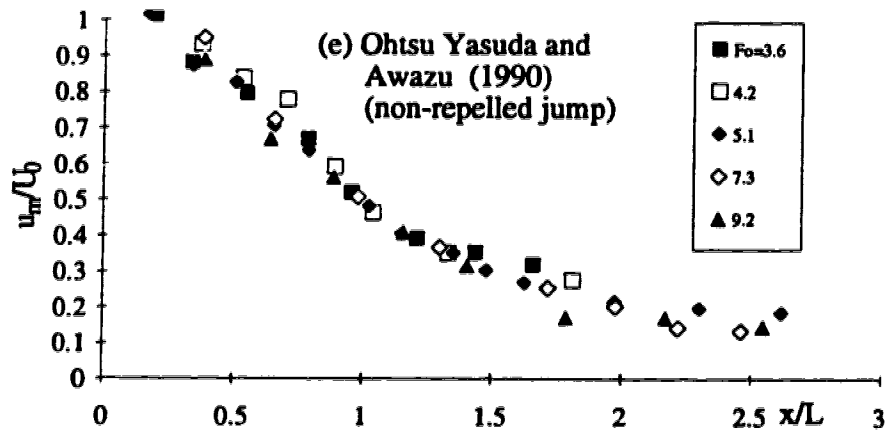
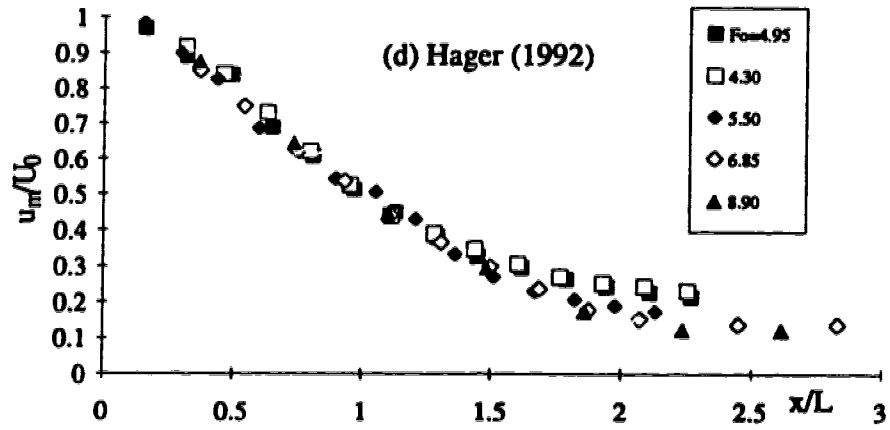


Fig. 4-10(d-f) Decay of the velocity scale in free jumps

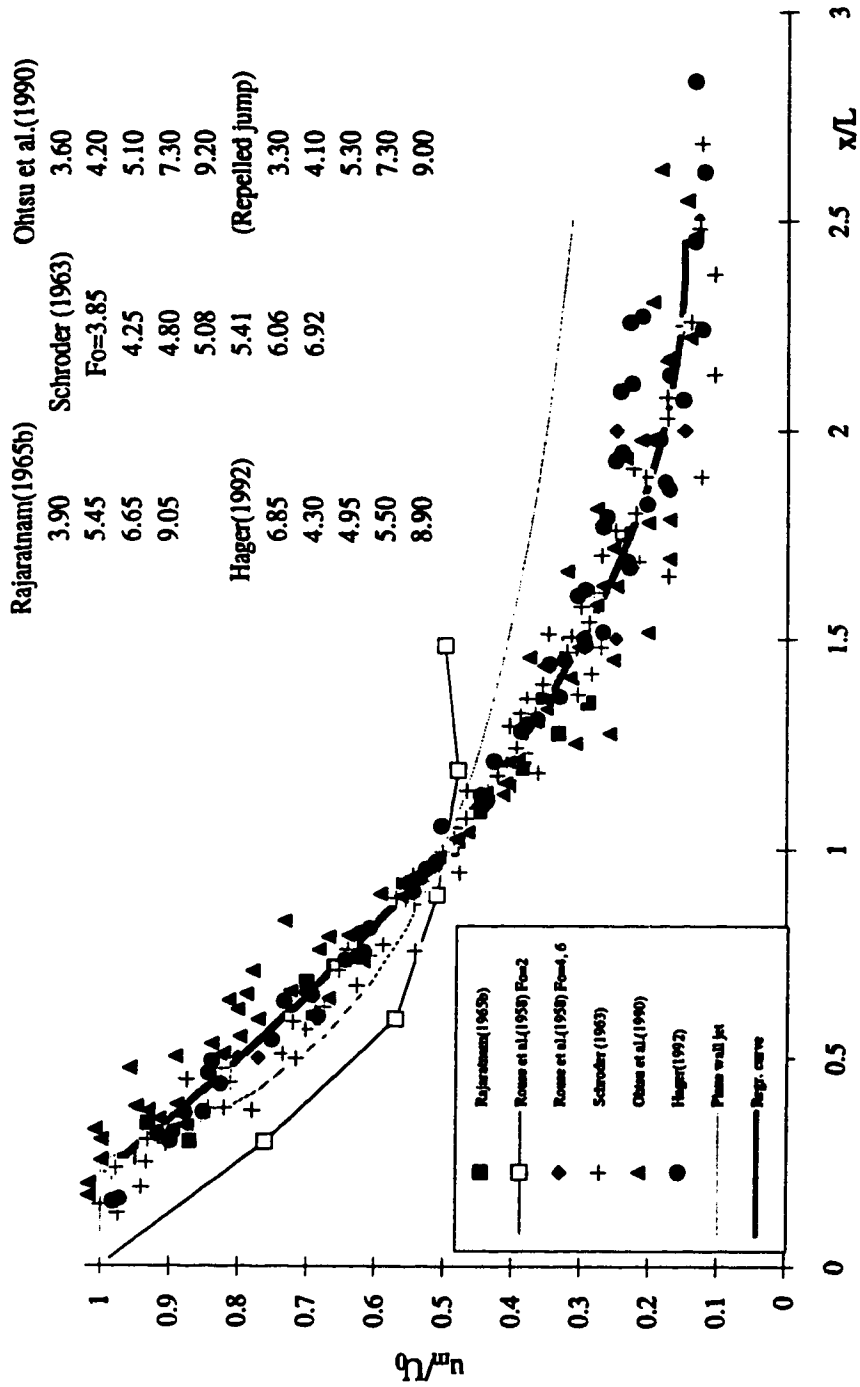


Fig. 4-11 Consolidated plot of the velocity scale decay in free jumps

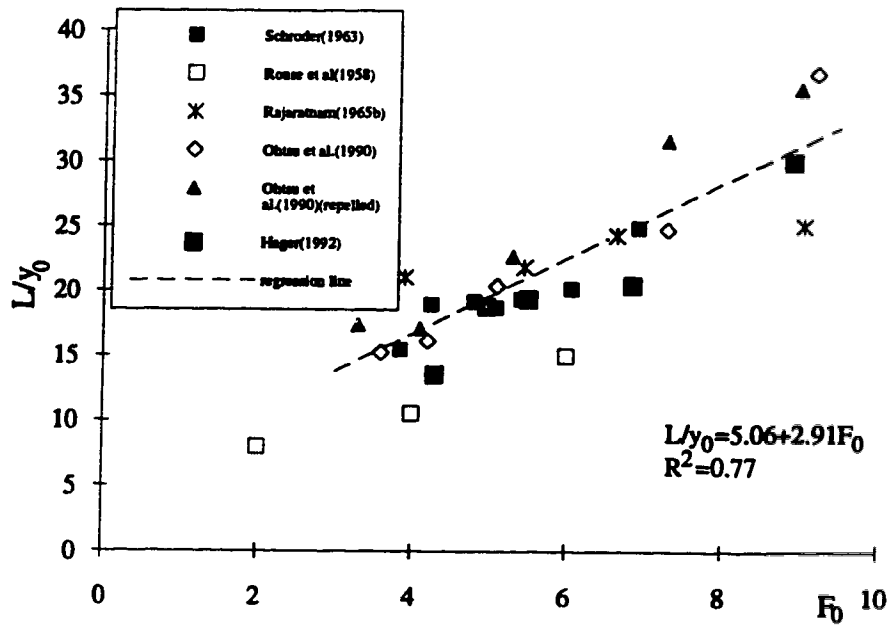


Fig. 4-12 Variation of the length scale L with  $F_0$  for the free jumps

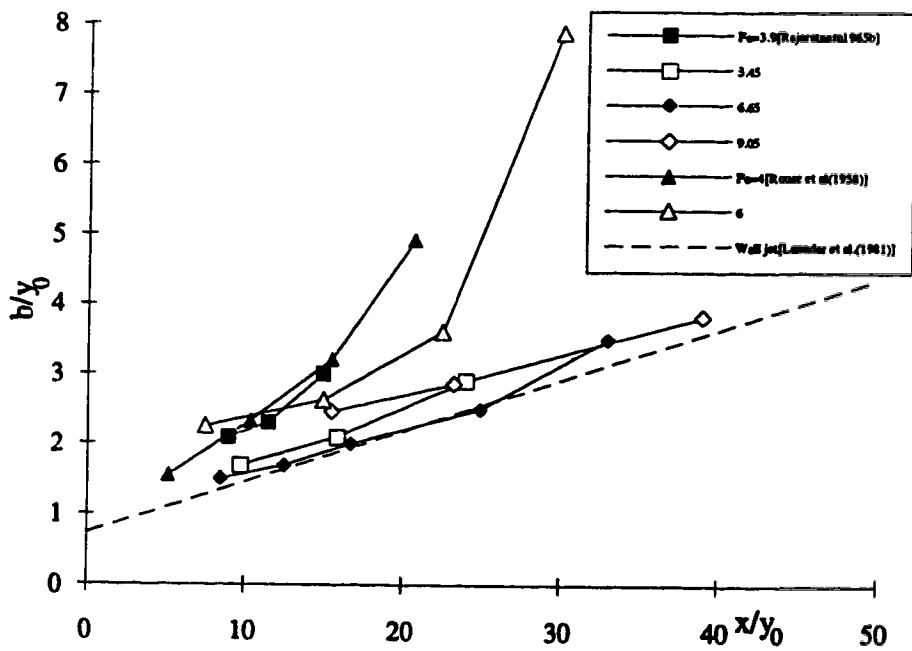


Fig. 4-13 Growth of the length scale b for the free jumps

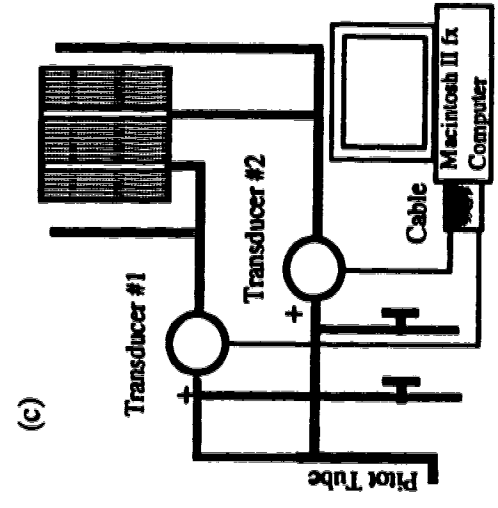
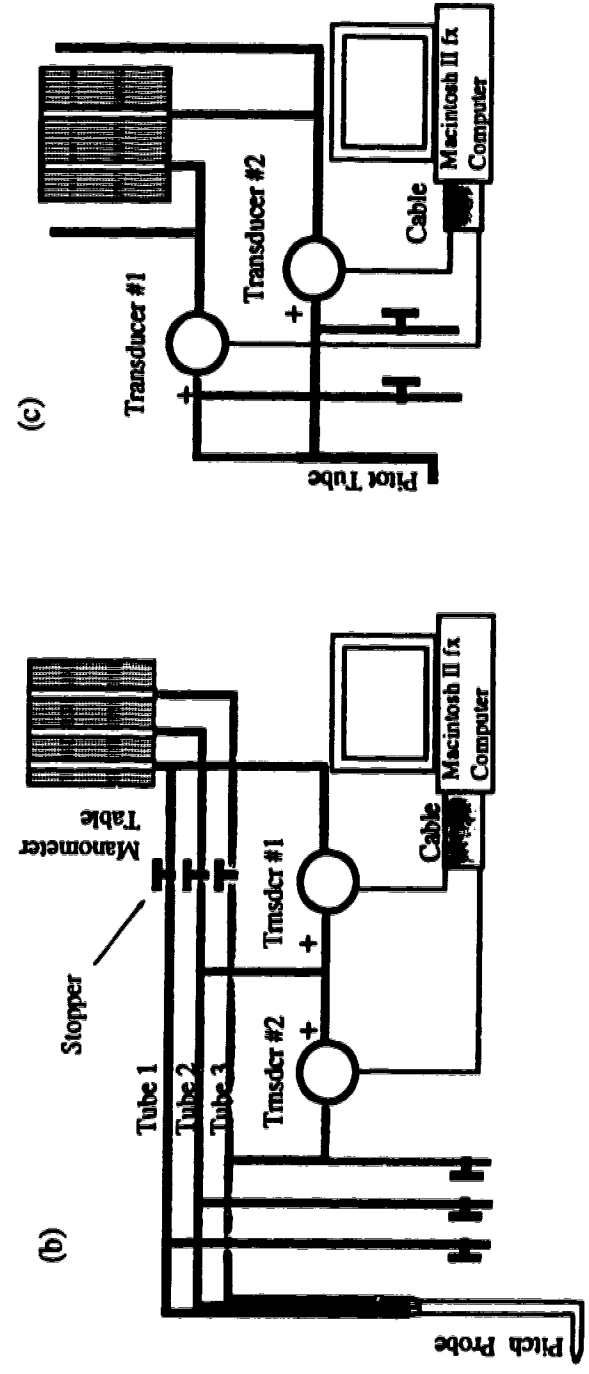
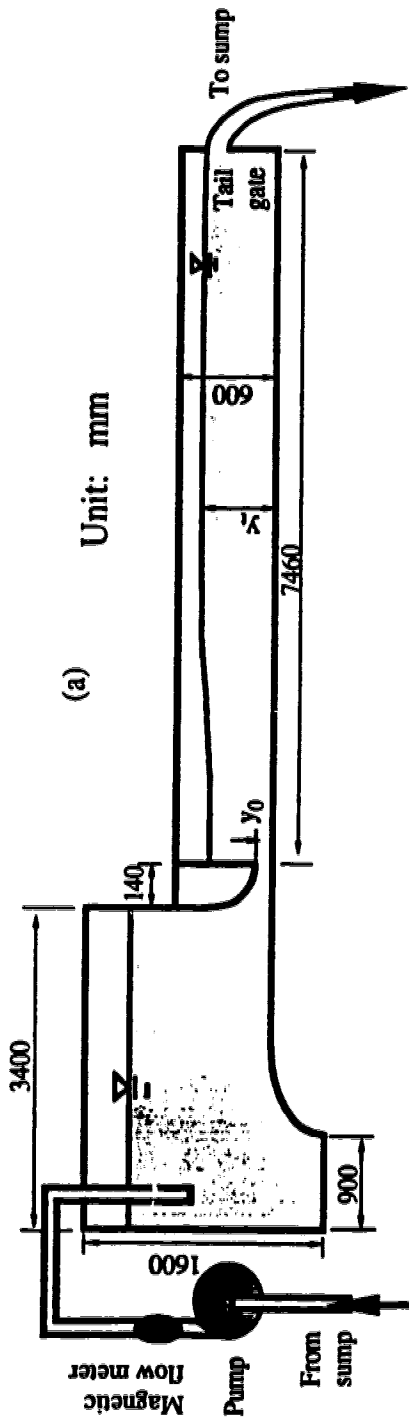


Fig. 4-14(a-c) Experimental arrangement

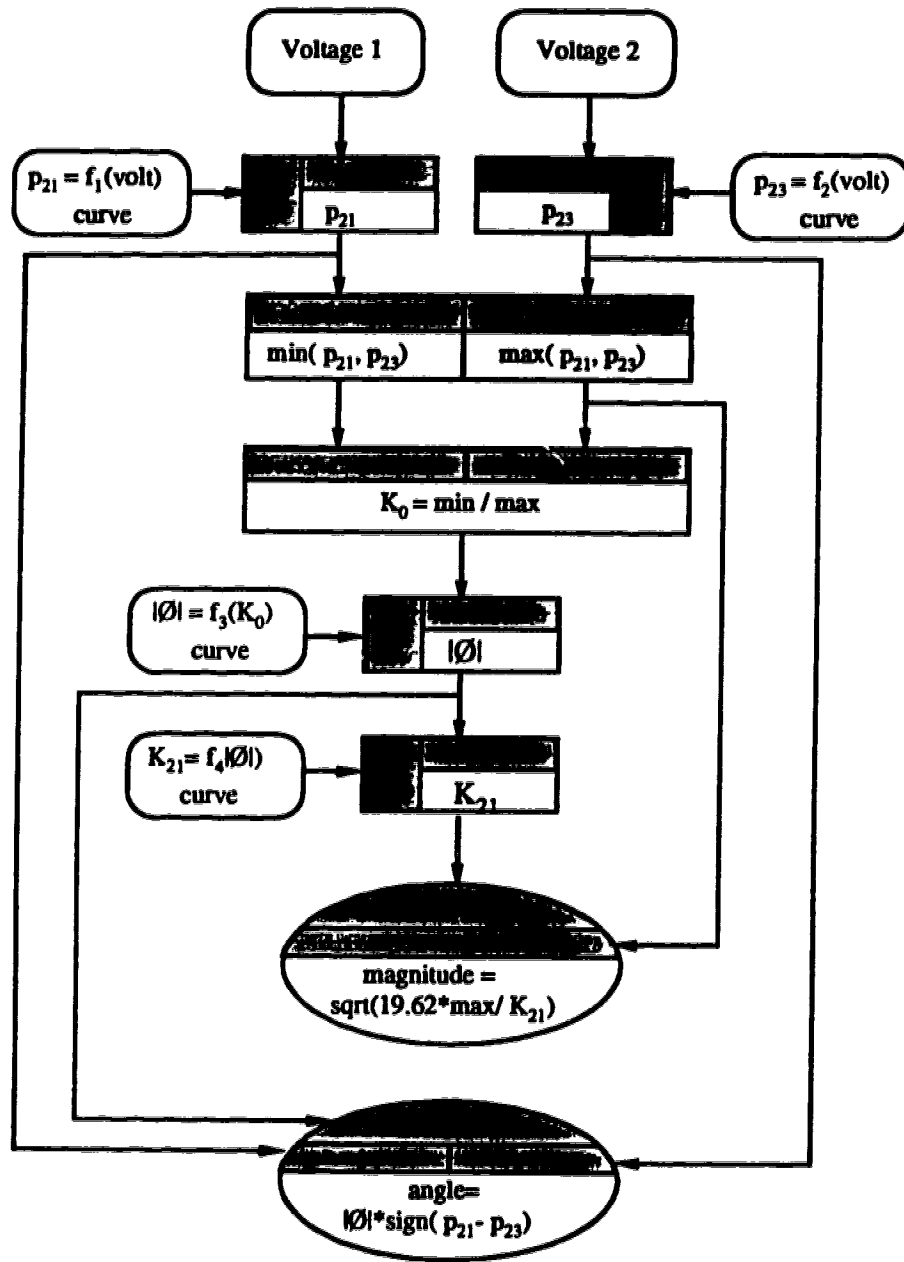


Fig. 4-15 Flow chart for sub-VI "From voltages to magnitude and angle"

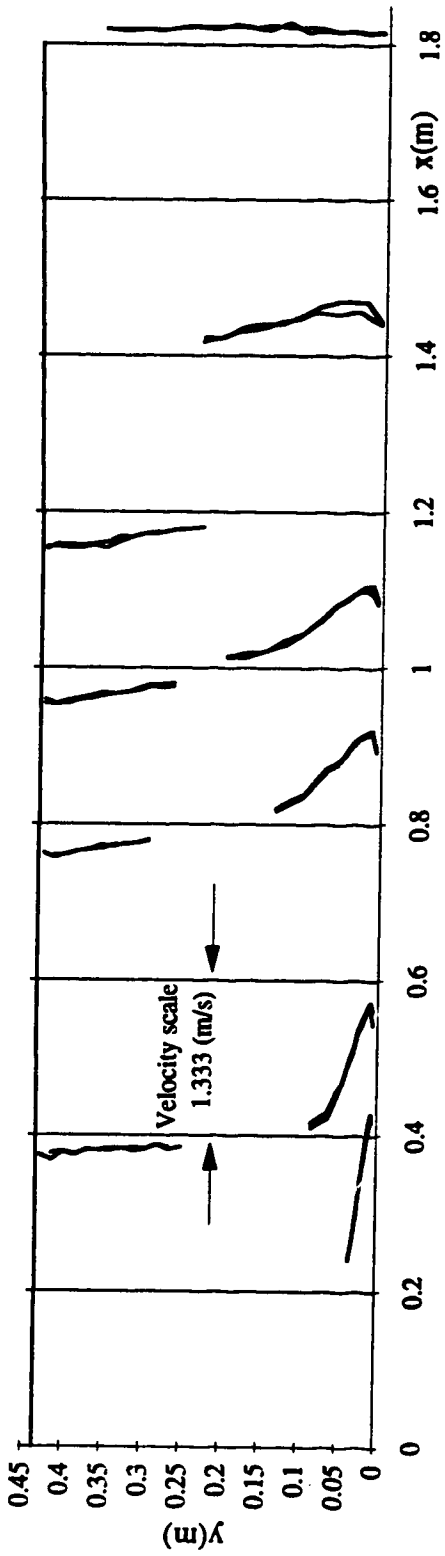


Fig. 4-16 Comparison of longitudinal velocity profiles of run 1 in  $z=0$  and  $z=0.1B$  planes

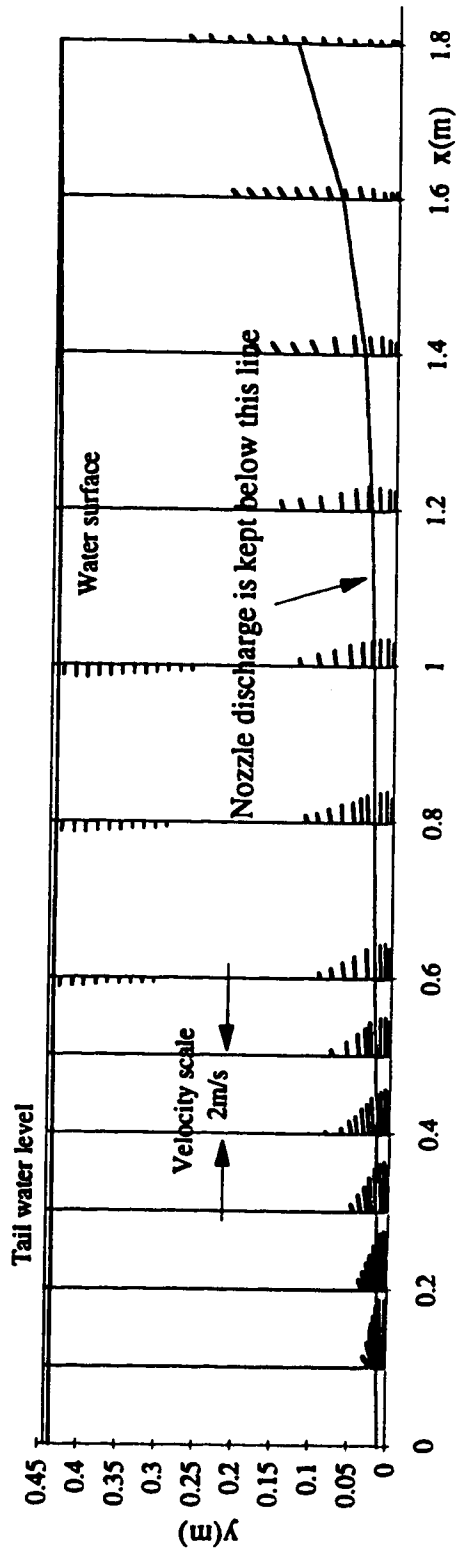


Fig. 4-17 Mean velocity field of run 1



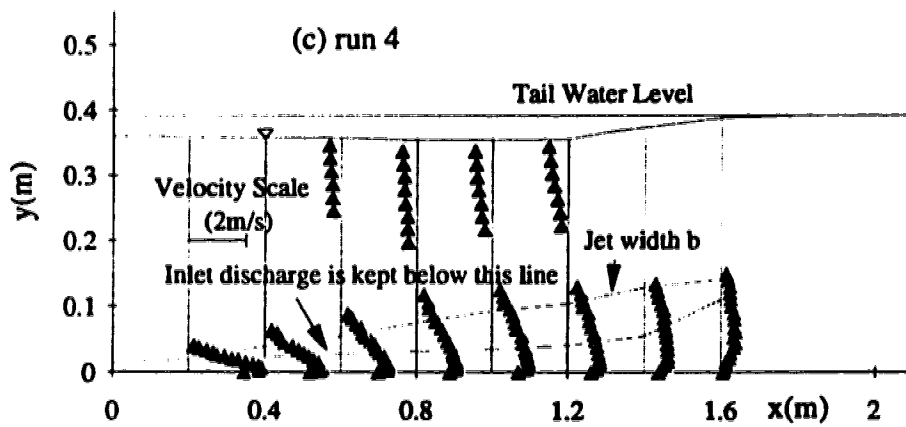
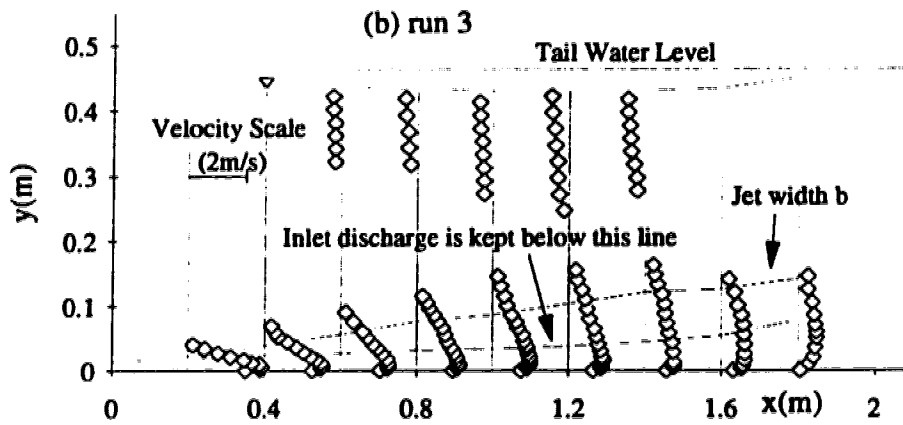
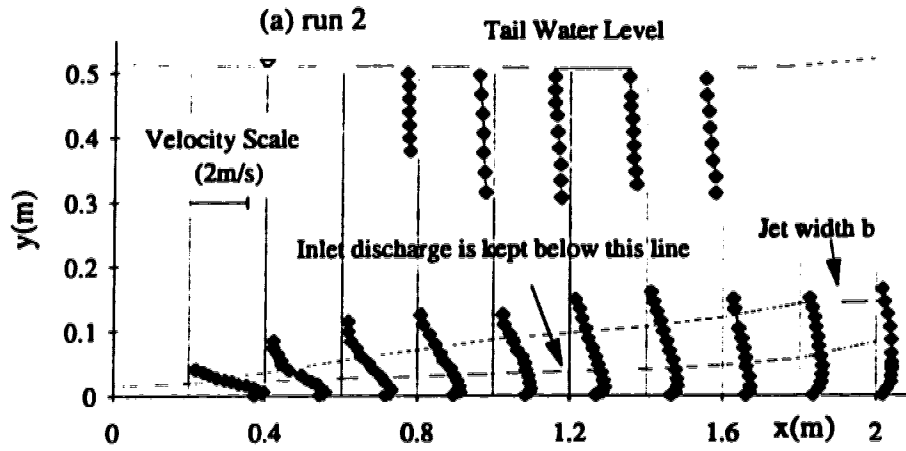


Fig. 4-18(a-c) Longitudinal velocity profiles for runs 2, 3 & 4

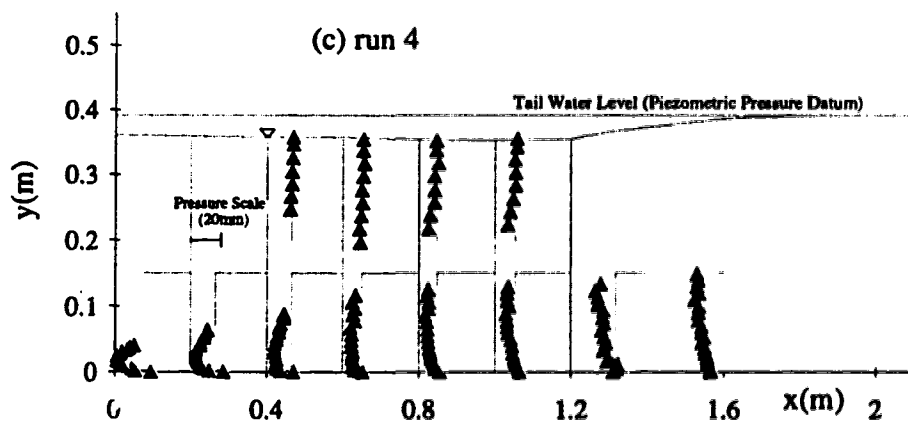
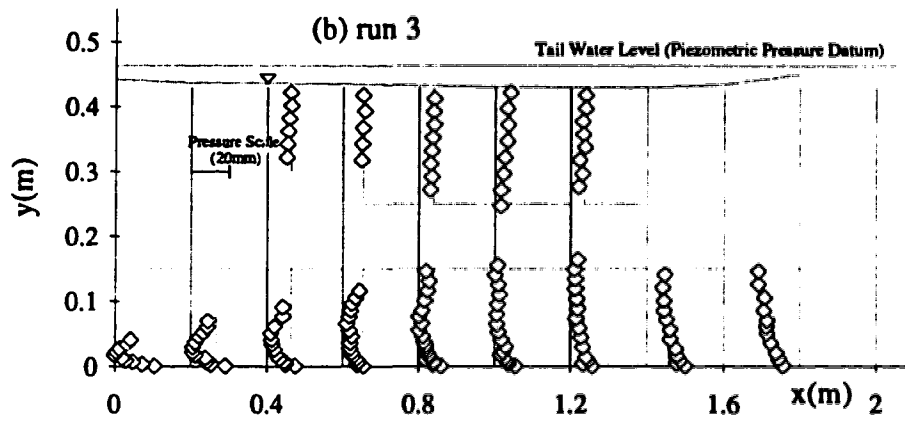
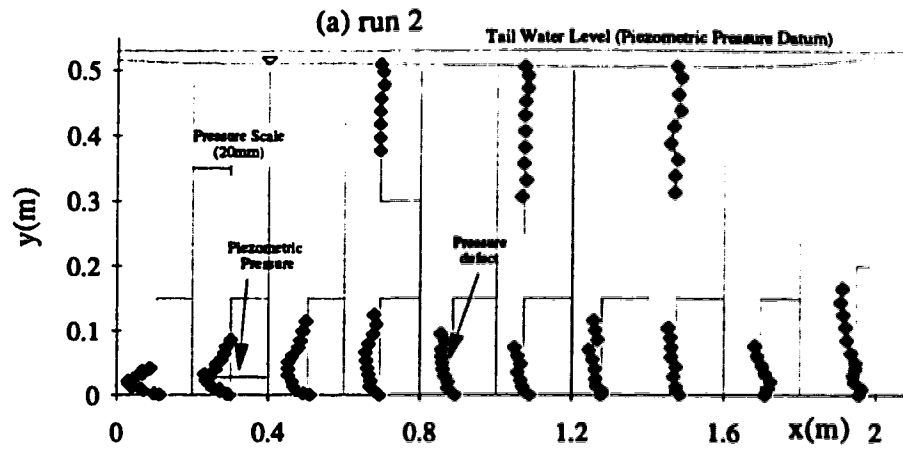


Fig. 4-19(a-c) Pressure profiles for runs 2,3 & 4

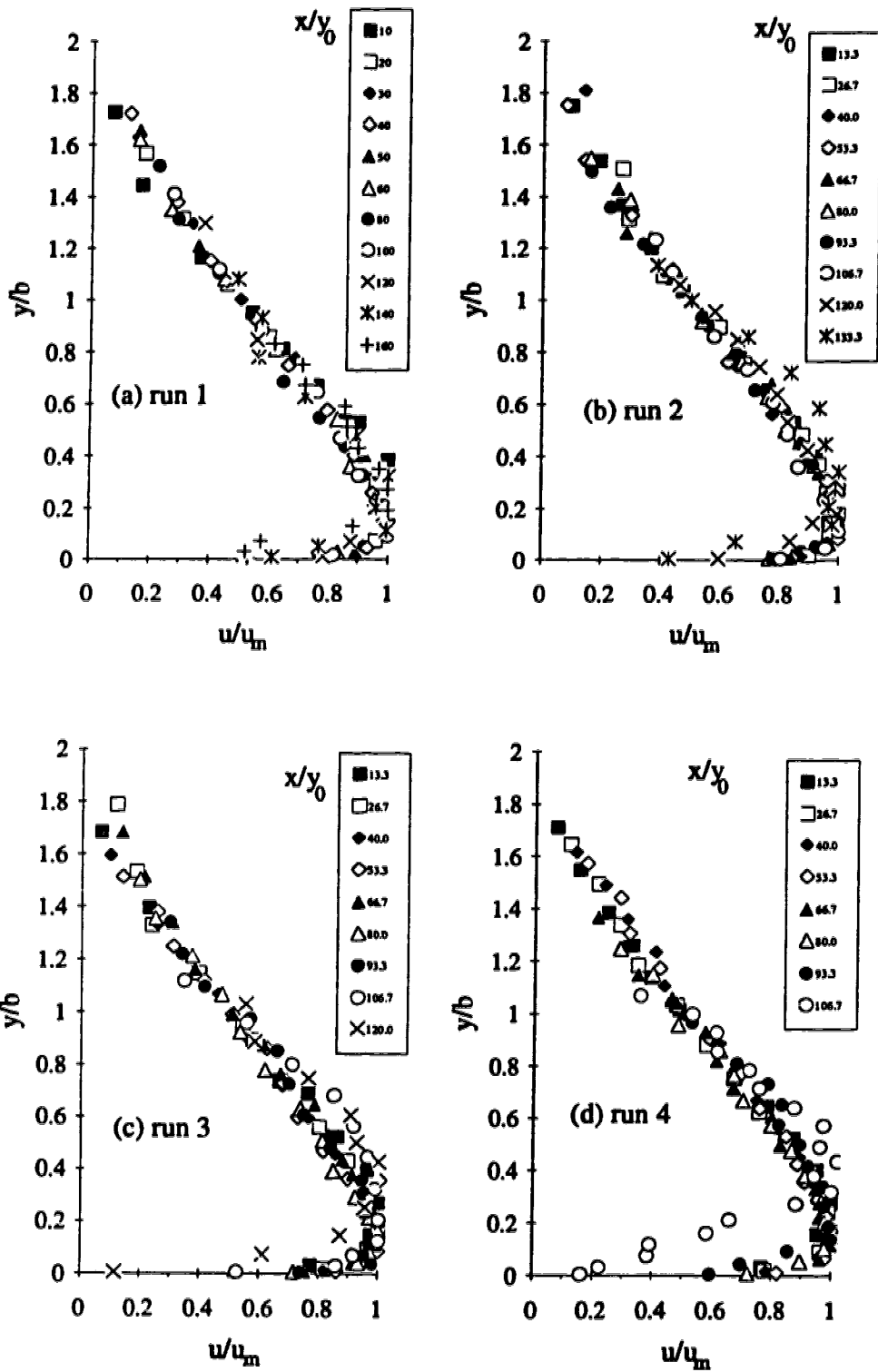


Fig. 4-20(a-d) Non-dimensional longitudinal velocity profiles for runs 1 ~ 4

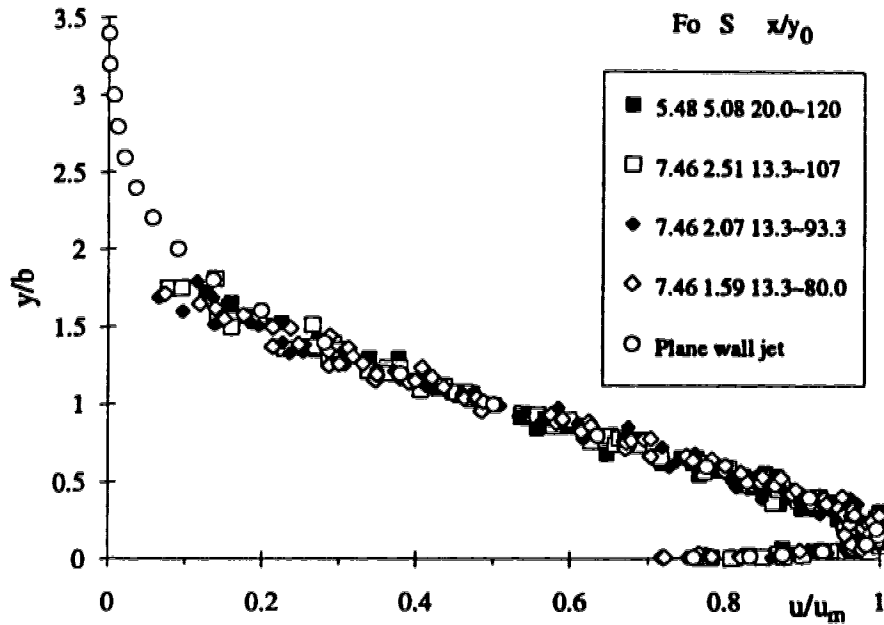


Fig. 4-21 Consolidated plot of the non-dimensional longitudinal velocity profiles of present experiments on submerged jumps

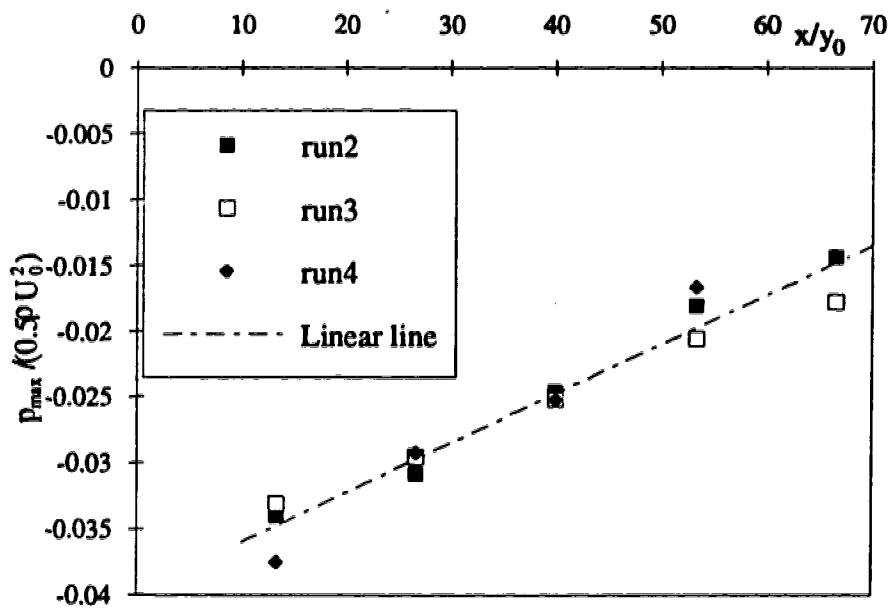


Fig. 4-22 Longitudinal variation of the maximum pressure defect in submerged jumps

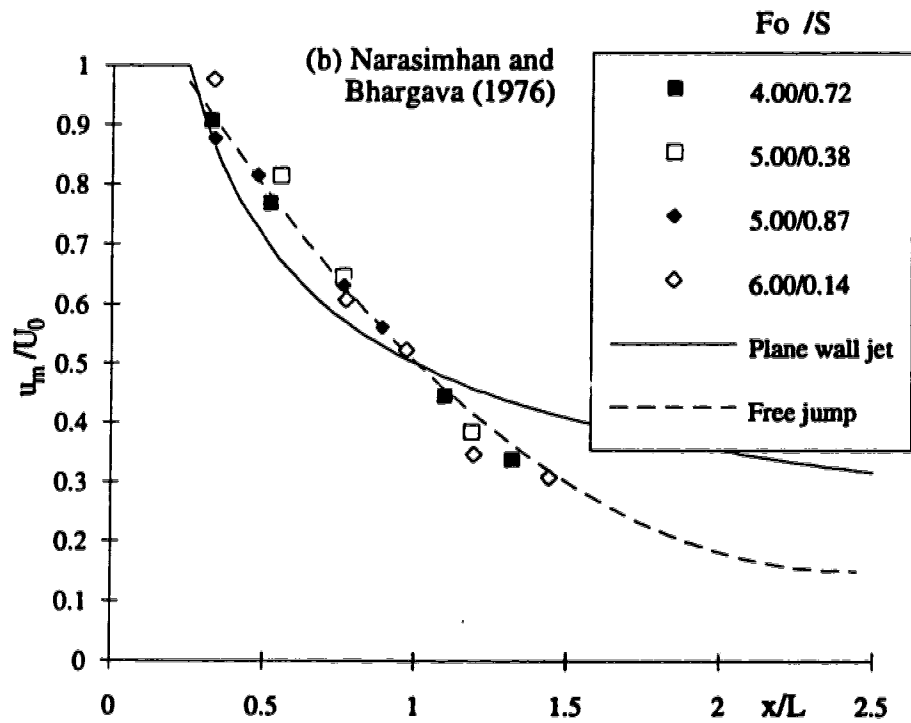
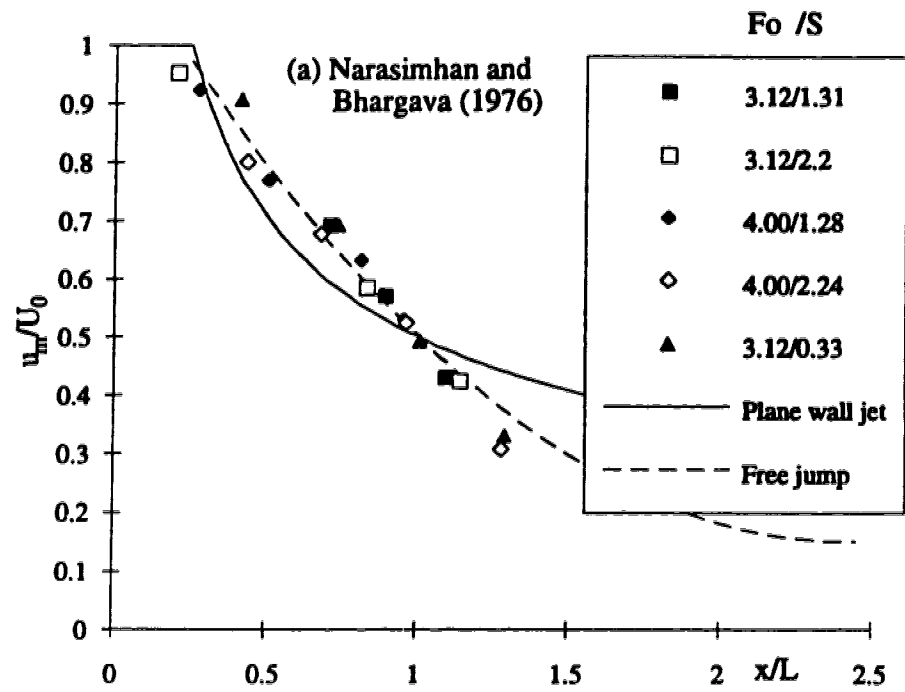


Fig. 4-23(a-b) Longitudinal variation of the velocity scale in submerged jumps

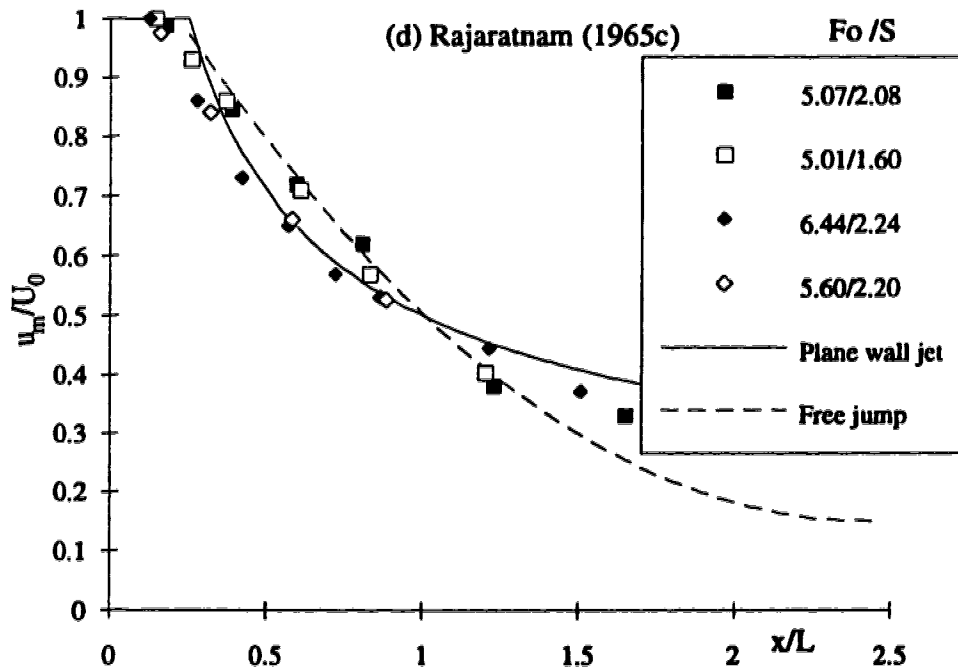
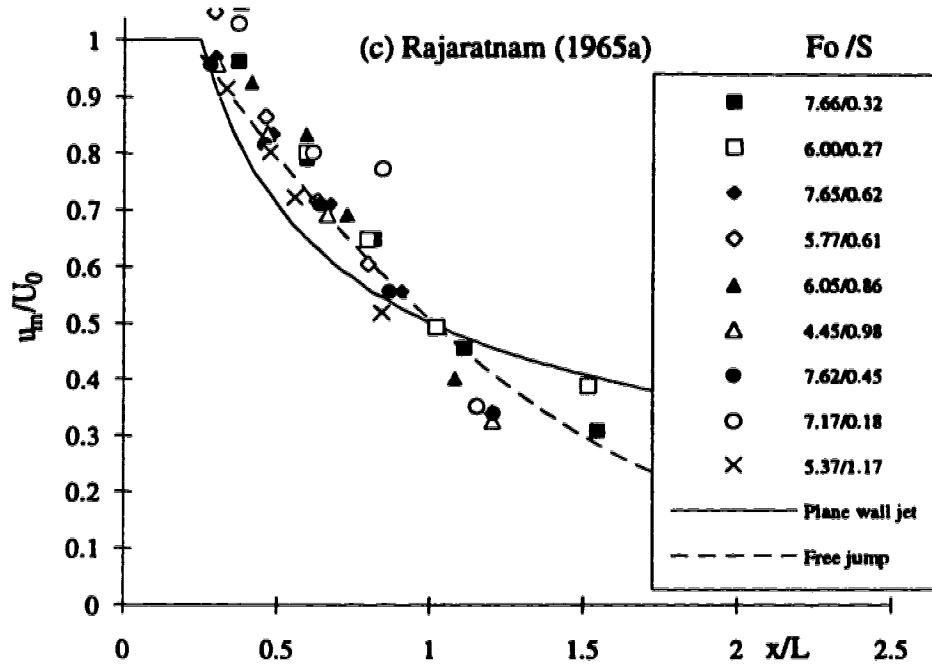


Fig. 4-23(c-d) Longitudinal variation of the velocity scale in submerged jumps

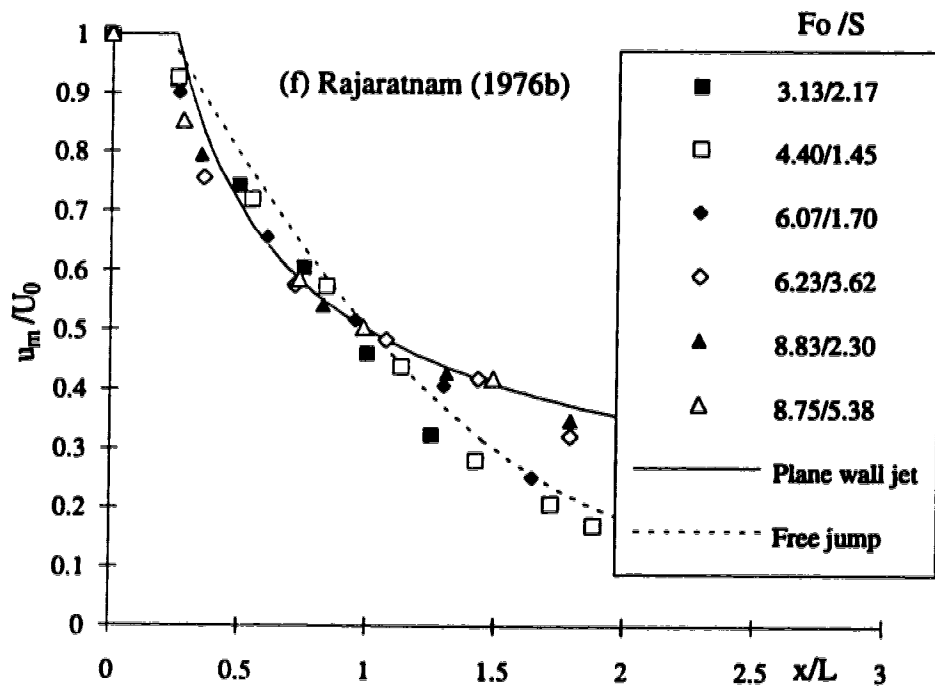
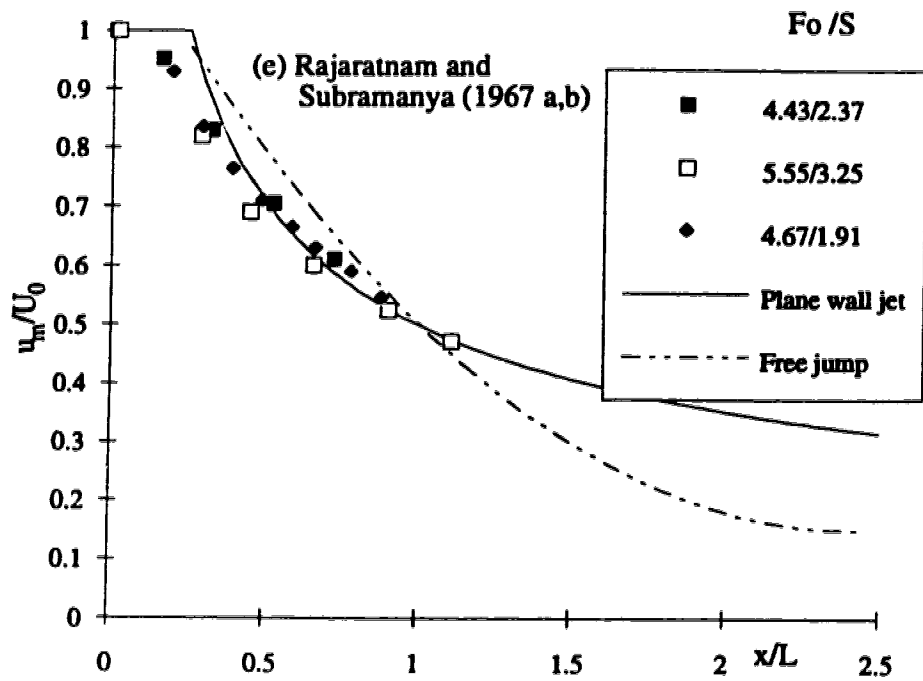


Fig. 4-23(e-f) Longitudinal variation of the velocity scale in submerged jumps

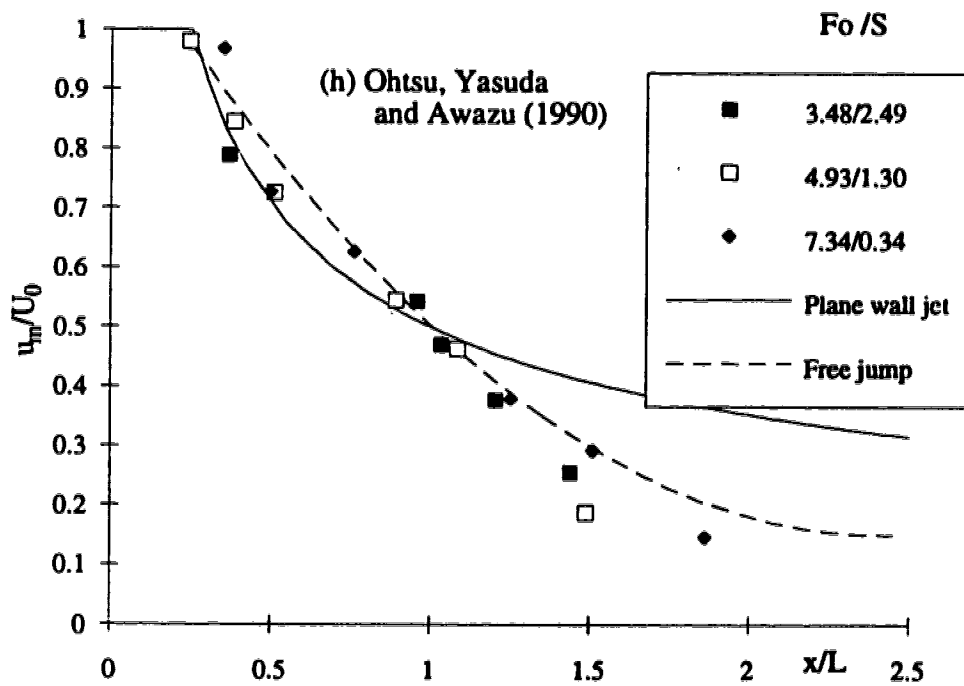
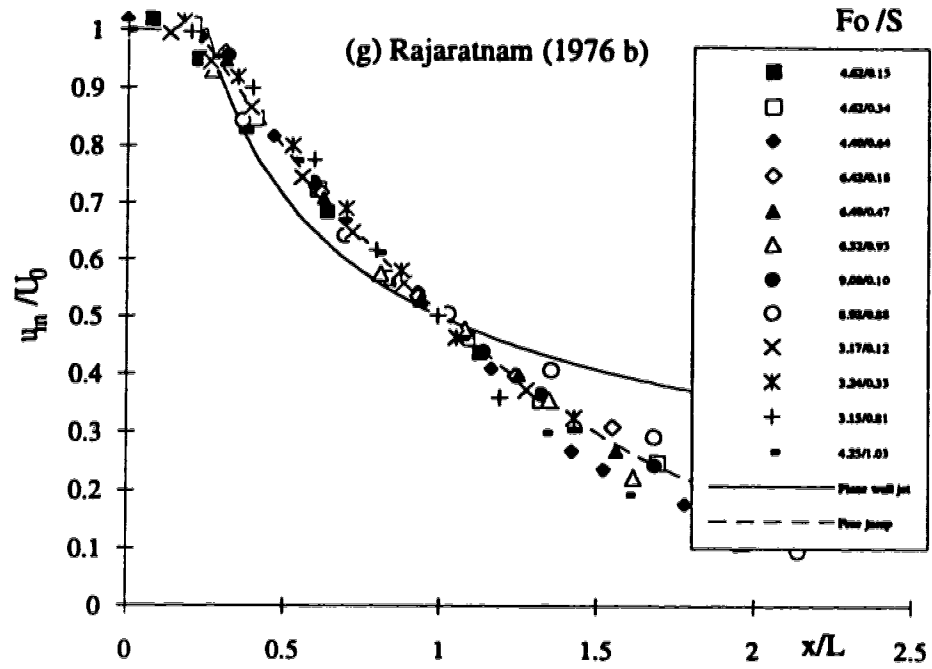


Fig. 4-23(g-h) Longitudinal variation of the velocity scale in submerged jumps



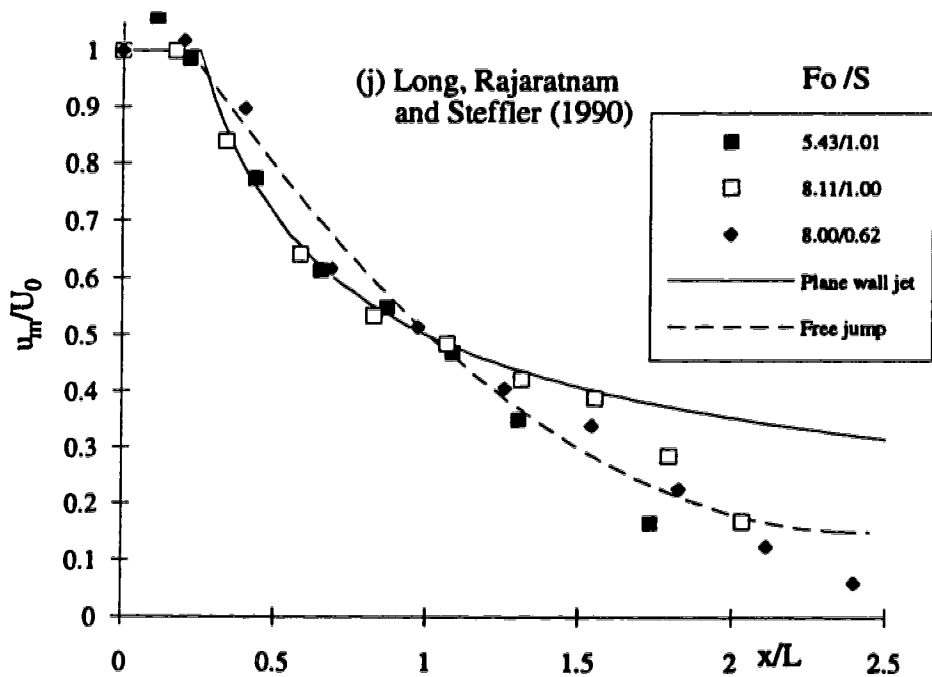
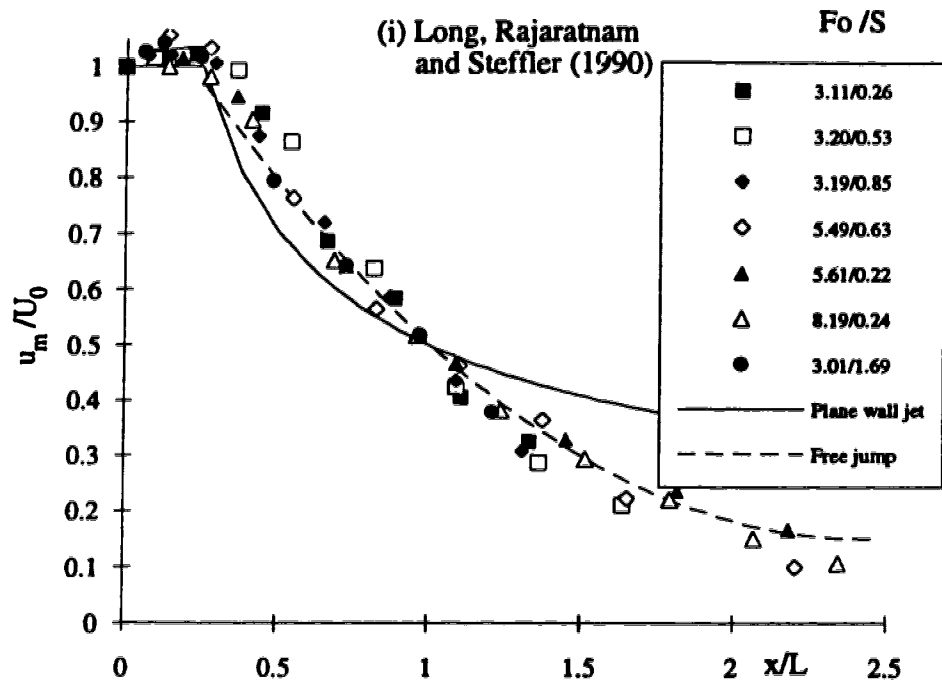


Fig. 4-23(i-j) Longitudinal variation of the velocity scale in submerged jumps

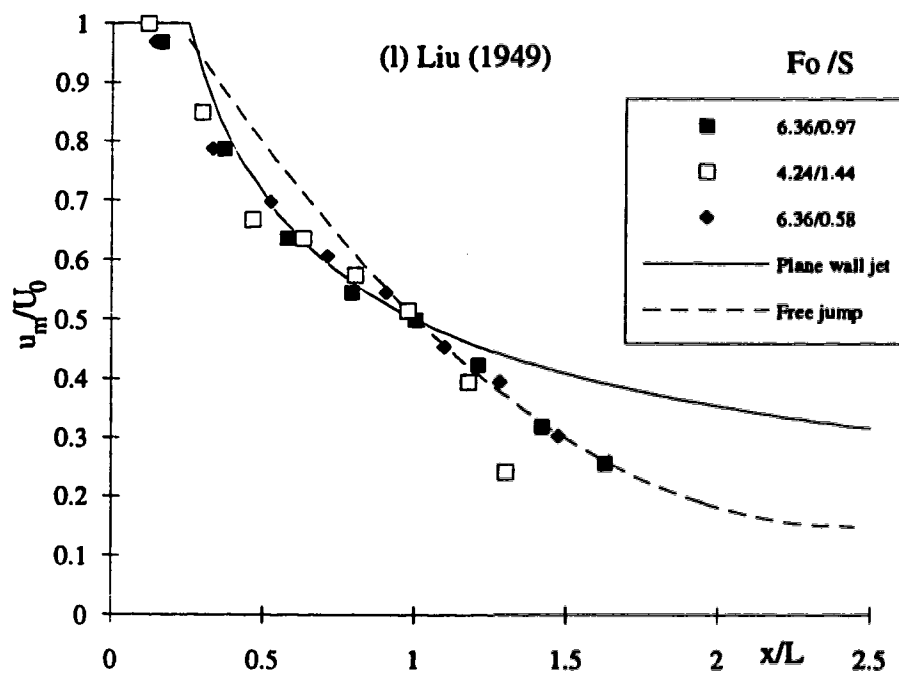
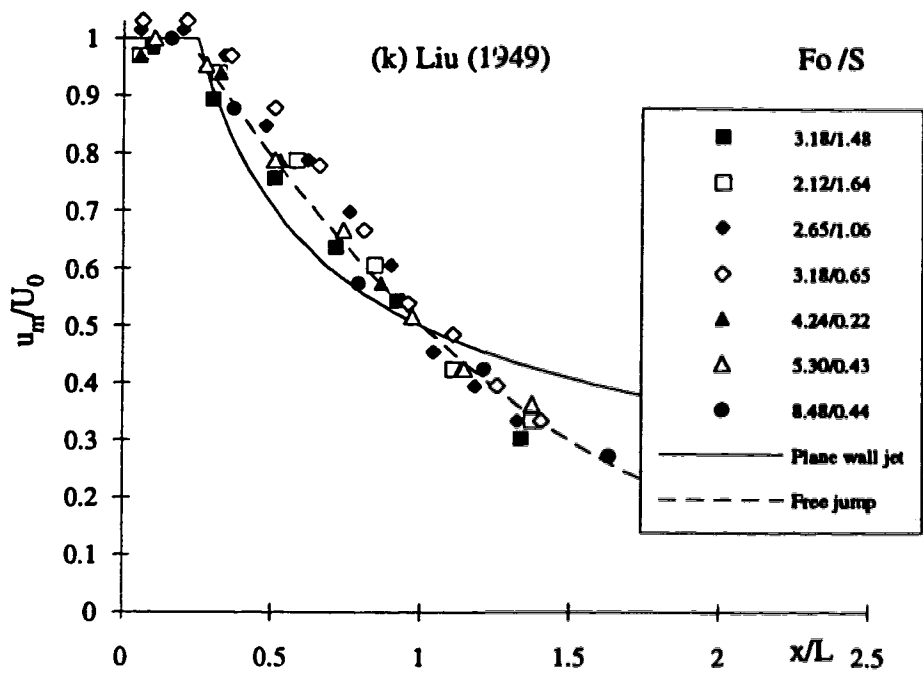


Fig. 4-23(k-l) Longitudinal variation of the velocity scale in submerged jumps

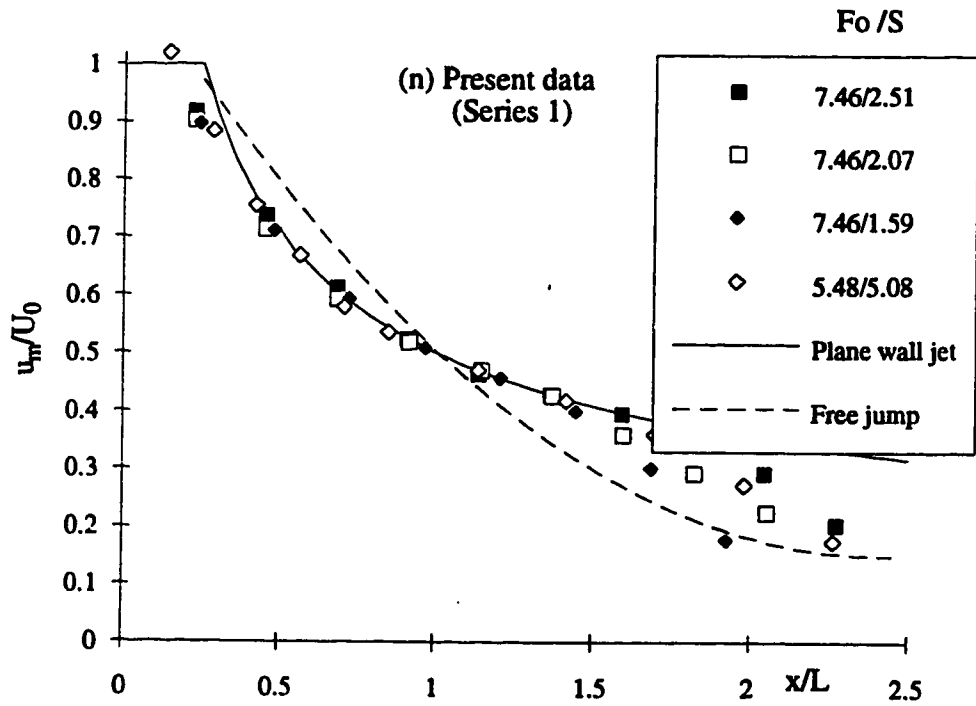
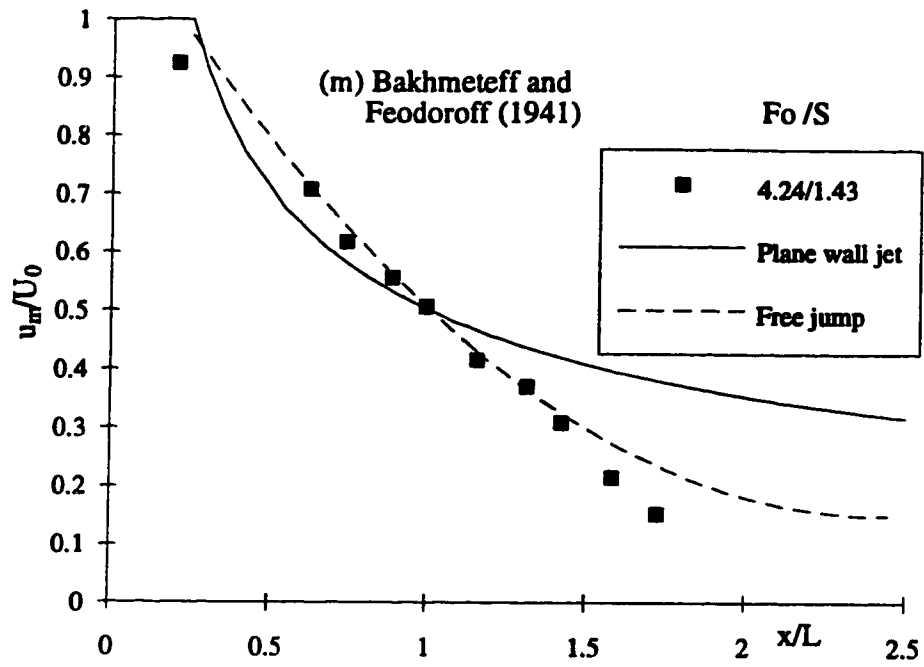


Fig. 4-23(m-n) Longitudinal variation of the velocity scale in submerged jumps

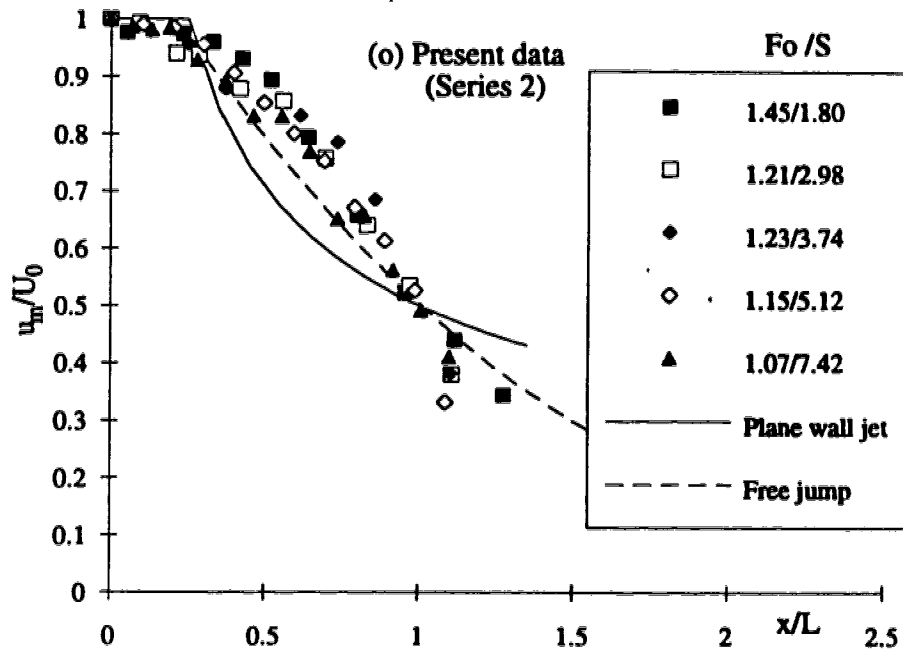


Fig. 4-23(o) Longitudinal variation of the velocity scale in submerged jumps

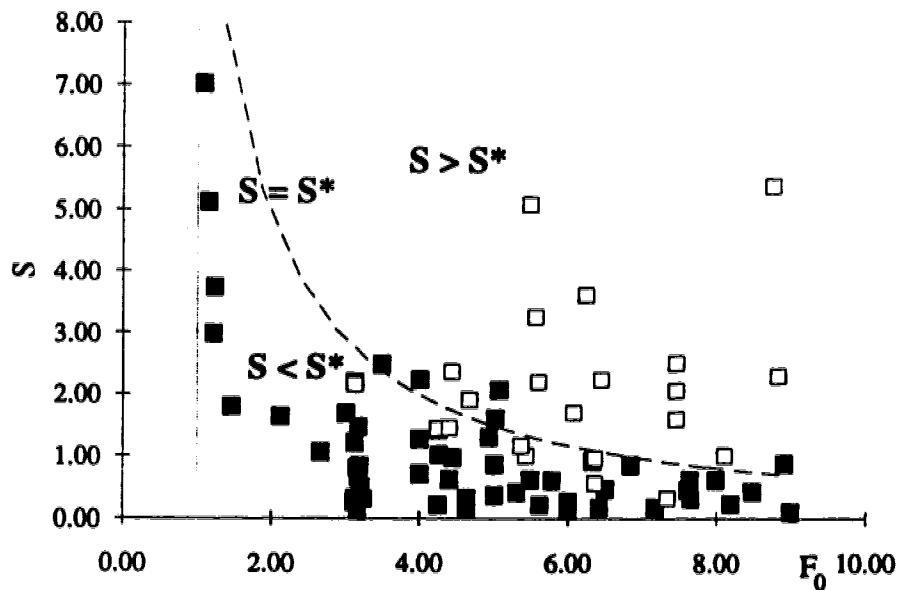


Fig. 4-24 Variation of  $S^*$  with  $F_0$

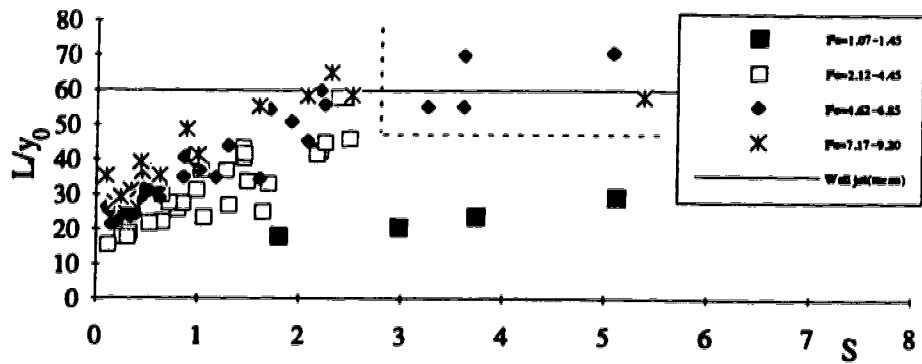


Fig. 4-25 Variation of the length scale  $L$  with  $F_0$  and  $S$  for submerged jumps

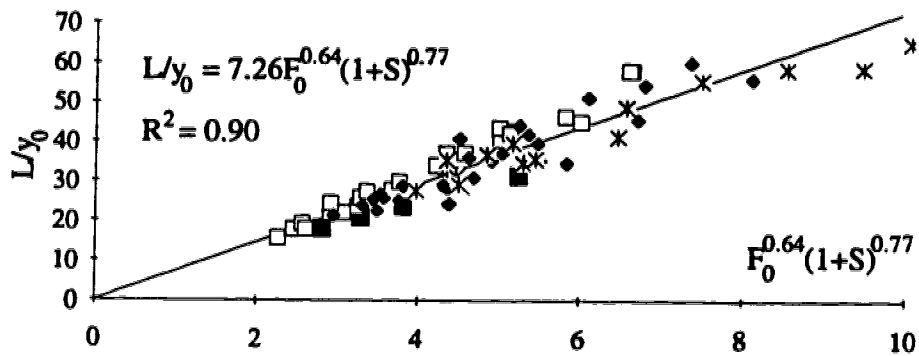


Fig. 4-26 Correlation between  $L/y_0$  and  $F_0$  and  $S$  for submerged jumps

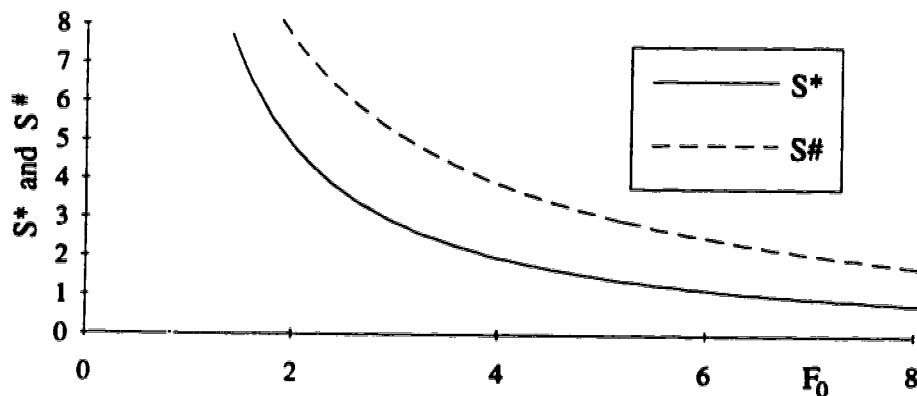


Fig. 4-27 Variation of  $S^*$  and  $S^\#$  with  $F_0$  for submerged jumps

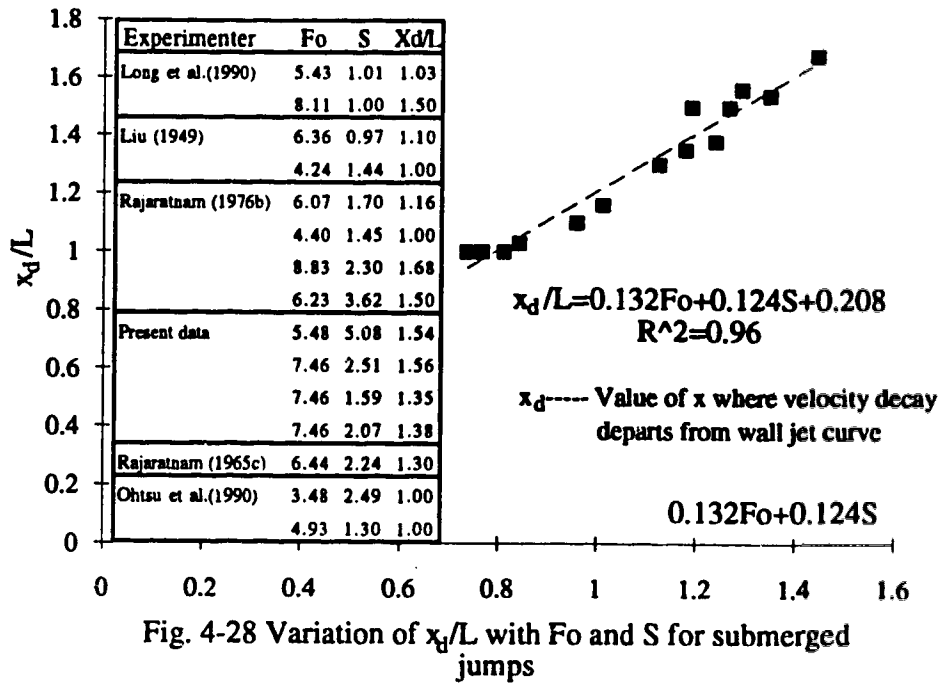


Fig. 4-28 Variation of  $x_d/L$  with Fo and S for submerged jumps

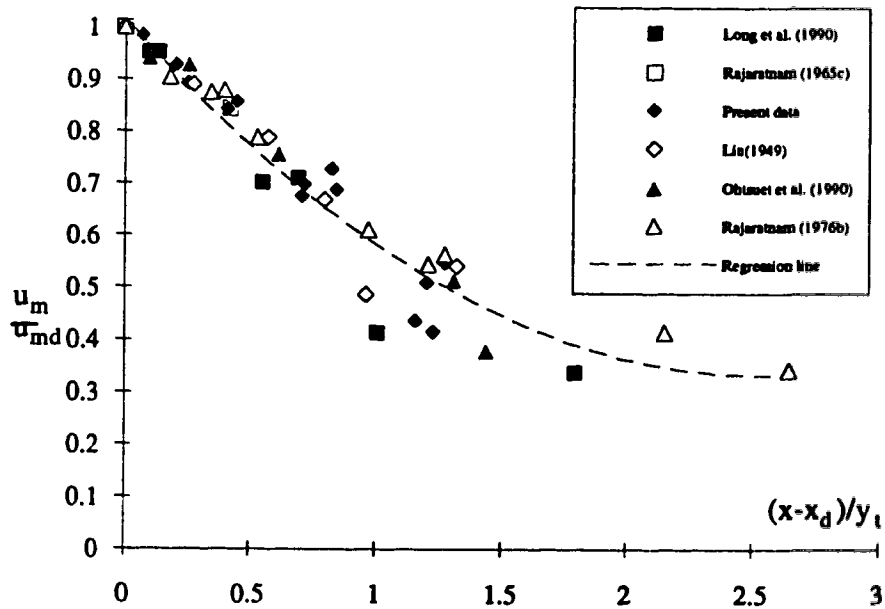


Fig. 4-29 Velocity scale decay of WJL jump in the region off the wall jet curve

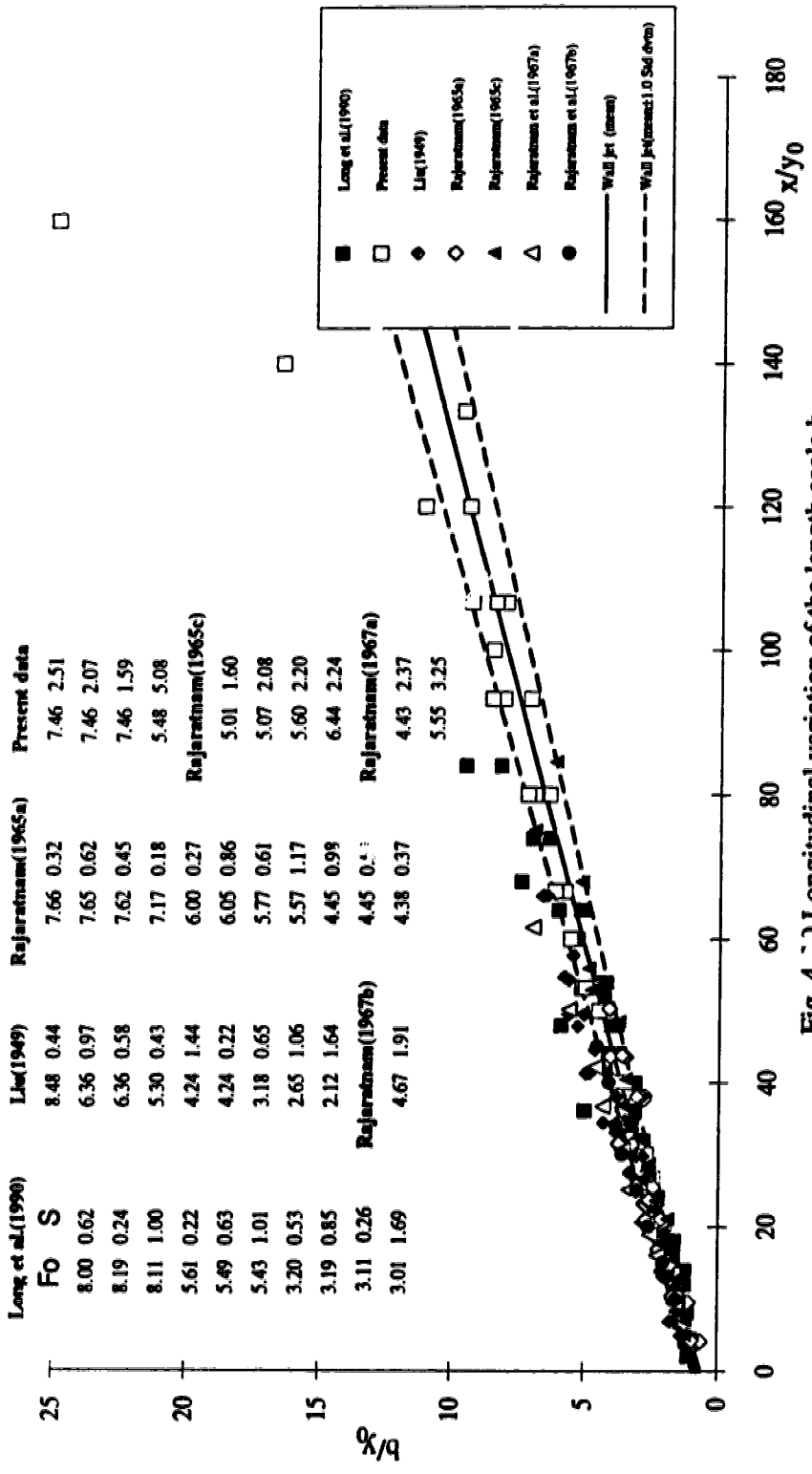


Fig. 4-3) Longitudinal variation of the length scale b for submerged jumps

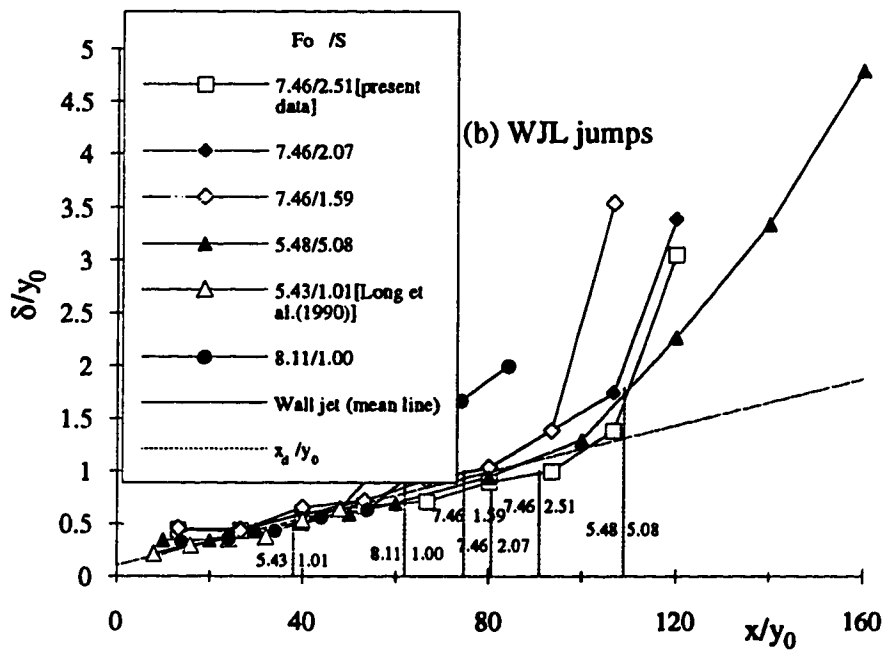
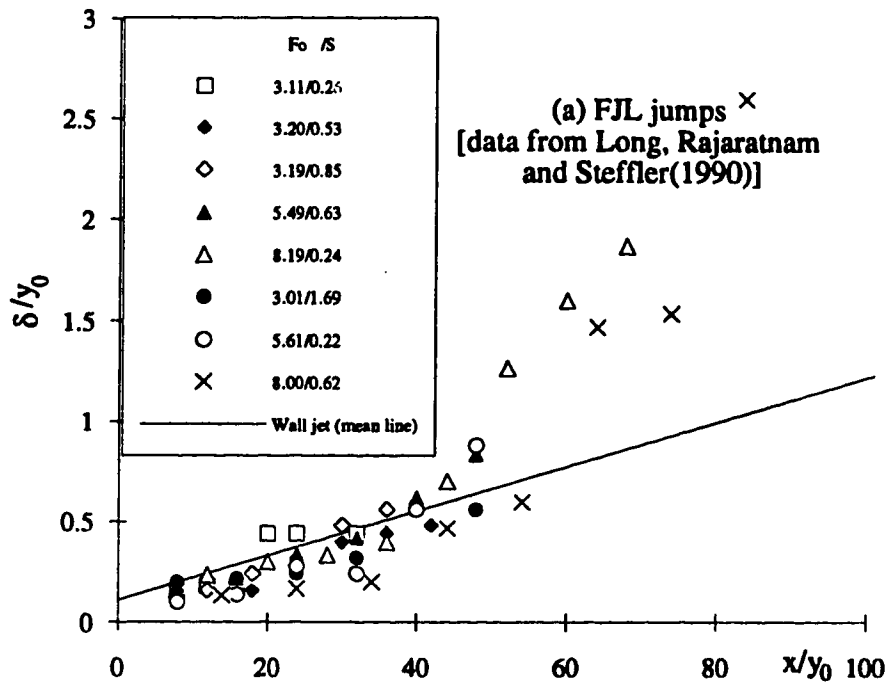


Fig. 4-31(a-b) Growth of the inner layer of submerged jumps



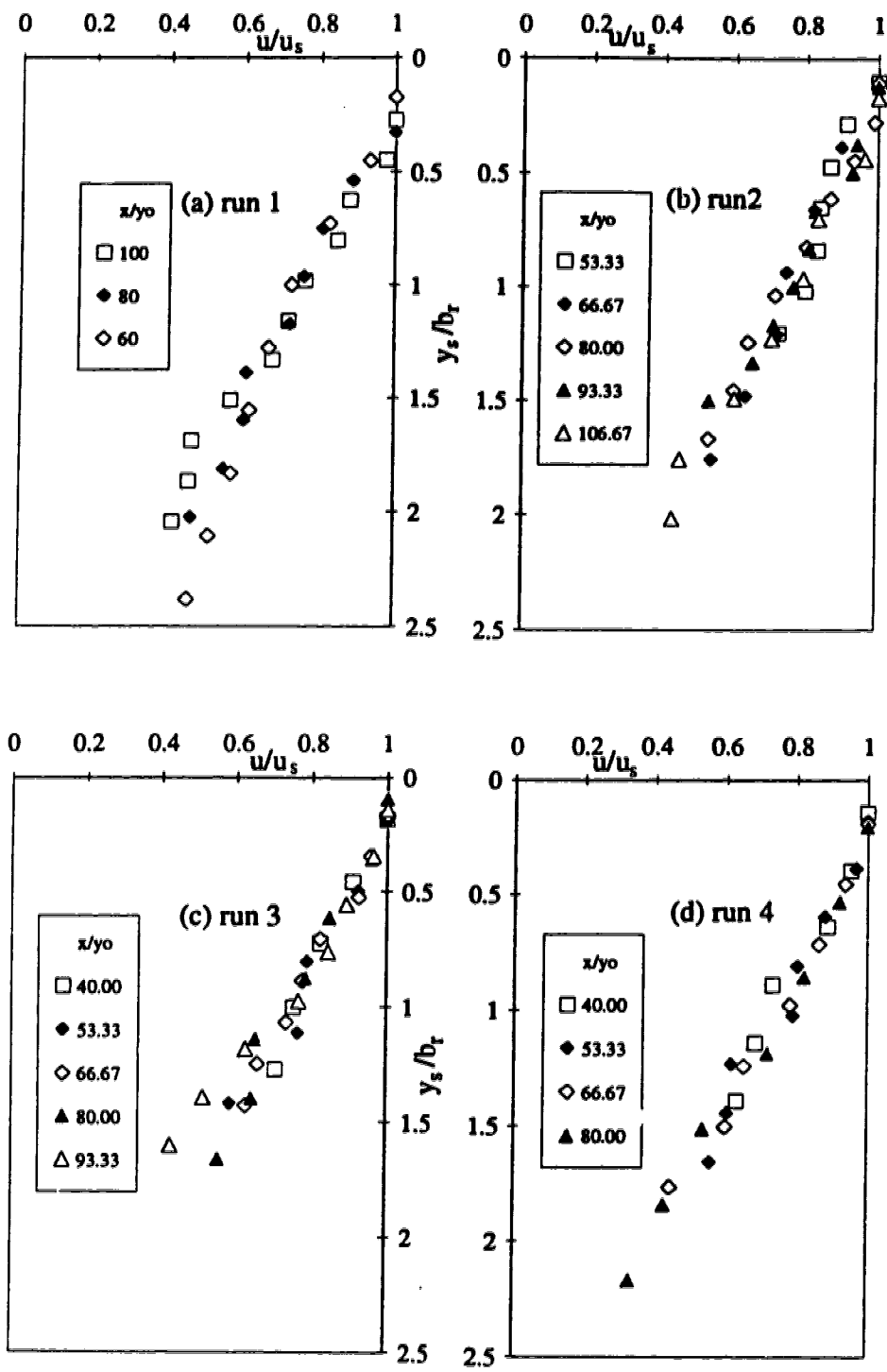


Fig. 4-32(a-d) Similarity of velocity profiles of the reverse flow in submerged jumps

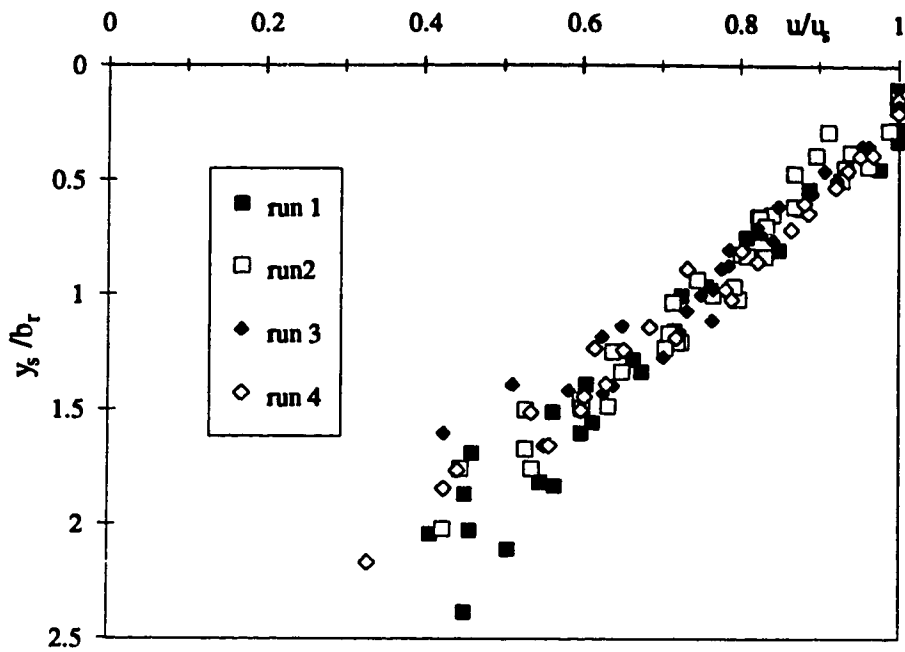


Fig. 4-33 Consolidated non-dimensional plot of the reverse flow velocity profiles in submerged jumps

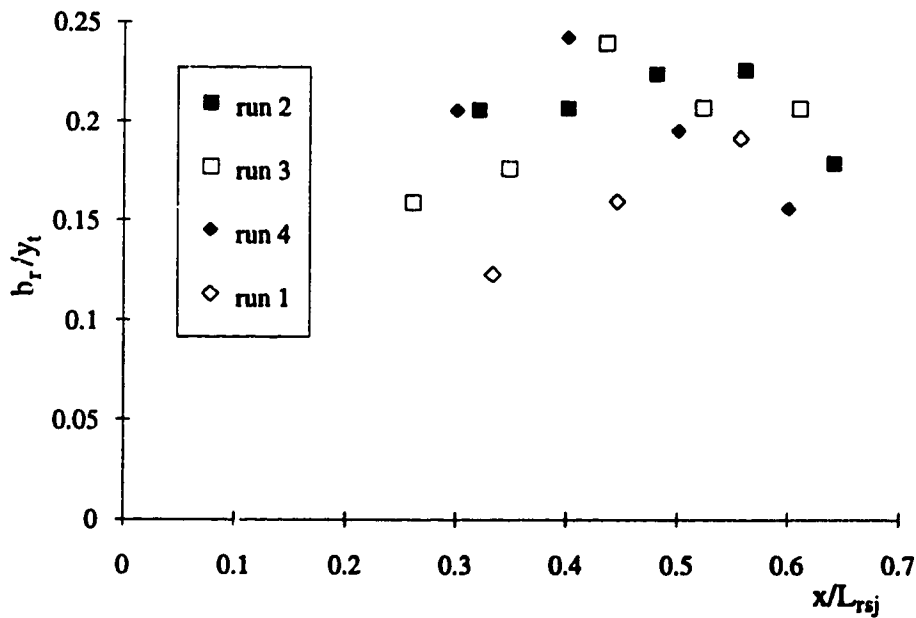


Fig. 4-34 Longitudinal variation of the length scale  $b_r$  of the reverse flow region of submerged jumps

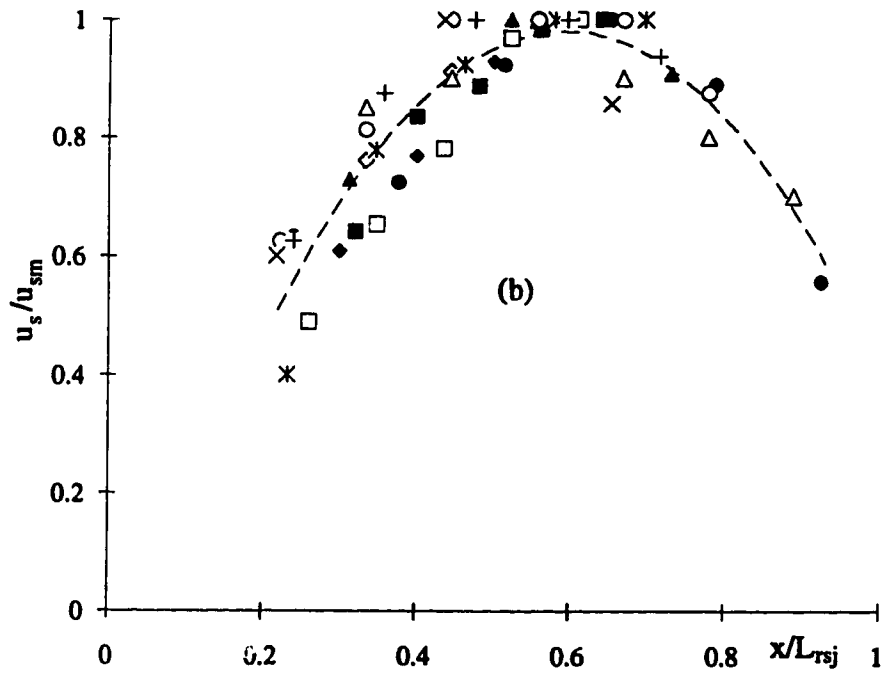
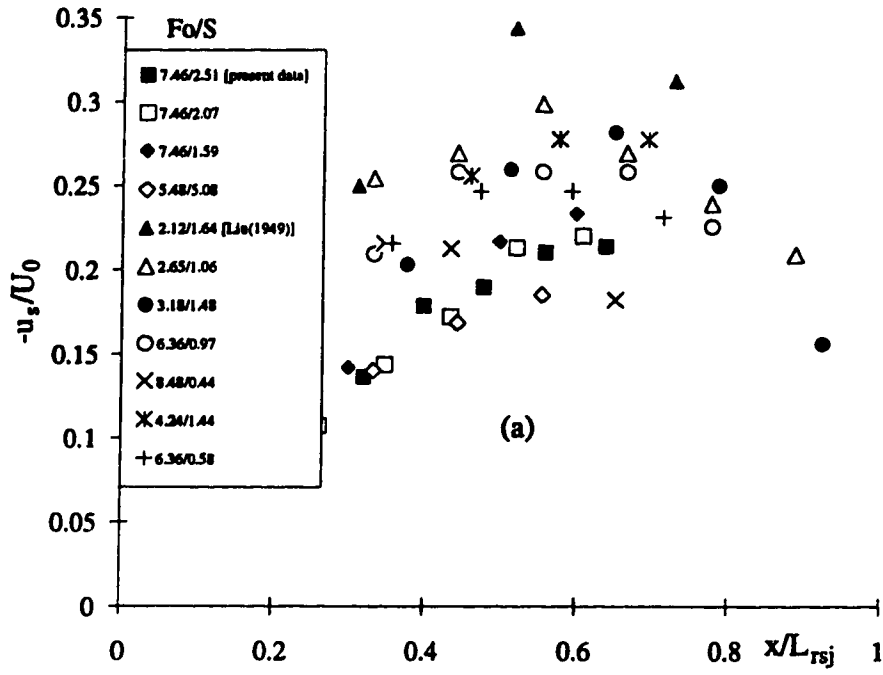


Fig. 4-35(a-b) Longitudinal variation of the reverse flow surface velocity in submerged jumps

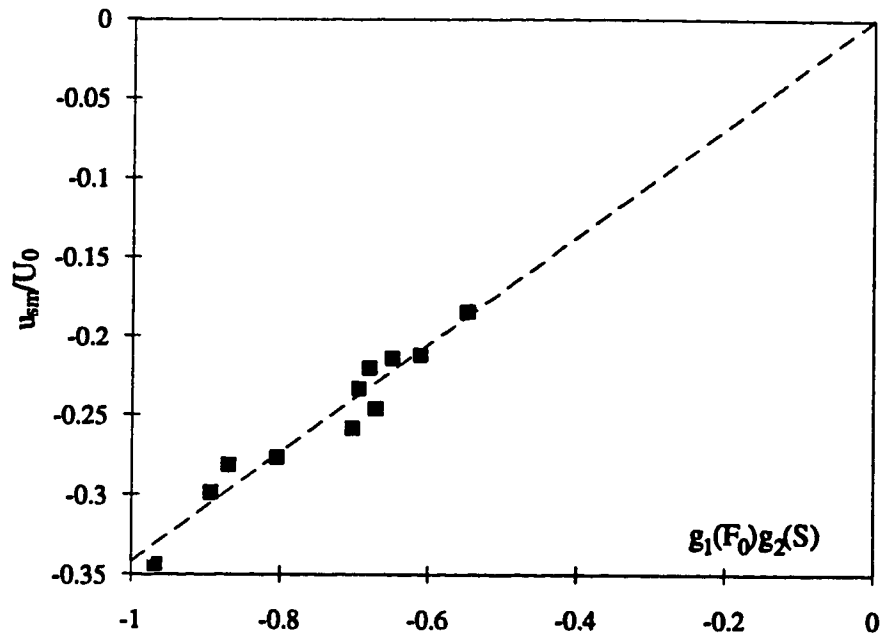


Fig. 4-36 Velocity scale  $u_{sm}$  as a function of  $F_0$  and  $S$

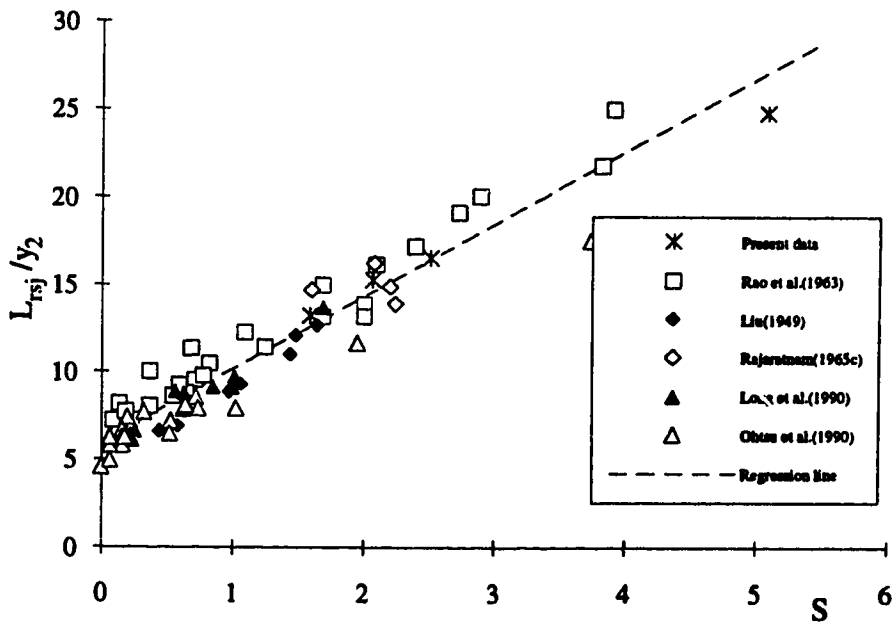


Fig. 4-37 Variation of the roller length with  $S$  for submerged jumps

Table 4-1 Data for the wall jet velocity scale

$x/L$	$u_m/U_0$	$x/L$	$u_m/U_0$	$x/L$	$u_m/U_0$	$x/L$	$u_m/U_0$
Myers et al. (1961)		Sigalla (1958)		Schwarz et al. (1961)		Forthmann (1934) (*)	
$R_0=36000$		$R_0=20000-40000$		$R_0=41600$		$R_0=53000$	
0.71865	0.583	0.06681	1.00472	0.51721	0.72636	0.04286	0.9769
0.64678	0.64	0.13754	1	0.61376	0.67065	0.10573	0.9769
1.07797	0.477	0.13754	1.00943	0.71248	0.61623	0.20574	0.93213
1.4373	0.412	0.26526	0.93774	0.81105	0.55942	0.28575	0.818
1.50916	0.4	0.40674	0.77925	1.00084	0.5054	0.34576	0.76298
1.94035	0.338	0.53544	0.65472	1.0956	0.47806	0.42862	0.70841
2.15595	0.341	0.53544	0.6717	1.19934	0.43927	0.51721	0.65186
2.37154	0.316	0.53544	0.68868		$R_0=30000$	0.57721	0.62297
2.83866	0.308	0.67789	0.59434	0.54007	0.72847	Tailland (1970)(*)	
2.83866	0.284	0.67789	0.60377	0.62847	0.68574	$R_0=11000$	
3.23392	0.277	0.67789	0.63396	0.71892	0.6018	1.12896	0.45843
	$R_0=19000$	0.67789	0.69245	0.81639	0.59314	1.69205	0.37589
0.27688	0.845	0.80954	0.56604	0.89807	0.53846	2.24682	0.32387
0.83064	0.537	0.80954	0.57925	0.99519	0.49716	2.80159	0.29046
1.3844	0.416	0.94316	0.51415	1.09476	0.49476	3.37855	0.26436
1.93816	0.35	0.94316	0.52358	1.17233	0.45461		$R_0=18000$
2.49192	0.319	0.94316	0.54717		$R_0=20100$	1.02806	0.48255
3.04569	0.302	1.07874	0.47547	0.58117	0.64192	1.54083	0.39038
3.59945	0.28	1.07874	0.48491	0.58402	0.62658	2.04602	0.33621
4.15321	0.259	1.07874	0.5	0.673	0.60427	2.55121	0.30278
	$R_0=37000$	1.20842	0.45283	0.76424	0.59269	3.07661	0.27407
0.20243	0.933	1.20842	0.46226	0.85312	0.53935		$R_0=25000$
0.40486	0.762	1.34596	0.42453	0.95234	0.52266	0.95045	0.50092
0.67476	0.607	1.34596	0.43396	1.02482	0.48025	1.4245	0.40959
1.01215	0.496	1.34596	0.4434	1.11638	0.46314	1.89155	0.35194
1.34953	0.432				$R_0=13500$	2.3586	0.31545
1.68691	0.387	Gartshore et al.(1969)		0.63119	0.62289	2.84433	0.28736
2.02429	0.355	$R_0=30800$		0.75823	0.59636	Guitton (1970)(*)	
2.36167	0.324	0.04736	1	0.87803	0.5259	$R_0=30800$	
2.69906	0.31	0.12832	0.99	0.99951	0.50717	0.74317	0.58177
3.03644	0.3	0.27956	0.856	1.12123	0.46827	1.16284	0.45037
		0.5805	0.646	1.24857	0.46601	Patel (1962)(*)	
		0.88603	0.526	1.36345	0.4282	$R_0=30000$	
		1.39014	0.411			0.49569	0.66159
		1.89426	0.349			0.96596	0.49772
						1.43115	0.40213

(\*) : data from Launder and Rodi (1981)

Table 4-2 Data for the wall jet length scal L

Source	$R_0$	$L/y_0$	Source	$R_0$	$L/y_0$
Förthmann(1934)(*)	53000	57.37	Schwarz et al.(1961)	13510	49.15
Tailland (1970)(*)	11000	59.10		20100	67.84
	18000	64.90		30000	67.84
	25000	70.20		41600	63.00
Guitton (1970)(*)	30800	75.00	Patel (1962)(*)	30000	64.49
Sigalla(1958)	20000	47.50	Myers et al(1963)	19000	43.34
	40000	47.50		36000	55.66
Gartshore et al.(1969)	30800	65.46		37000	59.28
Mean value of $L/y_0 = 59.85$			Standard Deviation = 9.20		

(\*) : data from Launder and Rodi (1981)

Table 4-3 Data for the rate of growth of length scales for wall jet  
(data from Table 1 of Launder and Rodi (1981))

Source	$10^{-3}R_0$	$\frac{db}{dx}$	$\frac{d\delta}{dx}$	Source	$10^{-3}R_0$	$\frac{db}{dx}$	$\frac{d\delta}{dx}$
Förthmann	53	0.0820	0.0139	Mogahan	6.8	0.0790	0.0119
Sigalla	20-40	0.0640	0.0096	Patel	30	0.0710	0.0114
Geoge	6.8	0.0790	0.0119	Tailland	11	0.0760	0.0118
Bradshaw and Gee	6.08	0.0710			18	0.0740	0.0104
Schwarz & Cosart	13.5	0.0850	0.0136		25	0.0730	0.0096
	20	0.0690	0.0110	Guitton	30.8	0.0710	0.0107
	30	0.0560	0.0090	Verhoff	10.3	0.0816	
	41.6	0.0610	0.0098		12.1	0.0766	
Myers et al.	7.1-56	0.0770		Wilson	13	0.0760	0.0099
Giles et al.	20-100	0.0766	0.0107	Neale	33.5-49.6	0.0670	
Gartshore et al.	30.8	0.0700	0.0105			0.0660	
Mean of $db/dx = 0.0728$				Std. Dvtn=0.0071			
Mean of $d\delta/dx = 0.0110$				Std. Dvtn=0.0014			

Table 4-4 Data for the velocity scale of free jumps

$x/L$	$u_m/U_0$	$x/L$	$u_m/U_0$	$x/L$	$u_m/U_0$	$x/L$	$u_m/U_0$	$x/L$	$u_m/U_0$	$x/L$	$u_m/U_0$
Schröder (1963)				Hager (1992)				Ohtsu et al. (1990)			
Fo=4.8		Fo=6.06		Fo=4.95		Fo=6.85		(Non-repelled jump)		(Repelled jump)	
0.1532	0.9737	0.2237	0.9836	0.1595	0.9717	0.3691	0.8504	0.1972	1.0169	0.3699	0.9322
0.3031	0.9316	0.4474	0.8740	0.3190	0.8937	0.5409	0.7502	0.3380	0.8814	0.5918	0.7712
0.4537	0.8107	0.6731	0.6276	0.4908	0.8370	0.7413	0.6261	0.5493	0.7966	0.7299	0.6186
0.6164	0.6792	0.8809	0.5575	0.6503	0.6910	0.9322	0.5364	0.7887	0.6695	0.9616	0.5169
0.7705	0.5898	1.1284	0.4381	0.8099	0.6074	1.1135	0.4391	0.9577	0.5212	1.1342	0.4407
0.9246	0.5320	1.3560	0.3811	0.9694	0.5125	1.3076	0.3644	1.2113	0.3941	1.4548	0.3771
1.0735	0.4688	1.5777	0.3022	1.1289	0.4473	1.4985	0.2971	1.4366	0.3559		
1.2276	0.3847	1.8014	0.2223	1.2933	0.3807	1.6862	0.2342	1.6620	0.3220	0.3515	0.9153
1.2927	0.4057	2.0291	0.1763	1.4479	0.3254	1.8771	0.1789				
1.3869	0.3058	2.2567	0.1423	1.6197	0.2942	2.0712	0.1520				
1.5410	0.2900	2.4804	0.1292	1.7915	0.2630	2.4498	0.1370				
1.6865	0.2175	2.6823	0.1270	1.9461	0.2418	2.8315	0.1370				
1.8269	0.2059			2.1105	0.2276						
				2.2700	0.2134						
Fo=3.85		Fo=6.92		Fo=4.3		Fo=6.9		Fo=3.6		Fo=3.3	
0.1227	0.9750	0.2346	0.9777	0.3151	0.9176	0.3657	0.8771	1.0391	0.4661	1.3057	0.3644
0.2521	0.9351	0.4745	0.8249	0.4618	0.8421	0.7346	0.6436	1.3321	0.3517	1.5819	0.2797
0.3782	0.8203	0.7091	0.6542	0.6329	0.7322	1.1035	0.4440	1.8117	0.2797	1.9334	0.2373
0.5092	0.7354	0.9385	0.5460	0.7959	0.6223	1.4850	0.2950				
0.6336	0.6875	1.1818	0.3641	0.9508	0.5262	1.8602	0.1736				
0.7597	0.6406	1.4164	0.2860	1.1165	0.4369	2.2386	0.1245				
0.8840	0.5707	1.6511	0.1745	1.2795	0.3888	2.6169	0.1229				
1.0118	0.4928	1.8892	0.1265	1.4397	0.3476						
1.1395	0.4679	2.1325	0.1075	1.6027	0.3064						
1.3916	0.3580	2.3723	0.1075	1.7684	0.2693						
1.5042	0.3161			1.9287	0.2515						
Fo=4.25		Fo=5.08		Fo=5.5		Rouse et al. (1959)		Fo=5.1		Fo=5.3	
0.1275	0.9744	0.0000	0.9997	0.20917	0.2446						
0.2488	0.9334	0.1468	0.9997	2.2547	0.2309						
0.3733	0.7798	0.2937	0.9048								
0.4992	0.7163	0.4405	0.8110								
0.6221	0.6744	0.5874	0.7209	0.1540	0.9826	0.0000	1.0000				
0.7450	0.6088	0.7342	0.6359	0.2978	0.8987	0.2965	0.7600				
0.8679	0.5443	0.8810	0.5575	0.4365	0.8263	0.5931	0.5700				
0.9938	0.5034	1.0279	0.4865	0.5982	0.6845	0.8896	0.5100				
1.1167	0.4368	1.1747	0.4236	0.7522	0.6164	1.1861	0.4800				
1.2396	0.3958	1.3216	0.3689	0.8986	0.5441	1.4827	0.5000				
1.3671	0.3067	1.4684	0.3222	1.0552	0.5050						
1.4792	0.2730	1.6118	0.2832	1.2092	0.4283	0.0000	1.0000				
		1.7621	0.2513	1.3607	0.3313	0.5000	0.8000				
		1.9089	0.2257	1.5148	0.2691	1.0000	0.5000				
				1.6714	0.2300	1.5000	0.3200				
				1.8228	0.2054	2.0000	0.2500				
				1.9769	0.1880						
				2.1309	0.1735						
Fo=5.41						Fo=2		Fo=7.3		Fo=9	
0.1890	0.9408					0.0000	1.0000				
0.3780	0.8440					0.2965	0.7600				
0.5670	0.7021					0.5931	0.5700				
0.7560	0.5429					0.8896	0.5100				
0.9450	0.4783					1.1861	0.4800				
1.1340	0.4375					1.4827	0.5000				
1.3230	0.3901										
1.5120	0.3493										
1.7010	0.2718										
1.8900	0.2084										
2.0790	0.1772										
2.2491	0.1530										
				Rajaratnam (1965 b)				Fo=9.2			
Fo=3.90		Fo=6.65		Fo=9.05		Fo=5.45		0.3856		0.8898	
0.2581	0.9400	0.3401	0.9300	0.2981	0.8700	1.0000	0.4900	0.6426	0.6695	0.8880	0.5636
0.4488	0.8200	0.6802	0.7000	0.5962	0.6900	1.1134	0.4400	1.1568	0.4110	1.4080	0.3178
0.7181	0.6600	1.0203	0.4800	0.9135	0.5600	1.1918	0.3860	1.5000	0.2500	1.7877	0.1737
1.0884	0.4500	1.3604	0.3600	1.4904	0.3100	1.2742	0.3340	2.0000	0.1500	2.1733	0.1737
1.3465	0.2900	1.7521	0.2400	2.5472	0.1483			2.5000	0.1300	2.5472	0.1483

Table 4-5 Data for the length scale L of free jumps

Source	$F_0$	$L/y_0$	Source	$F_0$	$L/y_0$
Schroder (1963)	4.80	19.135	Ohtsu et al. (1990) (Non-repelled jump)	3.60	15.236
	3.85	15.464		4.20	16.109
	4.25	18.934		5.10	20.305
	5.41	19.347		7.30	24.730
	6.06	20.126	9.20	36.731	
	6.92	24.901	(repelled jump)	3.30	17.406
5.08	18.699	4.10		17.093	
Rouse et al. (1959)	2.00	8.000		5.30	22.665
Rouse et al. (1959)	4.00	10.600	7.30	31.661	
	6.00	15.000	9.00	35.677	
	Hager (1992)	4.30	13.523	Rajaratnam (1965b)	3.90
4.95	18.824	5.45	21.827		
5.50	19.327	6.65	24.257		
6.85	20.459	9.05	25.096		
8.90	29.970				

Table 4-6 Data for the length scale b of free jumps

Source	$F_0$	$x/y_0$	$b/y_0$
Rouse et al. (1959)	4.00	5.180	1.554
		10.360	2.331
		15.540	3.212
		20.720	4.921
	6.00	7.500	2.250
		15.000	2.625
22.500		3.600	
30.000		7.875	
Rajaratnam(1965b)	3.90	9.000	2.100
		11.500	2.300
		15.000	3.000
	5.45	9.750	1.700
		15.850	2.100
		24.000	2.900
		6.65	8.500
	12.500	1.700	
		16.750	2.000
		24.950	2.500
		33.000	3.500
	9.05	15.500	2.460
23.250		2.860	
39.000		3.820	



Table 4-8 Data of Fo and S for submerged jumps  
(a) data for FJL jumps ( $S < S^*$ )

Source	Fo	S	Source	Fo	S
Long et al (1990).	3.01	1.69	Rajaratnam(1965a)	4.45	0.98
	3.11	0.26		5.77	0.61
	3.19	0.85		6.00	0.27
	3.20	0.53		6.85	0.86
	5.49	0.63		7.17	0.18
	5.61	0.22		7.62	0.45
	8.00	0.62		7.65	0.62
	8.19	0.24		7.66	0.32
Bakhmeteff(1941)	2.12	1.64	Rajaratnam(1976 b)	3.15	0.81
Liu(1949)	2.65	1.06		3.17	0.12
	3.18	1.48		3.24	0.33
	3.18	0.65		4.25	1.03
	4.24	1.43		4.40	0.64
	4.24	0.22		4.62	0.15
	5.30	0.43		4.62	0.34
	8.48	0.44		6.32	0.93
Narasimhan et al. (1976).	3.12	1.21		6.42	0.18
	3.12	2.20		6.49	0.47
	3.12	0.33	8.92	0.88	
	4.00	1.28	9.00	0.10	
	4.00	2.24	Ohtsu et al.(1990)	3.48	2.49
	4.00	0.72		4.93	1.30
	5.00	0.38	Present data	1.07	7.02
	5.00	0.87		1.15	5.12
6.00	0.14	1.21		2.98	
Rajaratnam(1965c)	5.01	1.60		1.23	3.74
	5.07	2.08	1.45	1.80	

(b) data for WJL jumps ( $S > S^*$ )

Source	Fo	S	Source	Fo	S
Long et al. (1990).	5.43	1.01	Rajaratnam(1976)	3.13	2.17
	8.11	1.00		4.40	1.45
Present data	5.48	5.08		6.07	1.70
	7.46	2.51		6.23	3.62
	7.46	2.07		8.75	5.38
	7.46	1.59	8.83	2.30	
Liu(1949)	4.24	1.44	Rajaratnam(1965c)	6.44	2.24
	6.36	0.58		5.60	2.20
	6.36	0.97	Ohtsu et al.(1990)	7.34	0.34
Rajaratnam(1965a)	5.37	1.17	Rajaratnam(1967a)	4.43	2.37
Rajaratnam(1967b)	4.67	1.91		5.55	3.25

Table 4-9 Velocity scale data for submerged jumps

x/L	um/Uo	x/L	um/Uo	x/L	um/Uo	x/L	um/Uo	x/L	um/Uo	x/L	um/Uo
Rajaratnam(1976 b)						Long et al.(1990)				Narasimhan et al. (1976)	
Fo/S=4.62/0.15		9.00/0.10		4.25/1.03		3.11/0.26		8.19/0.24			
0.000	1.000	0.000	1.000	0.000	1.000	0.000	1.000	0.000	1.000		3.12/1.31
0.075	1.018	0.318	0.957	0.266	0.955	0.111	1.019	0.138	0.999	1.100	0.431
0.226	0.950	0.591	0.737	0.533	0.775	0.222	1.023	0.276	0.981	0.900	0.569
0.376	0.833	0.864	0.561	1.065	0.463	0.444	0.915	0.414	0.903	0.714	0.692
0.639	0.686	1.137	0.439	1.331	0.300	0.667	0.688	0.689	0.652		3.12/2.2
1.128	0.438	1.319	0.366	1.598	0.194	0.889	0.584	0.965	0.517	1.147	0.423
1.429	0.314	1.682	0.244	0.799	0.613	1.111	0.405	1.241	0.382	0.838	0.585
1.993	0.189	2.319	0.128	1.802	0.150	1.333	0.324	1.516	0.293	0.205	0.954
4.62/0.34		8.92/0.88		4.40/1.45		3.20/0.53		1.792		0.219	
0.000	1.000	0.000	1.000	0.000	1.000	0.000	1.000	2.068	0.152	0.959	0.529
0.203	1.009	0.362	0.846	0.256	0.927	0.091	1.014	2.343	0.108	0.817	0.631
0.406	0.847	0.692	0.643	0.548	0.720	0.182	1.019		8.00/0.62	0.508	0.769
0.609	0.724	1.021	0.505	0.841	0.573	0.364	0.993	0.000	1.000	0.274	0.923
0.846	0.568	1.350	0.407	1.133	0.439	0.545	0.865	0.200	1.017		4.00/2.24
1.083	0.462	1.680	0.294	1.425	0.280	0.818	0.638	0.400	0.897	1.285	0.308
1.320	0.355	2.141	0.098	1.718	0.207	1.091	0.425	0.686	0.616	0.966	0.523
1.692	0.249		3.17/0.12	1.882	0.171	1.364	0.287	0.971	0.514	0.681	0.677
2.031	0.183	0.000	1.000		6.07/1.70	1.636	0.211	1.257	0.406	0.435	0.800
4.40/0.64		0.131		0.994		0.000		1.000		3.12/0.33	
0.000	1.018	0.261	0.945	0.260	0.901	0.000	1.000	1.829	0.227	1.293	0.331
0.232	0.988	0.392	0.867	0.606	0.655	0.073	1.020	2.114	0.124	1.010	0.492
0.464	0.817	0.556	0.746	0.953	0.516	0.145	1.021	2.400	0.060	0.740	0.692
0.697	0.671	0.719	0.649	1.299	0.406	0.291	1.006		3.01/1.69	0.414	0.908
0.929	0.544	0.882	0.558	1.646	0.252	0.436	0.875	0.000	1.000		4.00/0.72
1.161	0.410	1.275	0.373		6.23/3.62	0.655	0.720	0.061	1.027	1.321	0.338
1.419	0.268		3.24/0.33	0.000	1.000	0.873	0.585	0.121	1.043	1.096	0.446
1.522	0.237	0.000	1.000	0.358	0.755	1.091	0.435	0.242	1.017	0.520	0.769
1.780	0.177	0.175	1.014	0.717	0.575	1.309	0.306	0.485	0.794	0.323	0.938
6.42/0.18		0.350		0.919		1.075		0.483		5.00/0.38	
0.000	1.000	0.524	0.800	1.434	0.418	0.000	1.000	0.970	0.519	1.188	0.385
0.310	0.961	0.699	0.689	1.792	0.322	0.138	1.057	1.212	0.377	0.762	0.646
0.619	0.718	0.874	0.581		8.83/2.30	0.275	1.033		5.43/1.01	0.551	0.815
1.239	0.397	1.049	0.462	0.000	1.000	0.551	0.763	0.000	1.000		5.00/0.87
1.548	0.310	1.428	0.324	0.347	0.795	0.826	0.564	0.108	1.061	0.890	0.562
0.929	0.535		3.15/0.81	0.829	0.542	1.102	0.463	0.217	0.986	0.765	0.631
2.168	0.182	0.000	1.000	1.310	0.428	1.377	0.363	0.434	0.774	0.478	0.815
6.49/0.47		0.198		0.997		1.791		0.349		1.653	
0.000	1.000	0.397	0.900	2.272	0.235	2.204	0.100	0.867	0.548		6.00/0.14
0.312	0.950	0.595	0.776		8.75/5.38		5.61/0.22	1.084	0.470	1.441	0.308
0.624	0.709	0.794	0.616	0.000	1.000	0.000	1.000	1.301	0.351	1.194	0.346
0.937	0.529	0.992	0.501	0.278	0.851	0.182	1.017	1.735	0.166	0.971	0.523
1.249	0.399	1.190	0.360	0.732	0.586	0.364	0.947		8.11/1.00	0.771	0.608
1.561	0.269		3.13/2.17	0.985	0.503	0.727	0.642	0.000	1.000	0.331	0.977
1.873	0.162	0.000	1.000	1.490	0.417	1.091	0.466	0.170	1.000		Rajaratnam (1967 b)
6.32/0.93		0.250		0.921		2.247		0.352		0.840	
0.000	1.000	0.500	0.743	3.005	0.300	1.455	0.328	0.339	0.642		4.67/1.91
0.269	0.931	0.750	0.605			1.818	0.236	0.582	0.642	0.196	0.930
0.808	0.576	1.001	0.461			2.182	0.168	0.824	0.536	0.294	0.835
1.078	0.478	1.251	0.323					1.067	0.486	0.392	0.765
1.347	0.355							1.309	0.422	0.490	0.710
1.617	0.223							1.552	0.389	0.588	0.665
1.963	0.110							1.794	0.286	0.667	0.630
								2.036	0.168	0.784	0.590
										0.882	0.546

Table 4-9 (continued)

x/L	um/Uo	x/L	um/Uo	x/L	um/Uo	x/L	um/Uo	x/L	um/Uo	x/L	um/Uo
Rajaratnam (1965a)		Liu (1949)				Present data				Rajaratnam (1965 c)	
		3.18/1.48		8.48/0.44		7.46/2.51		1.45/1.80			
7.66/0.32		0.096	0.985	0.161	1.000	0.228	0.918	0.000	1.000		
0.372	0.963	0.302	0.894	0.371	0.879	0.455	0.737	0.054	0.977		5.07/2.08
0.595	0.790	0.509	0.757	0.791	0.576	0.683	0.612	0.235	0.975	0.176	0.990
0.817	0.648	0.716	0.636	1.210	0.424	0.910	0.524	0.330	0.961	0.387	0.845
1.111	0.457	0.923	0.545	1.630	0.273	1.138	0.463	0.425	0.932	0.598	0.720
1.546	0.309	1.129	0.424	6.36/0.58		1.365	0.428	0.520	0.895	0.809	0.620
6.00/0.27		1.336	0.303	0.140	0.969	1.593	0.395	0.642	0.795	1.231	0.380
0.380	1.068	2.12/1.64		0.333	0.788	1.820	0.344	0.800	0.657	1.653	0.330
0.596	0.802	0.056	0.969	0.522	0.697	2.048	0.292	0.958	0.522	5.01/1.60	
0.794	0.648	0.319	0.939	0.711	0.606	2.275	0.204	1.116	0.441	0.145	1.000
1.018	0.494	0.583	0.788	0.904	0.545	7.46/2.07		1.274	0.345	0.261	0.930
1.514	0.389	0.846	0.606	1.097	0.454	0.228	0.904	1.07/7.42		0.371	0.860
7.65/0.62		1.110	0.424	1.281	0.394	0.457	0.713	0.000	1.000	0.609	0.710
0.299	0.969	1.373	0.333	1.474	0.303	0.685	0.594	0.067	0.988	0.832	0.570
0.486	0.833	2.65/1.06		6.36/0.97		0.914	0.519	0.136	0.982	1.203	0.404
0.675	0.710	0.060	1.015	0.162	0.969	1.142	0.469	0.188	0.985	6.44/2.24	
0.909	0.556	0.200	1.015	0.371	0.788	1.371	0.426	0.279	0.931	0.125	1.000
5.77/0.61		0.340	0.969	0.581	0.636	1.599	0.358	0.370	0.894	0.277	0.860
0.296	1.049	0.481	0.848	0.791	0.545	1.827	0.293	0.461	0.834	0.421	0.730
0.463	0.864	0.621	0.788	1.001	0.500	2.056	0.226	0.553	0.837	0.571	0.650
0.631	0.716	0.762	0.697	1.210	0.424	7.46/1.59		0.644	0.772	0.723	0.570
0.798	0.605	0.902	0.606	1.420	0.318	0.241	0.897	0.735	0.653	0.866	0.530
1.202	0.340	1.042	0.454	1.630	0.258	0.482	0.711	0.826	0.656	1.214	0.445
6.05/0.86		1.183	0.394	4.24/1.44		0.724	0.593	0.917	0.563	1.511	0.370
0.417	0.926	1.323	0.333	0.116	1.000	0.965	0.507	1.009	0.493	5.60/2.20	
0.596	0.833	3.18/0.65		0.296	0.848	1.206	0.457	1.100	0.411	0.161	0.975
0.727	0.691	0.063	1.030	0.464	0.666	1.447	0.399			0.320	0.840
1.082	0.401	0.213	1.030	0.631	0.636	1.688	0.301			0.582	0.660
4.45/0.98		0.362	0.969	0.803	0.576	1.929	0.179	1.15/5.12		0.883	0.525
0.305	0.957	0.511	0.879	0.975	0.515	5.48/5.08		0.000	1.000	Ohtsu et al. (1990).	
0.467	0.833	0.660	0.779	1.179	0.394	0.142	1.020	0.104	0.991		
0.664	0.691	0.809	0.666	1.302	0.242	0.283	0.883	0.202	0.985		
1.202	0.327	0.958	0.539			0.425	0.754	0.300	0.957	3.48/2.49	
7.62/0.45		1.107	0.485			0.566	0.667	0.398	0.907	0.369	0.789
0.281	0.957	1.257	0.394			0.708	0.579	0.496	0.854	0.960	0.543
0.459	0.815	1.406	0.333			0.849	0.535	0.594	0.802	1.034	0.470
0.638	0.710	4.24/0.22				1.132	0.469	0.692	0.753	1.206	0.378
0.867	0.556	0.057	0.969			1.416	0.417	0.791	0.671	1.440	0.256
1.207	0.340	0.327	0.939	Bakhmeteff et al. (1941)		1.699	0.359	0.889	0.612	4.93/1.30	
7.17/0.18		0.529	0.788			1.982	0.272	0.987	0.526	0.243	0.980
0.372	1.031	0.866	0.576			2.265	0.175	1.085	0.331	0.383	0.844
0.616	0.802	1.135	0.424	4.24/1.43		1.21/2.98		1.23/3.74		0.511	0.725
0.842	0.772	5.30/0.43		0.209	0.924	0.000	1.000	0.000	1.000	0.895	0.545
1.151	0.352	0.107	1.000	0.626	0.709	0.095	0.994	0.129	0.979	1.086	0.464
5.37/1.17		0.280	0.954	0.744	0.616	0.211	0.942	0.250	0.958	1.488	0.189
0.334	0.914	0.510	0.788	0.889	0.555	0.283	0.939	0.372	0.879	7.34/0.34	
0.476	0.802	0.741	0.666	0.997	0.505	0.420	0.880	0.494	0.857	0.353	0.968
0.556	0.722	0.971	0.515	1.158	0.416	0.557	0.858	0.615	0.832	0.498	0.727
0.841	0.519	1.144	0.424	1.316	0.370	0.694	0.759	0.737	0.786	0.761	0.626
		1.375	0.364	1.424	0.308	0.832	0.641	0.858	0.684	1.253	0.380
				1.583	0.216	0.969	0.535	0.980	0.523	1.510	0.293
				1.728	0.154	1.106	0.380	1.102	0.383	1.864	0.148

Table 4-10 Data for the length scale L for submerged jumps

Source	S	Fo	L/yo	Source	S	Fo	L/yo
Present data	1.590	7.460	55.287	Rajaratnam (1965a)	0.980	4.450	31.500
	2.070	7.460	58.368		0.610	5.770	31.500
	2.510	7.460	58.600		0.270	6.000	25.000
	5.080	5.480	70.645		0.860	6.850	35.000
	1.800	1.450	18.080		0.320	7.660	28.500
	2.980	1.210	20.820		0.450	7.620	36.500
	3.740	1.230	23.709		0.620	7.650	34.500
	5.120	1.150	29.130		1.170	5.370	35.000
	7.020	1.070	31.328		0.180	7.170	27.500
Long et al.(1990)	0.260	3.110	17.877	(1963).	0.390	6.850	24.133
	0.530	3.200	21.882		0.520	6.800	30.815
	0.850	3.190	27.400		0.610	6.840	34.924
	0.220	5.610	22.462	(1967a)	2.372	4.426	58.000
	1.690	3.010	33.247		3.253	5.549	55.362
	0.630	5.490	29.043	(1967b)	1.913	4.668	51.000
	0.240	8.190	29.019		2.080	5.070	45.500
	1.010	5.430	36.890	(1965c)	1.600	5.010	34.500
	0.620	8.000	35.310		2.240	6.440	56.000
	1.000	8.110	41.250		2.200	5.600	60.000
Rajaratnam (1976b)	0.098	9.000	35.246	Liu(1949)	1.640	2.120	25.052
	0.108	6.420	26.467		1.060	2.650	23.512
	0.116	3.170	15.612		1.480	3.180	31.932
	0.150	4.620	21.275		0.650	3.180	22.132
	0.315	3.240	17.875		1.440	4.240	40.382
	0.340	4.620	23.639		0.220	4.240	24.503
	0.465	6.490	31.404		0.430	5.300	28.628
	0.640	4.400	29.907		0.970	6.360	39.339
	0.810	3.150	25.714		0.580	6.360	35.887
	0.884	8.920	48.654		0.440	8.480	39.348
	0.927	6.320	41.635	Narasimhan et al. (1976).	0.330	3.120	19.217
	1.030	4.250	36.988		1.309	3.120	27.184
	1.450	4.400	42.092		2.197	3.120	42.644
	1.703	6.070	54.450		0.719	4.000	27.638
	2.171	3.130	41.641		1.278	4.000	36.849
	3.620	6.230	70.000		2.244	4.000	45.035
	2.300	8.830	65.000		0.381	5.000	25.494
5.380	8.750	58.000	0.867	5.000	40.604		
				0.138	6.000	25.201	
Bakhmeteff et al. (1941).	1.433	4.244	43.500	Ohtsu et al.(1990)	2.486	3.480	46.300
					1.296	4.930	44.000
					0.344	7.340	31.000

Table 4-11 Data for the length scale b for submerged jumps

x/yo	b/yo	x/yo	b/yo	x/yo	b/yo	x/yo	b/yo	x/yo	b/yo	x/yo	b/yo	x/yo	b/yo	x/yo	b/yo	x/yo	b/yo
Long et al. (1990)				Present data		Rajaratnam et al. 1967b)		Liu(1949)				Rajaratnam (1965a)					
Fo/S=3.11/0.26		5.49/0.63		7.46/2.51		5.02/1.69		6.36/0.97		6.36/0.58		7.62/0.45		7.66/0.32			
2.00	1.05	4.00	1.10	13.33	1.59	10.00	1.56	8.25	1.49	6.93	1.73	4.48	1.00	4.60	0.93		
4.00	1.10	8.00	1.20	26.67	2.41	15.00	2.04	16.50	2.15	13.86	2.08	10.43	1.51	10.12	1.60		
8.00	1.20	16.00	1.70	40.00	3.64	20.00	2.60	24.76	2.81	20.63	2.59	16.87	2.00	17.18	2.11		
12.00	1.40	24.00	2.40	53.33	4.72	25.00	3.00	33.01	3.63	27.40	3.30	23.01	2.67	23.13	2.73		
16.00	1.60	32.00	2.80	66.67	5.80	30.00	3.58	41.26	4.95	34.33	3.80	31.47	2.84	31.47	3.07		
20.00	2.00	40.00	3.10	80.00	6.40	34.00	3.83	49.51	5.03	41.26	4.16	43.56	3.47	43.56	4.04		
24.00	2.60	48.00	4.00	93.33	7.11	40.00	4.08	57.77	5.45	47.86	5.28	4.45/0.98		7.17/0.18			
8.11/1.0		8.0/6.2		106.7	8.03	45.00	4.53	66.02	6.44	54.79	5.78	4.41	0.78	10.43	1.67		
7.00	1.28	7.00	1.18	120.0	9.47							9.86	1.28	16.87	2.20		
14.00	1.56	14.00	1.22	133.3	9.70			2.12/1.64		8.48/0.44		15.05	1.90	23.62	2.56		
24.00	2.22	24.00	2.30			Rajaratnam		3.30	1.16	8.25	1.32	20.97	2.68	31.47	3.73		
34.00	3.30	34.00	3.20	7.46/2.07		(1965c)		9.90	1.49	16.50	1.98	5.57/1.17		7.65/0.62			
44.00	4.10	44.00	3.80	13.33	1.60			16.50	2.15	33.01	3.80	6.67	1.20	4.29	0.93		
54.00	4.50	54.00	4.20	26.67	2.60	5.07/2.08		23.11	2.44	49.51	5.61	15.14	1.83	10.43	1.43		
64.00	5.10	64.00	5.00	40.00	3.80	8.00	1.40	29.71	2.97	66.02	6.60	21.01	2.23	16.75	2.07		
74.00	6.40	74.00	7.00	53.33	5.11	17.60	2.07					24.72	2.49	23.31	2.53		
84.00	8.20	84.00	9.50	66.67	5.77	27.20	2.58	2.65/1.06		3.18/0.65		38.19	2.76	31.29	3.20		
5.43/1.01		3.19/0.85		80.00	6.90	36.80	3.60	3.30	1.16	3.30	1.16	50.37	4.09	43.74	3.60		
4.00	1.10	2.00	1.00	93.33	8.13	56.00	4.87	6.60	1.32	6.60	1.40	5.77/0.61&					
8.00	1.20	4.00	1.05	106.7	8.42	75.20	6.90	9.90	1.49	9.90	1.57	6.05/0.86		4.45/0.59			
16.00	1.70	8.00	1.10	120.0	9.47			13.20	1.98	13.20	1.82	4.14	0.60	3.94	0.70		
24.00	2.40	12.00	1.20			5.01/1.6		16.50	2.15	16.50	2.15	9.58	1.20	9.50	1.20		
32.00	2.80	18.00	1.80	7.46/1.59		5.01	1.22	19.81	2.31	19.81	2.15	9.58	1.07	14.59	1.90		
40.00	3.10	24.00	2.30	13.33	1.63	9.00	1.40	23.11	2.64	23.11	2.48	14.83	1.93	21.08	2.45		
48.00	3.80	30.00	2.80	26.67	2.61	12.80	1.55	26.41	3.05	26.41	2.72	14.83	1.83	25.63	3.03		
64.00	6.00	36.00	5.00	40.00	3.66	21.00	1.90	29.71	3.14	29.71	3.05	14.83	1.72				
8.19/0.24		3.2/0.53		53.33	4.99	28.70	2.60			33.01	3.80	19.96	2.20	4.38/0.37			
4.00	1.15	2.00	1.00	66.67	6.13	41.50	4.27	5.3/0.43		4.24/0.22		19.78	1.95	0.64			
8.00	1.25	4.00	1.05	80.00	6.93			4.95	1.32	3.30	1.12	21.01	2.11	1.70	1.98		
12.00	1.40	8.00	1.10	93.33	8.53	6.44/2.24		9.90	1.49	9.90	1.49	25.21	2.67	21.08	2.52		
20.00	2.00	12.00	1.20	106.7	9.33	7.00	1.20	16.50	2.10	14.85	1.90	25.34	2.51	25.09	3.03		
28.00	2.60	18.00	1.60			15.50	1.65	23.11	2.48	23.11	2.20	25.34	2.40				
36.00	3.10	24.00	2.20	5.48/5.08		23.60	2.30	29.71	2.81	29.71	3.19	37.70	2.80	6/0.27			
44.00	3.70	30.00	2.80	10.00	1.42	32.00	2.86	34.66	3.47			38.01	2.89	4.02	0.71		
52.00	4.30			20.00	1.98	40.50	3.50					38.01	3.04	9.58	1.24		
60.00	5.30	3.01/1.69		30.00	2.70	48.50	3.75	3.18/1.48		4.24/1.44							
68.00	7.40	2.00	1.05	40.00	3.49	68.00	5.15	4.95	1.24	6.60	1.49	Rajaratnam et al. (1967a)					
5.61/0.22		4.00		50.00	4.46	84.60	6.14	11.55	1.57	13.86	1.82						
4.00	1.10	8.00	1.20	60.00	5.56			18.15	1.90	20.63	2.81	4.76/2.12		5.97/2.93			
8.00	1.20	16.00	1.90	80.00	7.20	5.62/2		24.76	2.81	27.40	3.30	9.45	1.57	16.00	2.26		
16.00	1.70	24.00	2.40	100.0	8.51	9.65	1.42	31.36	3.14	34.33	4.29	18.90	2.51	25.00	3.29		
24.00	2.20	32.00	2.90	120.0	11.16	19.20	2.08	37.96	3.80	41.26	4.82	30.60	3.60	36.60	4.32		
32.00	2.90	40.00	3.60	140.0	16.50	34.90	3.26	44.56	4.62	49.51	5.61	42.20	4.63	50.20	5.60		
40.00	3.60	48.00	5.90	160.0	25.00	53.00	4.77			54.46	5.61			61.60	6.99		

Table 4-12 Data for the length scale  $\delta$  for submerged jumps

$x/y_0$	$\delta/y_0$	$x/y_0$	$\delta/y_0$	$x/y_0$	$\delta/y_0$
Present data		Long et al. (1990)			
Fo/S=7.46/2.51		3.11/0.26		3.01/1.69	
13.33	0.44	8.00	0.16	8.00	0.20
26.67	0.44	12.00	0.18	16.00	0.22
40.00	0.59	16.00	0.18	24.00	0.24
53.33	0.67	20.00	0.44	32.00	0.32
66.67	0.72	24.00	0.44	40.00	0.56
80.00	0.90	32.00	0.44	48.00	0.56
93.33	1.00				
106.67	1.39		3.20/0.53		5.43/1.01
120.00	3.06	8.00	0.16	8.00	0.22
		12.00	0.16	16.00	0.30
	7.46/2.07	18.00	0.16	24.00	0.36
13.33	0.44	24.00	0.32	32.00	0.38
26.67	0.46	30.00	0.40	40.00	0.54
40.00	0.59	36.00	0.44	48.00	0.64
53.33	0.72	42.00	0.48	64.00	1.44
66.67	0.92				
80.00	1.03		8.00/0.62		8.11/1.00
93.33	1.39	14.00	0.13	14.00	0.33
106.67	1.74	24.00	0.17	24.00	0.37
120.00	3.39	34.00	0.20	34.00	0.43
		44.00	0.47	44.00	0.57
	7.46/1.59	54.00	0.60	54.00	0.63
13.33	0.46	64.00	1.47	64.00	1.00
26.67	0.44	74.00	1.53	74.00	1.67
40.00	0.66	84.00	2.60	84.00	2.00
53.33	0.72				
66.67	0.92		3.19/0.85		5.61/0.22
80.00	1.04	8.00	0.12	8.00	0.10
93.33	1.39	12.00	0.16	16.00	0.14
106.67	3.54	18.00	0.24	24.00	0.28
		24.00	0.28	32.00	0.24
	5.48/5.08	30.00	0.48	40.00	0.56
10.00	0.35	36.00	0.56	48.00	0.88
20.00	0.35				
30.00	0.45		8.19/0.24		5.49/0.63
40.00	0.51	12.00	0.23	8.00	0.18
50.00	0.60	20.00	0.30	16.00	0.22
60.00	0.70	28.00	0.33	24.00	0.34
80.00	0.95	36.00	0.40	32.00	0.42
100.00	1.30	44.00	0.70	40.00	0.62
120.00	2.27	52.00	1.27	48.00	0.84
140.00	3.35	60.00	1.60		
160.00	4.80	68.00	1.87		

Table 4-13 Scale data for the reverse flow of present experiments

run	$L_{Tij}(m)$	$x(m)$	$b_j(m)$	$-u_s(m/s)$
1	1.8	0.6	0.0543	0.2405
		0.8	0.0706	0.2887
		1.0	0.0846	0.3169
2	2.5	0.8	0.1090	0.3916
		1.0	0.1095	0.5110
		1.2	0.1186	0.5428
		1.4	0.1199	0.6012
		1.6	0.0949	0.6115
3	2.3	0.6	0.0735	0.3084
		0.8	0.0817	0.4118
		1.0	0.1108	0.4914
		1.2	0.0958	0.6100
		1.4	0.0957	0.6300
4	2.0	0.6	0.0803	0.4055
		0.8	0.0946	0.5119
		1.0	0.0764	0.6189
		1.2	0.0610	0.6669

Table 4-14 Surface profile data of present experiments

run 1		run 2		run 3		run 4	
x(m)	y(m)	x(m)	y(m)	x(m)	y(m)	x(m)	y(m)
0	0.435	0	0.516	0	0.442	0	0.361
0.2	0.434	0.1	0.513	0.2	0.437	0.2	0.359
0.4	0.433	0.2	0.511	0.4	0.436	0.4	0.357
0.6	0.435	0.4	0.510	0.6	0.436	0.6	0.357
0.8	0.434	0.6	0.511	1	0.431	0.8	0.354
1	0.434	0.8	0.509	1.4	0.430	1	0.353
1.2	0.434	1	0.507	1.6	0.434	1.2	0.354
1.8	0.442	1.2	0.505	1.8	0.450	1.3	0.366
		1.45	0.506			1.6	0.387
		1.6	0.505			1.8	0.391
		1.8	0.509			2	0.391
		2	0.520				

## Chapter 5 Effect of Baffles on Submerged Jumps \*

### 1. Introduction

In hydraulic structures like dams and outlet structures, when the tail water depths are larger than the subcritical sequent depth required for free jumps so that submerged jumps might form, the general practice is to avoid submerged jump as the energy dissipating element. The main reason for this appears to be the concern that the high velocity supercritical stream might continue for relatively large distances without appreciable dissipation thereby causing serious erosion. It appears that this can be remedied by the provision of stilling basins of baffle wall or baffle block types. At this time, even though submerged jumps are well-understood ( Liu, 1949; Rao and Rajaratnam, 1963; Rajaratnam, 1965a, 1965b; Narasimhan and Bhargava, 1976; Long, Rajaratnam and Steffler, 1990; Ohtsu, Yasuda, and Awazu, 1990), hardly any work has been done on submerged jumps with baffle walls or baffle blocks. This chapter presents the results of an experimental study on the behavior of submerged hydraulic jumps with baffle walls. It would be interesting and useful to continue this work with baffle blocks, which might enhance the energy dissipation even more.

Fig. 5-1 shows a definition of a submerged jump with a baffle wall where  $y_0$  and  $U_0$  are respectively the depth and mean velocity of the supercritical stream ( leaving the gate);  $h$  is the height of the baffle located at a distance of  $x_0$  from the gate and  $y_t$  is the tail water depth. The supercritical Froude number is  $F_0$  and  $S$  is the submergence factor, equal to  $(y_t - y_2)/y_2$ .

---

\* The main content of this chapter has been sent to Journal of Hydraulic Engineering, American Society of Civil Engineers for publication.



In this chapter, we present the experimental arrangement and then the results of a series of experiments which demonstrate that in the case of submerged jumps with baffles, one might get either a stable reattached jet on the bed or a stable deflected surface jet or a bi-stable state in which either of these might occur. This is followed by a detailed study of submerged jumps with baffles, regarding the structure of the mean velocity field.

## **5.2 Experimental arrangement**

The experiments were done in the T. Blench Hydraulics Laboratory of the University of Alberta. Fig. 5-2 shows the experimental arrangement used. The flume was 7.60 m long, 0.466 m wide and 0.60 m deep. The horizontal bottom was made of aluminum and the side walls were made of glass. Water was pumped to the head tank from the sump and the discharge was measured by a magnetic flowmeter located in the supply line. Water entered the flume under a sluice gate with a streamlined lip, which produced a supercritical stream with a thickness equal to the gate opening. The tail water depth was controlled by a vertical tail gate located at the downstream end of the flume.

The horizontal baffles used in the experiments were made with wood. The length of the baffles was equal to the width of the flume and the height  $h$  of the baffles ranged from 6 to 27 mm. The thickness was 20 mm for the baffles lower than or equal to 20 mm and 30 mm for the baffles higher than 20 mm.

For the measurement of the time-averaged velocity and pressure fields, two arrangements were used and these are shown in Fig. 5-3(a) and (b). The arrangement shown in Fig. 5-3(a) was used with a pitch probe. The pitch probe was made of three tubes of external diameters of 1.0 mm. and was made and calibrated in the Hydraulics laboratory (Rajaratnam and Muralidhar, 1967).

Three transducers of the Validyne model DP45-16 were used to measure the pressure differences. The output ends of the transducers were connected to a flat cable which in turn was connected to a Macintosh IIfx computer. Transducer #1 measured the pressure difference between the middle and the upper tubes of the pitch probe and #2 between the middle and the lower tubes. Transducer #3 was used to measure the pressure difference between the middle tube and a reference level. The transducers were used when the pressure differences were within the range of transducers #1 and #2 (-2.54 cm to 2.54 cm). When the observations were made, the computer first took the samples from transducers #1 and #2 at the desired sampling rate and coupled every sequence of two signals to obtain the magnitude of the velocity and attack angle and displayed the magnitude and angle on a strip chart on the screen in real time. When the desired number of samples were taken, the computer processed all the samples to obtain the mean values and the standard deviations for the magnitude and the attack angle and saved the results in an open file. The computer program used for this two-dimensional velocity measurement was the same as that described in Chapter 4. After the velocity data sampling, the computer took samples from transducer #3 and showed the pressure difference on the screen in real time. The mean value of this difference was recorded to the same file at the end of sampling. The computer program used for transducer #3 was the same as the one designed for Pitot tube in Chapter 4. The mean value of the piezometric pressure at the measuring point can be calculated from the three mean values recorded in the file. If the pressure differences were out of the range of the transducers, the three horizontal tube stoppers in Fig. 5-3 (a) were opened and results were obtained from the manometers and typed into the computer. Fig. 5-3(b) shows the arrangement for use with the Pitot tube with an external diameter of 2.4 mm.

This setup and the computer program were the same as that shown in Fig 4-14(c).

### **5.3 Possible flow states**

Some preliminary experiments on submerged jumps with baffle walls were performed which showed that in any particular experiment, one might get a stable deflected jet which would eventually form a surface jet ( see Fig. 5-4(a)) or a stable reattached wall (bed) jet, after an initial separation at the baffle ( see Fig. 5-4(b)). These states are referred to as the **deflected surface jet flow** and **reattaching jet flow patterns** respectively. There was also a transition state in which either of these could form.

In the deflected surface jet flow regime, the flow from the gate was deflected at the baffle towards the surface and formed a surface hump downstream the baffle. The main flow in the downstream channel was near the water surface below which a big eddy was formed. Another eddy was formed before the baffle near the gate which had significant circulation. This flow state might be favorable for the protection of the channel but might induce wave attack on the banks of the downstream channel.

The flow state shown in Fig. 5-4 (b) is different from that of Fig. 5-4 (a). The main flow passes over the baffle and gets reattached to the flume floor. Behind the baffle, a small eddy was formed and its length was of the same order as the baffle height. A very large elongated eddy was formed above the baffle and the size of which was comparable with the length of submerged jumps, with corresponding upstream conditions. This flow state should be avoided in

practice because the main flow, after reattachment, might possess high velocity and could cause severe erosion in the downstream channel.

Preliminary experiments indicated that for a given gate opening  $y_0$ , downstream channel depth  $y_t$  and baffle position  $x_0$ , there were two critical baffle heights  $h_{c1}$  and  $h_{c2}$ . If baffle height was smaller than  $h_{c1}$ , the flow would be stable in reattaching wall jet state. If baffle height was bigger than  $h_{c2}$ , the flow would be stable in the deflected surface jet state. If baffle height was between  $h_{c1}$  and  $h_{c2}$ , the flow could be in either of these two states, depending on initial conditions. If the flume water depth was initially smaller than the given  $y_t$  and increased to  $y_t$ , the flow would start at deflected surface jet state and be stable in this state. If the flume water depth was initially bigger than the given  $y_t$  and decreased to stay at  $y_t$ , the flow would start at reattaching wall jet state and be stable in this state. It was also found that in the transition state, the flow could be switched from one state to the other by means of a square wooden plate of side of 450 mm. This was not true when the baffle was a little shorter than  $h_{c2}$  or a little higher than  $h_{c1}$ . In the first case the flow was unstable in reattaching jet state. A small external disturbance could change the flow to deflected jet state. Once in deflected jet state the flow was stable and could not be changed back to reattaching jet by external interference. In the second case the flow was unstable in deflected jet state. A small disturbance could change the flow to reattaching jet state. Once in reattaching jet state the flow was stable and could not be changed back to deflected jet state by external interference.

It is believed that the oscillation of the eddy above the main flow jet was responsible for the instability of the flow. Let us consider the flow state of Fig. 5-4(a) as an example. It was observed that while the water surface downstream of the hump was relatively stable, there existed a strong oscillation of the water

surface upstream the hump. This oscillation caused a pressure oscillation on the upstream side of the main flow. If the pressure on upstream side decreased, the main flow would be pushed backwards by the force from the downstream side and become steeper to compact the upstream eddy. This, together with the increase in reverse flow ( by the increased water surface slope ), resulted in the pressure recovery on the upstream side. When the pressure on the upstream side of the main flow increased, the main flow would be pushed forwards to become flatter. This produced an expansion in the upstream side eddy and a decrease in its pressure on the main flow.

For a given baffle position, the oscillation frequency increased with baffle height. For a short baffle (e.g., shorter than  $h_{c1}$  ) the oscillation frequency was low and the oscillation period could be long enough for the flow state to change. On the other hand, for a high baffle (e.g., higher than  $h_{c2}$  ) the deflected main flow was steep, and the oscillation frequency was high. The deflected flow state was stable because the oscillation period was not long enough for the state to change.

Flow history played an important role in flow state determination and this resulted in the existence of the transition state. The history effect can be seen in many cases and one simple example is that of the critical Reynolds number for the transition from laminar flow to turbulent flow which is different from that required for the transition from turbulent flow to laminar flow.

Two series of experiments were done. The first series of experiments were performed to define these flow states and the second series were performed, mainly to study the structure of flow of mostly the deflected surface jet flow.

### 5.3.1 Experimental results and analysis ( Series 1)

In the experiments of series 1, four gate openings of 10, 12, 15 and 17 mm were used. For each opening, experiments were performed with different gate Froude numbers, baffle positions, baffle heights and tail water depths.

The values of the lower critical baffle height  $h_{c1}$  were found through the following steps: (1) Fix a baffle on the flume floor; open the tail gate completely and start the pump to obtain the desired discharge. Under these conditions, the high velocity flow sprayed over the baffle. (2) Slowly raise the tail gate in small increments and wait for the flow to become stable. (3) Repeat step (2) until the reattaching flow state was formed. The baffle height is the lower critical height  $h_{c1}$  corresponding to the given  $y_0$ ,  $F_0$ ,  $x_0$  and the final stable tail water depth  $y_t$ .

The values of the upper critical baffle height  $h_{c2}$  were found through the following steps: (1) Fix a baffle on the flume floor and close the tail gate to get a large tail water depth. Start the pump to obtain the desired discharge. In this step, the flow would be in reattaching wall jet state because of the deep tail water. (2) Lower the tail gate slowly in small increments and wait for the flow to become stable. (3) Repeat step (2) until the deflected surface jet state occurs. This baffle height is the critical height  $h_{c2}$  corresponding to the given  $y_0$ ,  $F_0$ ,  $x_0$  and the final stable tail water depth  $y_t$ .

The results for the critical heights are listed in Tables 5-1 and 5-2. It was found that when the ratio  $x_0/y_0$  was greater than about 10, the critical baffle heights were independent of the gate Froude number  $F_0$ . All the data for the critical heights are plotted in Fig. 5-5(a) and (b) in two different scales. In Fig. 5-5(a), the gate opening  $y_0$  is used as the scale for both  $x_0$  and  $h_c$ . It can be seen that while the data for  $h_{c1}/y_0$  might be given an average value of about 0.7, the

data for  $h_{c2}/y_0$  do not show any systematic variation. It is important to note that more than 90% of the  $h_{c2}/y_0$  data are equal to or greater than 1. In Fig. 5-5(b), the using of the tail water depth  $y_t$  as the scale enables all the  $h_{c2}$  data to collapse into a narrow range around the regression curve represented by the equation

$$\frac{h_{c2}}{y_t} \pm 0.003 = 0.0382 \pm 0.00072 - 0.0078 \pm 0.00064 \frac{x_0}{y_t} + 0.0261 \pm 0.000143 \sin^2\left(\frac{x_0}{y_t}\right) \quad (5-2)$$

(with the correlation coefficient of 0.91). It is seen from Fig. 5-5(b) that the relative critical baffle height  $h_{c2}/y_t$  increases with  $x_0/y_t$  to reach its peak value at  $x_0/y_t$  equal to about 1.5. As the baffle was moved farther downstream, the reattaching wall jet was affected by the impact of the tail water more and more and the critical baffle height necessary to deflect the jet decreased. The mean value of  $h_{c1}/y_0$  is 0.200 and the standard deviation is 0.0038. The two sets of data merge at  $x_0/y_t \approx 2.7$  and beyond this point the baffle almost lost its effect.

The  $h_{c2}/y_t \sim x_0/y_t$  curve shown in Fig. 5-5 can be used as a reference curve for baffle height design in submerged baffle stilling basin. For given  $x_0$  and  $y_t$ , the critical baffle height  $h_{c2}$  can be found from the curve. If the designed baffle is equal to or higher than  $h_{c2}$ , the flow will always be deflected to form surface jet so that the downstream channel bed will be protected. The designed baffle height should not be much higher than  $h_{c2}$  because it would be subjected to an unnecessarily large impact force. For a rough estimation,  $x_0/y_t$  and  $h_{c2}/y_t$  can be chosen the values of 1.00 and 0.05 respectively. At the same time the baffle should not be lower than the gate opening according to Fig. 5-5(a).

### 5.3.2 Mean flow structure

Experiments of series 2 were performed to study the mean flow structure of the two stable flow states, especially the deflected surface jet. Nine

experiments were conducted, the details of which are given in Table 5-3. As indicated in Table 5-3, only one experiment was done on the reattaching jet while the rest were devoted to the deflected surface jet. Detailed measurements of the velocity and the (piezometric) pressure fields were performed in all these nine experiments.

Experiments 1 to 3 were performed to study the mean velocity field of the deflected surface jet for three different values of  $F_0$  with approximately constant values of  $y_0$ ,  $y_t$ ,  $x_0$  and  $h$ . The results are shown in Fig. 5-6 (a) to (c). It is seen from these figures that the deflected jet hits the surface at an approximate distance 0.4m from the gate and this location is marked by the presence of a hump in the water surface. For a distance greater than 0.6m, the deflected flow behaves like a surface jet, in which the velocity vectors are almost horizontal, with the maximum velocity occurring near the free surface. Fig. 5-6(d) shows the mean velocity field for run 4 for which the conditions are the same as those of run 1 except for the baffle height. It can be seen that the deflected jet in Fig. 5-6 (d) has a steeper slope than that of Fig. 5-6 (a) because the baffle in run 4 is 1.47 times as high as that in run 1.

Table 5-3 Details of experiments of series 2

Run	$y_0$ (mm)	$F_0$	$y_t$ (mm)	S	$x_0$ (mm)	h (mm)	$x_0/y_t$	$h/y_t$	Flow state	Remarks
1	10	5.48	442	5.08	200	11.6	0.452	0.026	defld. jet	Bi-stable
2	10	6.85	447	3.86	200	11.6	0.447	0.026	defld. jet	Bi-stable
3	10	2.74	424	11.4	200	11.6	0.472	0.027	defld. jet	Bi-stable
4	10	5.48	442	5.08	200	17.0	0.452	0.038	defld. jet	Stable jet
5	10	5.48	440	5.08	400	11.6	0.909	0.026	defld. jet	Bi-stable
6	10	5.48	440	5.08	400	11.6	0.909	0.026	rtchg. jet	Bi-stable
7	10	5.48	440	5.08	600	11.6	1.364	0.026	defld. jet	Bi-stable
8	10	5.48	440	5.08	600	22.8	1.364	0.052	defld. jet	Stable jet
9	15	7.46	466	2.09	300	19.0	0.644	0.041	defld. jet	Stable jet



Figs. 5-6 (e) to (h) show the velocity and piezometric pressure fields for runs 5 and 6. The flows in these two experiments were in totally different states even though they had the same boundary conditions. A strong eddy upstream of the baffle for the deflected jet in run 5 is shown clearly in Fig. 5-6 (e). In the center of the eddy the piezometric pressure reached its lowest value and the pressure distribution in the surface jet region was almost hydrostatic as can be seen from Fig. 5-6 (f). Fig. 5-6 (g) shows that the main flow in run 6 passed over the baffle, impinged on the flume floor strongly and formed a reattached wall jet downstream. The water surface was almost horizontal and the reverse flow intensity was weaker than that for the flow without baffle (run 1 in Chapter 4). The pressure distribution downstream the baffle for the reattaching flow was almost hydrostatic as shown in Fig. 5-6 (h).

Figs. 5-6 (i) and (j) show the velocity and pressure fields for run 7 which was different from runs 1 and 5 with regard to the position of the baffle. We can see by comparison of the velocity and pressure fields of runs 1, 5 and 7 that as  $x_0$  is increased, the deflected jet becomes less and less steep; the eddy before the baffle becomes weaker and the free surface became flatter.

The velocity and pressure fields shown in Fig. 5-6 (k) and (l) are those for run 8 with the same boundary conditions as run 7 except that run 8 had a higher baffle. Even though the baffle height of run 8 was 1.97 times as big as that of run 7 the velocity and pressure fields of the two runs are not very different because the baffles were so far away from the gate.

In Figs. 5-6 (m) and (n), the velocity and pressure fields for run 9 are shown. Run 9 had a different gate opening from those of the other runs and the gate Froude number was also higher. The measurements were made by means of

a Pitot tube except that the curved jet was measured by the pitch probe. Because the initial momentum of run 9 was much higher than those of the other runs, the surface hump was much more prominent.

Let us now have a look at the velocity fields in detail. The distribution of the longitudinal forward velocity components before the baffle in runs 5 to 8 are shown in Figs. 5-7 (a) to (d) and the corresponding non-dimensional forms are presented in Figs. 5-8 (a) to (d). All these data are shown together in Fig. 5-9 in a consolidated form. The wall jet structure of these flows can be seen in these plots. For comparison, the corresponding curve of plane turbulent wall jet (Rajaratnam, 1976 ) is also shown in Fig. 5-9. In Figs. 5-7 to 5-9,  $u$  is the horizontal velocity component,  $u_m$  is the maximum value of  $u$  at the measuring section,  $b$  is the distance from the bed where  $u = 0.5u_m$  and  $\partial u/\partial y < 0$ , and  $y$  is vertical distance from the bed. It is seen that in the lower part where most of the momentum flux is transported, the velocity profiles are similar and well represented by the plane wall jet curve. For the deflected surface jets, the large surface eddy before the baffle adds induced velocity to the flow in the upper part of the forward flow. For the reattaching jet ( run 6), the reverse flow almost had no effect on the forward velocity profiles.

The decay of the velocity scale  $u_m$  before baffle is shown in Fig. 5-10 for runs 5 to 8. The corresponding variation for the wall jet ( from Chapter 4 ) is also shown in the same figure. It appears from Fig. 5-10 that the velocity scales for runs 7 and 8 decay somewhat more slowly than for the wall jet, whereas those for runs 5 and 6 decay at the same rate as the wall jet. This means that as we increase the baffle distance, the eddy before baffle will affect the main flow more.

The growth of the length scale  $b$  in the region before baffle is shown in Fig. 5-11 for runs 5 to 8 along with the corresponding variation for the wall jet (from Chapter 4 ). It can be seen that the growth of the length scale  $b$  is not affected by the presence of the baffles till the jet gets very close to them.

Fig. 5-12 (a) and (b) display the decay of maximum velocity (vector)  $v_m$  and the locus of the maximum velocity filament for the deflected surface jets with three different gate Froude numbers. For these three experiments, the gate opening, the tail water depth, the baffle height and the baffle position were kept about the same and only the discharge was changed. Concerning the decay of the velocity scale in the region downstream of the baffle, the following three stages can be noticed: (1) a rapid decrease in the curved jet region to reach its minimum value right below the surface hump; (2) an increase from below the hump upwards to reach its maximum value at the free surface apparently due to the convergence; (3) steady decrease near the free water surface downstream the hump. In this region, the flow behaved just like a surface jet originating some where upstream of the gate. Compared to the corresponding velocity scale decay of wall jet, the velocity scale of these submerged jumps with baffles decayed much faster. At  $x/y_0 = 140$ , the relative maximum velocity  $v_m/U_0$  for these submerged jumps is only half as that of the corresponding value for wall jet. From Fig. 5-12, it seems that the gate Froude number did not have any effect either on the maximum velocity or the locus of the maximum velocity filament.

A comparison of the decay of the maximum velocity (vector) and its locus for runs 5 and 6 is shown in Fig. 5-13 (a) and (b). These two runs had the same boundary conditions but the flow patterns were different. Fig. 5-13 (a) shows that in the case of the reattaching wall jet, the decay of the velocity scale behind the baffle shows the following four stages: (1) the slow decay from  $x/y_0$

= 40 to 50 because of flow convergence; (2) the rapid decay stage from  $x/y_0 = 50$  to 60; in this stage, the main flow diverged to impinge on the flume floor. (3) the slow decay stage from  $x/y_0 = 60$  to 80; in this stage, the impinged flow converged again. (4) submerged jump decay stage from  $x/y_0 = 80$  and further downstream. In this stage, the main flow behaved like that of a submerged jump whose toe section was at  $x/y_0 < 0$ . Compared to the case of the deflected surface jet, the velocity scale of the reattaching wall jet decayed slower up to the region where the shallowness of the tail water was felt by the flow. Fig. 5-13 (b) clearly shows the impingement of the reattaching main flow on the flume floor.

In runs 1, 4, 5, 7 and 8, the gate opening, the gate Froude number and the tail water depth were kept the same but different baffle heights and baffle positions were used. The decay and the locus of the maximum velocity are plotted in Fig. 5-14 (a) and (b). For comparison, the velocity scale decay curves for the plane wall jet and submerged jump without baffle ( same submergence, result from Chapter 4) are also plotted in Fig. 5-14 (a). In Fig. 5-14 (a), the broken vertical lines represent the positions of the baffles. As we can see, all the velocity scale data for the submerged jumps with baffles show the three decay stages and they all decayed faster than the wall jet and the submerged jump without baffle. As the baffle was moved farther away from the gate while its height was kept the same, the curved jet became increasingly flatter. As the baffle height was increased at a given position, the curved jet became progressively steeper and the velocity scale minimum point moved closer to the gate. The velocity scale data for run 9, which is the only run with a different gate opening, are also plotted in Fig. 5-14 (a) and they show a trend, consistent with all the other data except for the minimum point.

Let us now have a look at the velocity distribution in the region of surface jet. Figs. 5-15 (a) - (f) show the forward velocity profiles of runs 1, 2, 5, 7, 8 and 9 in non-dimensional form. The data for all the runs are plotted together in Fig. 5-15 (g). For comparison, a Gaussian curve representing the ordinary surface jet velocity distribution ( Rajaratnam and Humphries, 1984) is also plotted in Fig. 5-15 (g). In Fig. 5-15,  $u_s$  is the surface velocity,  $y_s$  is the water depth and  $b_s$  is the depth where  $u = 0.5u_s$ . Figs. 5-15 (a-g) show that although the forward velocities are similarly distributed, the distribution is different from the Gaussian distribution. This might be due to the shallow tail water.

The variation of forward discharge of the surface jets with the longitudinal distance is shown in Fig. 5-16 and the boundaries of the jet are shown in Fig. 5-17 (a). In Fig. 5-16,  $q$  is the unit discharge ( or discharge per unit width) and  $q_{nozl}$  is the unit discharge at the gate. Because it was very difficult to measure the velocities near the jet boundaries, the forward discharges and the jet boundaries were determined by using the data on surface velocity and velocity slope and assuming a linear velocity distribution. As indicated by Fig. 5-16, the forward discharge was as high as about 2.5 times the gate discharge before the start of the surface jet. The increase of the forward discharge is due to the enhanced entrainment by the curved jet. In the surface jet region of runs 1 and 2, the forward discharge increased for a certain distance and then decreased. Runs 5, 7 and 8 had the same boundary conditions as those of runs 1 and 2 but had bigger  $x_0$ . The forward discharge decreased all the way in the surface jet region of these three runs. The submergence of run 9 was smaller than that for all the other runs and its forward discharge also decreased all the way in the surface jet region. From Fig. 5-16 we can estimate the length of the eddy behind the baffles by looking at the crossing points of the data curves with the

horizontal line  $q/q_{nozl}=1$ . We can see that as the other boundary conditions were kept the same, bigger baffle position would result in a shorter eddy behind the baffle.

In Fig. 5-17 (b), the growth of length scale  $b_s$  in the surface jet region is shown in which  $x_{sm}$  is the value of  $x$  where maximum surface velocity occurred. For comparison, the straight line for ordinary surface jet ( Rajaratnam and Humphries, 1984 ) is also plotted in the same figure. According to Fig. 5-17 (b), only part of the surface jet region of runs 1 and 2 can be viewed as a normal surface jet, starting somewhere different from the gate. In all the other runs, the surface jet part was affected by the shallowness of the tail water from the beginning of the region, although the submergence was as high as 5.1. Fig. 5-17 (b) shows that at the beginning of the surface jet region, the jet half width  $b_s$  was about 7 times the gate opening and that the slope 0.07 of the ordinary surface jet was the maximum slope.

Let us consider the velocity scale of the surface jet region. Because the maximum velocity occurs at the surface, it was easy to measure. Therefore detailed measurements were done by using the setup shown in Fig. 5-3 (b) and the results are presented below.

In Fig. 5-18 (a), the longitudinal variation of surface velocities for four different gate Froude numbers is shown. In the four experiments of Fig. 5-18 (a), the gate opening, the tail water depth, the baffle height and baffle position were kept constant and only the discharge was varied. It is seen from Fig. 5-18 (a) that as the discharge was increased, the maximum surface velocity,  $u_{sm}$  was increased, the location of maximum surface velocity  $x_{sm}$  moved upstream and the decay of surface velocity became faster. The data points shown in Fig. 5-18

(a) are replotted in Fig. 5-18 (b) in non-dimensional form from which we can see that the surface velocity decayed in a similar way. In Fig. 5-18 (c), the variations with gate Froude number  $F_0$  of the following four variables are presented in non-dimensional form: the maximum surface velocity  $u_{sm}$ ; the distance of the top of surface hump from the baffle  $x_{top}-x_0$ ; the height of the surface hump  $h_h$  ( above tail water surface) and the distance from the position of the maximum surface velocity to the baffle  $x_{sm}-x_0$ . It is seen from Fig. 5-18 (c) that as  $F_0$  was increased,  $h_h/y_0$  and  $(x_{sm}-x_0)/y_0$  changed linearly with it but  $u_{sm}/U_0$  and  $(x_{top}-x_0)/y_0$  remained constant. The relevant linear equations and constants are given in Table 5-4.

Fig. 5-19 (a) presents the results for the longitudinal variation of surface velocities obtained for five different submergences. The experiments were done by fixing the discharge, the gate opening, the baffle height and position and changing the tail water depth only. The same data are shown in Fig. 5-19 (b) in non-dimensional form ( with the same scales as those for Fig. 5-18(b)) and the similarity is also shown for the surface velocity decay. The variations with submergence  $S$  of  $u_{sm}/U_0$ ,  $(x_{top}-x_0)/y_0$ ,  $h_h/y_0$  and  $(x_{sm}-x_{top})/y_0$  are shown in Fig. 5-19 (c). It is seen from Fig. 5-19 (c) that the four non-dimensional variables all change linearly with  $S$ . The equations describing these linear variations are given in Table 5-4.

The results shown in Fig. 5-20 (a) and (b) were obtained from the five experiments whose boundary conditions were the same except the different baffle positions. The variations with baffle position of the maximum surface velocity and its position are shown in Fig. 5-20 (c) in non-dimensional forms. Also shown in Fig. 5-20 (c) are the variations of  $(x_{top}-x_0)/y_0$  and  $h_h/y_0$  with the relative baffle position  $x_0/y_0$ . From Fig. 5-20(c) it seems that the baffle position

did not have obvious effect on all the four non-dimensional variables. The mean values of these variables are given in Table 5-4.

The results obtained from the four experiments with different baffle heights are shown in Fig. 5-21 (a) and (b) in original and non-dimensional forms. Fig. 5-21 (c) shows the results of  $u_{sm}/U_0$ ,  $(x_{top}-x_0)/y_0$ ,  $h_b/y_0$  and  $(x_{sm}-x_0)/y_0$ . All these four variables vary linearly with the relative baffle height  $h/y_0$  and the relations are given in Table 5-4.

The surface velocity data shown in Figs. 5-18(a), 5-19(a), 5-20(a), 5-21(a) and the data for run 9 are plotted together in Fig. 5-22 in non-dimensional form. As we can see that the surface velocity decayed linearly after the maximum velocity was reached and this is different from the -0.5 power law of the decay of the surface velocity of ordinary surface jet ( Rajaratnam and Humphries, 1984). The regression expressions are obtained for the data shown in Fig. 5-22:

$$\frac{u_s}{u_{sm}} \Big|_{(\pm 0.031)} = 1.001_{(\pm 0.013)} + 0.134_{(\pm 0.138)} \frac{x-x_{sm}}{y_t} - 0.723_{(\pm 0.310)} \left( \frac{x-x_{sm}}{y_t} \right)^2 \quad x < x_{sm} \quad (5-3)$$

$$\frac{u_s}{u_{sm}} \Big|_{(\pm 0.028)} = 1.008_{(\pm 0.026)} - 0.295_{(\pm 0.003)} \frac{x-x_{sm}}{y_t} \quad x \geq x_{sm} \quad (5-4)$$

Finally, let us have a look at the eddies before baffles. It was difficult to measure the distribution of vorticity  $\zeta$  inside the eddies, and the velocity distributions indicated that the vorticity could be assumed to be uniformly distributed. The vorticity was calculated by using the formula for circular vortex ( Pao, 1961 ) :



$$\omega = \frac{2\pi r v_{\theta}}{\pi r^2} = 2 \frac{v_{\theta}}{r} \quad (5-5)$$

where  $r$  is the distance from vortex center to the point of measurement and  $v_{\theta}$  is the tangential velocity.

The vorticity was calculated for runs 1, 2, 3, 4, 5, 7 and 8, and the results are given in Table 5-5 below. Once we get the vorticity, we can estimate the circulation  $\Gamma$  of the eddy by multiplying the vorticity with the cross-sectional area of the eddy which we can estimate from the original velocity field plot (Fig. 5-5). The results of circulation are also given in Table 5-5.

From Table 5-5 we can see that the vorticity and circulation of run 7 do not differ much from those of run 8 although the baffle heights were different. Due to this reason and the fact that the tail water depth almost did not change in the experiments listed in Table 5-5, the baffle position  $x_0$  was combined with gate velocity  $U_0$  to form the scale for the circulation. The non-dimensional circulation  $\Gamma/(U_0 * x_0)$  is plotted against  $x_0/y_0$  in Fig. 5-23 in which a horizontal line is plotted to represent the mean value. In the last column of Table 5-5, the ratios of eddy circulation discharges to the gate discharges are listed and as we can see that the ratios could be as high as 3.3.

#### 5.4 Conclusions

This chapter presents the results of an exploratory experimental study on the effect of two dimensional baffles on submerged hydraulic jumps. Experiments of series 1 were done for gate opening equal to 10, 12, 15 and 17 mm. The gate Froude number ranged from 1.4 to 12 and submergence ranged from 0.5 to 32. Based on the results of experiments of series 1, the following conclusions can be formulated:

(1) For submerged hydraulic jumps with baffle walls, there exists two different stable flow states: deflected surface jet state and reattaching wall jet state. In deflected surface jet state, the main flow is deflected to the water surface to form surface jet downstream the baffle. In the region below the surface jet, the water flows slowly towards the baffle. In the reattaching wall jet state, the main flow passes over the baffle to impinge and reattach to the bed immediately downstream the baffle.

(2) For a given tail water depth and baffle position, there exists two critical baffle heights  $h_{c1}$  and  $h_{c2}$  and they are independent of gate opening and gate Froude number. If baffle height is smaller than  $h_{c1}$ , the flow will be in stable reattaching wall jet state. If baffle height is bigger than  $h_{c2}$ , the flow will be in stable deflected surface jet state. If baffle height is between  $h_{c1}$  and  $h_{c2}$ , the flow can be stable in either states depending on initial flow state and the flow can be changed from one state to the other by external interference. The mean value of the ratio of  $h_{c1}$  to the tail water depth is 2% and the regression equation for  $h_{c2}$  is

$$\frac{h_{c2}}{y_t} = 0.0382 - 0.0078 \frac{x_0}{y_t} + 0.0261 \sin^2\left(\frac{x_0}{y_t}\right) \quad (5-2)$$

Based on the results of the detailed measurements in experiments of series 2, the following conclusions can be formulated:

(1) In the region upstream of the baffle, the forward velocity profiles are similar in the lower part and can be described by the corresponding wall jet curve. They are not similar in the upper part due to the effect of the strong surface eddy formed upstream of the baffle. The jet half width  $b$  in this region is not affected by the baffle but the velocity scale, the maximum forward velocity, is somewhat higher than that of the wall jet.

(2) In the deflected surface jet, the maximum velocity decays continuously to reach its minimum value somewhere below the water surface and then increases to reach its maximum value on the water surface. After this it decays continuously. In the reattaching wall jet state, the maximum velocity decays all the way from the gate. For the same boundary conditions, the decay of the maximum velocity is faster in the deflected surface jet state than that in the reattaching wall jet state.

(3) In the surface jet region of the deflected surface jet flow state, the forward velocity profiles are similar. These similar profiles are generally different from those of the ordinary surface jet because of the effect of the shallowness of tail water. Also due to this reason the growth rate of the length scale  $b_s$  is smaller than 0.07 which is the growth rate for the half width of the ordinary surface jet.

(4) The scales for the surface jet( the maximum surface velocity, the surface hump height, the position of maximum surface velocity and the position of the top of surface hump ) are generally affected by the following four variables: tail water depth, gate Froude number, baffle position and baffle height.

(5) For the deflected surface jet flow state, the circulation of the eddy before baffle is about 1.5 times the product of the gate velocity and the baffle position from the gate. The circulating discharge can be as large as 3.3 times the gate discharge.

## **5.5 References**

1. Liu, H. K. (1949), Diffusion of Flow from Submerged Sluice Gate, Thesis presented to the State Univ. of Iowa, Iowa, in partial fulfillment of the requirements for the degree of M. Sc., 32p.
2. Long, D, Rajaratnam, N. and Steffler, P. M. (1990), LDA Study of Flow Structure in Submerged Hydraulic Jump, Jour. of Hyd. Res., Vol. 28, No. 4, pp. 437-460.
3. Narasimhan, S. and Bhargava, V. P. (1976), Pressure Fluctuations in Submerged Jump, ASCE Jour. of Hyd. Div., Vol. 102, HY3, pp. 339-350.
4. Ohtsu, I., Yasuda, Y. and Awazu, S. (1990), Free and Submerged Hydraulic Jumps in Rectangular Channels, Report of the Research Institute of Science and Technology, Nihon University, No. 35, Feb. 1990, 50 p.
5. Pao, Richard H. F. (1961) Fluid Mechanics, John Willy & sons, Inc., 502p.
6. Rajaratnam, N. (1965a), Submerged Hydraulic Jump, ASCE Jour. of Hyd. Div., Vol. 91, HY4, pp. 71-96.
7. Rajaratnam, N. (1965b), Flow below a Submerged Sluice Gate as a Wall Jet Problem, 2nd Australation Conf. on Hydraulics and Fluid Mechanics, Auckland, New Zealand, pp. B131-146.
8. Rajaratnam, N. (1976), Turbulent Jets, Elsevier Scientific Publishing Co., 304p.
9. Rajaratnam, N. and Humphries, J. A. (1984), Turbulent Non-Buoyant Surface Jet, Jour. of Hyd. Res., Vol. 22, No. 2, pp. 103-114.
10. Rao, N. S. G. and Rajaratnam, N. (1963), The Submerged Hydraulic Jump, ASCE Jour. of Hyd. Div., Vol. 89, HY1, pp. 139-162.

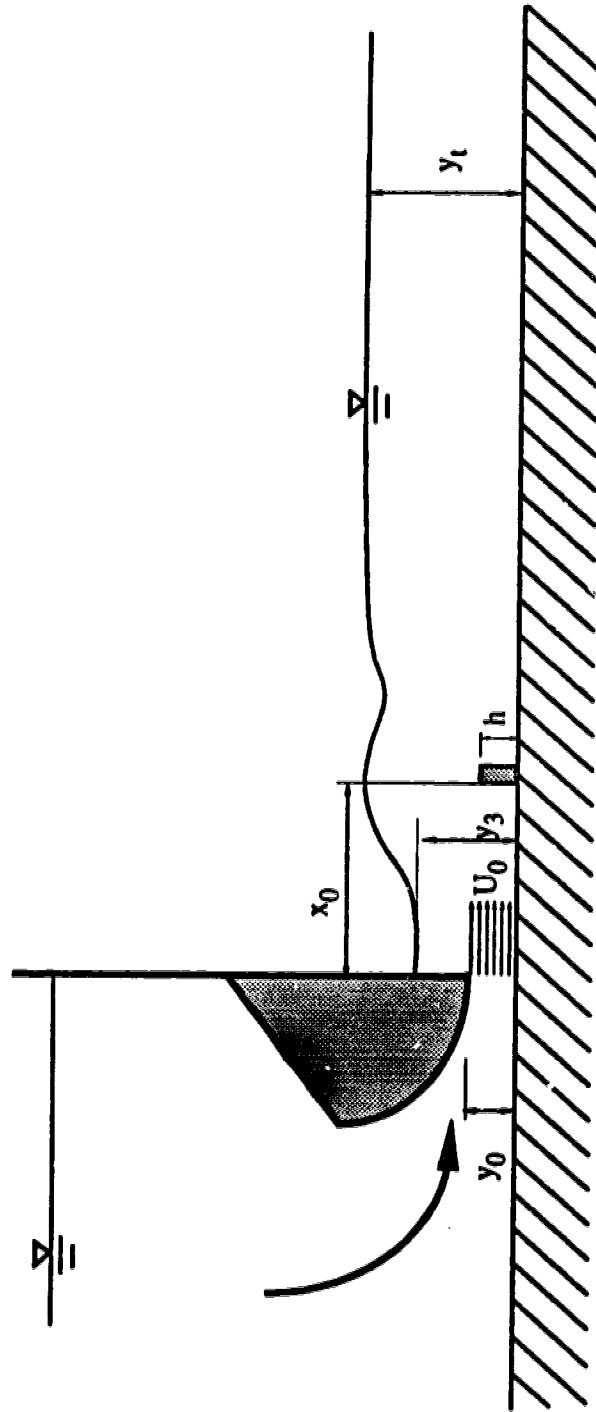


Fig. 5-1 Flow configuration of hydraulic jump forced by a two-dimensional baffle

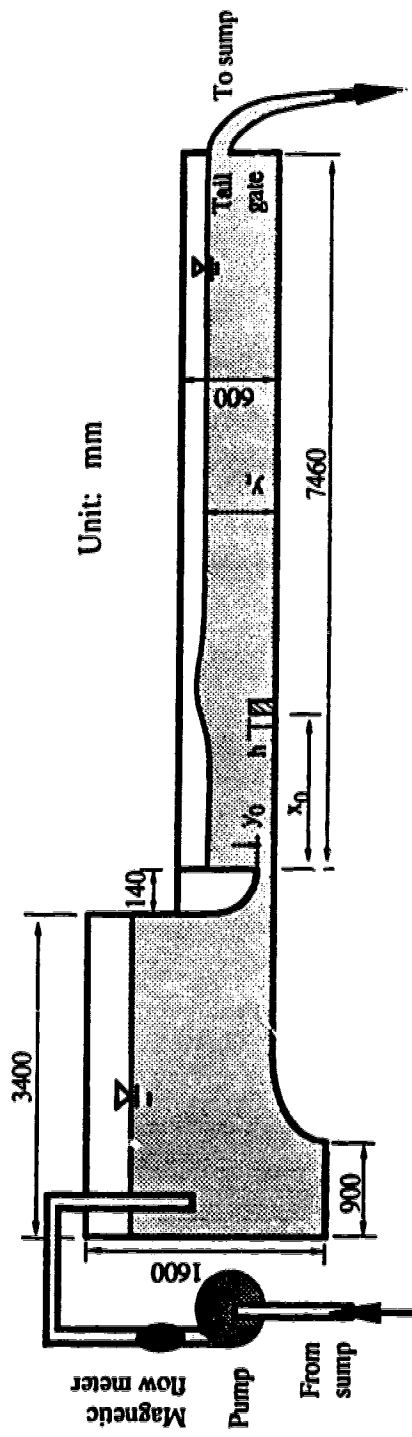


Fig. 5-2 Experimental flume

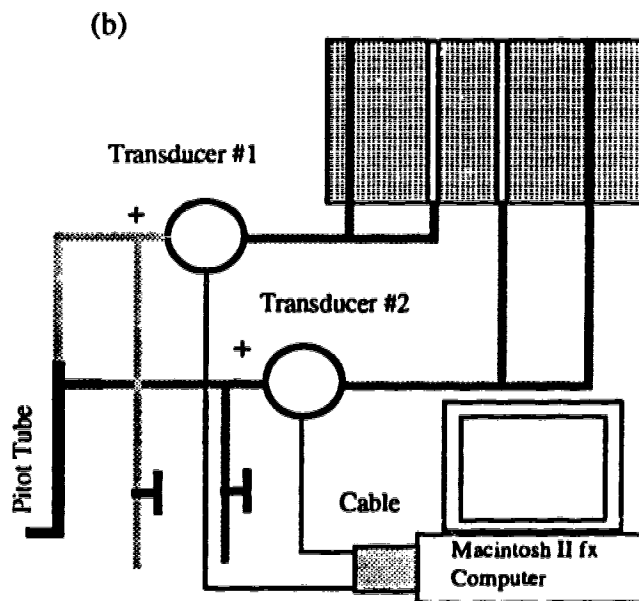
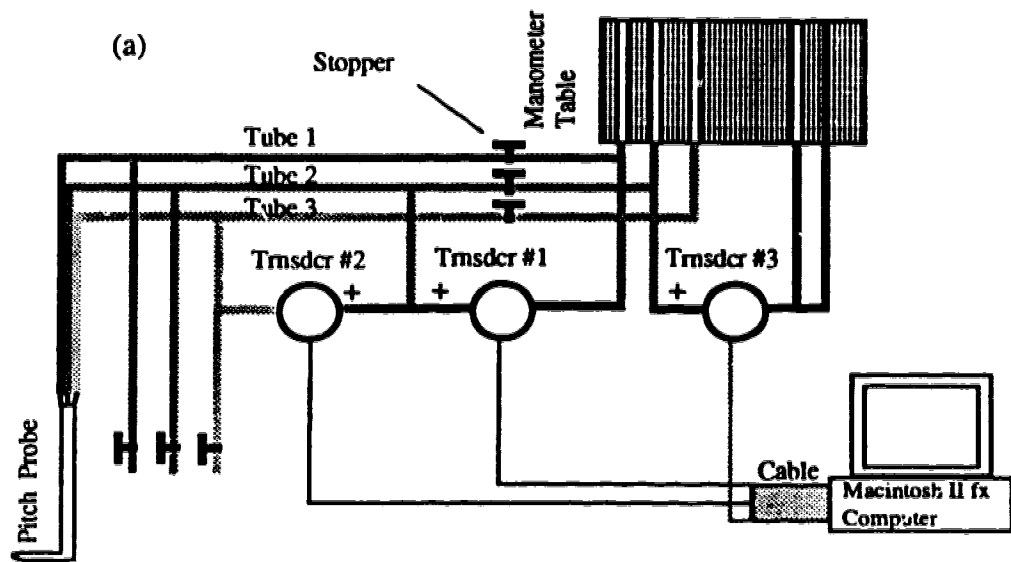


Fig. 5-3(a-b) Experimental setup for velocity and pressure measurements

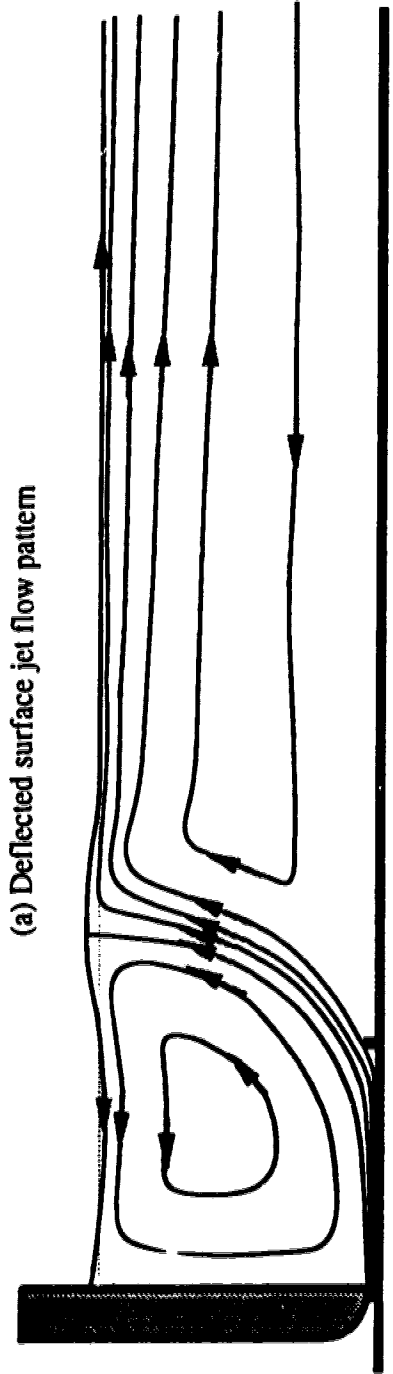


Fig. 5-4 (a)-(b) Schematic flow patterns



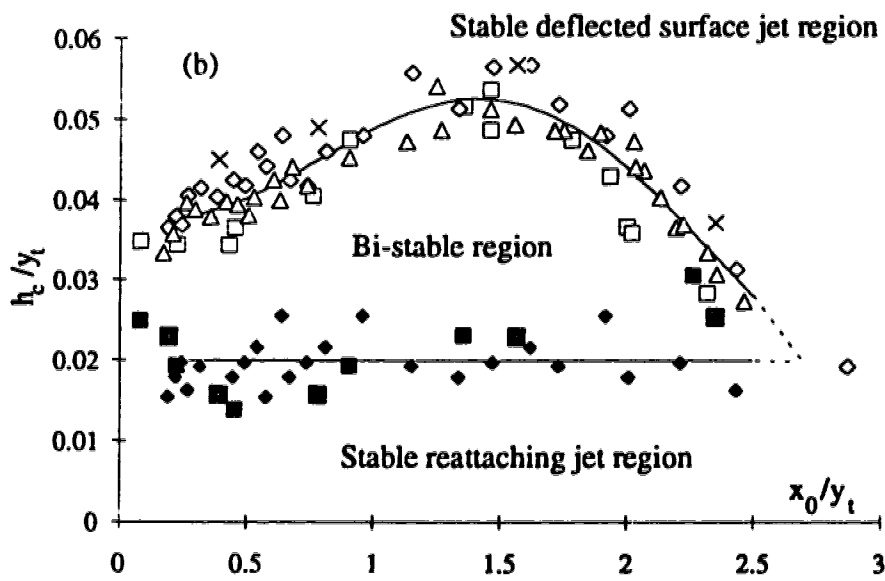
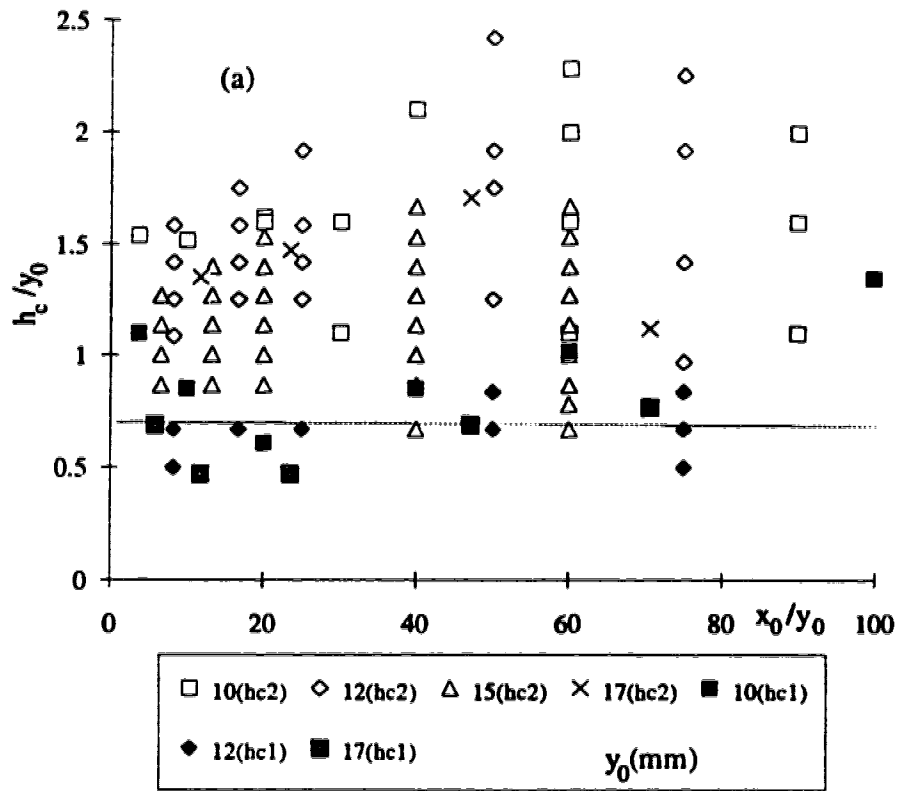


Fig. 5-5(a-b) Variation of the critical baffle heights with baffle position

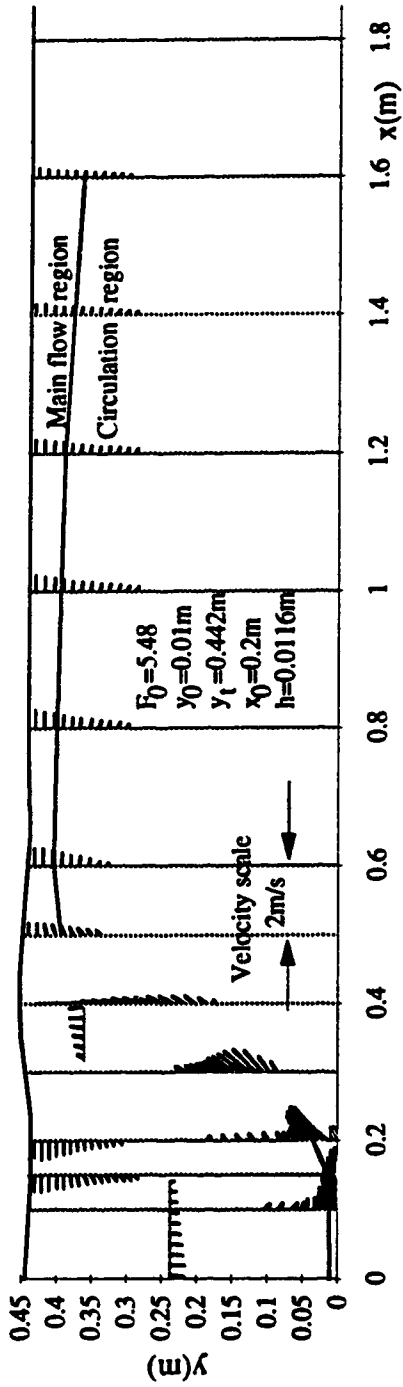


Fig. 5-6 (a) Velocity field of run 1

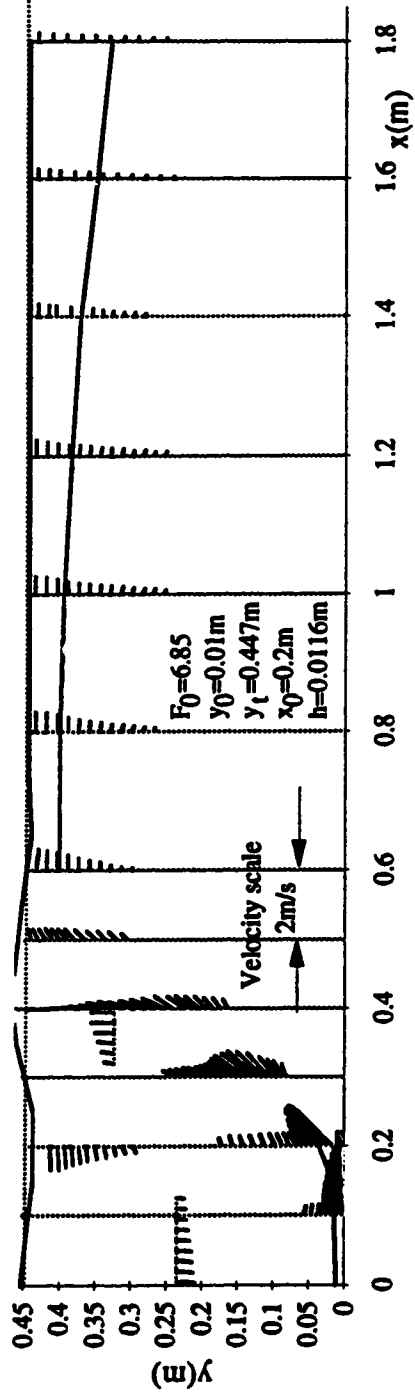


Fig. 5-6 (b) Velocity field of run 2

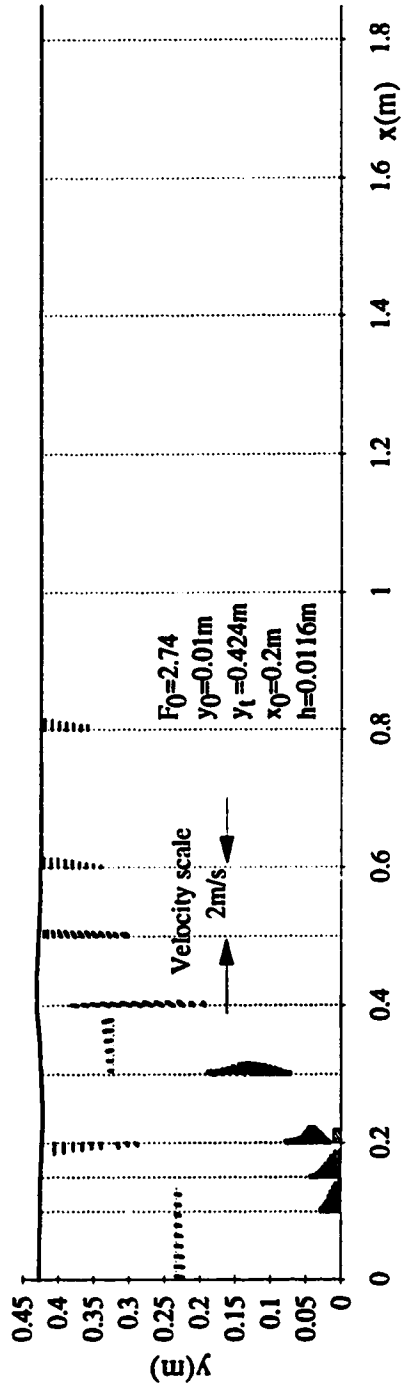


Fig. 5-6 (c) Velocity field of run 3

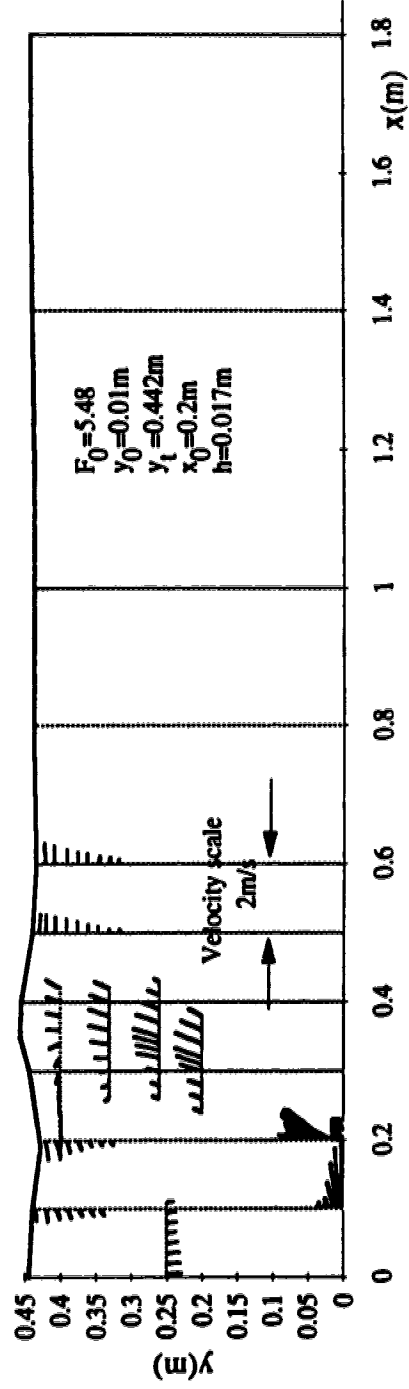


Fig. 5-6 (d) Velocity field of run 4

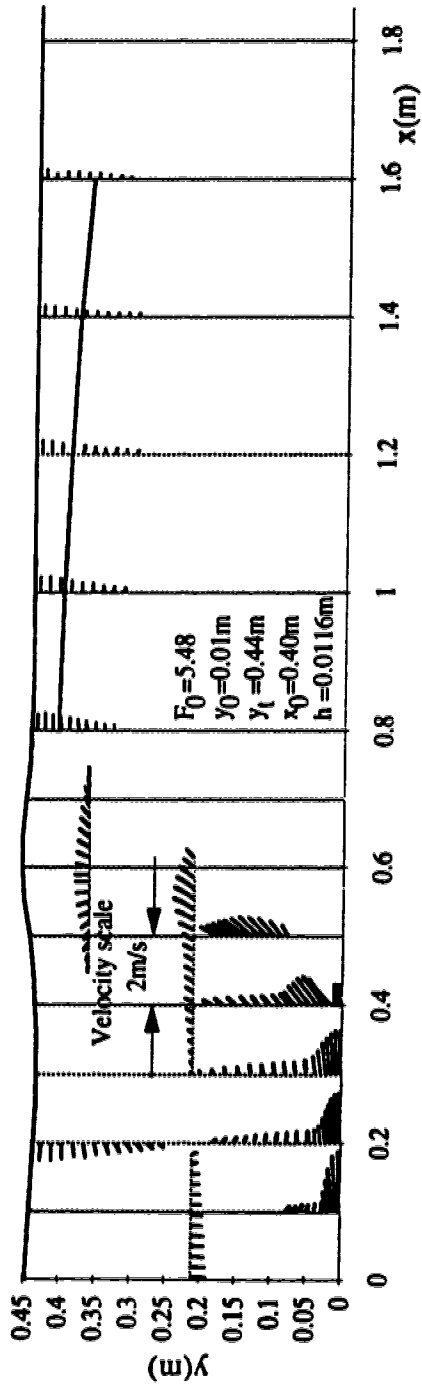


Fig. 5-6 (e) Velocity field of run 5

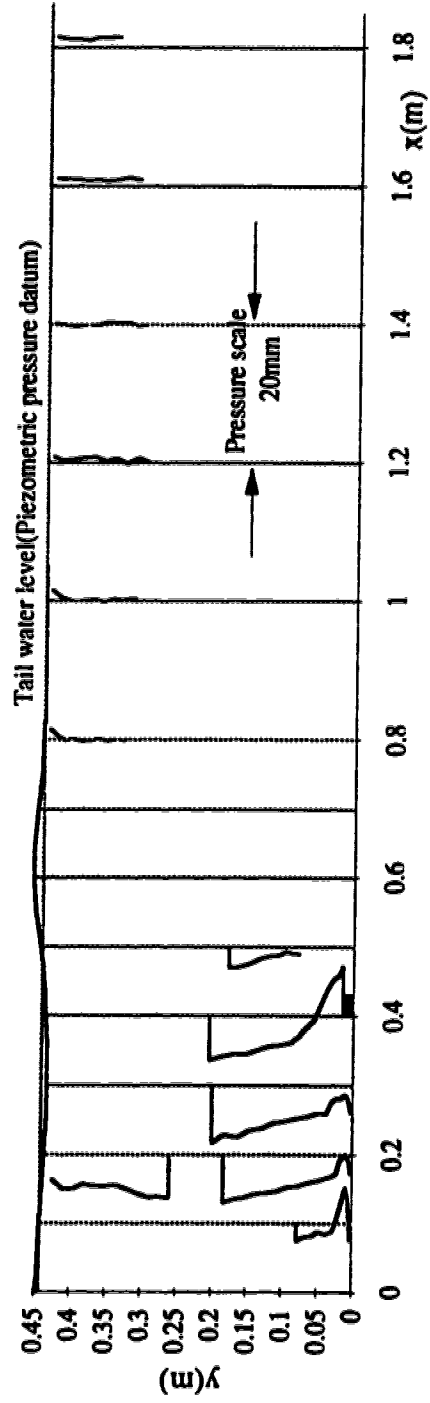


Fig. 5-6 (f) Piezometric pressure field of run 5

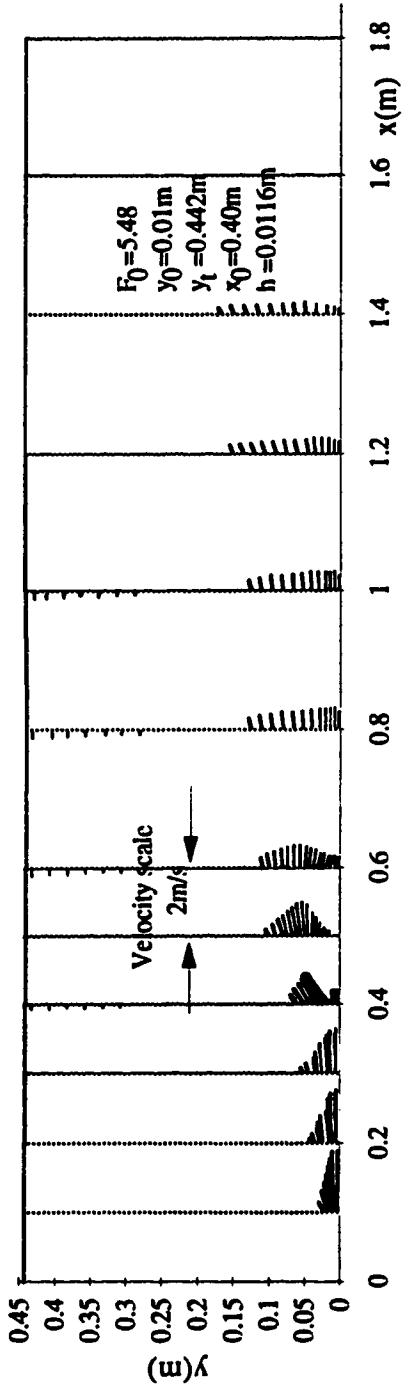


Fig. 5-6 (g) Velocity field of run 6

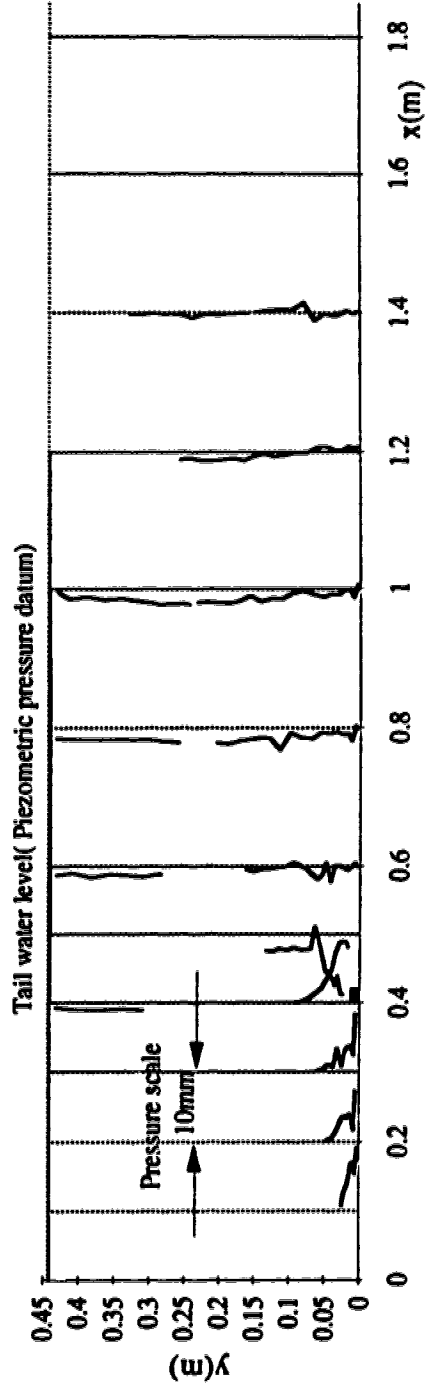


Fig. 5-6 (h) Piezometric pressure field of run 6

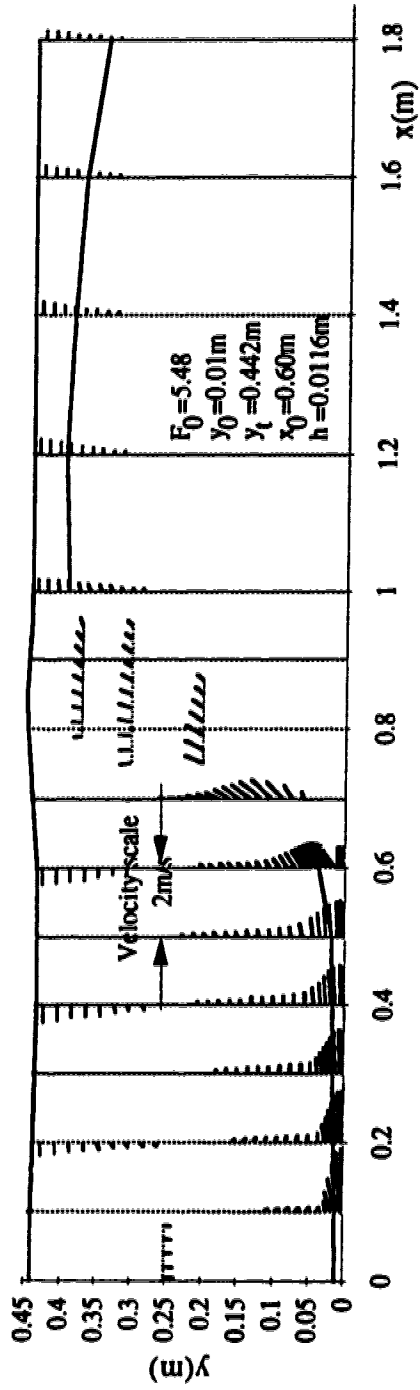


Fig. 5-6 (i) Velocity field of run 7

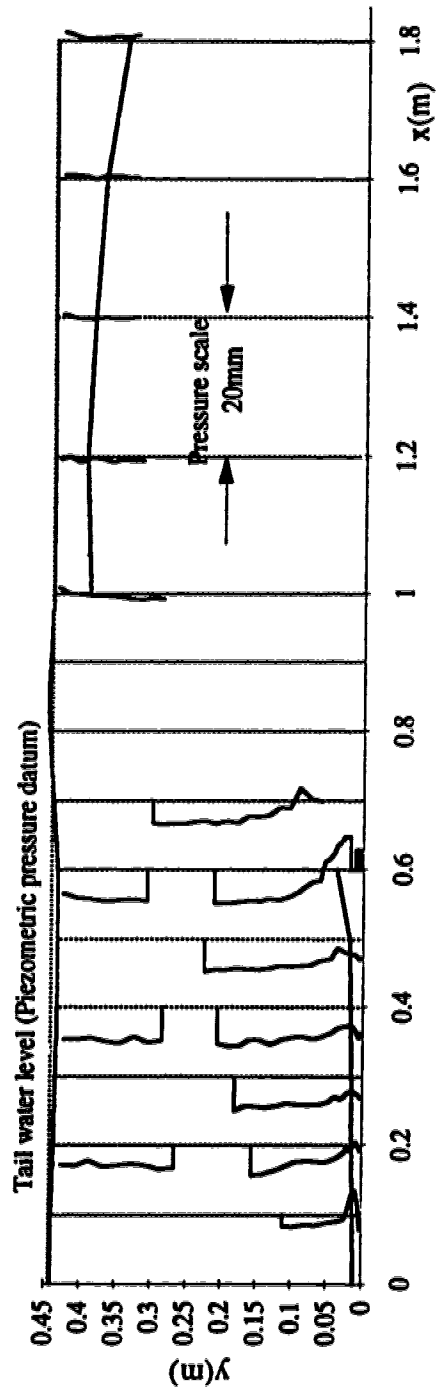


Fig. 5-6 (j) Piezometric pressure field of run 7

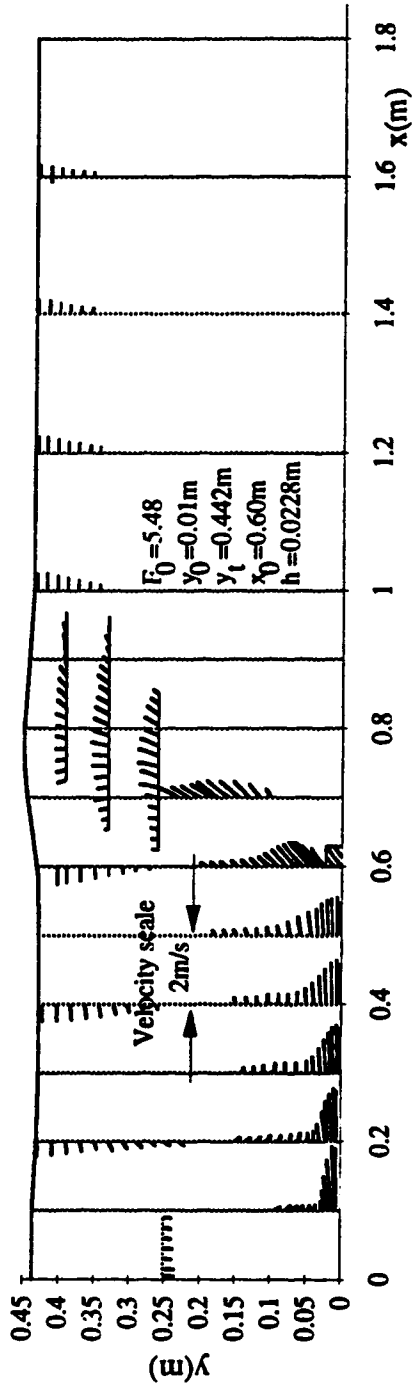


Fig. 5-6 (k) Velocity field of run 8

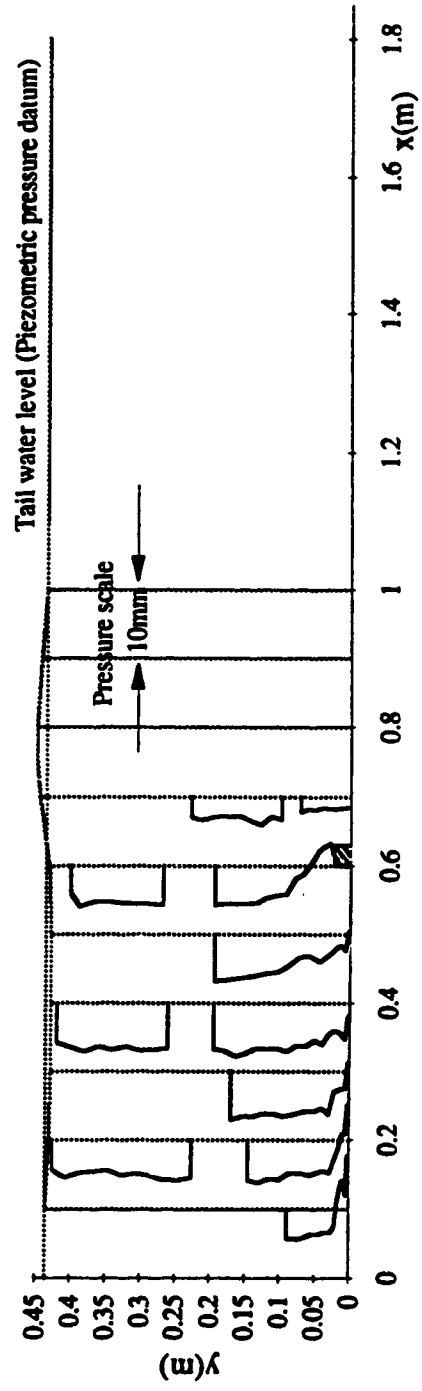


Fig. 5-6 (l) Piezometric pressure field of run 8

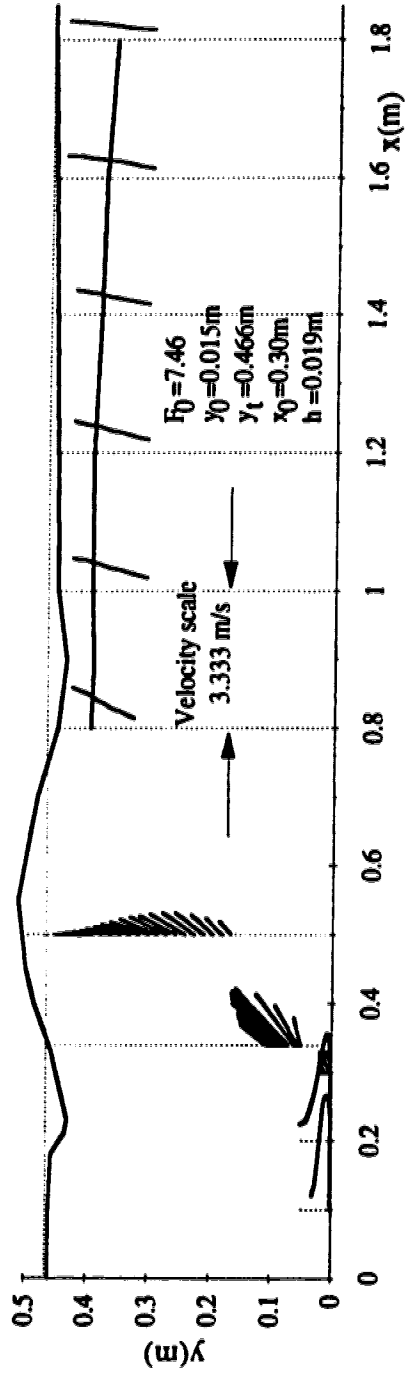


Fig. 5-6 (m) Velocity field of run 9

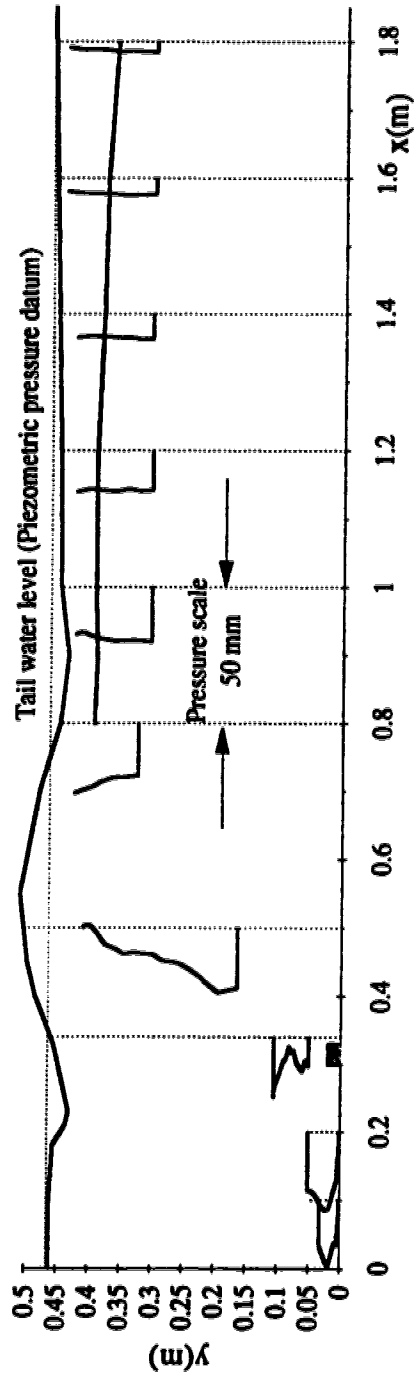


Fig. 5-6 (n) Piezometric pressure field of run 9



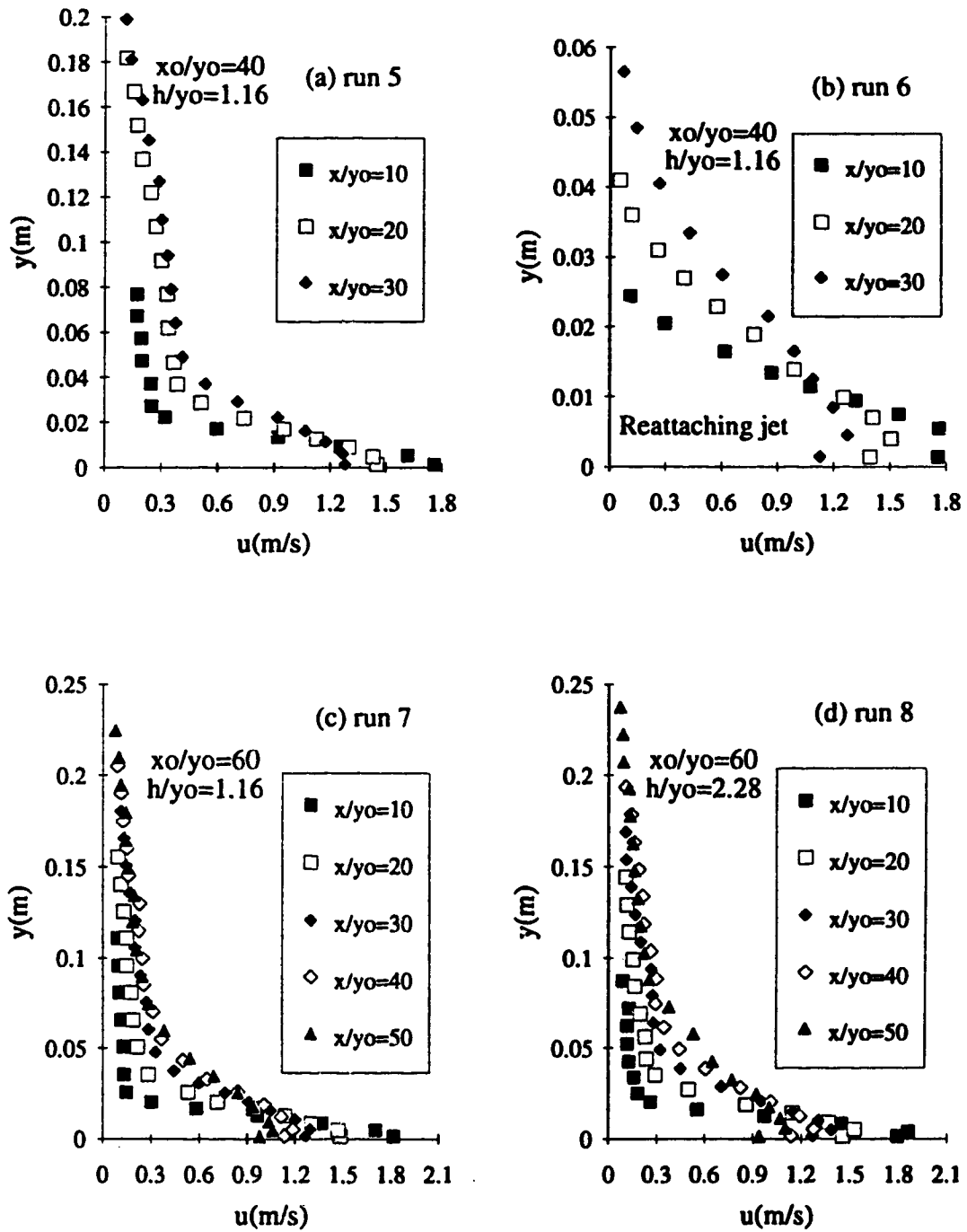


Fig. 5-7 (a)-(d) Distribution of longitudinal velocity component before baffle

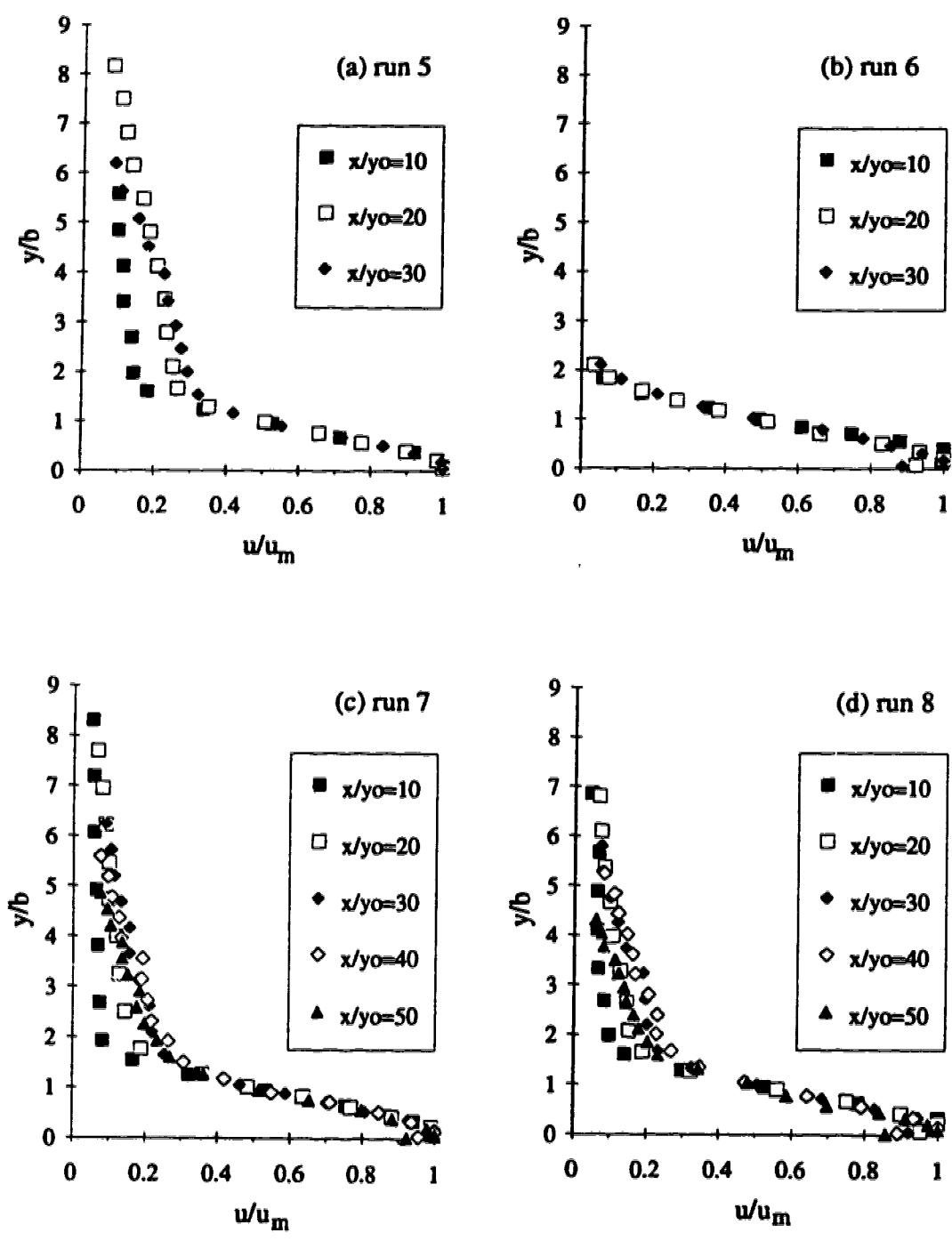


Fig. 5-8 (a)-(d) Non-dimensional profiles of the longitudinal velocity component before baffle

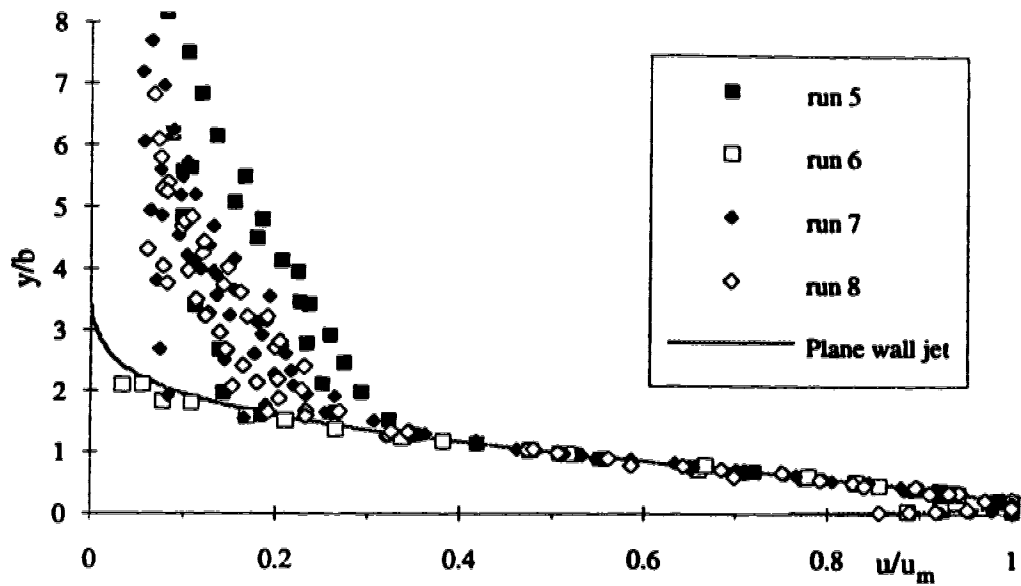


Fig. 5-9 Consolidated non-dimensional profiles of the longitudinal velocity component before baffle

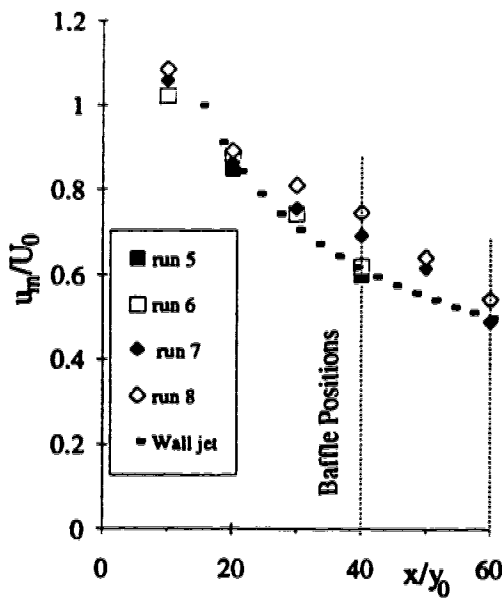


Fig. 5-10 Decay of the velocity scale before baffle

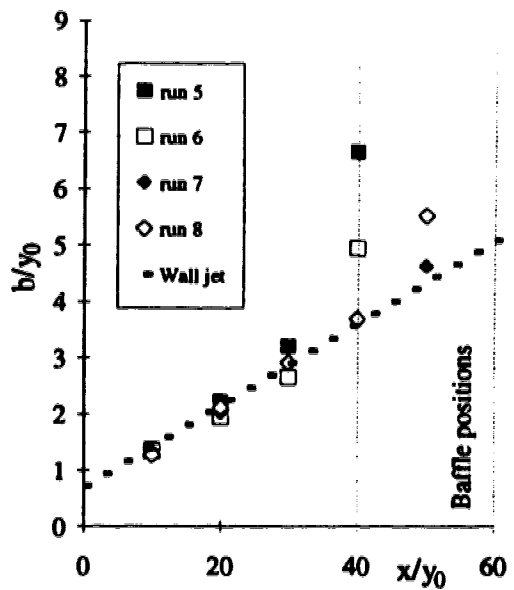


Fig. 5-11 Variation of the length scale  $b$  before baffle

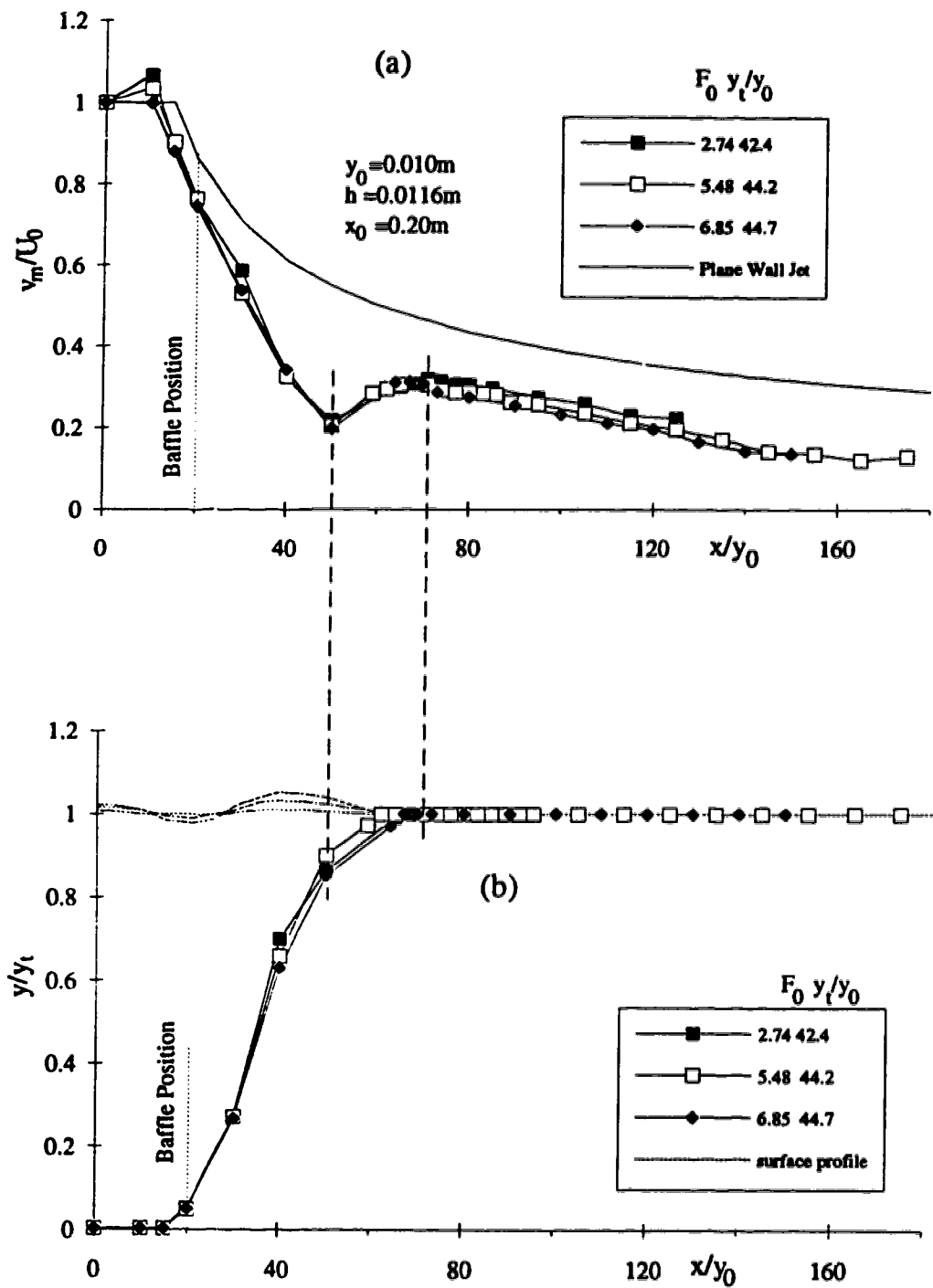


Fig. 5-12 (a)-(b) Effect of the gate Froude number on the decay of maximum velocity and its locus

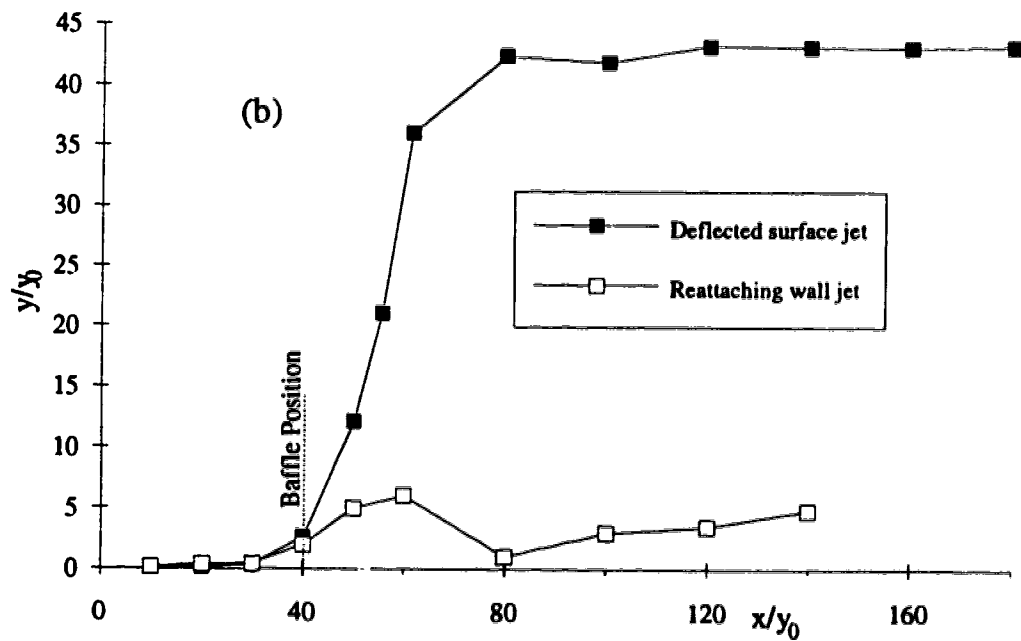
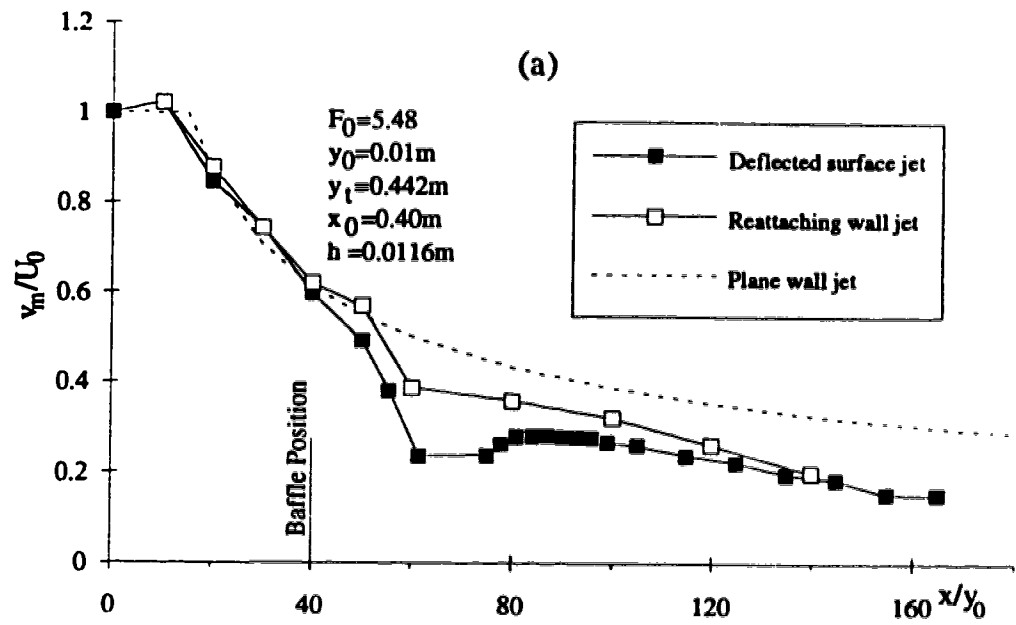


Fig. 5-13 (a)-(b) Comparison of the decay and locus of the maximum velocity for two different flow patterns

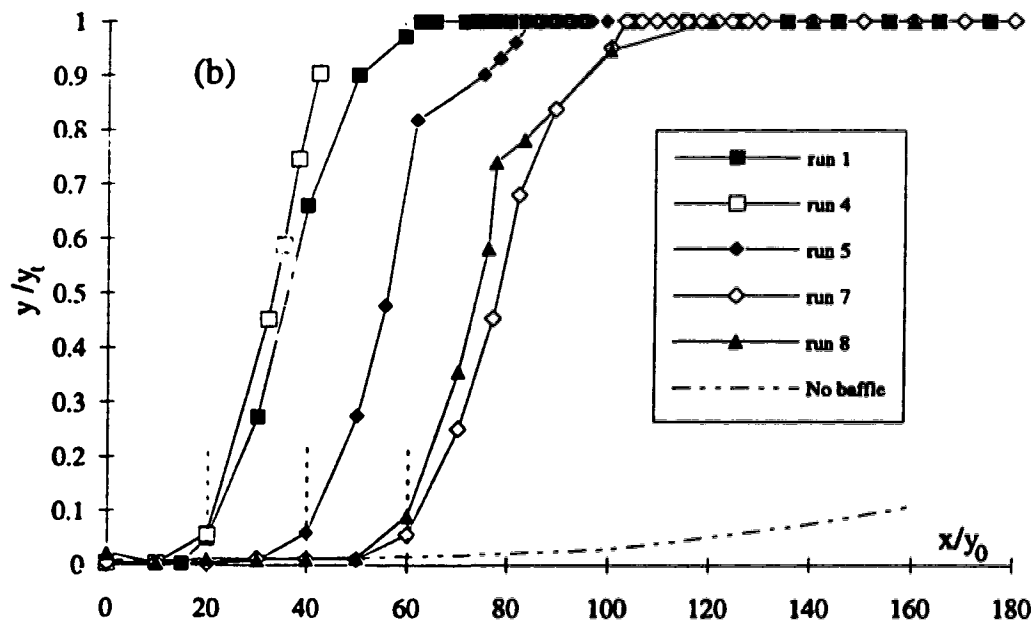
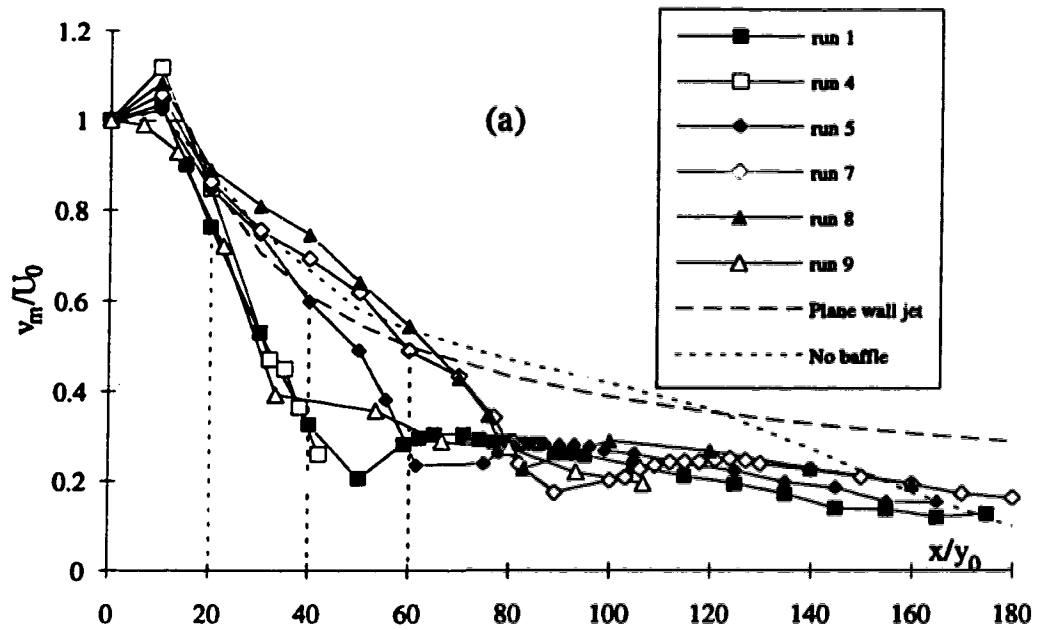


Fig. 5-14 (a-b) Effect of the baffle position and height on the decay and locus of the maximum velocity of deflected surface jets

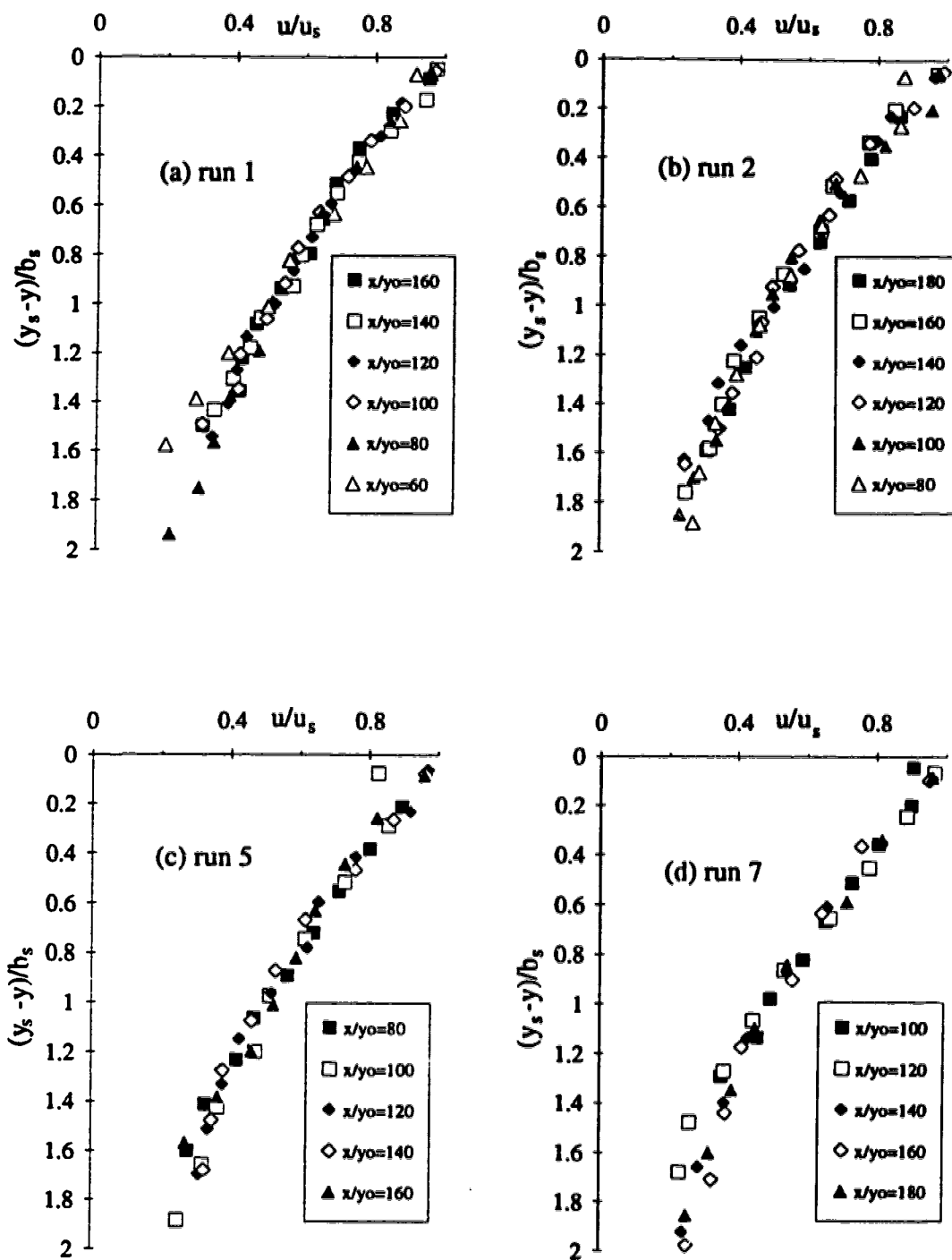


Fig. 5-15 (a)-(d) Non-dimensional forward velocity profiles in the region of surface jet

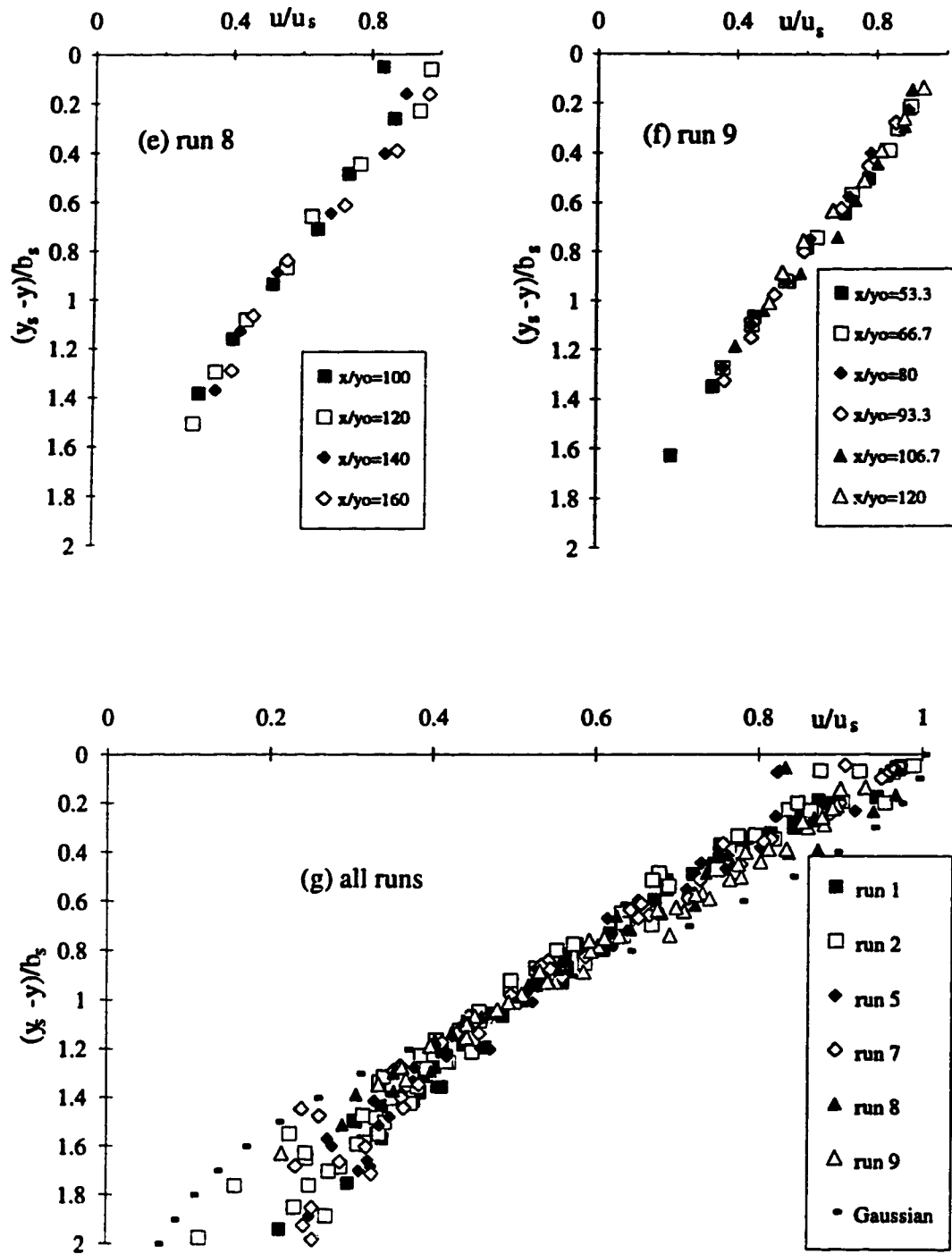


Fig. 5-15 (e)-(g) Non-dimensional forward velocity profiles in the region of surface jet



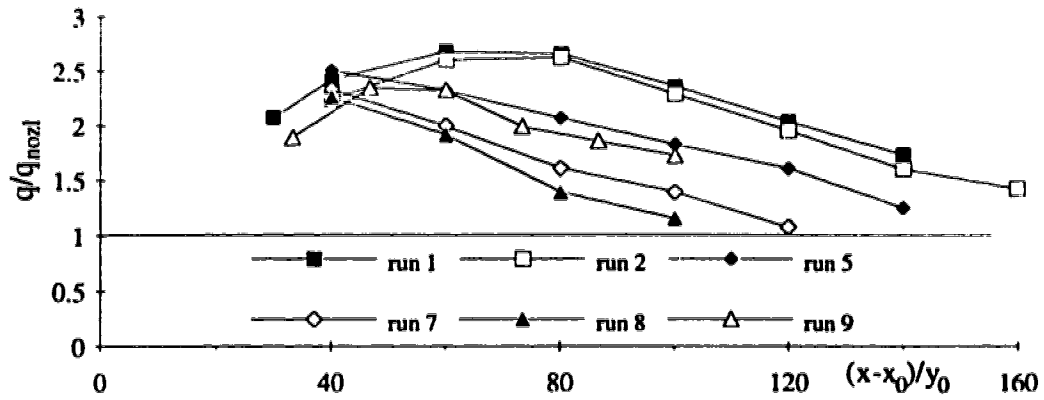


Fig. 5-16 Longitudinal variation of forward discharge of surface jets

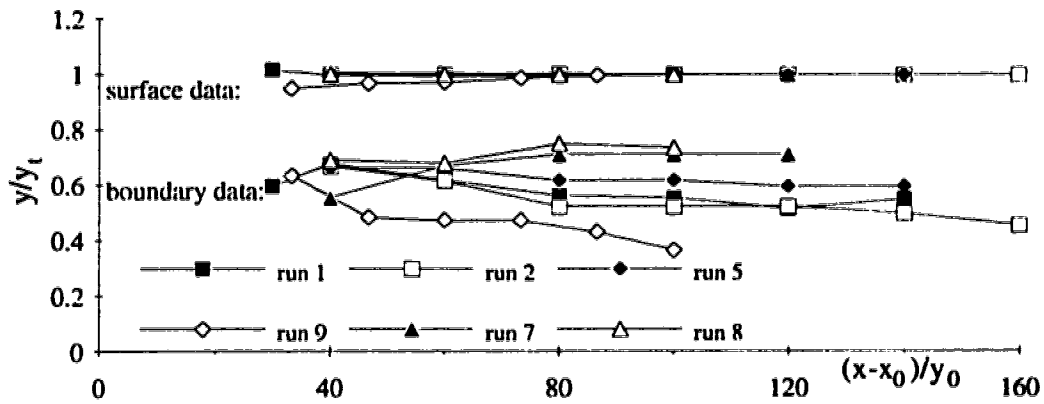


Fig. 5-17 (a) Longitudinal variation of surface jet boundary

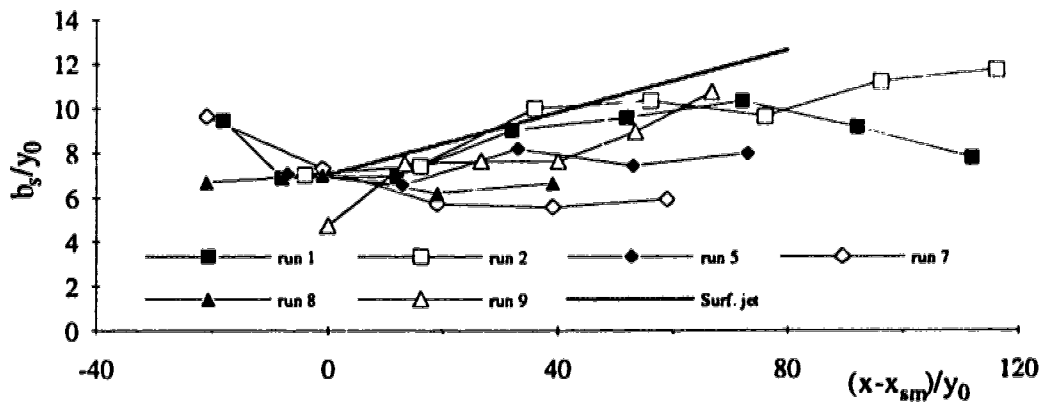


Fig. 5-17 (b) Growth of the length scale  $b_s$

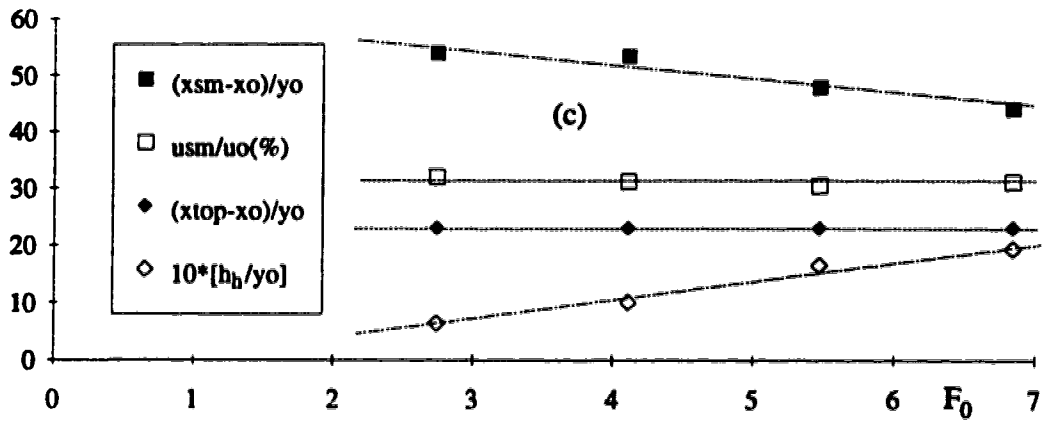
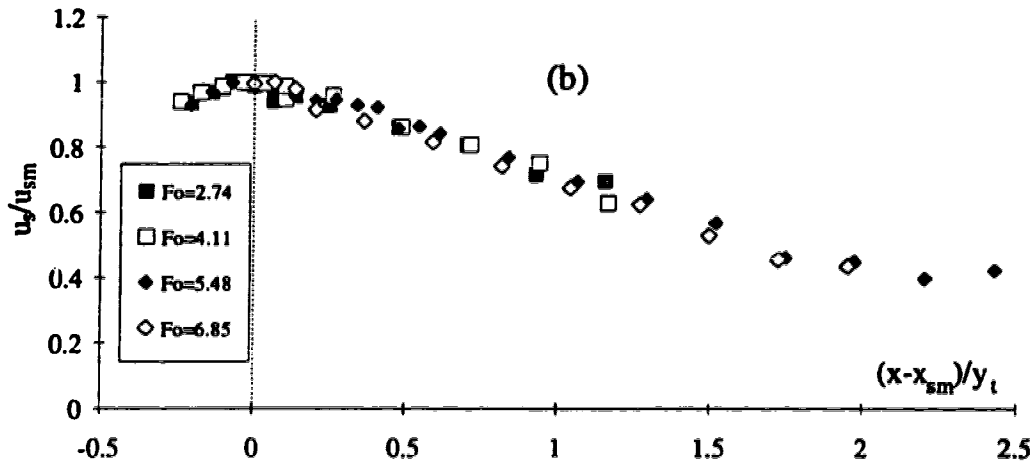
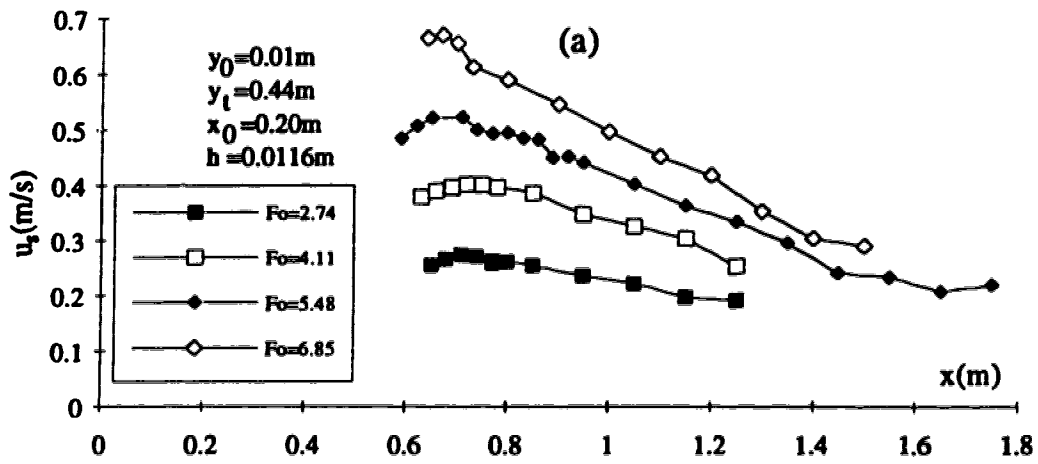


Fig. 5-18(a-c) Effect of gate Froude number on the scales on water surface

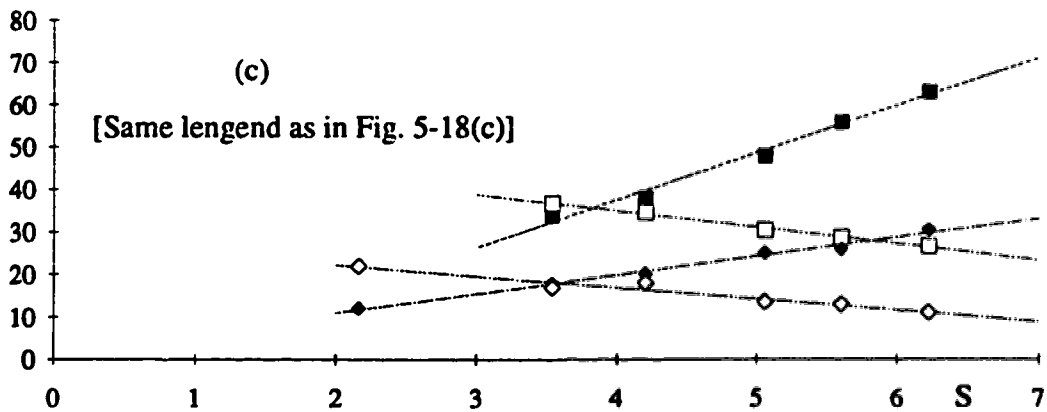
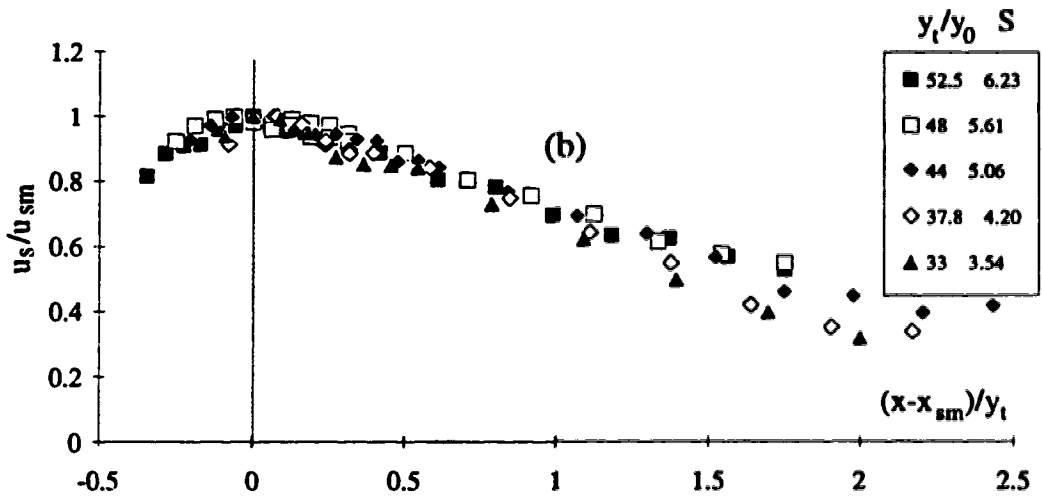
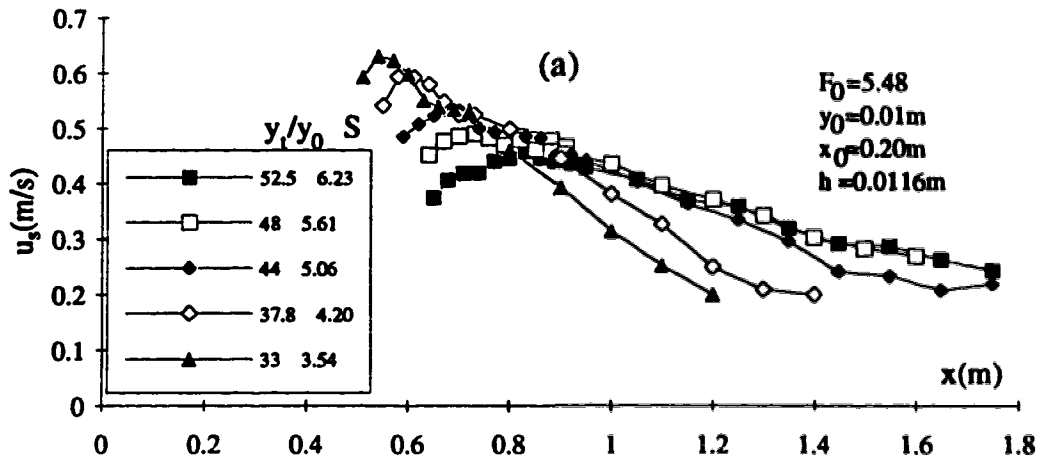


Fig. 5-19(a-c) Effect of submergence on the scales on water surface

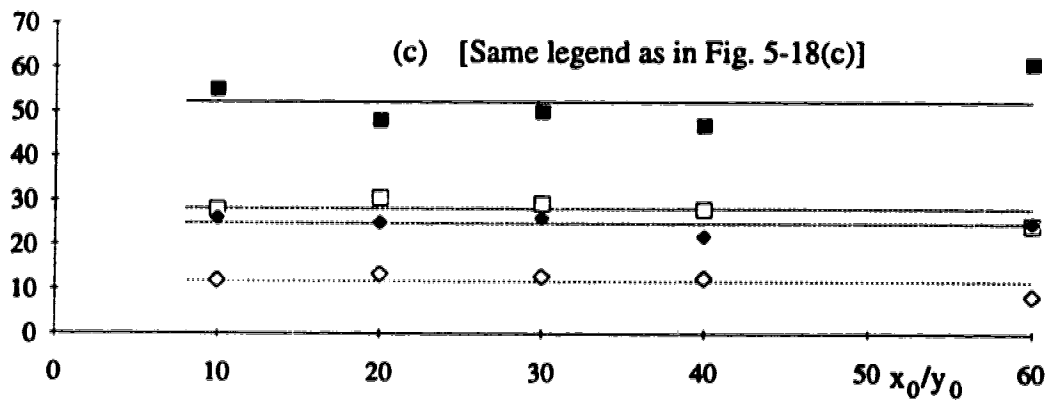
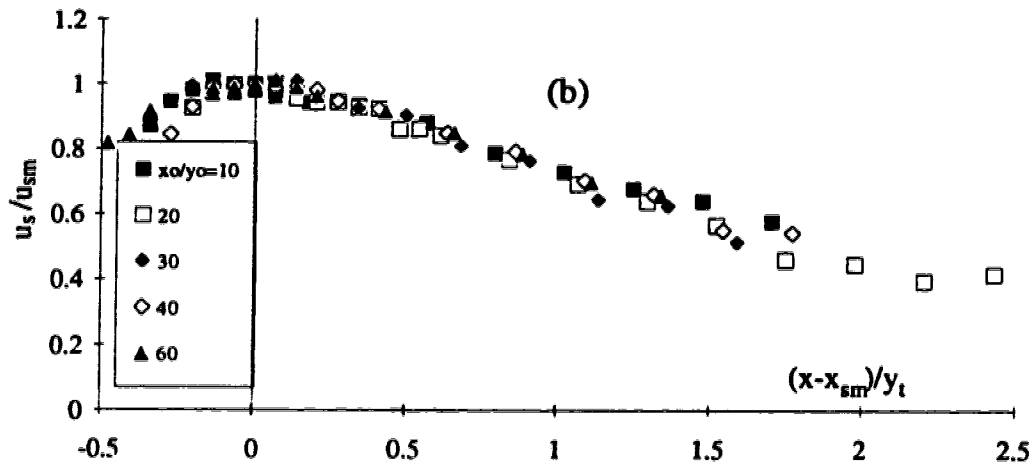
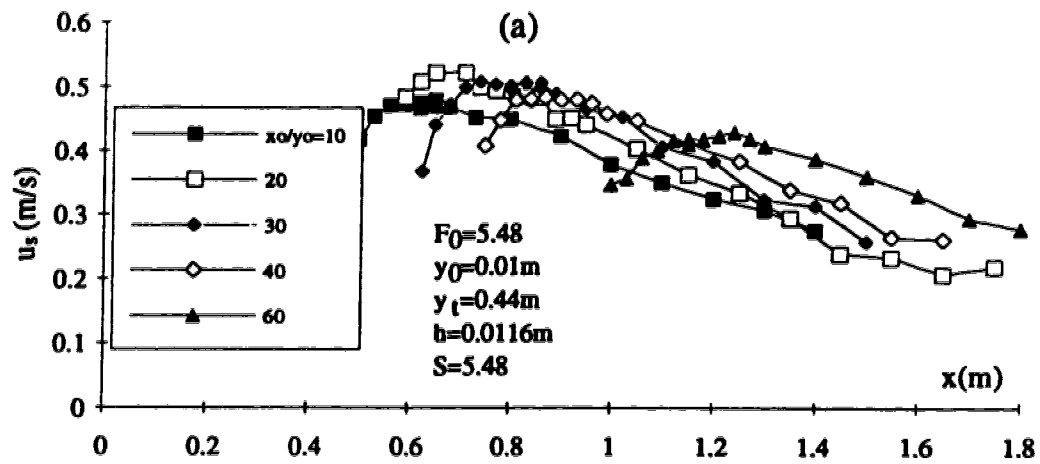


Fig. 5-20(a-c) Effect of baffle position on the scales on water surface

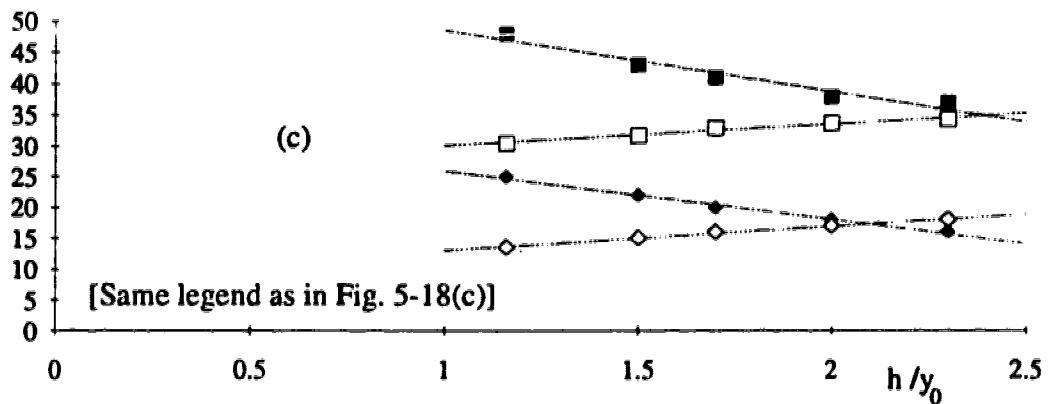
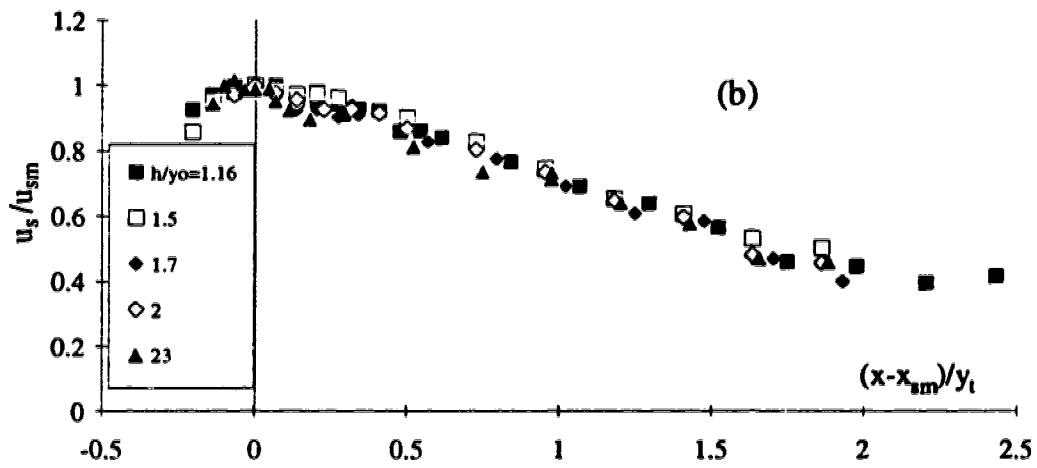
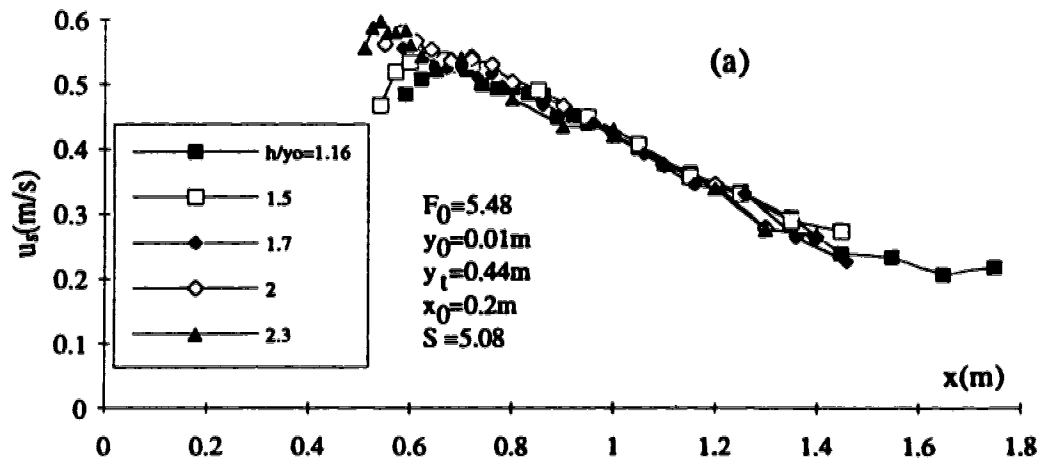


Fig. 5-21 (a-c) Effect of baffle height on the scales on water surface

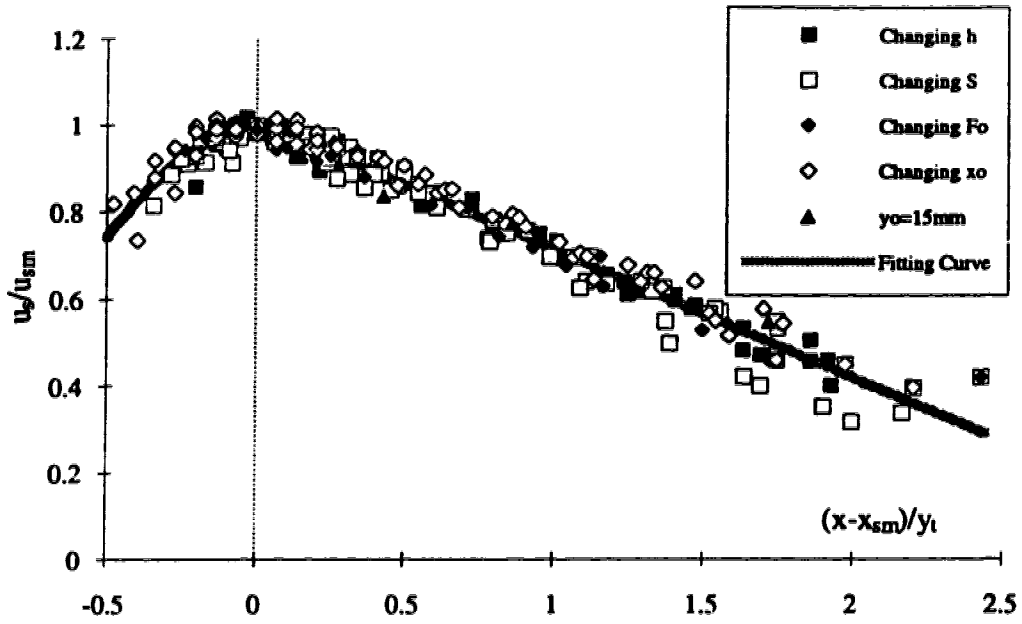


Fig. 5-22 Consolidated plot for the surface velocity decay

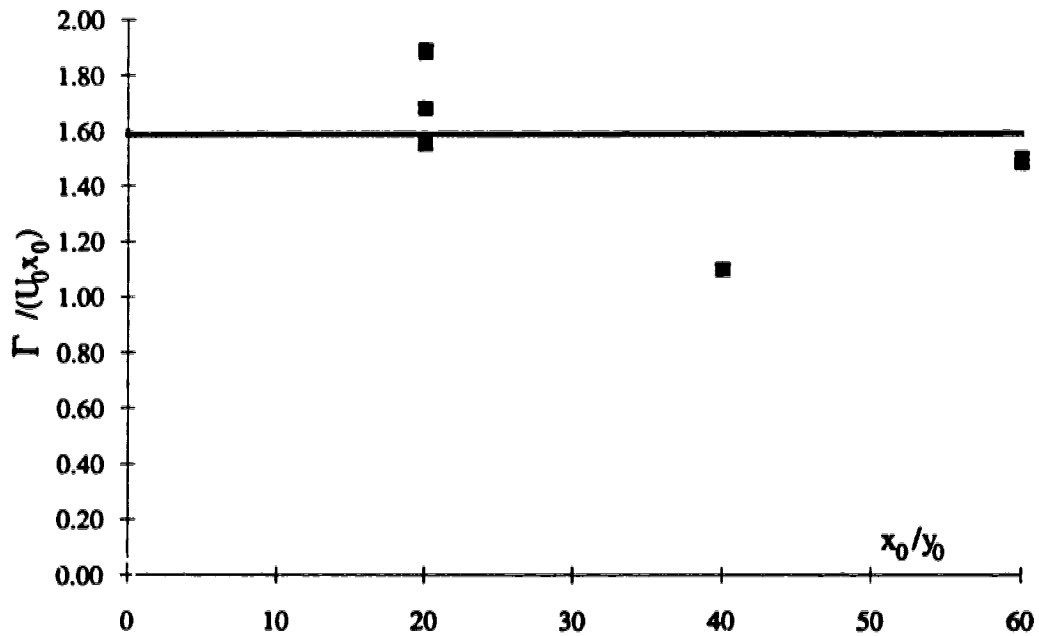


Fig. 5-23 Variation of circulation with baffle position

Table 5-1 Experimental results for critical baffle height  $h_{c1}$

$y_0 = 10$ (mm) $F_0 = 5.5 - 10.3$ $S = 2.1 - 5.1$				
$x_0$ (mm)	$h_{c1}$ (mm)	$y_t$ (mm)	$x_0 / y_t$	$h_{c1} / y_t$
38	11	442	0.086	0.025
100	8.5	442	0.226	0.019
200	6.1	442	0.452	0.014
400	8.5	442	0.905	0.019
600	10.2	442	1.357	0.023
1000	13.5	442	2.262	0.031
$y_0 = 17$ (mm) $F_0 = 2.6 - 5.7$ $S = 0.6 - 4.3$				
$x_0$ (mm)	$h_{c1}$ (mm)	$y_t$ (mm)	$x_0 / y_t$	$h_{c1} / y_t$
100	11.7	511	0.196	0.023
200	8	511	0.391	0.016
400	8	511	0.783	0.016
800	11.7	511	1.566	0.023
1200	13	511	2.348	0.025
$y_0 = 12$ (mm) $F_0 = 6.1 - 12$ $S = 0.58 - 4.32$				
$x_0$ (mm)	$h_{c1}$ (mm)	$y_t$ (mm)	$x_0 / y_t$	$h_{c1} / y_t$
100	8	520	0.192	0.015
200	8	520	0.385	0.015
300	8	520	0.577	0.015
600	10	520	1.154	0.019
900	10	520	1.731	0.019
100	8	448	0.223	0.018
200	8	448	0.446	0.018
300	8	448	0.670	0.018
600	8	448	1.339	0.018
900	8	448	2.009	0.018
100	8	407	0.246	0.020
200	8	407	0.491	0.020
300	8	407	0.737	0.020
600	8	407	1.474	0.020
900	8	407	2.211	0.020
100	6	370	0.270	0.016
200	8	370	0.541	0.022
300	8	370	0.811	0.022
600	8	370	1.622	0.022
900	6	370	2.432	0.016
100	6	313	0.319	0.019
200	8	313	0.639	0.026
300	8	313	0.958	0.026
600	8	313	1.917	0.026

Table 5-2 Experimental results for critical baffle height  $h_{c2}$

$y_0 = 10$ (mm) $F_0 = 1.37 - 10.28$ $S = 0.46 - 32$					$y_0 = 17$ (mm) $F_0 = 2.6 - 5.7$ $S = 0.6 - 4.3$				
$x_0$ (mm)	$h_{c2}$ (mm)	$y_t$ (mm)	$x_0 / y_t$	$h_{c2} / y_t$	$x_0$ (mm)	$h_{c2}$ (mm)	$y_t$ (mm)	$x_0 / y_t$	$h_{c2} / y_t$
38	15.4	442	0.086	0.035	200	23	511	0.391	0.045
100	15.2	442	0.226	0.034	400	25	511	0.783	0.049
200	16.2	442	0.452	0.037	800	29	511	1.566	0.057
400	21	442	0.905	0.048	1200	19	511	2.348	0.037
600	22.8	442	1.357	0.052					
$y_0 = 12$ (mm) $F_0 = 6.1 - 12$ $S = 0.58 - 4.32$					$y_0 = 15$ (mm) $F_0 = 3.73 - 7.46$ $S = 0.59 - 6.92$				
$x_0$ (mm)	$h_{c2}$ (mm)	$y_t$ (mm)	$x_0 / y_t$	$h_{c2} / y_t$	$x_0$ (mm)	$h_{c2}$ (mm)	$y_t$ (mm)	$x_0 / y_t$	$h_{c2} / y_t$
200	16	465	0.430	0.034	900	25	514	1.751	0.049
300	16	395	0.759	0.041	900	23	475	1.895	0.048
300	11	205	1.463	0.054	900	21	444	2.027	0.047
600	20	410	1.463	0.049	900	19	435	2.069	0.044
600	16	337	1.780	0.047	900	17	422	2.133	0.040
900	20	465	1.935	0.043	900	15	410	2.195	0.037
600	11	300	2.000	0.037	900	13	388	2.320	0.034
900	16	445	2.022	0.036	900	11.7	382	2.356	0.031
900	11	388	2.320	0.028	900	10	365	2.466	0.027
100	19	520	0.192	0.037	300	23	570	0.526	0.040
200	21	520	0.385	0.040	300	21	495	0.606	0.042
300	23	520	0.577	0.044	300	19	475	0.632	0.040
600	29	520	1.154	0.056	300	17	407	0.737	0.042
900	27	520	1.731	0.052	300	15	332	0.904	0.045
100	17	448	0.223	0.038	300	13	240	1.250	0.054
200	19	448	0.446	0.042	600	25	530	1.132	0.047
300	19	448	0.670	0.042	600	23	473	1.268	0.049
600	23	448	1.339	0.051	600	21	410	1.463	0.051
900	23	448	2.009	0.051	600	19	385	1.558	0.049
100	15	407	0.246	0.037	600	17	350	1.714	0.049
200	17	407	0.491	0.042	600	15	325	1.846	0.046
300	17	407	0.737	0.042	600	13	295	2.034	0.044
600	23	407	1.474	0.057	600	10	270	2.222	0.037
900	17	407	2.211	0.042					
100	15	370	0.270	0.041	200	21	555	0.360	0.038
200	17	370	0.541	0.046	200	19	478	0.418	0.040
300	17	370	0.811	0.046	200	17	432	0.463	0.039
600	21	370	1.622	0.057	200	15	395	0.506	0.038
900	11.6	370	2.432	0.031	200	13	295	0.678	0.044
100	13	313	0.319	0.042	100	19	570	0.175	0.033
200	15	313	0.639	0.048	100	17	475	0.211	0.036
300	15	313	0.958	0.048	100	15	378	0.265	0.040
600	15	313	1.917	0.048	100	13	335	0.299	0.039
900	6	313	2.875	0.019					



Table 5-4 Regression equations for the scales on water surface

Experimental conditions	Regression equations	R <sup>2</sup>
F <sub>0</sub> = 5.48 y <sub>0</sub> = 0.01m x <sub>0</sub> = 0.20 m h = 0.0116m S=3.54-6.23	$u_{sm}/U_0(\%)_{\pm 0.394} = 50.420_{\pm 0.921} - 3.854_{\pm 0.184} S$ $(x_{top}-x_0)/y_0_{\pm 0.782} = 2.149_{\pm 1.103} + 4.426_{\pm 0.236} S$ $h_h/y_0_{\pm 0.105} = 2.754_{\pm 0.148} - 0.264_{\pm 0.318} S$ $(x_{sm}-x_0)/y_0_{\pm 1.643} = -7.311_{\pm 2.842} + 11.187_{\pm 0.765} S$	0.993 0.989 0.945 0.986
y <sub>1</sub> = 0.44m y <sub>0</sub> = 0.01m x <sub>0</sub> = 0.20 m h = 0.0116m F <sub>0</sub> =2.74-6.85	$u_{sm}/U_0(\%) = 31.240_{\pm 0.5241}$ $(x_{top}-x_0)/y_0 = 23.000_{\pm 0.000}$ $h_h/y_0_{\pm 0.104} = -0.280_{\pm 0.117} + 0.330_{\pm 0.034} F_0$ $(x_{sm}-x_0)/y_0_{\pm 1.61} = 62.300_{\pm 2.643} - 2.590_{\pm 0.525} F_0$	0.979 0.924
y <sub>1</sub> = 0.44m y <sub>0</sub> = 0.01m F <sub>0</sub> = 5.48 h = 0.0116m x <sub>0</sub> /y <sub>0</sub> =10-60	$u_{sm}/U_0(\%) = 28.107_{\pm 2.165}$ $(x_{top}-x_0)/y_0 = 24.800_{\pm 1.643}$ $h_h/y_0 = 1.190_{\pm 0.195}$ $(x_{sm}-x_0)/y_0 = 52.200_{\pm 5.805}$	
y <sub>1</sub> = 0.44m y <sub>0</sub> = 0.01m F <sub>0</sub> = 5.48 x <sub>0</sub> = 0.20 m h/y <sub>0</sub> =1.16-2.3	$u_{sm}/U_0(\%)_{\pm 0.359} = 26.740_{\pm 0.724} + 3.417_{\pm 0.407} (h/y_0)$ $(x_{top}-x_0)/y_0_{\pm 0.353} = 33.878_{\pm 0.712} - 7.897_{\pm 0.401} (h/y_0)$ $h_h/y_0_{\pm 0.018} = 0.906_{\pm 0.036} + 0.395_{\pm 0.020} (h/y_0)$ $(x_{sm}-x_0)/y_0_{\pm 1.141} = 58.227_{\pm 2.300} - 9.716_{\pm 1.295} (h/y_0)$	0.959 0.992 0.992 0.949

Table 5-5 Data for the vorticity, circulation and circulation discharge of the eddy upstream the baffle

run	data source	ζ (1/s)	area (m <sup>2</sup> )	Γ (m <sup>2</sup> /s)	U <sub>0</sub> *x <sub>0</sub> (m <sup>2</sup> /s)	$\frac{\Gamma}{U_0 * x_0}$	$\frac{q_{circ}}{q_{noz}}$
(1)	(2)	(3)	(4)	(5)=(3)*(4)	(6)	(7)	(8)
1	downward section in Fig. 5-6 (a)	4.622	0.140	0.649	0.343	1.889	2.461
2	downward section in Fig. 5-6 (b)	4.758	0.140	0.666	0.429	1.552	2.638
3	downward section in Fig. 5-6 (c)	2.393	0.135	0.323	0.172	1.879	3.286
4	downward section in Fig. 5-6 (d)	4.589	0.126	0.576	0.343	1.678	2.605
5	downward section in Fig. 5-6 (e)	3.373	0.224	0.755	0.687	1.100	3.330
7	section x=0.4(m), backwards, Fig. 5-6(i)	4.926	0.313	1.543	1.030	1.498	3.034
8	section x=0.4(m), backwards, Fig. 5-6(k)	5.039	0.303	1.526	1.030	1.481	3.296

**Table 5-6 Magnitude and locus of the maximum velocity**

run 1			run 2				run 3			
x(m)	v <sub>m</sub> (m/s)	δ(m)	x(m)	v <sub>m</sub> (m/s)	δ(m)		x(m)	v <sub>m</sub> (m/s)	δ(m)	
0.00	1.716	0.001	0.00	2.145	0.001		0.00	0.858	0.001	
0.10	1.774	0.002	0.10	2.139	0.002		0.10	0.915	0.002	
0.15	1.549	0.002	0.15	1.884	0.002		0.15	0.771	0.002	
0.20	1.311	0.022	0.20	1.602	0.023		0.20	0.653	0.022	
0.30	0.909	0.121	0.30	1.149	0.120		0.30	0.502	0.116	
0.40	0.559	0.292	0.40	0.736	0.282		0.40	0.278	0.297	
0.50	0.352	0.398	0.50	0.422	0.380		0.50	0.186	0.365	
0.59	0.486	0.430	0.64	0.666	0.433		0.65	0.257	0.420	
0.62	0.508	0.442	0.67	0.670	0.447		0.68	0.265	0.424	
0.65	0.522	0.442	0.70	0.656	0.447		0.71	0.274	0.424	
run 4			run 5				run 6			
x(m)	v <sub>m</sub> (m/s)	δ(m)	x(m)	v <sub>m</sub> (m/s)	δ(m)	b(m)	x(m)	v <sub>m</sub> (m/s)	δ(m)	b(m)
0.00	1.717	0.001	0.00	1.716	0.001		0.00	1.716		
0.10	1.921	0.002	0.10	1.756	0.002	0.014	0.10	1.755	0.002	0.013
0.20	1.457	0.026	0.20	1.454	0.002	0.022	0.20	1.507	0.004	0.020
0.32	0.809	0.200	0.30	1.278	0.004	0.032	0.30	1.275	0.005	0.027
0.35	0.772	0.260	0.40	1.027	0.026	0.067	0.40	1.063	0.020	0.049
0.38	0.626	0.330	0.50	0.841	0.121		0.50	0.974	0.050	
0.42	0.447	0.400	0.56	0.653	0.210		0.60	0.665	0.061	
			0.615	0.405	0.361		0.80	0.615	0.011	
			0.75	0.408	0.398		1.00	0.550	0.030	
			0.78	0.449	0.411		1.20	0.448	0.035	
			0.81	0.482	0.424		1.40	0.345	0.049	
			0.81	0.479	0.424					
			0.84	0.479	0.442					
run 9			run 7				run 8			
x(m)	v <sub>m</sub> (m/s)	δ(m)	x(m)	v <sub>m</sub> (m/s)	δ(m)	b(m)	x(m)	v <sub>m</sub> (m/s)	δ(m)	b(m)
0.00	2.862	0.002	0.00	1.716	0.001		0.00	1.716	0.010	
0.10	2.832	0.004	0.10	1.815	0.002	0.013	0.10	1.859	0.002	0.013
0.20	2.658	0.007	0.20	1.481	0.002	0.020	0.20	1.529	0.005	0.021
0.34	2.058	0.069	0.30	1.296	0.006	0.029	0.30	1.389	0.005	0.029
0.50	1.124	0.255	0.40	1.186	0.005	0.037	0.40	1.279	0.006	0.037
0.80	1.018	0.466	0.50	1.058	0.005	0.046	0.50	1.099	0.006	0.055
1.00	0.822	0.466	0.60	0.840	0.025	0.127	0.60	0.933	0.041	0.154
1.20	0.784	0.466	0.70	0.743	0.111		0.70	0.736	0.158	
1.40	0.627	0.466	0.77	0.585	0.200		0.76	0.596	0.257	
1.60	0.559	0.466	0.82	0.410	0.300		0.78	0.504	0.327	
			0.89	0.300	0.370		0.83	0.390	0.345	
			1.00	0.347	0.420		1.00	0.498	0.418	
			1.03	0.357	0.442		1.20	0.459	0.442	
			1.06	0.3886	0.442		1.40	0.3934	0.442	

Table 5-7 Data for the surface profiles

run 1		run 2		run 3		run 4		run 5	
x(m)	y <sub>s</sub> (m)	x(m)	y <sub>s</sub> (m)	x(m)	y <sub>s</sub> (m)	x(m)	y <sub>s</sub> (m)	x(m)	y <sub>s</sub> (m)
0.000	0.444	0.000	0.453	0.000	0.425	0.000	0.444	0.000	0.446
0.050	0.443	0.050	0.451	0.050	0.424	0.100	0.439	0.150	0.439
0.100	0.440	0.100	0.447	0.100	0.422	0.190	0.427	0.250	0.434
0.150	0.435	0.150	0.436	0.150	0.422	0.300	0.443	0.350	0.433
0.200	0.432	0.200	0.433	0.200	0.422	0.350	0.457	0.440	0.437
0.250	0.436	0.250	0.436	0.250	0.421	0.400	0.455	0.500	0.443
0.300	0.440	0.300	0.451	0.300	0.423	0.500	0.439	0.550	0.451
0.350	0.449	0.350	0.460	0.350	0.426	0.600	0.433	0.600	0.454
0.400	0.451	0.400	0.466	0.400	0.426	0.700	0.436	0.650	0.453
0.450	0.450	0.450	0.464	0.450	0.426	0.800	0.437	0.750	0.444
0.500	0.447	0.500	0.460	0.500	0.424	1.000	0.436	1.850	0.441
0.550	0.443	0.550	0.453	0.550	0.423	1.200	0.437		
0.600	0.440	0.600	0.445	0.600	0.422	1.400	0.440		
0.650	0.435	0.650	0.440	0.650	0.422	1.600	0.441		
0.700	0.437	0.700	0.440	0.700	0.422	1.800	0.442		
1.850	0.437	1.800	0.443	1.800	0.422				
run 6		run 7		run 8		run 9			
x(m)	y <sub>s</sub> (m)	x(m)	y <sub>s</sub> (m)	x(m)	y <sub>s</sub> (m)	x(m)	y <sub>s</sub> (m)		
0.000	0.442	0.000	0.440	0.000	0.435	0.000	0.460		
0.200	0.441	0.100	0.440	0.100	0.435	0.100	0.460		
0.400	0.441	0.200	0.437	0.200	0.430	0.180	0.456		
0.600	0.439	0.400	0.433	0.300	0.428	0.210	0.435		
0.800	0.439	0.600	0.433	0.400	0.428	0.230	0.430		
1.000	0.441	0.750	0.443	0.500	0.428	0.330	0.456		
1.200	0.442	0.800	0.446	0.590	0.430	0.400	0.485		
1.800	0.442	0.850	0.448	0.700	0.444	0.450	0.498		
		0.950	0.443	0.750	0.449	0.550	0.511		
		1.000	0.441	0.800	0.449	0.700	0.481		
		1.200	0.441	0.900	0.442	0.800	0.448		
		1.400	0.441	1.000	0.436	0.900	0.435		
		1.600	0.441	1.800	0.435	1.000	0.449		
		1.800	0.441			1.100	0.450		
						1.200	0.451		
						1.850	0.464		

Table 5-8 Length scale and discharge data in the surface jet region

run 1					run 2				
x(m)	b <sub>s</sub> (m)	y <sub>u=0</sub> (m)	y <sub>noz1</sub> (m)	q/q <sub>noz1</sub>	x(m)	b <sub>s</sub> (m)	y <sub>u=0</sub> (m)	y <sub>noz1</sub> (m)	q/q <sub>noz1</sub>
0.50	0.095	0.260	0.392	2.07	0.60	0.070	0.294	0.401	2.24
0.60	0.069	0.295	0.401	2.42	0.80	0.074	0.270	0.401	2.60
0.80	0.070	0.270	0.397	2.68	1.00	0.100	0.230	0.395	2.63
1.00	0.090	0.245	0.392	2.66	1.20	0.103	0.230	0.385	2.29
1.20	0.096	0.242	0.387	2.36	1.40	0.096	0.230	0.372	1.96
1.40	0.103	0.225	0.375	2.04	1.60	0.112	0.220	0.349	1.61
1.60	0.091	0.240	0.363	1.74	1.80	0.117	0.200	0.329	1.43
run 5					run 7				
x(m)	b <sub>s</sub> (m)	y <sub>u=0</sub> (m)	y <sub>noz1</sub> (m)	q/q <sub>noz1</sub>	x(m)	b <sub>s</sub> (m)	y <sub>u=0</sub> (m)	y <sub>noz1</sub> (m)	q/q <sub>noz1</sub>
0.80	0.071	0.290	0.404	2.51	1.00	0.096	0.242	0.389	2.34
1.00	0.066	0.290	0.399	2.32	1.20	0.073	0.292	0.395	2.00
1.20	0.082	0.270	0.390	2.07	1.40	0.057	0.310	0.384	1.61
1.40	0.074	0.270	0.380	1.83	1.60	0.056	0.310	0.370	1.39
1.60	0.080	0.260	0.363	1.61	1.80	0.059	0.310	0.340	1.08
run 8					run 9				
x(m)	b <sub>s</sub> (m)	y <sub>u=0</sub> (m)	y <sub>noz1</sub> (m)	q/q <sub>noz1</sub>	x(m)	b <sub>s</sub> (m)	y <sub>u=0</sub> (m)	y <sub>noz1</sub> (m)	q/q <sub>noz1</sub>
1.00	0.067	0.300	0.399	2.26	0.80	0.071	0.295	0.396	1.90
1.20	0.071	0.295	0.392	1.92	1.00	0.113	0.225	0.395	2.35
1.40	0.062	0.325	0.380	1.39	1.20	0.115	0.220	0.394	2.33
1.60	0.067	0.320	0.364	1.16	1.40	0.114	0.220	0.387	1.99
					1.60	0.134	0.200	0.379	1.86
					1.80	0.161	0.170	0.364	1.73

- b<sub>s</sub>..... Surface jet half width.
- y<sub>u=0</sub>..... Value of y where u=0.
- q ..... The unit width forward discharge of surface jet.
- q<sub>noz1</sub> ..... Unit width nozzle discharge.
- y<sub>noz1</sub>..... Value of y above which the unit width forward discharge equals to q<sub>noz1</sub>

Table 5-9(a) Surface velocity data for varying gate Froude numbers

$x_0=0.2(m)$ $h=11.6(mm)$ $y_0=10(mm)$ $y_1=0.440(m)$							
$F_0=2.74$		$F_0=4.11$		$F_0=5.48$		$F_0=6.85$	
x(m)	u(m/s)	x(m)	u(m/s)	x(m)	u(m/s)	x(m)	u(m/s)
0.650	0.257	0.630	0.380	0.590	0.486	0.640	0.666
0.680	0.265	0.660	0.391	0.620	0.508	0.670	0.670
0.710	0.274	0.690	0.396	0.650	0.522	0.700	0.656
0.740	0.271	0.690	0.397	0.710	0.523	0.730	0.613
0.770	0.258	0.720	0.403	0.740	0.501	0.800	0.589
0.770	0.263	0.750	0.402	0.770	0.493	0.900	0.546
0.800	0.262	0.780	0.398	0.800	0.495	1.000	0.497
0.850	0.254	0.850	0.387	0.830	0.486	1.100	0.452
0.950	0.236	0.950	0.348	0.860	0.483	1.200	0.418
1.050	0.222	1.050	0.326	0.890	0.450	1.300	0.354
1.150	0.196	1.150	0.303	0.920	0.452	1.400	0.305
1.250	0.191	1.250	0.253	0.950	0.440	1.500	0.290
				1.050	0.403		
				1.150	0.363		
				1.250	0.334		
				1.350	0.296		
				1.450	0.240		
				1.550	0.234		
				1.650	0.207		
				1.750	0.219		

Table 5-9(b) Surface velocity data for varying baffle heights

$x_0=0.2(m)$ $F_0=5.48$ $y_0=10(mm)$ $y_1=0.440(m)$							
$h=15(mm)$		$h=17(mm)$		$h=20(mm)$		$h=23(mm)$	
x(m)	u(m/s)	x(m)	u(m/s)	x(m)	u(m/s)	x(m)	u(m/s)
0.540	0.467	0.585	0.556	0.550	0.563	0.510	0.556
0.570	0.520	0.610	0.566	0.580	0.579	0.525	0.588
0.600	0.535	0.640	0.547	0.610	0.567	0.540	0.598
0.630	0.545	0.670	0.524	0.640	0.547	0.555	0.581
0.660	0.538	0.700	0.525	0.640	0.554	0.570	0.581
0.690	0.531	0.730	0.511	0.680	0.537	0.590	0.585
0.720	0.532	0.760	0.516	0.680	0.537	0.600	0.562
0.720	0.532	0.860	0.469	0.720	0.542	0.620	0.545
0.750	0.525	0.960	0.439	0.720	0.538	0.650	0.526
0.850	0.491	1.060	0.392	0.760	0.531	0.650	0.528
0.950	0.450	1.160	0.345	0.800	0.503	0.700	0.537
1.050	0.408	1.260	0.331	0.900	0.466	0.700	0.541
1.150	0.357	1.360	0.266	1.000	0.425	0.800	0.479
1.250	0.331	1.460	0.228	1.100	0.375	0.900	0.435
1.350	0.290			1.200	0.346	1.000	0.432
1.450	0.275			1.300	0.279	1.000	0.420
				1.400	0.266	1.100	0.377
						1.200	0.340
						1.300	0.277
						1.400	0.270

**Table 5-9(c) Surface velocity data for varying submergences**

$x_0=0.2(m)$ $F_0=5.48$ $y_0=10(mm)$ $h=11.6(mm)$							
$S=6.23$		$S=5.61$		$S=4.20$		$S=3.54$	
$x(m)$	$u(m/s)$	$x(m)$	$u(m/s)$	$x(m)$	$u(m/s)$	$x(m)$	$u(m/s)$
0.650	0.374	0.640	0.453	0.550	0.542	0.510	0.594
0.680	0.406	0.670	0.477	0.580	0.594	0.540	0.631
0.710	0.418	0.700	0.487	0.610	0.593	0.570	0.625
0.740	0.419	0.730	0.491	0.640	0.580	0.600	0.599
0.770	0.440	0.760	0.488	0.670	0.542	0.630	0.551
0.800	0.445	0.760	0.482	0.670	0.548	0.660	0.539
0.830	0.459	0.790	0.482	0.700	0.531	0.660	0.538
0.860	0.446	0.790	0.471	0.700	0.525	0.690	0.535
0.890	0.439	0.820	0.487	0.730	0.526	0.720	0.533
0.920	0.436	0.820	0.479	0.730	0.526	0.720	0.535
0.950	0.427	0.850	0.481	0.800	0.499	0.720	0.531
1.050	0.407	0.850	0.461	0.900	0.444	0.800	0.461
1.150	0.370	0.880	0.478	1.000	0.380	0.900	0.393
1.250	0.359	0.880	0.459	1.100	0.325	1.000	0.313
1.350	0.319	0.910	0.466	1.200	0.250	1.100	0.252
1.450	0.291	0.910	0.454	1.300	0.209	1.200	0.201
1.550	0.287	1.000	0.435	1.400	0.201		
1.650	0.263	1.100	0.395				
1.750	0.244	1.200	0.371				
		1.300	0.343				
		1.400	0.303				
		1.500	0.284				
		1.600	0.270				

**Table 5-9(d) Surface velocity data for varying baffle positions**

$y_t=0.44(m)$ $F_0=5.48$ $y_0=10(mm)$ $h=11.6(mm)$							
$x_0=0.10(m)$		$x_0=0.20(m)$		$x_0=0.40(m)$		$x_0=0.60(m)$	
$x(m)$	$u(m/s)$	$x(m)$	$u(m/s)$	$x(m)$	$u(m/s)$	$x(m)$	$u(m/s)$
0.500	0.419	0.625	0.368	0.750	0.408	1.000	0.347
0.530	0.454	0.650	0.441	0.780	0.449	1.030	0.357
0.560	0.472	0.680	0.473	0.810	0.482	1.060	0.389
0.590	0.486	0.710	0.499	0.810	0.479	1.090	0.401
0.590	0.473	0.740	0.508	0.840	0.479	1.120	0.416
0.620	0.473	0.770	0.504	0.840	0.481	1.150	0.411
0.620	0.467	0.800	0.501	0.870	0.483	1.150	0.419
0.620	0.475	0.800	0.496	0.900	0.479	1.180	0.416
0.650	0.480	0.830	0.506	0.930	0.480	1.180	0.419
0.650	0.470	0.860	0.497	0.960	0.474	1.210	0.424
0.680	0.469	0.860	0.507	0.990	0.458	1.240	0.430
0.730	0.453	0.890	0.489	1.050	0.446	1.270	0.420
0.800	0.449	0.950	0.464	1.150	0.410	1.300	0.408
0.900	0.424	1.020	0.453	1.250	0.383	1.400	0.388
1.000	0.378	1.100	0.405	1.350	0.340	1.500	0.360
1.100	0.350	1.200	0.383	1.450	0.318	1.600	0.332
1.200	0.325	1.300	0.324	1.550	0.266	1.700	0.295
1.300	0.307	1.400	0.313	1.650	0.263	1.800	0.279
1.400	0.277	1.500	0.258				

Table 5-10 Data of surface bump position, surface bump height, maximum surface velocity and its position for varying nozzle Froude numbers, submergences, baffle heights and baffle positions

	$F_0$	$x_{sm}(m)$	$u_{sm}(m/s)$	$x_{top}(m)$	$h_h (mm)$
$x_0=0.2(m)$	2.74	0.74	0.2744	0.43	6.5
$h=0.0116(m)$	4.11	0.735	0.403	0.43	10.0
$y_0=0.010(m)$	5.48	0.68	0.5234	0.43	16.5
$y_t=0.440(m)$	6.85	0.64	0.67	0.43	19.5
	$h(mm)$	$x_{sm}(m)$	$u_{sm}(m/s)$	$x_{top}(m)$	$h_h (mm)$
$x_0=0.2(m)$	15	0.63	0.5448	0.42	15.0
$F_0=5.48$	17	0.61	0.5663	0.4	16.0
$y_0=10(mm)$	20	0.58	0.57916	0.38	17.0
$y_t=0.440(m)$	23	0.57	0.5884	0.36	18.0
	S	$x_{sm}(m)$	$u_{sm}(m/s)$	$x_{top}(m)$	$h_h (mm)$
$x_0=0.2(m)$	6.23	0.83	0.45896	0.505	11.0
$F_0=5.48$	5.21	0.76	0.49144	0.46	13.0
$y_0=10(mm)$	4.20	0.58	0.59384	0.4	18.0
$h=11.6(mm)$	3.54	0.54	0.63059	0.38	17.0
	$x_0(m)$	$x_{sm}(m)$	$u_{sm}(m/s)$	$x_{top}(m)$	$h_h (mm)$
$y_t=0.44(m)$	0.10	0.650	0.480	0.360	12.0
$F_0=5.48$	0.30	0.800	0.502	0.560	13.0
$y_0=10(mm)$	0.40	0.870	0.483	0.620	13.0
$h=11.6(mm)$	0.60	1.210	0.424	0.850	9.0

$u_{sm}$  ..... Maximum surface velocity.  
 $x_{sm}$  ..... Position of maximum surface velocity.  
 $x_{top}$  ..... Position of the top of surface hump.  
 $h_h$  ..... Height of surface hump (above tail water surface)

## **Chapter 6 General discussion**

**In the preceding four chapters, four problems were studied in the field of hydraulic engineering using the theory of turbulent jets. In this last chapter, a brief general discussion is presented on these contributions.**

**The first contribution is the finding of roughness effect on the characteristics of circular wall jets. Chapter 2 investigated the effects in the following respects: (1) the effect on the distribution of mean longitudinal velocity; (2) the effect on the growth of length scales; (3) the effect on the decay of mean velocity scale; and (4) the effect on boundary shear stress. The analysis of the results of the experimental study and the conclusions of Chapter 2 provide necessary information required to predict the development of circular jets on rough boundaries.**

**Due to the restriction of the measuring equipment, the study of Chapter 2 was not extended to cover the roughness effect on the turbulent structure of circular wall jets. This can only be accomplished with the help of three dimensional Laser Doppler Anemometer. The investigation on the roughness effect in this respect will help the hydraulic engineers to predict the diffusion and energy dissipation of the circular wall jets on boundaries with different roughnesses.**

**The second contribution of the thesis is the revelation of the mean flow structures of two intersecting jets with different momentum fluxes. For a fixed intersection angle of 60 degrees, detailed results are presented in Chapter 3 for the mean longitudinal velocity and pressure field measurements made for the momentum flux ratio  $R$  ranging from 0 to about 0.8. The study of Chapter 3 showed the existence of similarity in the mean velocity distribution in both**



transverse and vertical directions before and after the intersection point. By using the analysis results in Chapter 3, for intersecting jets with the same intersection angle we can predict the jet development before and after the intersection point. This includes (1) the direction of the resultant jet; (2) the decay of the axial mean velocity; (3) the jet thickness in vertical and transverse directions; and (4) the axial variation of the mean pressure.

The study of Chapter 3 is the extension to the study of Rajaratnam and Khan (1992), but it only concentrated on one fixed angle (60 degrees). To complete the work, further investigations on intersection jets of different momentum fluxes are needed for different intersection angles. In addition, it will be interesting to see how the turbulent structure of intersection jets is affected by different intersection angles and different momentum flux ratios.

As a third contribution, Chapter 4 of the present thesis investigated the free hydraulic jumps, submerged jumps together with two dimensional wall jets. This chapter collected all the available existing data for free jumps, submerged jumps and wall jets. It also presented the detailed experiment results obtained by the advanced probe-transducer-computer systems. The contribution is reflected mainly in the following respects: (1) The analysis of the velocity data indicated that the vertical distribution of forward longitudinal velocity is very insensitive to nozzle Froude number  $F_0$  and submergence  $S$ ; The velocity profiles are similar in each of the three flow configurations. (2) Based on all the existing data Chapter 4 derived a general velocity scale decay law for free jumps which is comparable with that of wall jet; (3) Chapter 4 investigated the variation of relative length scale  $L/y_0$  with nozzle Reynolds number  $R_0$  for wall jets and with  $F_0$  and  $S$  for hydraulic jumps, and derived regression equations for these variations. This relative length scale played a very important role in the

comparison of the decay of the velocity scales of free jumps, submerged jumps and wall jets. (4) For the longitudinal velocity scale of submerged jumps, Chapter 4 investigated as to how its decay changed from the free jump style to the wall jet style with increase of submergence and proposed a criteria for this changing. In addition to these, Chapter 4 also investigated in detail the boundary layer thickness, the jet half width and the length of jump roller. With the work of Chapter 4 we can now predict the main characteristics of hydraulic jumps of any submergence.

Chapter 4 concentrated on the mean characteristics of free jumps, submerged jumps and two dimensional wall jets. It did not consider the turbulence in these flows. In fact the turbulent characteristics of the three flow configurations were studied separately by Rouse, Siao and Nagaratnam (1959), Long, Rajaratnam and Steffler (1992) and Mathieu and Tailland (1965). It will be interesting to study them together and find the turbulent characteristics which are common to free jumps, submerged jumps and wall jets.

The fourth contribution of the thesis is of two fold. Firstly, the investigation in Chapter 5 found out the existence and the formation conditions of the three flow states, namely the stable deflected surface jet, the stable reattaching wall jet and the bistable state. The knowledge of the formation conditions of these flow regions is very important in designing the dimensions of baffle structures for deeply submerged flow. For example, we can design a 2D baffle structure so that a stable deflected surface jet will form to protect the river bed. Secondly, the present investigation revealed the mean flow structure of both reattaching wall jet and deflected surface jet states, especially the later flow state. The revelation will help us to predict the following features for given boundary conditions: (1) the decay and locus of the main flow; (2) the velocity

distribution; (3) the entrainment by the main flow and (4) the vorticity caused by a 2D baffle.

The purpose of this study in Chapter 5 was to commence an investigation on deeply submerged flows with baffles. Even for the simple two dimensional baffle case, the present study is not complete. For example, the force acting on the baffles was not investigated at this time. As we can expect, the two dimensional baffles are simple to construct but they can not cause sufficient mixing and dissipation when the flow is deeply submerged. In order to have sufficient energy dissipation it is necessary to use baffle blocks. The study of the baffle block effect on submerged jumps is a large field. For different value of the nozzle Froude number, downstream water level, different block sizes and combinations, we need to find the flow structures, energy dissipation rates and forces acting on the blocks. The accomplishment of the study on submerged energy dissipators needs further extension.

#### **References:**

1. Long, D, Rajaratnam, N. and Steffler, P. M. (1990), LDA Study of Flow Structure in Submerged Hydraulic Jump, Jour. of Hyd. Res., Vol. 28, No. 4, pp. 437-460.
2. Mathieu, S. and Tailland, A. (1965), Jet Parietal, Comptes Rendus, Académie des Sciences, Paris, Vol. 261, pp. 2282-2286.
3. Rouse, H. Siao, T. T. and Nagaratnam, S. (1959). Turbulence Characteristics of the Hydraulic Jump, Trans. ASCE, Vol. 124, pp. 926-966.
4. Rajaratnam, N. and Khan, A. A. (1992), Intersecting Circular Turbulent Jets, Journal of Hyd. Res., IAHR, Vol. 30, No. 3, pp. 373-387.